

# **HYDRODYNAMIC MODELLING OF SECONDARY SETTLING TANKS**


**(January 1997 to December, 2000)**

**Part 1: By GA Ekama and P Marais**

**Part 2: By D Kleine and BD Reddy**

**WRC Report No. 835/1/02**



**Water Research Commission** 

#### **Disclaimer**

This report emanates from a project financed by the Water Research Commission (WRC) and is approved for publication. Approval does not signify that the contents necessarily reflect the views and policies of the WRC or the members of the project steering committee, nor does mention of trade names or commercial products constitute endorsement or recommendation for use.

#### **Vrywaring**

Hierdie verslag spruit voort uit 'n navorsingsprojek wat deur die Waternavorsingskommissie (WNK) gefinansier is en goedgekeur is vir publikasie. Goedkeuring beteken nie noodwendig dat die inhoud die siening en beleid van die WNK of die lede van die projek-loodskomitee weerspieël nie, of dat melding van handelsname of -ware deur die WNK vir gebruik goedgekeur of aanbeveel word nie.

UNIVERSITY OF CAPE TOWN

Faculty of Engineering and the Built Environment

*Water Research Group, Department of Civil Engineering  
Centre for Research in Computational and Applied Mechanics*

FINAL REPORT

to the Water Research Commission

on the contract K5/835

## **HYDRODYNAMIC MODELLING OF SECONDARY SETTLING TANKS**

(January 1997 to December, 2000)

### **PART 1: APPLICATION OF A HYDRODYNAMIC MODEL TO FULL SCALE SECONDARY SETTLING TANKS**

by

**GA Ekama and P Marais**

### **Part 2: DEVELOPMENT OF A FINITE ELEMENT 2D HYDRODYNAMIC MODEL FOR SECONDARY SETTLING TANKS**

by

**D Kleine and BD Reddy**

ISBN No 1 86845 860 1  
WRC Report No 835/1/02  
WRC Contract No K5/835

Water Research Group (WRG)  
Research Report No W107

**March 2002**

## EXECUTIVE SUMMARY

This research project comprised two principal objectives, i.e.

- 1) to simulate with a commercially available 2 dimensional (2D) hydrodynamic secondary settling tank (SST) model (SettlerCAD) a number of fullscale SSTs in different countries (South Africa, Netherlands and USA) that have been hydraulically and solids loading rate stress tested, to determine the applicability for design and operation of fullscale SSTs the widely used 1D idealized flux theory (1DFT), and
- 2) to develop a finite element program for 2D hydrodynamic modelling of fullscale SSTs.

The research work flowing from meeting these two objectives are presented in two parts in this executive summary and in the more detailed final report that follows.

### PART 1 - APPLICATION OF A HYDRODYNAMIC MODEL TO FULL SCALE SECONDARY SETTLING TANKS

#### 1.1 INTRODUCTION

Application of the idealized steady state 1D flux theory (1DFT) to full scale circular (and rectangular) SSTs indicate that the design procedures based on this theory over-predict the permissible solids loading rate (SLR) by about 25 percent (Ekama *et al.*, 1997). This means that fullscale SSTs have a flux rating or capacity of about 80% on the 1DFT calculated SLR. The reason for this loss of SST capacity was believed to be due to poor hydraulics caused by (i) turbulence and density currents, (ii) poor effluent weir and baffle placement, (iii) effects of sludge collection mechanisms and inlet arrangements, (iv) absence of flocculating centre and stilling wells and (v) wind and temperature effects. However, there was no convincing evidence that this 25% correction needed to be applied for all types of SST, and therefore a crucial unanswered question was whether or not the observed SST failures on which the 25% reduction was based, were specific to the particular design of the tested SSTs. Because the 1DFT based procedures are widely used for design and operation of SSTs for activated sludge plants, it is important to determine the applicability of the 1DFT to the design and operation of full scale SSTs.

#### 1.2 OBJECTIVES

In this task, the two dimensional (2D) hydrodynamic model SettlerCAD (Zhou *et al.*, 1998) was applied to simulate full scale circular secondary settling tank (SSTs) with the principle aim to:



- (1) establish whether or not it “automatically” reproduces a flux rating  $< 1.0$  with respect to the steady state 1D idealized flux theory (1DFT), where the flux rating is the capacity of the SST as a % of the 1DFT calculated maximum surface overflow rate (SOR) and solids loading rate (SLR) and;
- (2) determine what factors influence this flux rating.

To do this, SST solids loading rate (SLR) stress tests reported in the literature were simulated. The tests simulated were;

- (1) the 4 tests done by de Haas *et al.* (1998) on four 35m diameter SSTs with Stamford baffle of the Darvill wastewater treatment plant (WWTP), Pietermaritzburg, South Africa;
- (2) the 15 tests done by Watts *et al.* (1996) on a single 28.96m diameter SST at the Kanapaha WWTP (Florida, USA), and
- (3) 6 each on the Rijen and Oss SSTs of the STOWa (1981) SST test data set in which 47 tests were done on 25 different SSTs in Holland with 30 to 46m diameter (Stofkoper and Trentelman, 1982).

Some details of the SSTs simulated are given in Table 1.

**Table 1:** Geometrical features of circular SSTs simulated with SettlerCAD.

	Darvill		Watts	STOWa	
	New	Old		Rijen	Oss
Diameter, $\phi_{ST}$ , m	35	35	28.96	45.5	41.8
Side water depth, SWD, m	4.10	2.50	3.66	2.25	2.00
Bottom slope	1:10	Flat	1:15.4	1:12	1:12
Average depth, $H_{ave}$ , m	4.68	2.50	3.97	2.88	2.58
$\phi_{ST}/H_{ave}$ ratio	7.48	14.00	7.29	15.79	16.20
Sludge collection	Scraper	Suction	Suction	Scraper	Scraper
Feed	Centre	Centre	Centre	Centre	Centre
Effluent launder	Peripheral	Peripheral	Peripheral	Inset <sup>1</sup>	Inset <sup>1</sup>
Feed well skirt baffle $\phi$ , m	6.0	6.0	15.32	4.55 <sup>2</sup>	4.18 <sup>2</sup>
Stamford baffle	Yes	Yes	No	No	No

<sup>1</sup>The outside rim of the inset launder was blocked off so in effect it was peripheral.

<sup>2</sup>Actual dimensions not given - estimated from a survey of Dutch SSTs (STOWa, 1981c).

### 1.3 METHOD - FINDING THE MAXIMUM SOR AND ASSOCIATED SLR AND HLR OF SETTLER CAD

From the measured  $V_0$ ,  $n$  and feed concentration ( $X_f$ ) values of a particular SLR stress test, the maximum SOR, and associated SLR, hydraulic loading rate (HLR) and actual hydraulic retention

time ( $R_{ha}$ ), was calculated from the 1DFT. The data listed in the literature for the particular SST and SLR stress test to be simulated, was given as input to SettlerCAD. Keeping the recycle flow ( $Q_R$ ) and feed concentration ( $X_F$ ) constant at the test values, the influent flow ( $Q_I$ ), calculated as a % of the 1DFT limit value, was increased for successive simulation runs from a low value to a high value, first in 2% of 1DFT limit increments, and then in 0.25 % of 1DFT limit increments between consecutive safe and fail runs. SST failure was accepted to be an average effluent suspended solids (ESS)  $> 50$  mg/l over the final 2 actual hydraulic retention times ( $R_{ha}$ ) of the run. In this way the steady state influent flow rate ( $Q_I$ ) for ESS  $> 50$  mg/l was determined for SettlerCAD at an accuracy of 0.25 % of the 1DFT limit and the first run with ESS  $> 50$  mg/l was accepted as the SettlerCAD predicted maximum influent flow rate limit. The SettlerCAD predicted maximum SOR, and associated SLR, HLR and  $R_{ha}$ , was calculated from the predicted influent flow limit and the test  $Q_R$  and  $X_F$  values. The predicted ESS and RAS concentrations over the complete run were imported into a spreadsheet program, in which were calculated (i) the average ESS and RAS concentrations over the final 2 actual hydraulic retention times ( $2xR_{ha}$ ) and (ii) the % solids mass balance as the run proceeded. The outcome (fail or safe) of each simulation run was recorded by checking sludge blanket height in SettlerCAD at the end of each simulation and whether the average ESS concentration over the final  $2xR_{ha}$  was greater (fail), or less (safe) than 50 mg/l. The % mass balance at a particular time interval was calculated as the sum of the masses of sludge in the return and effluent flows as a % of the mass of sludge entering the SST with the influent and recycle flows.

Generally, the better the sludge settleability, the higher the  $V_0$  and the lower the  $n$  values in the semilog equation linking the zone settling velocity  $V_{zs}$  and sludge concentration  $X$  ( $V_{zs} = V_0 e^{-nX}$ ) and the higher the concentration  $X$ , the lower the  $V_{zs}$ . Therefore, the better the sludge settleability and lower the SST feed concentration ( $X_F$ ), the higher the term  $V_0/(nX_F)$ , called the flux load factor and the higher the flux load factor, the higher the SOR, SLR and HLR (and the shorter the  $R_{ha}$ ). High HLR are more likely to cause hydraulic disturbances in the SST than low HLR and therefore the flux rating of the SST can be expected to decrease as the flux load factor increases. For this reason the SettlerCAD predicted SOR or SLR flux ratings (as a % of the 1DFT maxima) for the SSTs were plotted versus the flux load factor  $V_0/(nX_F)$  of the different tests.

#### 1.4 VALIDATION OF SETTLERCAD PREDICTION ACCURACY

The only tests which were helpful to check the accuracy with which SettlerCAD simulated full scale SSTs were the Watts tests. Of all 15 Watts tests simulated, SettlerCAD correctly predicted the results of 12 tests, i.e. Tests 1, 2 and 4 to 10 (safe) and 11 to 13 (fail) but incorrectly predicted the results for 3 tests, i.e. Tests 3 (test safe, SettlerCAD fail) and 14 and 15 (test fail, SettlerCAD safe). Tests 4, 14, 13, 7, 9 and 12, which include 3 safe and 3 fail tests, fall in a very narrow

%1DFT SOR (and SLR) range of 2% of 1DFT SOR from 71.5 to 73.5% and the SettlerCAD predicted SOR limit versus flux load factor line falls very close to these 6 tests (Fig 1). This narrow range, indicates that apart from Test 3 and 15, SettlerCAD accurately identifies the SOR and SLR capacity of the Watts SST. The SettlerCAD results of the Watts tests gives a good indication that the SettlerCAD predictions are valid for the simulation of full scale stress tests. SettlerCAD correctly predicted the result of 2 of the 4 Darvill tests and all 12 Rijen and Oss tests simulated. However, these tests were not helpful to validate the accuracy with which SettlerCAD predicted SST capacity, because, unlike the Watts tests, the range between the highest loaded safe and lowest loaded fail tests was too large ( $>10\%$  of 1DFT SOR).

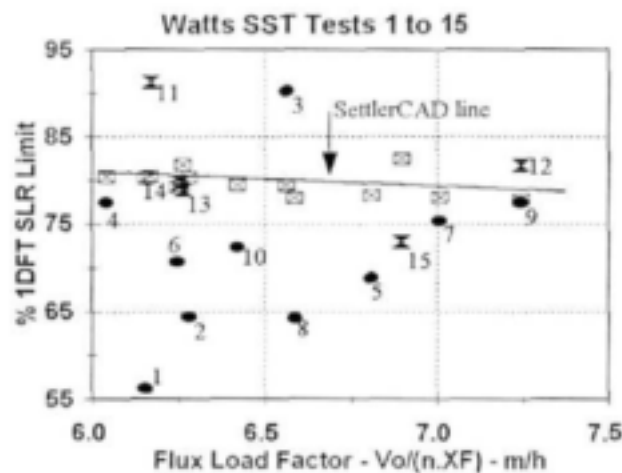


*Fig 1: SettlerCAD predicted maximum solids loading rate (SLR) as % of the 1DFT maximum limits versus flux load factor. Also shown are the positions and result (safe ●, fail ○) of the 15 actual tests identified by number.*

In all of the simulation runs, simulation times were selected which were  $>25$  times the actual hydraulic retention time ( $25 \times R_{hs}$ ). These run times were sufficiently long to establish a final steady state condition towards the end of the simulation, which was checked from the solids mass balance calculated at each time step of the run. In the solids mass balance, the mass of solids exiting the SST via the underflow and overflow is calculated as a % of the inflow mass of sludge. Steady state was accepted to have been established when the % mass balance no longer changed.

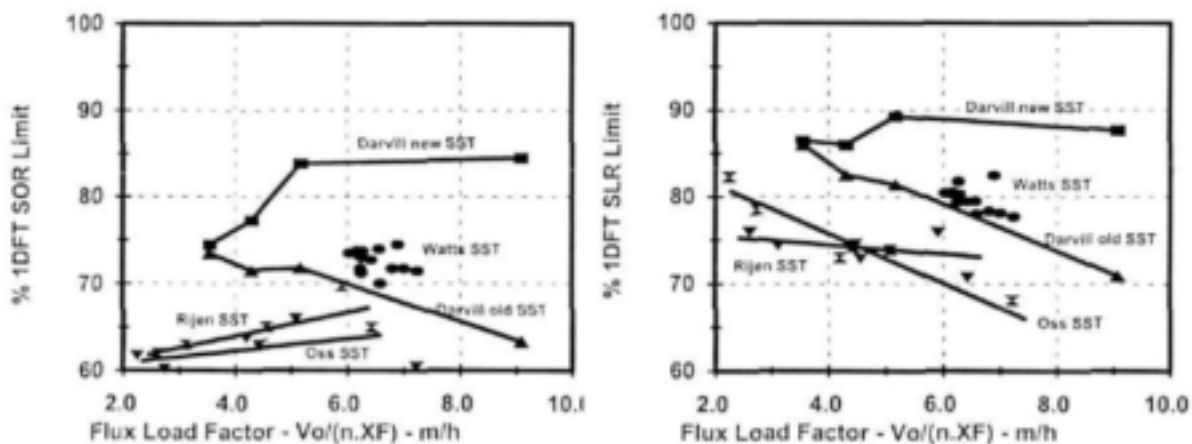
The final ESS ( $X_E$ ) and RAS ( $X_R$ ) concentrations accepted for each run were the averages of the predicted values over the last  $2 \times R_{hs}$  of the run. Provided the run ended safe ( $ESS < 50 \text{ mg/l}$ ), the final concentrations yielded a solids mass balance within 0.5% of 100%. In contrast, runs that ended in failure ( $ESS > 50 \text{ mg/l}$ ) yielded a lower than 99.5 % solids mass balance and the greater the SST overload (i.e. higher the ESS concentration) the lower the solids mass balance below 99.5 %, even as low as 86 % for some runs at 100 % of the 1DFT SOR. Halving the simulation time steps and/or doubling the number of iterations per time step yielded identical simulation results and no improvement in % mass balance and therefore it was accepted that the low % mass balance was not due to numerical instability. It is suspected that the low mass balance for the failed runs is due to a simple logical error in SettlerCAD. It seems that the RAS

concentration is “corrected” by subtracting from it the ESS concentration, because the higher the ESS concentration (or overload) the lower the RAS concentration. This is not consistent with the flux theory. Theoretically for increasing  $Q_i$  and constant  $Q_R$  and  $X_F$ , the RAS concentration should remain constant (at  $X_R = j_L/q_R$ ) once the SLR capacity (failure) has been reached. This error does not influence the SettlerCAD predicted SOR and SLR limits because the ESS is still low at the transition from safe to fail.

## 1.5 RESULTS

### 1.5.1 Flux rating of the simulated SSTs.

The results of the SettlerCAD predicted SOR, as % of the 1DFT calculated maximum SOR, and associated SLR, also as % of the 1DFT calculated maximum SLR, of all the simulated tests on the Darvill new and old, Watts, Rijen and Oss SSTs are plotted together in Figs 2a and b. The Rijen (▼) and Oss (⌘) SettlerCAD predicted SOR and SLR limit results lie below the Darvill old (▲) and new (■) and Watts (●) SST “lines”, but closer to the Darvill old SST line. Considering that with respect to external SST geometry (Table 1), the Rijen and Oss SSTs are closer in likeness to the old Darvill SST than the Darvill new and Watts SSTs, the expectation is that the Rijen and Oss results should fall near the old Darvill SST results, and this does indeed happen.



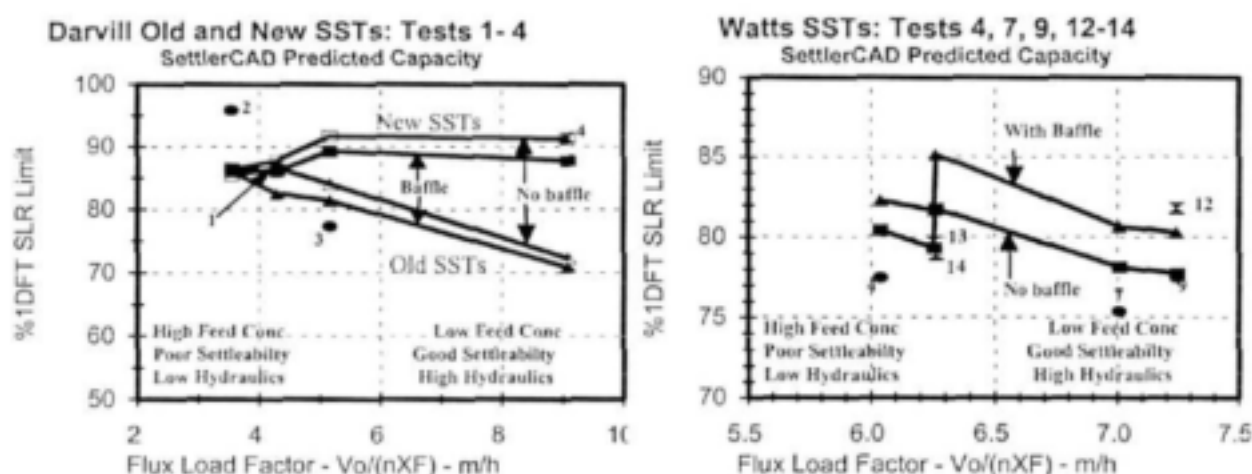
*Figs 2a and b: SettlerCAD predicted maximum SOR (Fig 2a, left) and SLR (Fig 2b, right), as a % of the 1DFT limit values versus flux load factor  $V_d/(nX_F)$  for the 4 tests on the Darvill new (■) and old (▲) SSTs, 15 of the 15 tests on the Watts' SST (●), 6 each of the 14 and 10 tests on the Rijen (▼) and Oss (⌘) SSTs.*

The simulations of SST stress tests with the 2D hydrodynamic model SettlerCAD indicate, as would be expected, that the SST hydraulic non-idealities are intrinsically part of the model and that SettlerCAD predicted maximum SOR and SLR were significantly below those calculated from the 1DFT. The simulations indicate that the *capacity*, or flux rating, of the 2.5m SWD flat bottom Darvill old SST decreases from 86% to 70% of the 1DFT maximum SLR as the flux load

factor  $V_0/(nX_F)$  increases (which increases HLR due to an improvement in sludge settleability and/or decrease in feed concentration). The shallow Rijen and Oss SSTs have a lower flux rating (SLR) than the Darvill old SST which decreases from 80% to 67% as flux load factor increases. The 4.1m SWD 1:10 sloping bottom Darvill new SST does not show this sensitivity of capacity (or flux rating) to the flux load factor (or HLR) and the flux rating remained approximately constant at around 87% of the 1DFT maximum SLR. The simulations show that the magnitude of the flux rating is not a constant value, and seems to be dependent on SST depth and HLR - the deeper the SST and the lower the HLR, the higher the flux rating. To determine the effect of the Stamford baffle and SWD on the flux rating, additional simulation runs were done on the Darvill SST (i) without the Stamford baffles and (ii) with interchanged SWD between the new and old SSTs and on the Watts SST (i) with a Stamford baffle and (ii) with 6.0m SWD.

### 1.5.2 The effect of the Stamford baffle on SST flux rating (capacity)

The SettlerCAD predicted maximum SLR (or flux rating) for the Darvill new and old and Watts SSTs with and without Stamford baffles are shown in Figs 3a and b.

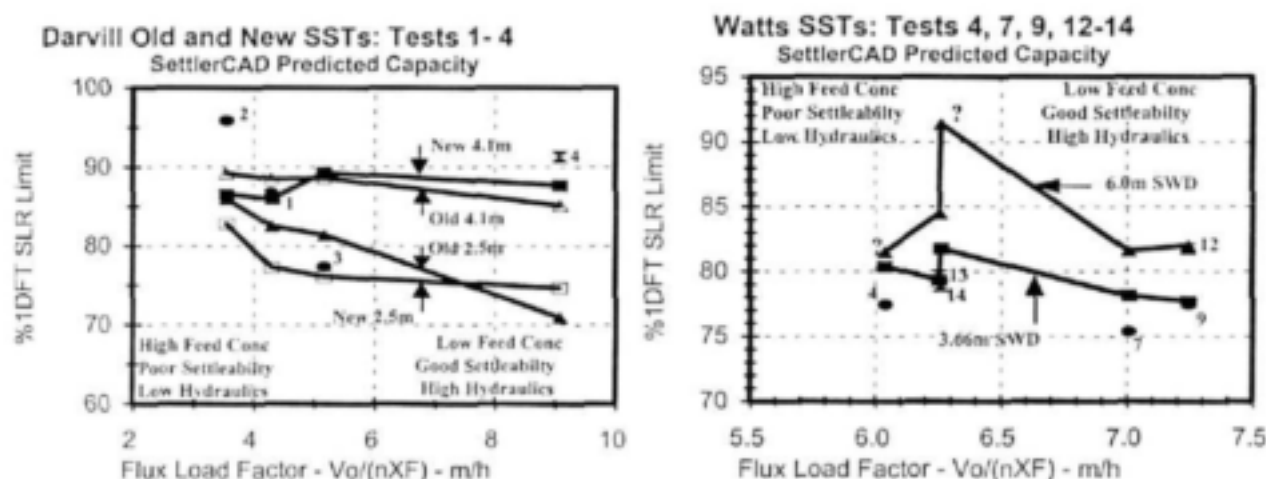


**Figs 3a and b:** SettlerCAD predicted maximum SLR for the Darvill (Fig 3a, left) and Watts (Fig 3b, right) SSTs with and without baffles. The actual test values, identified by number and result (safe ●, fail ⚡), are also shown.

For the Darvill SSTs, the SLR flux rating (Fig 3a) is about 2% of the 1DFT limit SLR *higher* without the Stamford baffle. In contrast, for the Watts SST, the flux rating is about 2% of the 1DFT limit SLR *lower* without the Stamford baffle. From this, it is concluded that while the Stamford baffle has a significant effect on the ESS concentration while the SST is underloaded, its influence on the flux rating (or capacity) of the SST is small.

### 1.5.3 The Effect of depth on SST flux rating (capacity)

The SettlerCAD predicted maximum SLR for the Darvill new and old SSTs with interchanged depths (i.e. new 2.5 m SWD, 1: 10 sloping bottom and scraper sludge collection and old 4.1 m SWD, flat bottom and suction sludge collection ) and the Watts SST with 6.0 m SWD are compared with that of the SSTs as built, (i.e. new 4.1 m SWD, 1: 10 sloping bottom and scraper sludge collection, old 2.5 m SWD, flat bottom and suction sludge collection and Watts with 3.66 m SWD, 1:15.4 sloping bottom and suction sludge collection) are plotted versus flux load factor in Figs 4a and b.



**Figs 4a and b:** SettlerCAD predicted maximum SLR for the Darvill new and old SSTs (Fig 4a, left) with interchanged SWD (old 4.1m and new 2.5m) and the Watts SST (Fig 4b, right) with a SWD of 6.0 m compared with the SSTs as built (new 4.1m, old 2.5m and Watts 3.66m). The actual test values, identified by number and result (safe ●, fail X) are also shown.

For the Darvill SSTs, the 4.1m SWD old SST has approximately the same flux rating (SLR) as the new 4.1 m SST (Fig 4a) and shows a small decrease from 89 to 85% of 1DFT SLR limit as flux load factor increases from 3 to 9 m/h. Likewise 2.5 m new SST has a similarly low flux rating as the 2.5 m old SST. The differences in flux rating between the new and old SSTs with the same SWD probably arise from the different SST bottoms and sludge collection systems, which for the old SST is flat and hydraulic suction and for the new SST is sloping 1:10 and scraper. While SettlerCAD can accommodate these differences, the accuracy with which simulates then is unknown.

For the Watts SST, 3.66 m SWD (as built) the 1DFT SLR limit (Fig 4b) shows a slight decreasing trend from 80 to 77% of 1DFT SLR as sludge load factor increases from 6.0 to 7.3 m/h. For Test 13 and 14 conditions ( $X_t$  and  $q_R$ ), the same flux load factor of 6.3 m/h leads to SettlerCAD predicted SLR predicted limits of 79 and 82% respectively. Ignoring Tests 4 and 14 (marked ?) for reasons detailed in Section 7.2 of the report, the Watts SST with a 6.0 m SWD



has a flux rating of about 5% of 1DFT SLR higher than with a 3.66 m SWD.

From the above it is clear that the greater the SWD, the higher the flux rating. For the Watts SST, an increase in SWD from 3.66 to 6.0m represents a 60% increase in SST volume. For a 5% of 1DFT SLR increase in flux rating this volume increase is definitely not cost efficient - it would be better to select the shallower SWD (3.66m for the Watts SST) and increase the surface area to accommodate the lower flux rating.

## 1.6 CONCLUSION

The simulations of the full-scale SST SLR stress tests with the 2D hydrodynamic model SettlerCAD indicate, as would be expected, that the SST hydraulic non-idealities are intrinsically part of the model and that appropriate flux ratings for the full scale SSTs are reproduced “automatically” in the model. The simulations therefore provide further convincing evidence that the 1DFT cannot be applied to the design of full-scale SSTs without an appropriate reduction factor. The SettlerCAD simulations of the Darvill 35 m Ø SSTs indicated that the *capacity*, or flux rating, of the old flat bottom shallow (2.5 m SWD) SSTs decreased from 86 to 70% of the 1DFT maximum SLR as the flux load factor (or HLR) increased from an improvement in sludge settleability and/or decrease in feed concentration. The new sloping bottom deep (4.1m SWD) SSTs did not show this sensitivity of capacity (or flux rating) to flux load factor (or HLR) and the flux rating remained approximately constant at around 87% of the 1DFT maximum SLR. The magnitude of the flux rating therefore is not a constant value, and is shown to be dependent on SST depth and HLR; the deeper the SST, the higher the flux rating and the less sensitive the flux rating to flux load factor. Simulations of the Darvill new and old SSTs with inter-changed SWD and the Watts SST with 6.0m SWD, confirmed the sensitivity of the flux rating to depth and HLR. Furthermore, although the Stamford baffle can significantly reduce effluent suspended solids (ESS) concentration while the SST is underloaded, it does not increase the flux rating (or capacity) of the SST.

From the simulations the flux rating of 80% of the 1DFT maximum SLR recommendation by Ekama and Marais (1986) remains a reasonable value to apply in the design of full scale SSTs – for deep SSTs (4m SWD) the flux rating could be increased to 85% and for shallow SSTs (2.5m SWD) decreased to 75%. It is recommended that (i) while the apparent interrelationship between SST flux rating and depth suggests some optimization of the volume of the SST, that this be avoided and that (ii) the depth of the SST be designed independently of the surface area as is usually the practice and once selected, the appropriate flux rating is applied to the 1DFT estimate of the surface area.

## **PART 2 - DEVELOPMENT OF A FINITE ELEMENT 2D HYDRODYNAMIC MODEL FOR SECONDARY SETTLING TANKS**

### **2.1 INTRODUCTION**

The flow in a sedimentation tank is characterized by the simultaneous flow of suspended solids and water. Hydrodynamic models have been developed for simulating secondary settling tanks (SST) to get a better understanding of the complex flow patterns in these tanks and to make design and optimization of the SST internal features possible. These models use mainly the finite volume method (FVM) as a method for obtaining numerical solutions. The development of a finite element program for (initially) 2D hydrodynamic modelling of secondary settling tanks is considered in this second task of the research project.

### **2.2 THE ADVANTAGES OF FEM**

In this work a program code is developed that is performed by the finite element method (FEM). Although this method has its origins in stress analysis, it is currently applied to sophisticated problems in other areas such as heat transfer and fluid flow.

All numerical solutions are discrete approximations to continuous solutions. Most of the differences in techniques arise from the choice of discretization of the problem. The most common methods are Finite Differences (FDM), Finite Volumes (FVM) and Finite Elements (FEM).

The finite difference method approximates the derivatives in the differential equations via a truncated Taylor series and combines the series of adjacent points to approximate the governing equations. The FDM is simple and efficient to code in one, two and three dimensions on structured grids, and it is easy to obtain higher-order schemes. The restriction to simple geometries, static meshes and problems with smoothly varying properties are significant disadvantages in complex flows.

The equations of fluid dynamics express the conservation of mass, momentum and energy in a volume closed by a surface. There are situations where an accurate representation of the conservation laws in their integral form is extremely important, for example, the imposition of the incompressibility constraint, as a conservation law for mass, determines the pressure field. The finite volume method achieves this by discretizing the integral form of the equations and not the differential form. Due to the combination of the formulation of a flow problem on control volumes, with the geometric flexibility in the choice of the grid and the flexibility in defining the



discrete flow variables, makes the FVM very attractive in engineering applications. Additionally the FVM approach is simple to understand and to program. The disadvantages of the FVM are the difficulties in defining the derivatives. Since the grid is not necessarily orthogonal, as in the FDM, the Taylor-expansion cannot be applied to define the derivatives. It is also not possible to convert higher order derivatives into lower ones with the mechanism of a weak formulation, as in the FEM. This is the main distinguishing feature of the finite element method. The equations are multiplied by a weighting function before they are integrated over the entire domain. The power of the finite element method lies in its ability to use an irregular grid. It provides more flexibility in fitting irregular domains and in providing local grid refinement. The flexible geometry of the FEM supports the description and adaptation of complex internal features of SSTs like inlet and outlet arrangements. Furthermore, the FEM deals with strongly varying internal properties and is applicable to Lagrangian moving-mesh problems. The disadvantage of the FEM is a significantly greater computational complexity.

### **2.3 DEVELOPMENT OF A FEM CODE FOR HYDRODYNAMIC MODELLING OF FULLSCALE SSTs**

In this work a program is developed that is based on the finite element method (FEM). Unlike the finite difference method (FDM) or the FVM, the finite element method is convenient for handling arbitrarily shaped domains and variable resolution meshes.

The performance of a settling tank is determined by the tank hydraulics and the transport and removal of solids. The hydrodynamic SST model solves the continuity, momentum and the solids transport equations, as well as equations that model turbulence. A density state equation and a settling velocity equation carry out the coupling of the solids transport and hydrodynamic equations.

The finite element approach leads to a fully coupled matrix equation. The present work generally follows the projection method to decouple the incompressible Navier-Stokes equations. For solving the coupled momentum and continuity equation a second-order accurate pressure correction scheme is deployed. The treatment of incompressibility is taken into account by splitting the coupled Navier-Stokes- and the continuity equations, and obtaining definite expressions for the velocities as well as for the pressure.

The fractional- $\theta$ -scheme is adopted to integrate the time derivative of the governing equations in the temporal domain. This method has the merit of incorporating both implicit Euler and Crank-Nicolson schemes as special cases.

In order to improve stability the standard Navier-Stokes formulation is modified using the Streamline Upwind Petrov-Galerkin (SUPG) method. The problem of convergence no longer simply associated with the convective nature of the equations, since in stratified flow fields, as in settling tanks, the gravity-production term reduces the efficiency of the upwinding scheme.

The piecewise bilinear test functions and the trial functions for the velocity correction equation and the pressure equation are same in the formulation. In case of the SUPG formulation the test functions for the equation to evaluate the provisional velocity are performed by adding a streamline upwind perturbation, which acts only in the flow direction.

The discretized mathematical model results in the solution of systems of linear equations to obtain the nodal solution. The whole system, consisting of six coupled partial differential equations, is decoupled through the use of an iterative scheme and linearisation of the system. Sophisticated Krylov subspace iterations are adopted to solve the linear problems. The resulting symmetric and positive definite linear problem is solved by the conjugate gradient method. The resulting non-symmetric linear problem of the discrete momentum equations is solved by the generalized minimal residual (GMRES) method.

In this work, the finite element model is applied to full scale circular SSTs, in two dimensions. The performance of the model is analysed with tests done by de Haas *et al.* (1998) on SSTs of the Darvill wastewater treatment plant (Pietermaritzburg, South Africa), as well as with stress tests done by Watts *et al.* (1996) on one of the four SSTs at the Kanapaha Water Reclamation Facility (Florida,USA).

The computational results show that the turbulent transport is strongly affected by buoyancy effects. Without the buoyancy source term in the  $k$ - $\varepsilon$ -model the turbulence is not damped due to stable stratification. The sediment eddy diffusivity is related to the eddy viscosity by using the Reynolds analogy between mass transport and momentum transport. By setting the Schmidt number to typical values in the range between 0.5 and 1.0 the diffusion coefficient in the concentration equation reaches the size of the settling velocity. In a stable stratification the movement in the vertical direction is only determined by diffusion and settling motion. The settlement of the sludge cannot take place when the motion due to diffusion is higher than the convective motion due to the settling velocity of the sludge. Furthermore, the required recycle concentration is not attainable, which must inevitably result in a failure of the SST. Especially at the bottom of the tank the situation is critical: the higher the concentration the smaller the settling velocity and the higher the influence of the diffusion on the settling motion is.

The question arises as to what extent the use of the Reynolds analogy is applicable, and whether attention has to be paid to the rheological properties of highly concentrated activated sludge. Due

The question arises as to what extent the use of the Reynolds analogy is applicable, and whether attention has to be paid to the rheological properties of highly concentrated activated sludge. Due to these uncertainties and the immense effect of the turbulent sizes on the settling process the computational results do not provide a definitive answer. To properly validate the model further information and calibration are needed. Unfortunately this information is not yet available in the literature.

From the computational point of view the code needs to be improved with regard to computational efficiency. This can be done by preconditioning, a more robust iterative treatment, the implementation of a multigrid technique and by the choice of another element pair, which is more robust, accurate and efficient. Furthermore, because of the progressive development of the program, it is somewhat inefficient in computer time, because of numerous operations are repeated several times, instead of having their results stored once in the computer memory. To save on memory the matrix should be stored in a special way, for example using compressed sparse row storage. More efficient streamlining of the calculation procedure and routines can also reduce computation time. Finally, before the program can be released, it is necessary to build up a user-friendly pre- and postprocessing procedure.

## ACKNOWLEDGEMENTS

The writers wish to express their gratitude to Reid Crowther Consulting Inc (Seattle, USA) (Dr Z Cello Vitasovic) for donation of the SettlerCAD model to the Water Research Group (WRG) at UCT on condition that it is used for exclusively for research.

A special word of thanks to Mr Jay Bhagwan of the Water Research Commission (WRC) as chairman of the research steering committee for this project, for his support, positive critical comment and advice on the research work and his efforts on the administration of the project.

Gratitude is also expressed to the following persons who were members of the steering committee for this project, for their contribution to the overall success of the research work:

<b>Project K5/835 -</b>	<b>Hydrodynamic modelling of secondary settling tanks (This project)</b>
Mr JN Bhagwan -	WRC and chairman of the steering committee for the project.
Dr I Msibi -	WRC
Prof BD Reddy -	Dean of Science UCT, and Director of the Centre for Research in Computational and Applied Mechanics (CERECAM) at UCT (Project leader).
Prof GA Ekama -	Dept of Civil Engineering, UCT (Project leader).
Ms D Kleine -	Research Officer, CERECAM, UCT
Mr C Brouckaert -	Dept of Chemical Engineering , University of Natal , Durban
Prof O Onyejekwe -	Dept of Civil Engineering, University of Durban Westville.
Mr SA van der Merwe -	Pretoria City Council
Dr A van Niekerk -	Wates Meiring and Barnard
Mr AR Pitman -	Greater Johannesburg Metropolitan Council
Mr P Gaydon -	Umgeni Water.
Mr MJ Arkley -	Cape Metropolitan Council
Mr P Marais -	V3 Consulting, Masters student, Dept of Civil Eng, UCT.

and also of the 2 related WRC computational fluid dynamics (CFD) research projects with whom joint steering committees were held:

<b>Project K5/1075 -</b>	<b>CFD modelling support to water research projects. Dept of Chemical Engineering, University of Natal, Durban (UND).</b>
Dr G Offringa -	WRC, chairman of the steering committee for the project.
Dr I Msibi -	WRC
Mr C Brouckaert -	Dept of Chemical Engineering, UND (Project Leader)

Prof CA Buckley -	Dept of Chemical Engineering, UND
Prof CGdeK du Toit -	Dept of Chemical Engineering , Potchefstroom Univ. for CHE
Prof J Haarhof -	Dept of Civil Engineering, Rand Afrikaans University (RAU)
Prof M Starzak -	Dept of Chemical Engineering, UND
Mr W Pulles -	Pulles, Howard and de Lange Consultants
Mr M Pryor -	Umgeni Water
Dr EP Jacobs -	Polymer Research Institute, University of Stellenbosch
Dr VL Pillay -	ML Sultan Technikon
and -	Mr SA van der Merwe, Profs BD Reddy, Onyejekwe and Ekama of the above project.

<b>Project K5/998</b>	<b>Modelling of flocculation, thickening and sedimentation in water treatment - Potchefstroom Univ. for CHE (PotCHE)</b>
Mr JN Bhagwan -	WRC and chairman of the steering committee for the project.
Dr I Msibi -	WRC
Prof CGdeK du Toit -	Dept of Chemical Engineering, PotCHE (Project Leader)
Mr TN Lemmer -	Doctoral Student, Dept of Chemical Engineering, PotCHE
Mr CF Pretorius -	Wates, Meiring and Barnard Consultants
Mr JC Geldenhuys -	Rand Water
Mr SA Pieterse -	Cape Metropolitan Council
and -	Mr CJ Brouckaert, Dr AR Pitman, Ms D Kleine and Profs CG du Toit, GA Ekama, J Haarhof and BD Reddy, of the above two projects.

## TABLE OF CONTENTS

<b>EXECUTIVE SUMMARY</b>	iii
<b>ACKNOWLEDGEMENTS</b>	xv
<b>TABLE OF CONTENTS</b>	xvii
<b>OUTPUTS DURING CONTRACT PERIOD</b> (January 1997 to June 2001)	xxi
<b>PART 1: ESTIMATING THE CAPACITY OF FULLSCALE SSTs WITH A 2D HYDRODYNAMIC MODEL</b>	
<b>1 INTRODUCTION</b>	1
1.1 SSTs limit wastewater treatment plant capacity.	1
1.2 Design of fullscale SSTs	2
1.3 Application of the 1DFT to fullscale SSTs	2
<b>2 OBJECTIVES</b>	5
<b>3 SIMULATION OF SST PERFORMANCE WITH SettlerCAD</b>	6
3.1 SettlerCAD description and input information	6
3.2 Finding the maximum SLR and HLR of SettlerCAD	8
<b>4 SIMULATING THE DARVILL SSTs WITH SettlerCAD</b>	11
4.1 The Darvill WWTP SST SLR stress tests	11
4.2 Finding the SettlerCAD maximum SOR and SLR for the Darvill SSTs	13
4.3 Conclusions from the Darvill SST simulations	19
<b>5 SIMULATING THE WATTS' SSTs WITH SettlerCAD</b>	21
5.1 The Watts' SST SLR stress tests	21
5.2 Finding the SettlerCAD maximum SOR and SLR for the Watts' SSTs	24
5.3 Conclusions from the Watts' SST simulations	29
<b>6 SIMULATING THE DUTCH STOWa SSTs WITH SettlerCAD</b>	31
6.1 The STOWa SSTs SLR stress tests	31
6.2 Simulating the Rijen SST SLR stress tests with SettlerCAD	32
6.3 Finding the SettlerCAD maximum SOR and SLR for the Rijen SST	33

6.4	Simulating the Oss SST SLR stress tests with SettlerCAD	41
6.5	Finding the SettlerCAD maximum SOR and SLR for the Oss SST	41
6.6	Conclusions from the Rijen and Oss SST simulations	49
<b>7</b>	<b>EFFECT OF BAFFLING AND DEPTH ON SST FLUX RATING</b>	<b>51</b>
7.1	The effect of baffling on SST flux rating (capacity)	51
7.2	The effect of depth on SST flux rating (capacity)	52
<b>8</b>	<b>CONCLUSIONS AND RECOMMENDATIONS</b>	<b>57</b>
8.1	Validation of SettlerCAD prediction accuracy	57
8.2	Flux rating of the simulated SSTs	58
8.3	The effect of the Stamford baffle on SST flux rating (capacity)	59
8.4	The effect of depth on SST flux rating (capacity)	60
8.5	Closure	61
8.6	Recommendations	61
<b>9</b>	<b>REFERENCES</b>	<b>62</b>

## **APPENDIX 1 - ESTIMATION OF SECONDARY SETTLING TANK CAPACITY WITH THE 1 DIMENSIONAL IDEALIZED FLUX THEORY (1DFT)**

<b>1</b>	<b>INTRODUCTION</b>	<b>A1</b>
<b>2</b>	<b>MEASUREMENT OF THE FLUX CONSTANTS <math>V_0</math> AND <math>n</math></b>	<b>A2</b>
<b>3</b>	<b>RELATIONSHIP BETWEEN ZONE SETTLING VELOCITY AND CONCENTRATION</b>	<b>A3</b>
<b>4</b>	<b>FLUX DUE TO GRAVITY SETTLING</b>	<b>A4</b>
<b>5</b>	<b>1D IDEALIZED FLUX THEORY - GRAPHICAL APPLICATION</b>	<b>A6</b>
<b>6</b>	<b>DYNAMIC CONDITIONS</b>	<b>A16</b>
<b>7</b>	<b>MATHEMATICAL APPLICATION OF THE 1D FLUX THEORY</b>	<b>A17</b>
7.1	Mathematical properties of the theoretical flux equation	A17
7.2	Application of the exponential flux equation to SST	A19
7.3	SST design and operating chart	A21
<b>8</b>	<b>DESIGN EXAMPLE</b>	<b>A23</b>
<b>9</b>	<b>REFERENCES</b>	<b>A27</b>

## **APPENDIX 2 - LIST OF ABBREVIATIONS AND SYMBOLS FOR PART 1**

## TABLE OF CONTENTS

### **PART 2: DEVELOPMENT OF A FINITE ELEMENT 2D HYDRODYNAMIC MODEL FOR SECONDARY SETTLING TANKS**

<b>1</b>	<b>INTRODUCTION</b>	<b>1</b>
<b>2</b>	<b>SECONDARY SETTLING TANKS</b>	<b>3</b>
2.1	Function of Secondary Settling Tanks	3
2.2	Hydrodynamic Modelling of SSTs	3
<b>3</b>	<b>FUNDAMENTAL EQUATIONS</b>	<b>5</b>
3.1	Conservation of Fluid Mass: Continuity Equation	5
3.2	Conservation of Momentum: The Navier-Stokes Equations	5
3.3	Conservation of Particulate Mass: Concentration Equation	6
3.4	Solid Settling Equation	7
3.5	Density-State Equation	8
3.6	Turbulence Modelling	9
<b>4</b>	<b>NUMERICAL MODELLING</b>	<b>11</b>
4.1	Spatial Discretization	11
4.2	Weak Formulation of the Finite Element Equations	13
4.3	Upwinding Technique - Streamline Upwind Petrov-Galerkin Method	13
4.4	Temporal Discretization	14
4.5	Derivation of the Navier-Stokes Solver	15
4.6	Equation Solution Technique	16



<b>5</b>	<b>EXAMPLE USE OF NUMERICAL MODEL AND EXPERIMENT</b>	<b>18</b>
5.1	Geometry and Boundary Conditions for 2D-Model	18
5.2	Simulating the Darvill Old and New SST	23
5.2.1	Temporal and Steady State Result of Darvill Old SST	26
5.2.2	Temporal and Steady State Result of Darvill New SST	29
5.3	Simulating the Watts SST	32
5.3.1	Watts Test 1	32
5.3.2	Watts Test 12	35
5.3.3	Watts Test 4	41
<b>6</b>	<b>CONCLUSION AND OUTLOOK</b>	<b>42</b>
<b>7</b>	<b>REFERENCES</b>	<b>44</b>

### APPENDIX 3

<b>1</b>	<b>LIST OF SYMBOLS FOR PART 2</b>	<b>A3.1</b>
<b>2</b>	<b>LIST OF FIGURES FOR PART 2</b>	<b>A3.3</b>
<b>3</b>	<b>LIST OF TABLES FOR PART 2</b>	<b>A3.4</b>

## OUTPUTS DURING CONTRACT PERIOD (January 1997 to June 2001)

### 1 PUBLICATIONS

#### 1.1 Books

- 1 Ekama GA, Barnard JL, Günthert FW, Krebs P, McCorquodale JA, Parker DS, Wahlberg EJ (1997) *Secondary settling tanks: Theory, design, modelling and operation*. IAWQ STR No 6, pp216, International Association on Water Quality, London.

#### 1.2 International Conferences

- 1 Ekama GA, Barnard JL, Günthert FW, Krebs P, McCorquodale JA, Parker DS, Wahlberg EJ (1997) Secondary settling tanks: Theory, design, modelling and operation". *2nd Int Conf. of the Association of Wastewater Treatment Experts of the Czech Republic (ACECR)*. 26-27 May, Jihlava, CZ, Ed: Wanner J., ACECR, Prague, 169-190.
- 2 Marais PM, Ekama GA and de Haas DW (2001) Comparison of the 1D flux theory and a 2D hydrodynamic model with full-scale secondary settling tank performance data. *Procs. 74<sup>th</sup> Water Environment Federation Conference and Exhibition*, Atlanta, 13-17 Oct. (2)

#### 1.3 National Conferences

- 1 Kleine D, Reddy BD, GP Mitchell (2000) Finite Element Analysis of Flows in Secondary Settling Tanks. *Procs. SACAM 2000 Applied Mechanics International Conference*, Durban, 11-13 Jan.
- 2 Marais PM, Ekama GA and de Haas DW (2000) Comparison of the 1D idealized flux theory and a 2D hydrodynamic model with full-scale secondary settling tank performance data. *Procs 6<sup>th</sup> biennial Water Institute of Southern Africa conference and exhibition*, Suncity, 28/5 to 1/6/2000. CD-ROM ISBN 0-620-25661-3.
- 3 Kleine D, Reddy BD (2000) Hydrodynamic Modelling of Secondary Settling Tanks. Presented at 6<sup>th</sup> biennial Water Institute of Southern Africa conference and exhibition, Suncity, 28/5 to 1/6/2000.

#### 1.4 Reports

- 1 Ekama GA and Marais P (2001) Hydrodynamic modelling of secondary settling tanks Part 1 - Application of a hydrodynamic model to full scale secondary settling tanks, Final report to Water Research Commission on contract K5/835, Report K5/835/1/01, WRC, PO Box 824, Pretoria, 0001, RSA.
- 2 Kleine D and Reddy BD (2001) Hydrodynamic modelling of secondary settling tanks

Part 1 -Development of a finite element code for 2D hydrodynamic modelling of secondary settling tanks, Final report to Water Research Commission on contract K5/835, Report K5/835/1/01, WRC, PO Box 824, Pretoria, 0001, RSA.

- 3 Marais P and Ekama (2001) Comparison of the 1D idealized flux theory and a 2D hydrodynamic model with full scale secondary settling tank performance data. Research Report No W111, Dept of Civil Eng., Univ. of Cape Town, Rondebosch, 7701, Cape, RSA.

## **2 POSTGRADUATE STUDENTS**

### **2.1 Doctoral**

- 1 PhD Dorothee Kleine - Development of a finite element code for hydrodynamic modelling of secondary settling tanks.

### **2.2 Masters**

- 1 MSc (Eng) Pierre Marais - Comparison of the 1D idealized flux theory and a 2D hydrodynamic model with full scale secondary settling tank performance data.

UNIVERSITY OF CAPE TOWN  
Department of Civil Engineering  
*Water Research Group*

**FINAL REPORT**  
to the Water Research Commission for the task

**APPLICATION OF HYDRODYNAMIC MODELS TO FULL SCALE  
SECONDARY SETTLING TANK (SST) BEHAVIOUR**

in the contract K5/835  
**HYDRODYNAMIC MODELLING OF SECONDARY SETTLING TANKS**

by

George A Ekama and Pierre Marais

## **1. INTRODUCTION**

### **1.1 SSTs limit wastewater treatment plant capacity.**

The secondary settling tank (SST) of activated sludge systems is the bottle neck limiting the capacity of the wastewater treatment plant (WWTP). Two main factors influence this (i) the settleability of the sludge and (ii) the hydraulics within the SST. In the past SSTs have been designed by empirical rules such as the surface overflow rate (SOR)  $< 1\text{m/h}$  at peak wet weather flow (PWWF), but many SSTs already begin to discharge high effluent suspended solids (ESS) concentrations ( $>30\text{mg/l}$ ) long before they reach this capacity even with good settling sludges (Diluted sludge volume index, DSVI  $< 100\text{ml/g}$ ). This causes a significant loss of SST, and therefore also of WWTP, capacity. The reason for this loss of SST capacity often is poor hydraulics caused by (i) turbulence and density currents, (ii) poor effluent weir and baffle placement, (iii) effects of sludge collection mechanisms and inlet arrangements, (iv) absence of flocculating centre and stilling wells and (v) wind and temperature effects. Current design procedures, even those that recognize sludge settleability and reactor concentration, give very little guidance on the design of these SST internal features and it has been shown that some of this guidance is inappropriate (e.g. limiting the effluent weir loading rate, Ekama *et al.*, 1997). Design of these internal features has therefore been very subjective and their effectiveness has depended mainly on the design engineer's experience.

## 1.2 Design of fullscale SSTs

Currently the design of SSTs is usually done in two stages; in the first, zone settling and thickening considerations are applied which lead to the specification of a surface area, and in some procedures, also a depth. The SST design procedures (see Ekama *et al.*, 1997 for explanation and use) essentially give the designer the means to determine these two basic dimensions which define the external shell of the SST. With the proper incorporation of internal features for good clarification, zone settling and thickening criteria usually govern the specification of the area and depth of the SST. The specification of the depth should accommodate both sludge accumulation and thickening as well as maximizing the clarification efficiency. After specifying surface area and depth, the clarification efficiency of the tank is optimized by considering detail design of the internal features of the tank which significantly influence this. These features, such as (i) inlet arrangement, (ii) tank configuration, (iii) control of hydraulic flow patterns, short circuiting and turbulence with baffling, (iv) flocculation chambers and (v) sufficient sludge transport and collection capacity, can make the difference between achieving a low or high ESS concentration for the design SOR and depth. In future, with the advent of hydrodynamic SST models, design and optimization for settling, thickening, flocculation and clarification will be done concomitantly in an integrated fashion.

Hydrodynamic (or glass box) models for SSTs allow design and optimization of the SST's internal features such as geometry, side wall depth, baffling, inlet and sludge collection arrangements. A few such models of various complexity and sophistication have been developed for simulating circular and rectangular SSTs (see Krebs, 1995 or Chapter 5 in Ekama *et al.*, 1997 for a review of these models). Although application is limited at this stage, these models are being used successfully in research programmes and design for 2D and 3D simulation of fullscale SSTs. Improvements in the design and development of the internal features based on the simulation results have shown improvement on SST capacity with a reduction in ESS concentration. While the description of the hydrodynamics of the SSTs has progressed dramatically with the advent of 2D and 3D hydrodynamic models, description of the sludge settling behaviour in these models has not progressed very much beyond that in the 1D flux theory models and remains the major weakness in the models.

## 1.3 Application of the 1DFT to fullscale SSTs

Application of the idealized steady state 1D flux theory (1DFT) to full scale circular (and rectangular) SSTs indicate that the design procedures based on this theory over-predicts the permissible solids loading rate (SLR) by about 25 percent (Ekama *et al.*, 1997). However, there was no convincing evidence that this 25% correction needed to be applied for all types of SST, and therefore a crucial unanswered question was whether or not the observed SST failures on which the 25% reduction was based, were specific to the particular design of the tested SSTs. Since data was limited on tank types, confirmation of the applicability of the 1DFT for other tank types remained a research need. Indeed, from the available information, which included that

obtained in the American Society of Civil Engineers - Clarifier Research Technical Committee (ASCE-CRTC) study (see Wahlberg *et al.*, 1995), it could not be definitively established whether the clarification optimization techniques to reduce ESS by modifying the internal features of the SST with baffling, inlet and outlet arrangements and sludge collection improvements, extends the SLR capacity of the SST in terms of the 1DFT, or whether the clarification optimization maintains low ESS concentrations within a fixed SLR capacity. The inability to definitively establish the applicability of the 1DFT to circular and rectangular SSTs is a major weakness in SST technology and is a high priority research need which requires the development of;

- (1) a unified procedure for relating the 1DFT to the design of full scale SSTs,
- (2) a unified procedure for evaluating the effect of the internal design features such as depth, inlet and outlet arrangements, sludge transport and collection systems and baffling on effluent quality, both magnitude and variability,
- (3) hydrodynamic models to simulate the effect of internal feature design on effluent quality.

The recent development of hydrodynamic models for SSTs allow a measure of tank geometry and internal feature optimization. With these models it has become possible to calculate the SLR capacity of different SST designs and layouts and compare these with the 1DFT predictions. The above 3 aspects were investigated in this research project.

In the idealized 1DFT for SSTs, solids move only in a vertical direction. Because fullscale SSTs have a very high surface area to diameter ratio, which results in liquid and solids flow in vertical and horizontal directions, the applicability of the 1DFT to predict the maximum SOR and SLR of full scale SSTs remains uncertain. Ekama and Marais (1986) found that the SLR to cause solids overload was about 80% of that predicted by the 1DFT for 47 stress tests conducted on 25 full scale circular SSTs in Holland by STOWa (1981). The SSTs were 30 to 46m in diameter, had 1.5 to 2.5m side water depths (SWD) and a 1:12 sloping bottom with scraped sludge collection. An evaluation of 15 SLR stress tests conducted by Watts *et al* (1996) on a 3.66m SWD, 28.96m diameter circular SST with centre feed, peripheral and radial effluent overflow and rotating multiple suction pipe sludge collection system indicated that this tank could only achieve about 70% of the 1DFT maximum SOR (or ~80% of the SLR) (Ekama *et al.*, 1997). Göhle *et al.* (1996), assessing a 470 m<sup>3</sup> (46 m long x 10.2 m wide) 5.6 m SWD longitudinal flow rectangular SST fitted with a counter-current scraper sludge collection system and seven transverse effluent launders distributed over the length of the tank, found raised sludge blankets (>2 m) when the applied SLR exceeded 80% of that predicted by the 1DFT, a value similar to that found for the shallow circular Dutch SSTs by Ekama and Marais (1986). Such reductions compared with the 1DFT calculated limits are not unexpected because it is well known that the capacity of SSTs is affected by their internal features such as (i) inlet arrangement, (ii) tank configuration, (iii) control of hydraulic flow patterns, short circuiting and turbulence with baffling, (iv) flocculation chambers and (v) sufficient sludge transport and collection capacity.

The 1DFT design procedure gives no information regarding the optimal arrangements of the various internal features. Accepting that these features affect tank performance, it would be valuable to determine with the aid of 2D SST hydrodynamic models how the arrangement of these features influences the SLR (and SOR) capacity of the SST in relation to the maximum SLR and (SOR) calculated from the 1DFT. By this means, a *flux rating* is established, the magnitude of which gives the measure whereby the arrangements of the internal features within the external shell of the SST (area and depth) have been optimized. In this respect the flux rating of the Dutch, Watts and Göhle SSTs would be about 0.8 because the maximum SLR was found to be about 0.8 of the 1DFT maximum SLR. With deeper tanks and with carefully designed and placed baffles and inlet and outlet arrangements determined from optimization studies with the newly developed hydrodynamic models, the flux rating could possibly be increased closer to 1.0, which is the theoretical maximum. In this way the flux rating could become a means for optimizing the internal features designed into the shell of the SST obtained from the 1DFT design procedure. This conforms to the suggestion of Wahlberg *et al.* (1998) who state that “the results of a state point analysis” (i.e. a steady state idealized 1DFT design) “should be considered a theoretical limit, and hydrodynamic models give us the tools to develop better secondary clarifier designs that can operate closer to this limit” (Fig 1). The primary objective of this task of the research project is to determine the flux rating with a 2D computational fluid dynamic (CFD) hydrodynamic model of different stress tested fullscale SSTs that have been reported in the literature.

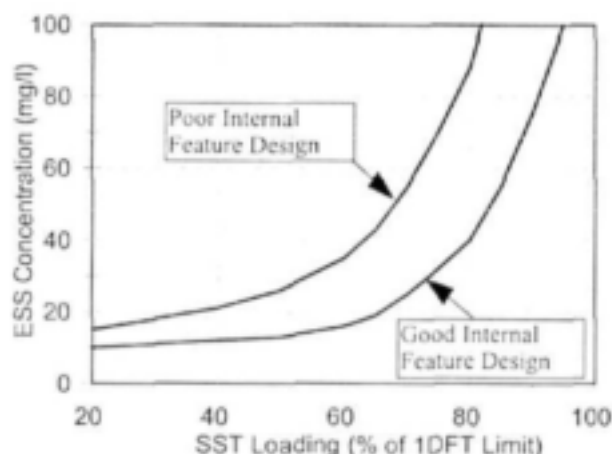


**Fig 1:** Hypothetical effluent suspended solids (ESS) concentration versus SST loading rate as a % of the 1DFT limit. With good internal feature design, the ESS remains low as the loading increases but with poor internal feature design the ESS increases more rapidly and from lower loading rates.

Non steady state 1D SST simulation models have been developed over the past 20 years and those of Ozinsky *et al.* (1994) and Watts *et al.* (1996) are recent examples of such models that incorporate many of the refinements and improvements developed over this time (Ekama *et al.*, 1997). In order for these 1D models to predict full-scale SST performance, a turbulent diffusion/dispersion coefficient is introduced into the partial differential equations describing the vertical motion of the solids in the SST. The effect of this coefficient is to introduce mixing between the elemental horizontal layers making up the water depth in the SST. The values of these coefficients have to be determined by calibration against full scale SST performance data.

This is not a simple matter because the values have been found to vary with depth, influent and recycle flow rate, tank geometry, baffling and other internal features of the tank. These coefficients therefore incorporate the effect of the internal features and hydrodynamics in a single lumped parameter. The values found are specific for the particular SSTs simulated and have the overall effect of reducing the flux rating, i.e. reduce the maximum SLR to lower values than calculated from the steady state 1DFT (Ozinsky et al., 1994; Watts et al, 1996).

Unlike in the non steady state 1D flux SST simulation models, in 2D hydrodynamic model SettlerCAD (Zhou *et al.*, 1998) there are no model “constants” that influence tank hydrodynamics that can be adjusted to improve the correlation between experimental and simulated results<sup>1</sup>. Therefore, the outcome of a stress test simulation (fail - raised sludge blanket and high ESS, or safe - stable sludge blanket and low ESS) can be compared with observed full scale SST performance without needing to do a major calibration exercise first. In this project the maximum SOR and SLR predicted by SettlerCAD is compared with that predicted by the 1DFT using as a basis the fullscale SST stress tests reported by de Haas *et al.* (1998), Watts *et al.* (1996) and STOWa (1981).

All the SST models mentioned above, i.e. the idealized steady state 1DFT, the dynamic non-steady state 1D models and the 2D hydrodynamic model SettlerCAD, have in common the specification of the sludge settleability. In all of them, this is in the conventional way of relating the solids vertical settling velocity with respect to the water due to gravity ( $V_s$ , m/h) to the local suspended solids concentration ( $X_t$ , kg/m<sup>3</sup>) with the empirical exponential equation, viz.

$$V_s = V_0 \exp(-nX_t) \quad \text{m/h} \quad (1)$$

This, in fact, forms the unified basis between the different models and allows them to be compared. It is only the hydraulic field in which solids settle that is modelled differently in the different models from the very simple to the very complex. In the steady state idealized 1DFT this is in the vertical direction only, in the dynamic non steady state 1D models, this is also in the vertical direction only but turbulent diffusion creates mixing in the SST to represent the non-idealities, and in the 2D hydrodynamic models such as SettlerCAD, this is modelled hydrodynamically in the more realistic vertical and horizontal directions.

## 2. OBJECTIVES

In this task, the 2D hydrodynamic model SettlerCAD (Zhou *et al.*, 1998) was applied to full scale circular SSTs with the principle aim to

---

<sup>1</sup>There are, of course, many model “constants” in 2D hydrodynamic models for SSTs which would significantly change the simulation results if changed (see Ekama *et al.*, 1997 for a review of 2D models). However, in SettlerCAD, except for those mentioned below, all the constants are in fact constant and cannot be changed by the user.



- (1) establish whether or not it “automatically” reproduces a flux rating  $< 1.0$  with respect to the 1DFT and
- (2) determine what factors influence the magnitude of this flux rating.

To do this, SST SLR stress tests reported in the literature were simulated. These were

- (1) the 4 tests done by de Haas *et al.* (1998) on 4 similar 35m diameter SSTs (2 new and 2 old) of the Darvill wastewater treatment plant (WWTP, Pietermaritzburg, South Africa)
- (2) the 15 tests done by Watts *et al.* (1996) on a single 3.66m SWD, 28.96m diameter circular SST with centre feed, peripheral and radial effluent overflow and rotating multiple suction pipe sludge collection system at the Kanapaha WWTP (Florida, USA), and
- (3) some of the 47 tests done by STOWa (1981) (Stopkoper and Trentelman, 1982) on 25 different SSTs with 30 to 46m diameter, 1.5 to 2.5m SWD and 1:12 sloping bottoms with scraped sludge collection.

### 3. SIMULATION OF SST PERFORMANCE WITH SettlerCAD

#### 3.1 SettlerCAD description and input information

The SettlerCAD model requires three groups of input viz., SST loading, SST geometry and sludge settleability.

- (1) The SST loading comprises the feed concentration ( $X_F$ ), recycle flow ( $Q_R$ ) and the influent flow to the WWTP ( $Q_I$ ) (i.e. excluding recycle flow). The recycle flow can be withdrawn uniformly over the tank bottom to simulate scraper sludge collection or by means of hydraulic suction by a specified number of siphons at specified radii from the centre, each with a specified proportion of the recycle flow. The influent and return sludge flows and feed concentration were constant throughout each simulation. The reactor concentration accepted for the simulation was the last value measured in the stress test, which could be up to about  $1 \text{ kgTSS/m}^3$  lower than the initial value due to sludge storage in the SSTs.
- (2) SST geometry requires specification of the side wall radius, side water depth (SWD) and bottom slope which together define the external shell of the SST. An inlet feedwell radius and depth and a feedwell skirt radius and depth, which together define the inlet arrangement also need to be specified. SettlerCAD makes provision for two types of baffle; a Crosby baffle, which is a small circular vertical wall on the bottom of the tank usually with a radius about half that of the tank to deflect the density current upwards into the tank to dissipate its energy, and a Stamford baffle, which is a horizontal plate

extending radially inwards immediately below the peripheral effluent launder to deflect the density induced current flowing upwards at the sidewall to the centre of the tank. The Crosby baffle height and radius from the centre of the SST and the Stamford baffle height above the bottom of the side wall are given as input; for SSTs without these baffles, zeros are given. Other internal features such as effluent launder placement and design cannot be modelled with SettlerCAD e.g., inboard (more than one average depth from the side wall) versus inset (close to sidewall) and single peripheral versus double sided inboard effluent launders. SettlerCAD models only single sided peripheral effluent launders.

- (3) The sludge settleability can be defined either in terms of the Specific Sludge Volume Index (SSVI) which is then internally converted to  $V_0$  and  $n$  values with the Wahlberg *et al.* (1988) relationships (see Ozinsky and Ekama, 1995 or Ekama *et al.*, 1997) or in terms of the Takács *et al.* (1991) double exponential equation. This equation is the usual exponential  $V_s - X_t$  equation (Eq 1 above) but includes an additional exponential term which seeks to take into account of the slow and non-settling discrete (pin-point floc) particles at low concentration ( $<100$  mg/l), viz.

$$V_s = V_0 [\exp\{-n(X_t - f_{ns}X_f)\} - \exp\{k_2(X_t - f_{ns}X_f)\}] \quad \text{m/h} \quad (2)$$

where  $X_f$  is the feed concentration from the biological reactor,  $f_{ns}$  the fraction of this solids concentration which does not settle at all ( $V_s=0$ ), and  $K_2$  an empirical constant which reduces  $V_s$  of the solids when the concentration  $X_t$  becomes low. In SettlerCAD, the fraction  $f_{ns}$  is fixed at zero so non-settling solids cannot be included. In the simulations, the  $K_2$  constant was set at a very high value (10) to eliminate the effect of second term on  $V_s$ . This reduced Eq 2 to be identical to Eq 1 so that the equation which defines the sludge settling velocity in the 1DFT (Eq 1) and in SettlerCAD are the same and dependent only on  $V_0$ ,  $n$  and  $X_t$ . This also eliminated the effect of the non- and slow settling solids on the ESS concentration predicted by SettlerCAD so that these would not confound the identification of SST failure from raised sludge blanket and ESS concentration predictions. The  $V_0$  and  $n$  values measured just prior to each of the SLR stress tests, or, where  $V_0$  and  $n$  were not measured, calculated from the measured DSVI or SSVI during the tests from the Ekama and Marais (1986) relationships (see Ekama *et al.*, 1997), served as input to define the sludge settleability.

SettlerCAD includes also a number of simulation parameters and those relevant in this research were the time step ( $\Delta t$ , min), total number of time steps ( $N_{TS}$ ) in the simulation and the total simulation time ( $T_{sim}$ ). The developers of SettlerCAD recommend a  $\Delta t$  between 1 and 3 min and this was adhered to. In an initial exploratory evaluation,  $N_{TS}$  was varied to examine (i)  $T_{sim}$  as a fraction of SST actual hydraulic retention time ( $R_{hyd}$ ) to obtain a sludge mass balance between 99 and 101% at the end of the simulation to ensure a final steady state had been achieved.

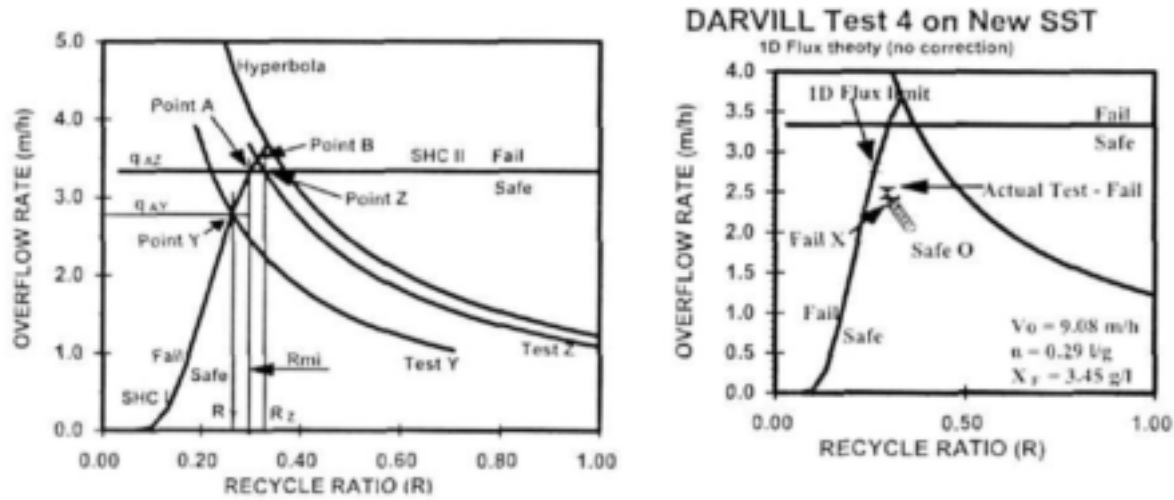
Generally  $T_{sim}$  had to be at least 15 times  $R_{ba}$ , but usually longer at 20 to 25 times  $R_{ba}$ . Simulation run times selected were generally  $>30$  times  $R_{ba}$  making them more than 10 times longer than the actual SLR stress test duration.

### 3.2 Finding the maximum SOR and SLR of SettlerCAD.

From the measured  $V_0$ ,  $n$  and feed concentration  $X_F$  values of a particular SLR test, the maximum SOR and minimum recycle ratio ( $R_{min}$ ) were calculated from the 1DFT. Details on how this calculation is done are given in Appendix A (see also Ekama *et al.*, 1997). The principles are shown in the 1DFT design & operating (D&O) chart (Fig 2a). The solids handling criterion (SHC) I and II lines and the hyperbola (which marks the boundary where the SHC I does and does not apply) are completely specified by the  $V_0$ ,  $n$  and  $X_F$  values. First the minimum recycle ratio ( $R_{min}$ ) for the maximum overflow rate ( $q_A = Q_1/A_{ST}$ , m/h) is determined (Point A) by setting the equations for SHC I and II equal and solving for  $R$  which is  $R_{min}$ . This  $R_{min}$  is used as a reference recycle ratio to check whether SHC I or SHC II governs the maximum capacity of the SST for the particular underflow rate ( $q_R = Q_R/A_{ST}$ , m/h) of the SLR test. For Test Y in Fig 2a, the locus of the SST operating point at constant underflow rate ( $q_R$ , m/h) and increasing SOR ( $q_A$ , m/h) cuts at SHC I line with an  $R$  value ( $R_Y$ )  $< R_{min}$  (at Point Y). This means that the SHC I fixes the maximum SOR and SLR of the SST for the fixed  $q_R$  and  $X_F$  of the particular test and the maximum SOR and SLR capacities in terms of the 1DFT are defined by Point Y, viz.  $SOR_{max} = q_{AY}$  m/h,  $SLR_{max} = (q_{AY} + q_{RY})X_F$  or  $q_{AY}(1 + R_Y)X_F$  kg/(m<sup>2</sup>h) and  $HLR_{max} = q_{AY}(1 + R_Y)$  or  $SLR_{max}/X_F$  m/h. For Test Z in Fig 2a, the locus of the SST operating point at constant  $q_R$  and increasing SOR ( $q_A$ ) cuts the SHC I line with an  $R$  value ( $R_Z$ )  $> R_{min}$  (at Point B). This means that the SHC II fixes the maximum SOR and SLR of the SST for the fixed  $q_R$  and  $X_F$  of the particular test and the maximum SOR and SLR capacities in terms of the 1DFT are defined by Point Z, viz.  $SOR_{max} = q_{AZ}$  m/h,  $SLR_{max} = (q_{AZ} + q_{RZ})X_F$  or  $q_{AZ}(1 + R_Z)X_F$  kg/(m<sup>2</sup>h) and  $HLR_{max} = q_{AZ}(1 + R_Z)$  or  $SLR_{max}/X_F$  m/h.

The input data listed above for a particular SST stress test to be simulated, was given as input to SettlerCAD. Keeping the recycle flow ( $Q_R$ ) and feed concentration ( $X_F$ ) constant at the test values, the influent flow ( $Q_1$ ), calculated as a % of the 1DFT limit value, was increased for successive simulation runs from a low value to a high value, first in 2% of 1DFT limit increments, and then in 0.25% of 1DFT limit increments between consecutive safe and fail runs. SST failure was accepted to be an average ESS  $> 50$  mg/l over the final 2 actual retention times ( $R_{ba}$ ) of the run. In this way the steady state influent flow rate ( $Q_1$ ) for ESS  $> 50$  mg/l was determined for SettlerCAD at an accuracy of 0.25% of the 1DFT limit and the first run with ESS  $> 50$  mg/l was accepted as the SettlerCAD predicted maximum influent flow rate limit. The SettlerCAD SOR, SLR and HLR limits were calculated from the predicted influent flow limit and the test  $Q_R$  and  $X_F$  values. Increasing  $Q_1$  ( $q_A$ ) for fixed  $Q_R$  ( $q_R$ ) moves the operating point in the steady state 1DFT D&O chart along the  $q_R$  line towards the SHC I or SHC II lines. Figure 2b shows the operating points for the SettlerCAD runs for Test 4 on the new Darvill SSTs (see

Section 4.2 below for details). The predicted ESS and RAS concentrations over the complete run were imported into a spreadsheet program, in which were calculated (i) the average ESS and RAS concentrations over the final 2 actual hydraulic retention times ( $2 \times R_{ha}$ ) and (ii) the % solids mass balance as the run proceeded. The outcome (fail or safe) of each simulation run was recorded by checking sludge blanket height in SettlerCAD at the end of each simulation and whether the average ESS concentration over the final  $2 \times R_{ha}$  was greater (fail) or less (safe) than 50 mg/l. The % mass balance at a particular time interval was calculated as the sum of the masses of sludge in the return and effluent flows as a % of the mass of sludge entering the SST with the influent and recycle flows.



**Figs 2a and 2b:** Design and operating (D&O) charts demonstrating the calculation method of the 1DFT (Fig 2a, left) and SettlerCAD (Fig 2b, right) SOR and SLR limit values. Figure 2b is for Test 4 on the new Darvill SSTs and the safe, fail and actual test positions are marked O, X and Z respectively.

With the 1DFT, the design of SST surface area ( $A_{ST}$ ) hinges round identifying Point A (in Fig 2a) for the specified  $X_f$  and  $V_0$  &  $n$ , where Point A is the SST operating position for the Peak Wet Weather Flow (PWWF,  $Q_{LPWWF}$ ). It gives the maximum overflow rate ( $q_{Amax}$ ) for the minimum recycle ratio ( $R_{min}$ ). From Point A, the design SST surface area  $A_{ST}$  is given by  $A_{ST} = Q_{LPWWF} / q_{Amax}$  and the recycle flow ( $Q_{RLPWWF}$ ) by  $Q_{RLPWWF} = R_{min} q_{Amax}$ . The maximum SLR and HLR associated with the design Point A are  $SLR_{max} = q_{Amax} (1 + R_{min}) X_f$  kg/(m<sup>2</sup>h) and  $HLR_{max} = q_{Amax} (1 + R_{min})$  or  $SLR_{max} / X_f$  m/h (see Appendix A for details).

Generally, from the 1DFT, the better the sludge settles i.e. the higher the  $V_0$  and the lower the  $n$ , and the lower the  $X_f$ , the higher the  $SOR_{max}$ ,  $SLR_{max}$  and  $HLR_{max}$ . The factor  $V_0 / (n X_f)$  (m/h), called the *flux load factor*, therefore is a relative measure for the  $HLR_{max}$ . The higher the  $V_0 / (n X_f)$ , the higher the  $HLR_{max}$ . So the better the sludge settles and the lower the  $X_f$ , the higher the flux load factor and the higher the  $HLR_{max}$ . The relationship between the  $HLR_{max}$  and flux load factor for the design Point A in Fig 2a for varying sludge settleability and  $X_f$  is shown in Fig 3. For Fig 3, the sludge settleability was varied from a SSVI of 40 to 160 ml/g and  $X_f$  from

2.5 to 4.5 g/l. The  $V_0$  &  $n$  values were calculated using the relationships of Ekama and Marais (1986) (see Ozinsky and Ekama, 1995). The range in  $V_0$  and  $n$  was from 10.74 to 3.18 m/h and 0.30 to 0.61 l/g respectively. The flux load factor varied from 1.15 to 14.28 m/h. It can be seen in Fig 3 that the higher the flux load factor, the higher the  $SOR_{max}$  and  $HLR_{max}$  and that the increase is quite consistent<sup>2</sup> with the flux load factor. This indicates that different  $V_0$ ,  $n$  and  $X_F$  making up the same flux load factor value, lead to approximately the same  $SOR_{max}$  and  $HLR_{max}$ . Because it is expected that the magnitude of the HLR affects the degree of the non-idealities (i.e. hydraulic disturbance), the flux rating (i.e. the % of the 1DFT maximum SLR that can be applied to full-scale SSTs) determined by SettlerCAD is expected to decrease with increasing flux load factor  $V_0/(nX_F)$ . Because the increase in  $SOR_{max}$  and  $HLR_{max}$  is consistent with increase in flux load factor, this consistency is not apparent for the  $SLR_{max}$ .

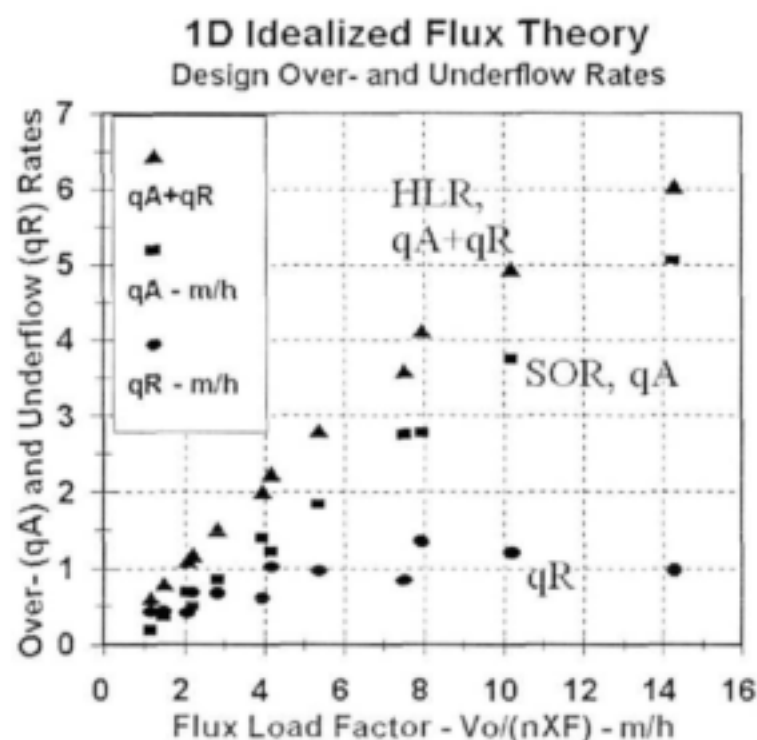


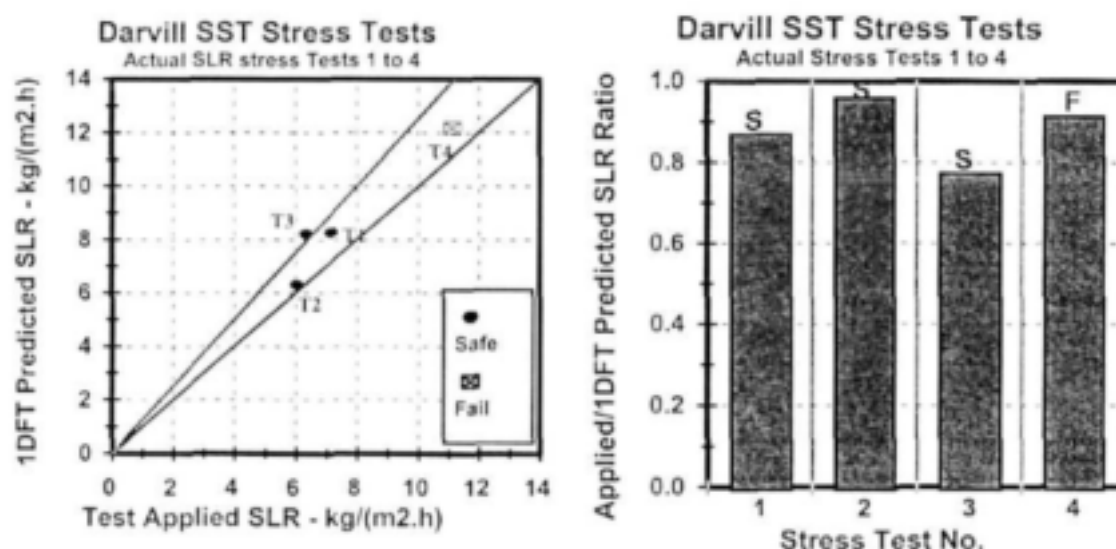
*Fig 3: Design overflow ( $SOR, q_A$  m/h) and underflow ( $q_R$  m/h) and hydraulic loading ( $HLR, q_A + q_R$  m/h) rates versus the flux load factor [ $V_0/(nX_F)$ , m/h] calculated from the 1DFT for the design Point A in Fig 1 for SSVI 40 to 160 mg (yielding  $V_0$  from 10.34 to 3.18 and  $n$  from 0.31 to 0.61), and  $X_F$  from 2.5 to 4.5 g/l. Note that an increase in the flux load factor leads to a consistent increase in  $SOR$  and  $HLR$ .*

<sup>2</sup>This appears true for  $V_0$  &  $n$  calculated from the SSVI relationship of Ekama and Marais (1986). It may not be as consistent for measured  $V_0$  &  $n$  values or other SSVI and  $V_0$  &  $n$  relationships that do not conform to the Ekama and Marais (1986) relationship.

## 4 SIMULATING THE DARVILL SSTs WITH SettlerCAD

### 4.1 The Darvill WWTP SST SLR stress tests.

The Darvill WWTP has five 35m diameter circular SSTs, 2 old and 3 new. Details of these SSTs are given in Table 1. The design capacity of the SSTs is  $7.5 \text{ kgSS}/(\text{m}^2\text{h})$  at a DSVI of around  $80 \text{ ml/g}$ , MLSS concentration of  $3.8 \text{ g/l}$ , a PWWF of  $162 \text{ Ml/d}$  and a recycle ratio of  $0.406$  viz.  $(162000/24) \times (1+0.406) \times 3.8 / (5 \times 962) = 7.5 \text{ kgSS}/(\text{m}^2\text{h})$ . Altogether four SLR stress tests were conducted on these SSTs, the first three (Tests 1 to 3) with four SSTs in operation (2 old and 2 new) and the fourth (Test 4) with two SSTs (1 old and 1 new) in operation. The tests were conducted by setting the sludge recycle (RAS) and influent (to WWTP) flows at rates that would cause critical loading conditions on the SSTs, i.e. at around 80% of the maximum SLR estimated from the 1DFT from the  $V_0$  and  $n$  values measured just prior to the stress tests. However, during the stress tests, the reactor concentration declined significantly below the normal operation value due to sludge storage in the SSTs. This reduced the applied SLR during the tests and so also the applied/test SLR ratio below the target 80% of the 1DFT maximum. The influent flow was kept constant and pumped from a diurnal flow balancing tank. The RAS and influent flows were controlled with computer controlled variable speed pumps (de Haas *et al.*, 1998) and the new and old SSTs were equally loaded. During the tests, which each lasted about 5 to 10h depending on the SOR and SLR, the reactor and underflow concentrations, the influent and RAS flow rates, the sludge blanket height and the ESS concentration were measured at about 1h intervals. A summary of the four tests is given in Tables 2 and 3.



**Figs 4a and 4b:** Calculated 1DFT maximum SLR versus test applied SLR (Fig 4a, left) and test applied to 1DFT calculated maximum SLR ratios (Fig 4b, right) for the four Darvill SLR stress tests on the new and old SSTs.

From the measured  $V_0$  and  $n$  values and the feed concentration ( $X_f$ ), the 1DFT predicted maximum SOR and SLR were calculated with the method described above and are listed in



Table 2. The 1DFT maximum and test applied SLRs and the test/1DFT maximum SLRs ratio from Table 2 are plotted in Figs 4a and b. From Fig 4b, the test/1DFT maximum SLR ratio for the four tests are 87, 96, 77 and 91% respectively. Of the four tests, only Test 4 on both the new and old SSTs ended in failure. From Table 2 it would therefore appear that the flux rating of the new and old SSTs are similar and somewhere between 77% (Test 3 - safe) and 91% (Test 4 - Fail).

**Table 1: Description of Darvill old and new SSTs.**

Parameter	Old SSTs (3 of) (Tanks A & E)	New SSTs (2 of) (Tanks B & C)
Diameter (m)	35	35
Side Water Depth (m)	2.5 ( $H_{we} = 2.50\text{m}$ )	4.1 ( $H_{we} = 4.68\text{m}$ )
Floor	Flat	Sloped (1:10)
Sludge Collection	Suction lift with manually controlled valves (six per SST)	Scraped to central hopper
Recycle pumps and control	4 centrifugal of 11 Mt/d each Level control in sump into which suction lift siphons discharge	2 variable speed drive pumps of 19 Mt/d each computer controlled to a selected set point.
Effluent launders	Single-sided peripheral	Single-sided peripheral
Inlet feed arrangement	1.0 m diam. centre feed well	1.0 m diam. centre feed well
Baffling	1. No scum board. 2. 6.0 m diameter skirt baffle acting as flocculator centre well to 1.8m water depth. Gap to floor 0.70m 3. Peripheral Stamford baffle extending 1.2 m from side wall	No scum board. 6.0m diameter skirt baffle acting as flocculator centre well to 2.7m water depth. Gap to floor 2.80m Peripheral Stamford baffle extending 1.7 m from side wall

**Table 2: Summary of the four SLR stress test results on the Darvill WWTP SSTs.**

Parameter		Test 1	Test 2	Test 3	Test 4
SST	Number of SSTs	4	4	4	2
	Surface area ( $A_{ST}$ m <sup>2</sup> )	4x 962	4x 962	4x 962	2x 962
Actual test loading conditions	Influent flow ( $Q_i$ Mt/d)	80	66	91	115
	Overflow rate ( $q_A$ SOR m/h)	0.866	0.715	0.985	2.49
	Recycle flow ( $Q_R$ Mt/d)	64	64	72	34
	Underflow rate ( $q_R$ m/h)	0.693	0.693	0.780	0.736
	Recycle ratio (R)	0.800	0.970	0.791	0.296
	Feed Concentration ( $X_F$ g/l)	4.60	4.30	3.60	3.45
	Applied flux [SLR kgSS/(m <sup>2</sup> .h)]	7.17	6.05	6.35	11.13
	Weir loading rate [WLR, m <sup>3</sup> /(h.m)]	7.57	6.25	8.62	21.78
	Hydraulic loading rate [ $q_A + q_R$ HLR m/h)]	1.56	1.41	1.76	3.27
Sludge settleability	$V_0$ (m/h)	7.71	7.83	8.00	9.08
	$n$ (l/g)	0.390	0.513	0.430	0.29
	DSVI (ml/g)	78	104	62	49
1DFT predicted limits	Maximum SLR <sub>max</sub> [kg/(m <sup>2</sup> .h)]	8.26	6.31	8.22	12.19
	Overflow rate SOR <sub>max</sub> (m/h)	1.104	0.775	1.503	2.796
	Influent flow (excl $Q_R$ ): 1 SST (m <sup>3</sup> /h)	1062	746	1446	2690
Flux ratings	Flux load factor [ $V_0/(nX_F)$ , m/h)]	4.30	3.55	5.17	9.08
	Test/1DFT SLR ratio	0.87	0.96	0.77	0.91
	Test/1DFT SOR ratio	0.79	0.92	0.66	0.89

**Table 3: Darvill WWTP SST SLR stress test results.**

Test No	Test 1		Test 2		Test 3		Test 4	
	New	Old	New	Old	New	Old	New	Old
SST type								
Feed concentration ( $X_f$ gSS/l)	4.60	4.60	4.30	4.30	3.60	3.60	3.45	3.45
Recycle concentration ( $X_R$ gSS/l)	10.0	9.5	9.0	9.0	9.0	8.0	15.0	16.0
Sludge blanket depth <sup>1</sup> (m)	2.2	1.0	2.6	1.4	2.7	1.6	1.6 <sup>1</sup>	0.3
Effluent SS (mg/l)	17	6	5	4	10	16	30	252
Actual hydraulic retention time ( $R_{hy}$ , h)	3.0	1.6	3.3	1.8	2.7	1.4	1.5	0.8
Test duration (hours)	10.5	10.5	12.0	12.0	10.0	10.0	5.0	5.0
Test duration (number of $R_{hy}$ )	3.5	6.6	3.6	6.7	3.7	7.1	3.3	6.3
Test outcome Fail/Safe <sup>2</sup>	Safe	Safe	Safe	Safe	Safe	Safe	Fail	Fail

<sup>1</sup> Sludge blanket depth is the depth of the top of the sludge blanket from the water surface.

<sup>2</sup> SST failure interpreted as raised sludge blanket to the water surface and gross solids loss.

<sup>3</sup> Test 4 had to be terminated when the old SST failed. Although the ESS concentration was still very low, the sludge blanket rise rate in the new SST was the same as in the old SST and therefore failure of the new SST seemed inevitable. The height of the sludge blanket was similar in the old and new SSTs. The onset of failure in the new SST was postponed due to its greater sludge storage capacity afforded by its greater depth (4.1 m SWD) compared with the old SST (2.5 m SWD).

**Table 4: Summary of the SettlerCAD simulations results for the SettlerCAD influent flow limit of Tests 1 to 4 on the new and old Darvill SSTs.**

PARAMETER	Test 1		Test 2		Test 3		Test 4	
	New	Old	New	Old	New	Old	New	Old
QI = Influent flow rate (m <sup>3</sup> /h)								
Flux load factor $V_d/(nX_f)$ - m/h	4.30	4.30	3.55	3.55	5.17	5.17	9.08	9.08
Influent Flow (m <sup>3</sup> /h) for 1 SST	820	759	556	548	1211	1038	2272	1702
% of 1DFT maximum $Q_I$	77.25	71.50	74.50	73.50	83.75	71.75	84.50	63.25
Overflow Rate (m/h)	0.87	0.84	0.69	0.73	1.23	1.21	1.88	1.88
Recycle Flow (m <sup>3</sup> /h)	667	666	667	667	750	750	708	708
Underflow Rate (m/h)	0.693	0.693	0.693	0.693	0.779	0.779	0.736	0.736
Recycle Ratio	0.80	0.82	1.00	0.95	0.64	0.64	0.39	0.39
Applied SLR (kgSS)/(m <sup>2</sup> .h)	7.17	7.05	5.96	6.11	7.22	7.17	9.02	9.02
% of 1DFT maximum SLR	86.0	82.5	86.5	86.0	89.3	81.4	87.7	70.9
Actual Retention Time (h)	3.0	1.6	3.4	1.8	2.3	1.3	1.8	1.0
Duration of Run (min)	6000	3600	6000	3600	6000	3600	3600	1800
Duration of Run (# of $R_{hy}$ )	33.0	35.6	27.1	30.3	43.5	44.6	39.7	30.1
Sim time Step (min)	2.5	2.5	2.5	2.5	2.5	2.5	1.25	1.25
Sim time Step (% $R_{hy}$ )	1.37	2.47	1.13	2.10	1.81	3.10	1.38	2.09
Effluent SS (mg/l)*	279	51	80	54	338	68	452	56
Recycle Conc (mg/l)*	9792	9728	7618	7718	8487	8349	13056	11560
Mass Balance (%)	98.8	99.5	97.5	99.0	95.9	98.4	99.9	99.6
Test Result (ESS>50mg/l)	Fail	Fail	Fail	Fail	Fail	Fail	Fail	Fail

\*Mean over the last 2  $R_{hy}$  values.

#### 4.2 Finding the SettlerCAD maximum SOR and SLR for the Darvill SSTs

The data listed in Tables 2 and 3, recalculated for a single SST, was given as input to SettlerCAD. For each test, 16 SettlerCAD runs were setup. For the new SST, runs 1 to 7 were at  $Q_I$  from 74 to 86% of the 1DFT limit in 2% increments and an 8<sup>th</sup> run at 100%. For the old SSTs, the 7 runs ranged from 60 to 72% with an 8<sup>th</sup> at 100%. Runs 9 to 15 were setup between consecutive safe and fail runs at 0.25% increments and the 16<sup>th</sup> run was at the actual test  $Q_I$ . The first run with ESS > 50 mg/l was accepted as the SettlerCAD predicted maximum influent flow

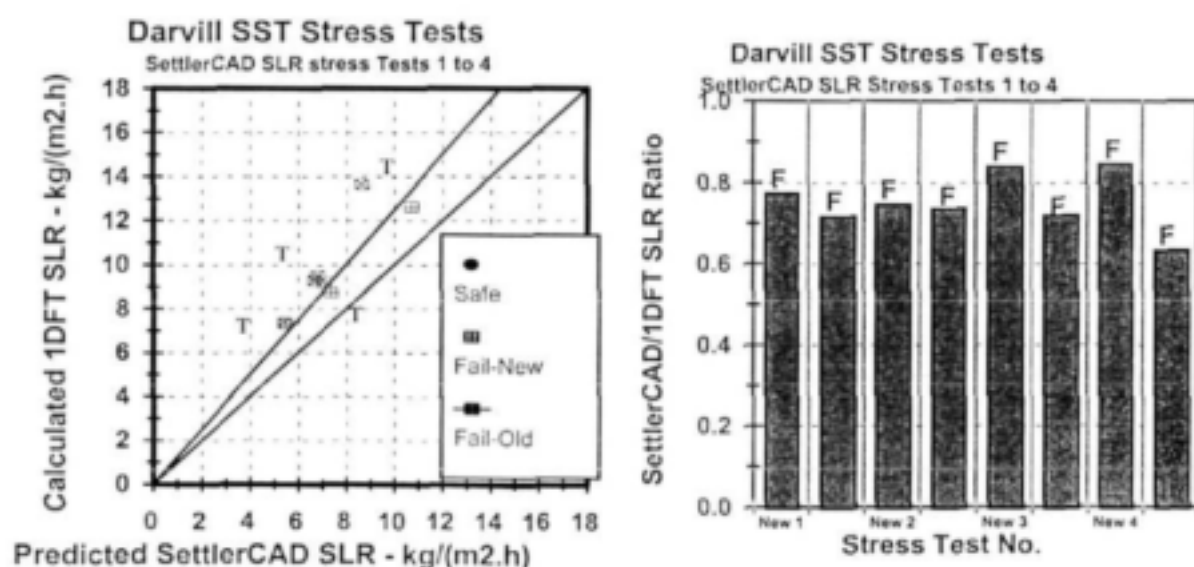


rate limit. The SettlerCAD SLR limit was calculated from the  $Q_L$  limit and the test  $Q_R$  and  $X_F$  values. The SettlerCAD predicted results of the first failure runs are given in Table 4 and are shown plotted in Figs 5a and b as 1DFT versus SettlerCAD predicted maximum SLR (Fig 5a) and SettlerCAD/1DFT maximum SLR ratio, or flux rating (Fig 5b). In Figs 5a and b it can be seen that the SettlerCAD predicted flux rating for the new SSTs ranges from 0.86 (Test 1) to 0.89 (Test 3) and for the old SSTs from 0.71 (Test 4) to 0.86 (Test 2). The simulation results of the runs at the actual test influent flow are given in Table 5.

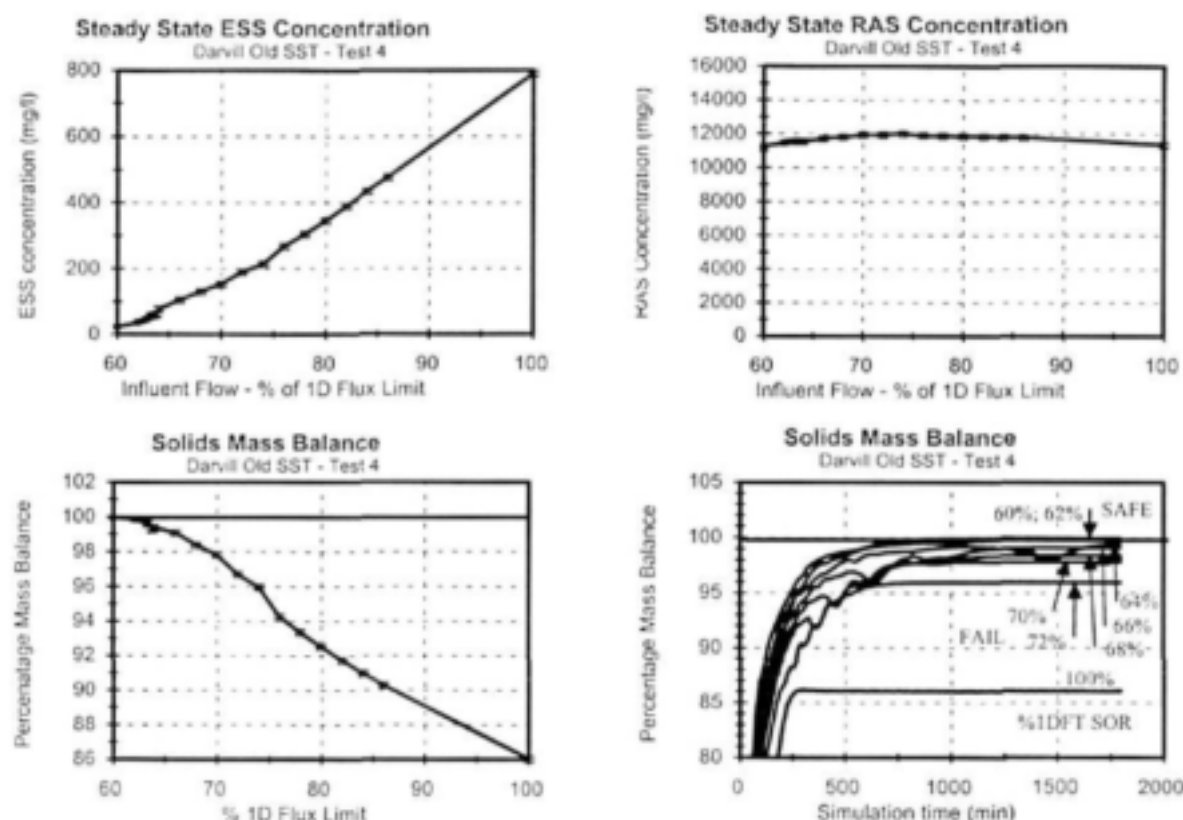
**Table 5: Summary of the SettlerCAD simulations results for the actual Tests 1 to 4 on the new and old Darvill SSTs.**

PARAMETER QI = Influent flow rate (m <sup>3</sup> /h)	Test 1		Test 2		Test 3		Test 4	
	New	Old	New	Old	New	Old	New	Old
Flux load factor $V_o/(nX_F)$ - m/h	4.30	4.30	3.55	3.55	5.17	5.17	9.08	9.08
Influent Flow (m <sup>3</sup> /h) for 1 SST	833	833	688	6888	948	948	2396	2396
% of 1DFT maximum $Q_L$	78.5	78.5	92.1	92.1	65.6	65.6	89.1	69.1
Overflow Rate (m/h)	0.87	0.87	0.71	0.71	0.99	0.99	2.49	2.49
Recycle Flow (m <sup>3</sup> /h)	667	666	667	667	750	750	708	708
Underflow Rate (m/h)	0.693	0.693	0.693	0.693	0.779	0.779	0.736	0.736
Recycle Ratio	0.80	0.80	0.97	0.97	0.79	0.79	0.296	0.296
Applied SLR (kgSS)/(m <sup>2</sup> .h)	7.17	7.17	6.05	6.05	6.36	6.35	11.13	11.13
% of 1DFT maximum SLR	86.8	86.8	95.9	95.9	77.3	77.3	91.3	91.3
Actual Retention Time (h)	3.0	1.6	3.3	1.8	2.7	1.4	1.5	0.8
Duration of Run (min)	6000	3600	6000	3600	6000	3600	3600	1800
Duration of Run (# of $R_{s2}$ )	33.3	37.4	30.0	33.8	37.7	42.3	41.3	38.7
Sim time Step (min)	2.5	2.5	2.5	2.5	2.5	2.5	1.25	1.25
Sim time Step (% $R_{s2}$ )	1.39	2.60	1.25	2.35	1.57	2.94	1.44	2.69
Effluent SS (mg/l)*	495	227	933	348	2.1	13.5	647	541
Recycle Conc (mg/l)*	9558	9666	7517	7745	8148	8119	12863	11751
Mass Balance (%)	98.3	96.1	97.1	92.8	100.0	99.8	99.6	89.8
Test Result (ESS>50mg/l)	Fail	Fail	Fail	Fail	Safe	Safe	Fail	Fail
Observed Result	Safe	Safe	Safe	Safe	Safe	Safe	Fail	Fail

\*Mean over the last 2  $R_{s2}$  values.



**Figs 5a and 5b: 1DFT calculated maximum SLR versus SettlerCAD predicted SLR (Fig 5a, left) and SettlerCAD predicted to 1DFT calculated maximum SLR ratios (Fig 5b, right) for the four Darvill SLR stress tests on the new and old SSTs.**

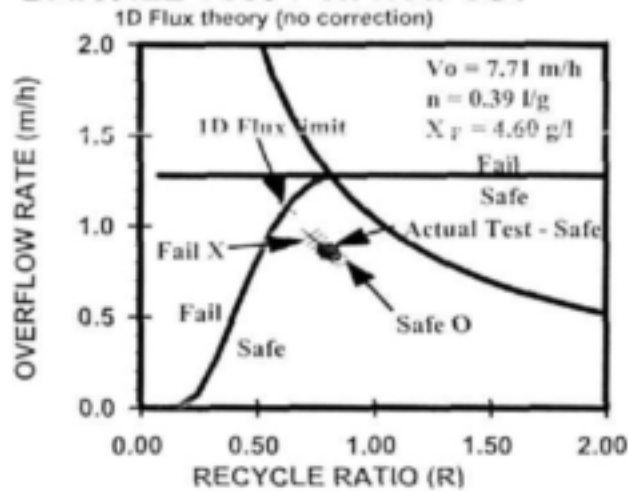


**Figs 6a to d:** Final ESS and RAS concentrations (Figs 6a, top left and Fig 6b, top right) and % mass balance (Fig 6c, bottom left) versus influent flow as % 1DFT limit showing runs ended safe (●) and fail (♠) and % mass balance versus simulation time (Fig 6d, bottom right) for the Test 4 SettlerCAD runs on the old Darvill SSTs.

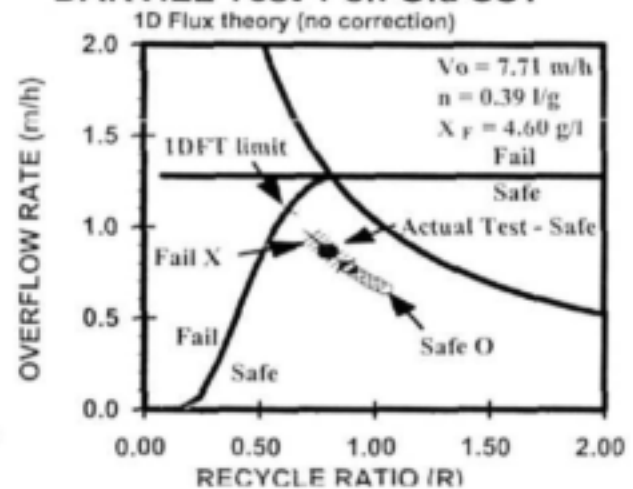
In the simulation runs, simulation times of 6000 and 3600 min were selected for the new and old SSTs respectively, which is more than 25x the actual hydraulic retention time ( $25 \times R_{\text{hyd}}$ ) for all the runs (see Table 4). These run times were sufficiently long to establish a final steady state condition. The final ESS ( $X_E$ ) and RAS ( $X_R$ ) concentrations accepted for each run were the average of the predicted values over the last  $2 \times R_{\text{hyd}}$ . The solids mass balance was based on these final average  $X_E$  and  $X_R$  concentrations (which are listed in Table 4). Provided the run did not in the failure ( $\text{ESS} < 50 \text{ mg/l}$ ) the run yielded a solids mass balance within 0.5% of 100%. Runs that ended in failure ( $\text{ESS} > 50 \text{ mg/l}$ ) yielded a lower than 99.5% solids mass balance and the greater the SST overload (i.e. the higher the ESS concentration), the lower the solids mass balance below 99.5%, even as low as 86% for Test 4 on the old SST at 100% of the 1DFT limit influent flow. The ESS, RAS and % mass balance versus influent flow (as % of the 1DFT limit  $Q_1$ ) for Test 4 on the new SST are given in Figs 6a to c. Halving the simulation time step and/or doubling the number of pressure iterations per time step yielded identical step by step simulation results and no improvement in % mass balance. From this it was accepted that the low % mass balance for the failed runs was not due to numerical instability in the algorithms of the programme. Figure 6d shows the % mass balance for the 8 runs at 60 to 72% and 100% 1DFT  $Q_1$  for Test 4 on the old SST as the simulation progressed and shows that the mass balance remains constant (indicating that ESS and RAS concentration did not change) at significantly

below 99.5%. It is suspected that there is a simple logical error in SettlerCAD. It seems that the RAS concentration is "corrected" by subtracting from it the ESS concentration, because the higher the ESS concentration (or overload), the lower the RAS concentration (Figs 6a and b). Theoretically, for increasing  $Q_i$  and constant  $Q_R$  and  $X_F$ , the RAS concentration should remain constant once the SLR capacity (failure) has been reached. This error does not influence the safe runs (because ESS concentration is low) and so does not influence the SettlerCAD predicted SOR and SLR limits.

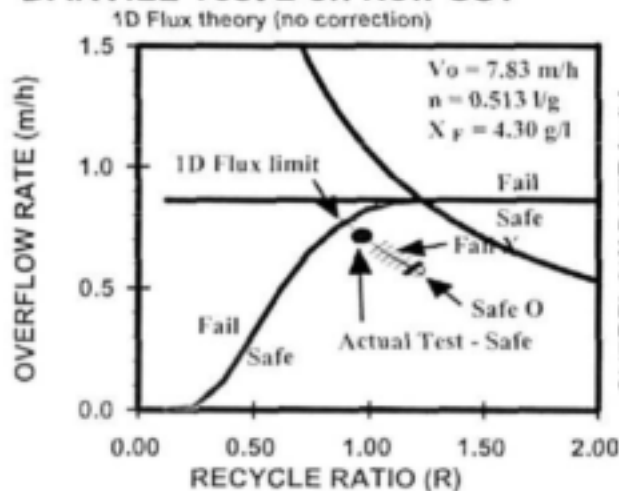
### DARVILL Test 1 on New SST



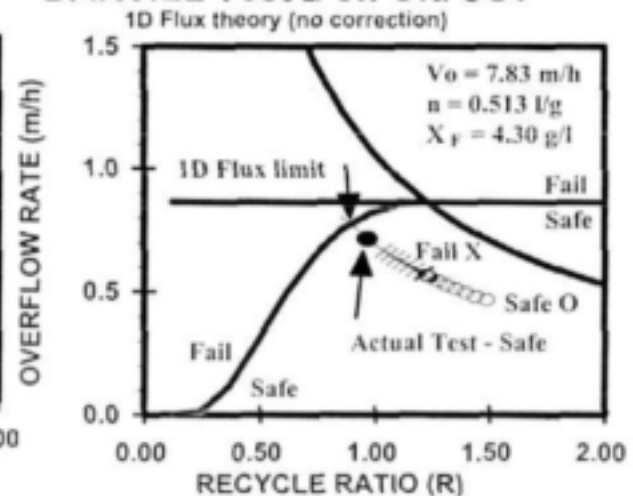
### DARVILL Test 1 on Old SST



### DARVILL Test 2 on New SST



### DARVILL Test 2 on Old SST

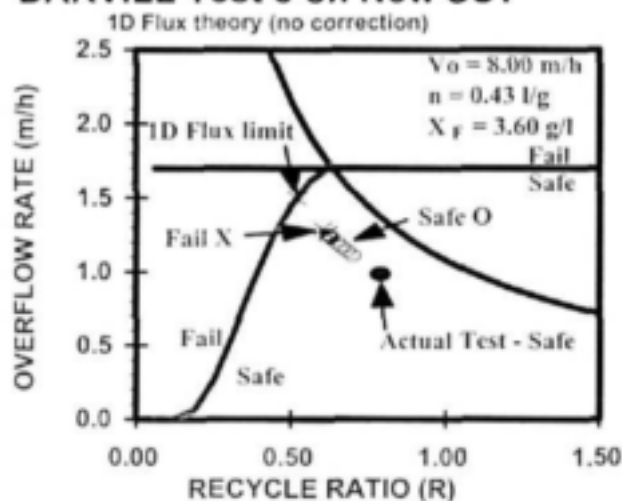


**Figs 7 a to d:** 1DFT D&O charts showing the SST operating position and result (safe O, fail X) of the SettlerCAD runs and actual tests (safe ●, fail X) for Tests 1 and 2 on the Darvill new and old SSTs.

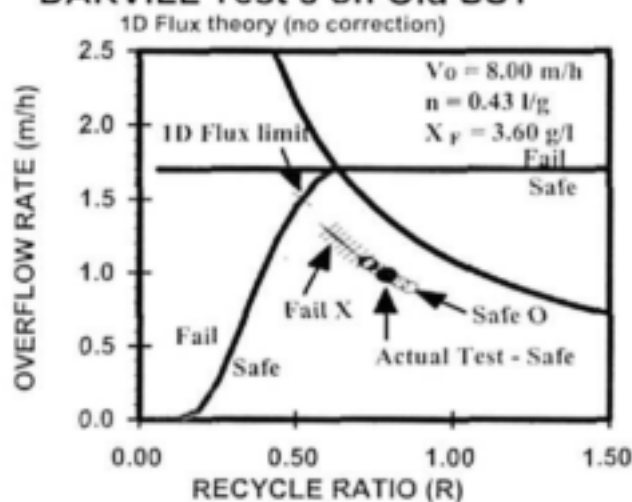
The position and result (safe O, fail X) of the SettlerCAD simulation runs for each of the 4 tests on the new and old SSTs are shown in the 1DFT D&O chart in Figs 7a to h. The actual test position (safe ●, fail X) and result also is indicated. In the charts, the SettlerCAD predicted SOR limit is given at the transition from the safe to the fail positions. If the actual test position safe

(●) is within the safe (O) runs, then SettlerCAD predicted a safe result for the actual test and if the actual test position fail (X) is within the fail (X) runs, then SettlerCAD predicted a fail result for the actual test. From this it can be seen that SettlerCAD predicted a fail result for Tests 1, 2 and 4 for both the new and old SSTs and a safe result for Test 3 on both new and old SSTs. Because the observed test results were safe for Tests 1, 2 and 3 and fail for Test 4, SettlerCAD predicted the result of Test 3 and 4 correctly i.e. safe and fail respectively, but predicted the result of Tests 1 and 2 incorrectly, i.e. fail for both when the observed result was safe for both. This aspect is discussed further below.

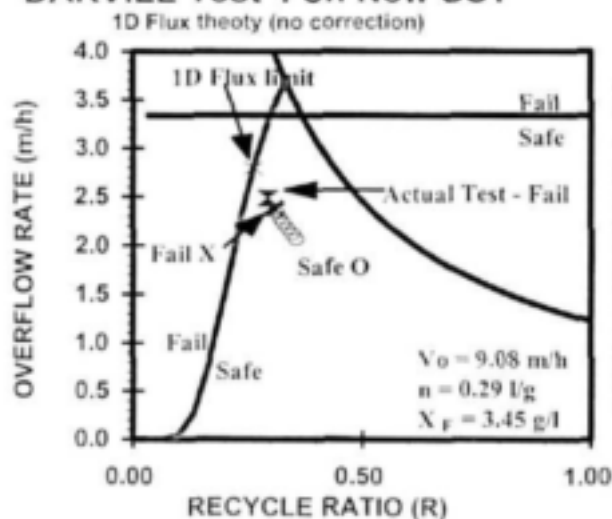
**DARVILL Test 3 on New SST**



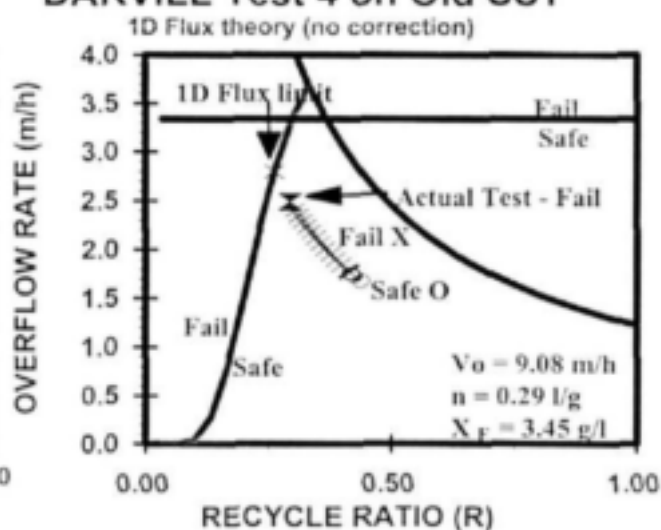
**DARVILL Test 3 on Old SST**



**DARVILL Test 4 on New SST**

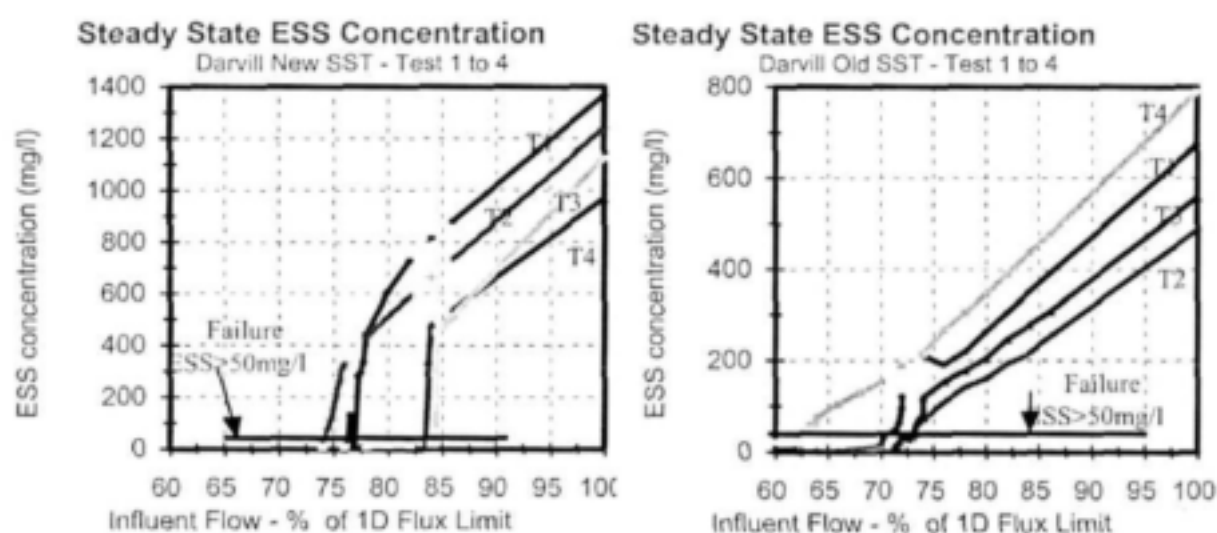


**DARVILL Test 4 on Old SST**



*Figs 7 e to h: 1DFT D&O charts showing the SST operating position and result (safe O, fail X) of the SettlerCAD runs and actual tests (safe ●, fail X) for Tests 3 and 4 on the Darvill new and old SSTs.*

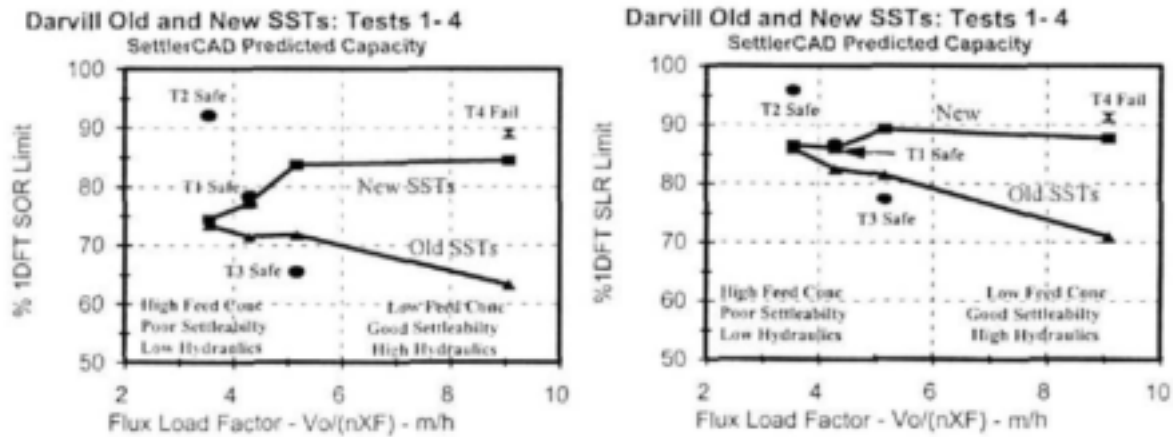
The ESS concentration versus  $Q_i$  (as a % of the 1DFT limit) for all the runs on the new and old SSTs are shown in Figs 8a and 8b. For the new SST (4.1m SWD) (Fig 8a), the ESS concentration increases precipitously above 50 mg/l at about 75% of the 1DFT limit influent flow for Tests 1 and 2 and about 84% for Tests 3 and 4. For the old SST (2.5m SWD) (Fig 8b), the increase in ESS concentration is much more gradual and increases above 50 mg/l at about 70% for Test 1, 72% for Tests 2 and 3 and 63% for Test 4. This reduced capacity and gradual increase in ESS concentration of the old SST is probably due to its shallowness (2.5m SWD) compared with the new SST (4.1m SWD). However, it is possible that the sludge collection system type also influenced this difference in behaviour - the 1:10 sloping bottom of the new SSTs adds considerable extra volume i.e.  $H_{ave} = 4.68\text{m}$ , compared with the flat bottom shallow old SSTs.



**Figs 8a and 8b:** SettlerCAD predicted ESS concentration versus influent flow (as % of 1DFT limit) for Tests 1 to 4 on the Darvill new (Fig 3a, left) and old (Fig 3b, right) SSTs.

SettlerCAD predicted maximum SOR and SLR, as a % of the 1DFT limits, were plotted versus the flux load factor for the new and old SSTs in Figs 9a and 9b. Also shown are the four actual test points. These figures show clearly the much greater sensitivity of the shallow old SSTs to the hydraulic flows compared with the new SSTs. As the 1DFT maximum SOR increases from the lowest value of Test 2 (0.78 m/h), through Test 1 (1.10 m/h) and Test 3 (1.50 m/h) to the highest value of Test 4 (2.80 m/h) (see Table 2), the SettlerCAD predicted capacity of the shallow old SST declines from 73% to 63% of the 1DFT SOR limit (or 85% to 70% of the 1DFT SLR limit). For the deeper new SSTs, the SettlerCAD predicted capacity increases from 73% to 83% of the 1DFT SOR limit (or 86% to 89% of the 1DFT SLR limit).

This indicates that for the shallow old SSTs, the lower the HLR, i.e. for poor settling sludges and/or and high  $X_r$ , the greater the SST capacity as a % of the 1DFT limit or flux rating, and the higher the HLR, i.e. good settling sludges and/or low  $X_r$ , the lower the flux rating. The new deep SSTs do not show this sensitivity to HLR.



**Figs 9a and 9b:** SettlerCAD predicted capacity as % of the 1DFT maximum SOR (Fig 9a, left) and SLR (Fig 9b, right) limits versus the flux load factor for the Darvill new (4.1m SWD, ■) and old (2.5m SWD, ▲) SSTs. The actual test positions and outcome are also shown (safe ●, fail X).

The actual test values and result are also shown in Figs 9a and b (safe ●, fail X). Compared with the SettlerCAD predicted limits, Test 2 is significantly above both the new (124%) and old (126%) SST lines, Test 1 on the new (102%) SST line but above the old (109%) SST line, Test 3 significantly below both the new (79%) and old (91%) SST line and Test 4 slightly above the new (105%) SST line but significantly above the old (141%) SST line (see Table 6). If SettlerCAD is realistic, then Tests 1, 2 and 4 should have ended in failure, whereas in fact only Test 4 ended in failure. Hence, SettlerCAD correctly predicts the result of Tests 3 and 4 only. For test 1, the test and SettlerCAD predicted maximum overflow rates are very close, so that had this test been run for longer, it may have ended in failure. However, this does not apply to Test 2, because this test was significantly overloaded with respect to the SettlerCAD limit (125%) so should have failed but didn't for both the new and old SSTs.

**Table 6:** Comparison of SettlerCAD predicted result with the actual Tests 1 to 4 on the new and old Darvill SSTs.

PARAMETER	Test 1		Test 2		Test 3		Test 4	
$Q_i$ = Influent flow (excl $Q_e$ )	New	Old	New	Old	New	Old	New	Old
Test $Q_i$ for 1 SST ( $m^3/h$ )	833	833	688	688	948	948	2396	2396
% of 1DFT maximum $Q_i$	78.5	78.5	92.1	92.1	65.6	65.6	89.1	89.1
1DFT predicted outcome	Safe	Safe	Safe	Safe	Safe	Safe	Safe	Safe
SettlerCAD predicted max $Q_i$ ( $m^3/h$ )	820.3	759.3	555.9	548.4	1211.1	1037.6	2273.4	1701.1
% of SettlerCAD predicted max $Q_i$	101.5	109.7	123.8	125.5	79.0	91.4	105.4	140.8
SettlerCAD predicted outcome	Fail	Fail	Fail	Fail	Safe	Safe	Fail	Fail
Observed test result	Safe	Safe	Safe	Safe	Safe	Safe	Fail	Fail

#### 4.3 Conclusions from the Darvill SST simulations

The simulations of 35m  $\phi$  Darvill full-scale SST SLR stress tests with the 2D hydrodynamic model SettlerCAD indicate, as would be expected, that the SST hydraulic non-idealities are intrinsically part of the model and that SettlerCAD predicted maximum SOR and SLR were



significantly below those calculated from the 1DFT. The simulations indicated that the *capacity*, or flux rating, of the old flat bottom shallow (2.5m SWD) SSTs decreased from 0.86 to 0.70 of the 1DFT maximum SLR as the flux load factor  $V_0/(nX_F)$  increased (which increases HLR due to an improvement in sludge settleability and/or decrease in feed concentration). The new deep 4.1m SWD 1:10 sloping bottom (average depth 4.68m) SSTs did not show this sensitivity of capacity (or flux rating) to the flux load factor (or HLR) and the flux rating remained approximately constant at around 0.87 of the 1DFT maximum SLR. The simulations showed that the magnitude of the flux rating is not a constant value, and seems to be dependent on SST depth and HLR - the deeper the SST and the lower the HLR, the closer the flux rating to 1.0. In Section 7 below, additional Darvill SST runs (i) without the Stamford baffles and (ii) with interchanged SWD between the new and old SSTs are discussed to evaluate the effect of the baffles and SWD on the flux rating.

With the Darvill SST tests, the accuracy of the SettlerCAD predicted flux rating could not be validated because the result of only two of the four tests (Tests 3 safe and 4 fail) on the new and old SSTs were predicted correctly. The highest flux rating of a safe test is 0.96 (Test 2) and the lowest flux rating of a fail test is 0.91, which is lower than that of the highest safe test. From the actual tests, the flux rating of the old and new SSTs appear to be approximately the same, but this may only appear to be so because none of the test SLRs and SORs fall between the old and new SST flux rating lines predicted by SettlerCAD in Figs 9a and b. Furthermore, the flux rating from the actual tests would seem to be much greater than that predicted by SettlerCAD, especially for the old SST. It is possible that for one of the tests not predicted correctly, i.e. Test 1 which loaded the SSTs at 78% of the 1DFT SLR, the test duration wasn't long enough to reach a steady state and had it been run for longer, the test, which was observed to end safe, may have ended fail. However, this does not apply to the other test not predicted incorrectly (Test 2). This test loaded the SST to 92% of the 1DFT SLR maximum, which is significantly higher than Test 4, which ended fail and was correctly predicted by SettlerCAD. Therefore, even though the HLR in Test 4 (3.23 m/h) was double that in Test 2 (1.61 m/h), it is likely that there was sufficient time in Test 2 to reach a steady state.

*Although the Darvill SST tests are not helpful for validating the SettlerCAD predicted flux ratings, the simulations nevertheless provide further convincing evidence that the 1D idealised flux theory (1DFT) should not be applied to the design of full-scale SSTs without an appropriate reduction factor (flux rating).*

## 5 SIMULATING THE WATTS' SSTs WITH SettlerCAD

Watts *et al.* (1996) conducted 15 SLR stress tests on one of the 4 SSTs at the Kanapaha Water Reclamation Facility (Florida, USA) over a 3 week period. The SSTs were 28.96 m in diameter with 3.66 m and 4.60 m side water and centre depths respectively, giving a bottom slope of 1:15.4 or 6.5%. The centre influent feed well was bounded by an annular skirt baffle 2.44 m deep (gap to floor 1.66 m) and occupying 28% of the SST surface area (i.e. 15.32 m diameter). Peripheral and radial effluent launders collected the surface overflow. Settled sludge was collected continuously via a rotating multiple pipe suctions system with 4 draw offs at radial distances of 1.5, 5.2, 8.6 and 12.2 m from the centre. Waste sludge was pumped from the sludge return flow and was included in the recycle flow in the simulations.

In the SLR tests, the influent and recycle flows were kept constant and each test lasted about 8 to 10 hours (3 to 6xR<sub>90</sub>). The feed ( $X_f$ ), effluent ( $X_e$ , ESS), underflow ( $X_u$ , RAS) and waste ( $X_w$ , WAS) sludge concentrations were measured hourly. Sludge blanket height (SBH) measurements were taken at about 15 min intervals and the position and movement of the sludge blanket height (SBH) was used to determine the test result. Where the SBH remained constant, the test was continued for at least 2 hours longer into the "steady state" period and the test ended safe. Where the SBH continued increasing, the test was stopped just prior the SBH reaching the effluent launders and the test ended fail.

During the three week testing period, the sludge settleability flux constants  $V_0$  &  $n$  were measured in 7 sets of 6 multiple batch settling tests at concentrations ranging from 2 to 14 g/l. After rejecting 2 sets, the remaining 5 were pooled and the average  $V_0$  &  $n$  determined for the 15 SLR tests, viz.  $V_0 = 7.62$  m/h and  $n = 0.3055$  m<sup>3</sup>/kg. In the 15 tests, of which the first 10 ended safe and the last 5 ended fail, the overflow and underflow rates ranged from 0.72 to 1.66 m/h and 0.36 and 1.14 m/h respectively and the feed concentration from 3.44 to 4.13 kg/m<sup>3</sup>. Because the  $V_0$  &  $n$  were accepted to be the same for all 15 tests, the flux load factor  $V_0/(nX_f)$  varied in a narrow range from 6.04 m/h for Test 4 to 7.24 m/h for Test 9 due to the small change in feed ( $X_f$ ) concentration. Details of the 15 tests are listed in Table 7.

From the measured  $V_0$ ,  $n$  and  $X_f$ , the 1DFT predicted maximum SOR and SLR were calculated with the method described earlier in Section 3.2 and are listed in Table 7. The 1DFT predicted and test applied SLRs and the Test/1DFT SLR ratio from Table 7 are plotted in Figs 10a and b. From Fig 10b, the Test/1DFT maximum SLR ratio for the 15 tests are between 0.56 (Test 1) and 0.91 (Test 11) and Tests 3, 4, 7 and 9, which ended safe, have higher Test/1DFT maximum SLR ratios than Test 15, which was the test with the lowest SLR test that ended fail. From Fig 8a, the line that best separates the safe (●) and fail (⊗) tests is about 0.80 indicating that the flux rating of the Watts SST is about 0.80.



**Table 7: Summary of the 15 SLR stress test results on the Kanapaha WWTP SSTs by Watts et al. (1996).**

Parameter		Test 1	Test 2	Test 3	Test 4	Test 5	Test 6	Test 7	Test 8	Test 9	Test 10	Test 11	Test 12	Test 13	Test 14	Test 15
SST	Number of SSTs	1	1	1	1	1	1	1	1	1	1	1	1	1	1	1
	Surface area (m <sup>2</sup> )	659	659	659	659	659	659	659	659	659	659	659	659	659	659	659
Actual test loading conditions	Influent flow (M/d)	11.4	14.9	18.9	18.8	18.8	18.8	22.4	18.8	24.4	18.6	24.5	26.3	24.5	24.5	24.2
	Overflow rate (m/h)	0.72	0.95	1.20	1.19	1.19	1.19	1.42	1.19	1.54	1.17	1.55	1.66	1.55	1.55	1.53
	Recycle flow (M/d)	9.5	9.6	5.8	9.5	9.5	11.4	9.5	13.3	9.5	9.5	9.5	9.5	13.3	17.1	18.1
	Underflow rate (m/h)	0.60	0.60	0.36	0.60	0.60	0.72	0.60	0.84	0.60	0.60	0.60	0.60	0.84	1.08	1.14
	Recycle ratio	0.837	0.639	0.304	0.508	0.507	0.606	0.426	0.706	0.391	0.514	0.389	0.363	0.543	0.698	0.746
	Feed Concentration (g/l)	4.053	3.972	3.801	4.130	3.664	3.994	3.560	3.787	3.444	3.885	4.044	3.444	3.987	3.983	3.618
	Applied SLR [kgSS/(m <sup>2</sup> .h)]	5.37	6.15	5.94	7.39	6.57	7.65	7.20	7.68	7.40	6.91	8.71	7.80	9.55	10.50	9.68
	Weir loading rate [m <sup>3</sup> /(h.m)]	5.22	6.84	8.67	8.59	8.62	8.62	10.26	8.60	11.19	8.50	11.23	12.04	11.24	11.24	11.10
	HLR [(qA+qR), m/h]	1.32	1.55	1.56	1.79	1.79	1.91	2.02	2.03	2.15	1.78	2.15	2.27	2.40	2.64	2.68
Sludge settleability	V <sub>0</sub> (m/h)	7.62	7.62	7.62	7.62	7.62	7.62	7.62	7.62	7.62	7.62	7.62	7.62	7.62	7.62	7.62
	n (l/g)	0.3055	0.3055	0.3055	0.3055	0.3055	0.3055	0.3055	0.3055	0.3055	0.3055	0.3055	0.3055	0.3055	0.3055	0.3055
	DSVI (ml/g)*	94	94	94	94	94	94	94	94	94	94	94	94	94	94	94
1DFT predicted limits	Maximum SLR [kg/(m <sup>2</sup> .h)]	9.54	9.55	6.58	9.54	9.55	10.81	9.55	11.94	9.55	9.55	9.54	9.55	11.98	13.31	13.27
	Overflow rate (m/h)	1.75	1.80	1.37	1.71	2.00	1.98	2.08	2.31	2.17	1.85	1.76	2.17	2.16	2.26	2.52
	Influent Q <sub>i</sub> (excl Q <sub>0</sub> ) (m <sup>3</sup> /h)	1153.9	1186.5	899.9	1124.2	1319.4	1307.4	1369.1	1523.8	1428.6	1221.7	1156.9	1428.6	1423.6	1486.9	1662.3
Flux ratings	Flux load factor [V <sub>0</sub> /(nX <sub>F</sub> ), m/h]	6.15	6.28	6.56	6.04	6.81	6.25	7.01	6.59	7.24	6.42	6.17	7.24	6.26	6.26	6.89
	Test/1DFT flux ratio	56.2	64.4	90.3	77.5	68.8	70.7	75.4	64.3	77.5	72.3	91.3	81.7	79.7	78.9	73.0
	Test/1DFT overflow rate ratio	41.2	52.5	87.7	69.5	59.4	60.1	68.2	51.4	71.2	63.3	88.3	76.7	71.8	68.8	60.7

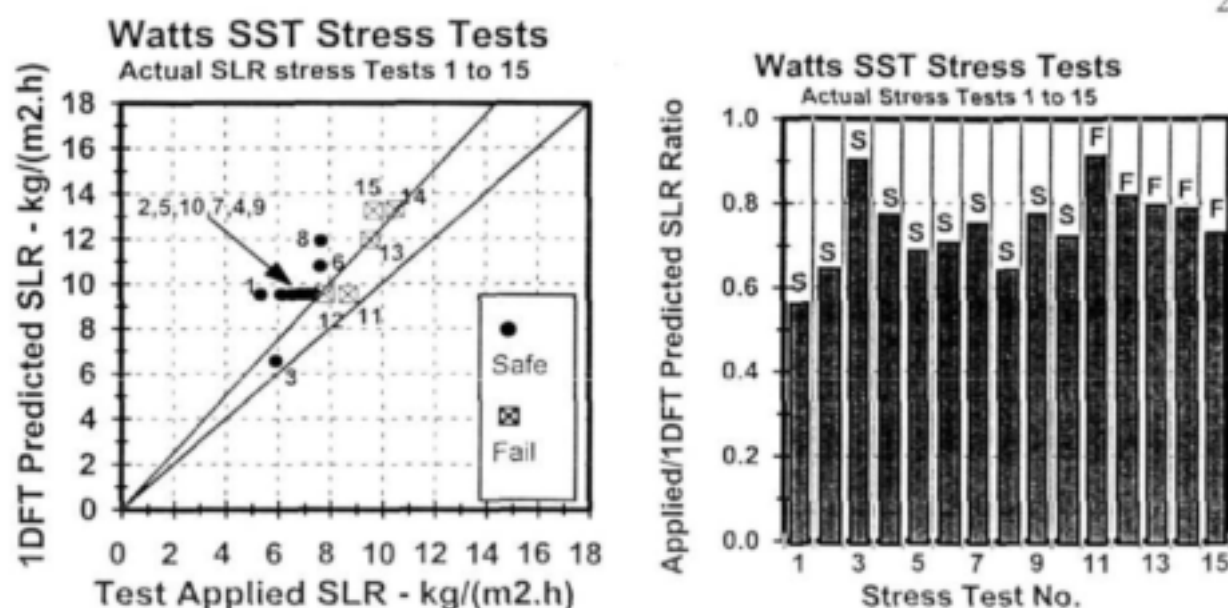
**Table 9: Comparison of SettlerCAD predicted result with the actual Tests 1 to 15 on the Watts SSTs.**

PARAMETER	Test 1	Test 2	Test 3	Test 4	Test 5	Test 6	Test 7	Test 8	Test 9	Test 10	Test 11	Test 12	Test 13	Test 14	Test 15
Q <sub>i</sub> = Influent flow (excl Q <sub>0</sub> )															
Test Q <sub>i</sub> for 1 SST (m <sup>3</sup> /h)	475.1	622.8	788.9	781.5	784.2	785.3	933.8	782.6	1107.8	773.5	1021.4	1095.2	1022.5	1022.8	1009.6
% of 1DFT maximum Q <sub>i</sub>	41.2	52.5	87.7	69.5	59.4	60.1	68.2	51.4	71.2	63.3	88.3	76.7	71.8	68.8	60.7
1DFT predicted outcome	Safe	Safe	Safe	Safe	Safe	Safe	Safe	Safe	Safe	Safe	Safe	Safe	Safe	Safe	Safe
SettlerCAD predicted max Q <sub>i</sub> (m <sup>3</sup> /h)	848.1	875.1	665.9	826.3	946.7	938.0	982.3	1066.6	1021.4	888.8	853.2	1021.4	1014.3	1085.5	1238.4
% of SettlerCAD predicted max Q <sub>i</sub>	56.0	71.2	118.5	94.6	82.8	83.7	95.1	73.4	99.6	87.0	119.7	107.2	100.8	94.2	81.5
SettlerCAD predicted outcome	Safe	Safe	Fail	Safe	Safe	Safe	Safe	Safe	Safe	Safe	Fail	Fail	Fail	Safe	Safe
Observed test result	Safe	Safe	Safe	Safe	Safe	Safe	Safe	Safe	Safe	Safe	Fail	Fail	Fail	Fail	Fail

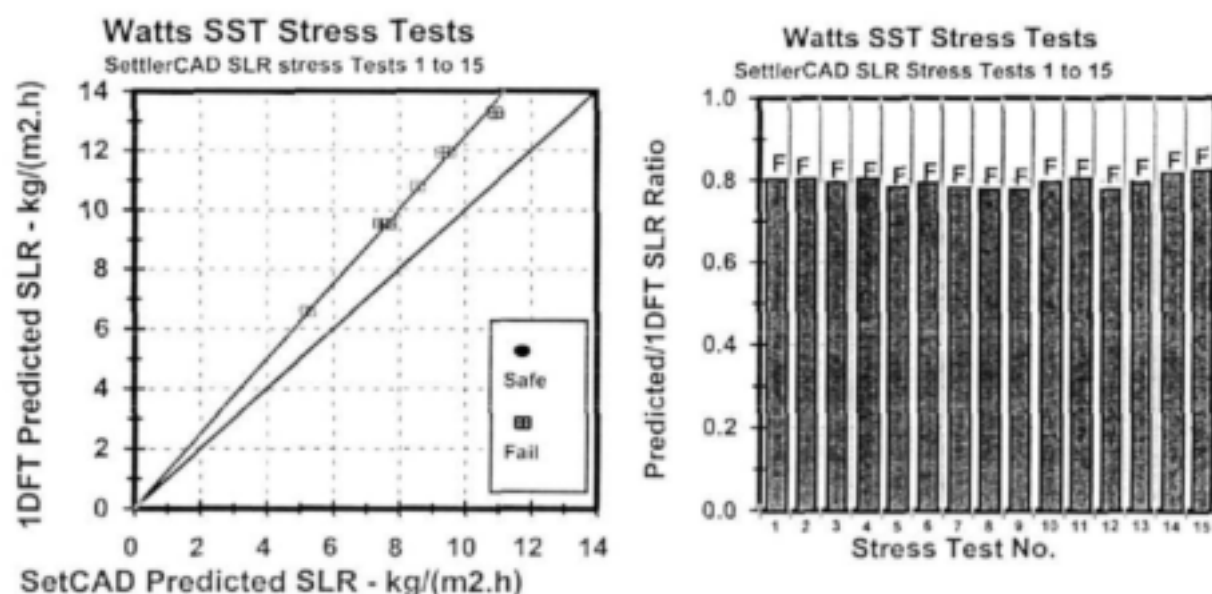
**Table 8:** Summary of the SettlerCAD simulation results for the SettlerCAD influent flow limit (top) and actual test influent flow (bottom) for the 15 SLR tests on the Watts SSTs ( $Q_i$  = Influent flow in  $m^3/h$ ).

SettlerCAD $Q_i$ LIMIT	Test 1	Test 2	Test 3	Test 4	Test 5	Test 6	Test 7	Test 8	Test 9	Test 10	Test 11	Test 12	Test 13	Test 14	Test 15
Flux factor $V_d/(nX_d)$ - $m/h$	6.15	6.28	6.56	6.04	6.81	6.25	7.01	6.59	7.24	6.42	6.17	7.24	6.26	6.26	6.89
Influent Flow ( $m^3/h$ ) for 1 SST	848.1	875.1	665.9	826.3	946.7	938.0	982.3	1066.6	1021.4	888.8	853.2	1021.4	1014.3	1085.5	1250.9
% of IDFT maximum $Q_i$	73.50	73.75	74.00	73.50	71.75	71.75	71.75	70.00	71.50	72.75	73.75	71.50	71.25	73.00	75.25
Overflow Rate ( $m/h$ )	1.29	1.33	1.01	1.25	1.44	1.42	1.49	1.62	1.55	1.35	1.30	1.55	1.54	1.65	1.90
Recycle Flow ( $m^3/h$ )	397.5	398.0	239.9	396.9	397.7	475.7	397.7	552.8	397.7	397.7	397.2	397.7	555.6	714.0	753.5
Underflow Rate ( $m/h$ )	0.603	0.604	0.364	0.603	0.604	0.722	0.604	0.839	0.604	0.604	0.603	0.604	0.843	1.084	1.144
Recycle Ratio	0.47	0.45	0.36	0.48	0.42	0.51	0.40	0.52	0.39	0.45	0.47	0.39	0.55	0.66	0.60
Applied Flux ( $kgSS/(m^2 \cdot h)$ )	7.66	7.68	5.23	7.67	7.48	8.57	7.46	9.31	7.42	7.59	7.68	7.42	9.50	10.88	11.01
% of IDFT maximum flux	80.3	80.3	79.5	80.4	78.3	79.3	78.1	78.0	77.7	79.4	80.5	77.7	79.3	81.8	83.0
Actual Retention Time (h)	2.1	2.1	2.9	2.1	1.9	1.9	1.9	1.6	1.8	2.0	2.1	1.8	1.7	1.5	1.3
Duration of Run (min)	6000	6000	6000	6000	6000	6000	6000	6000	6000	6000	6000	6000	6000	6000	6000
Duration of Run (# of $R_{90}$ )	47.6	48.6	34.6	46.7	51.4	54.0	52.7	61.9	54.2	49.1	47.8	54.2	60.0	68.7	76.6
Sim time Step (min)	2.5	2.5	2.5	2.5	2.5	2.5	2.5	2.5	2.5	2.5	2.5	2.5	2.5	2.5	2.5
Sim time Step (% $R_{90}$ )	1.98	2.03	1.44	1.95	2.14	2.25	2.20	2.58	2.26	2.05	1.99	2.26	2.50	2.86	3.19
Effluent SS ( $mg/l$ )*	53.5	51.4	55.0	57.7	81.0	97.2	92.2	50.6	50.2	54.5	52.2	50.2	52.0	50.5	64.2
Recycle Conc ( $mg/l$ )*	12492	12479	14152	12459	11988	11431	11909	10927	11888.7	12337.1	12488.8	11888.7	11079.7	9911.2	9431.0
Mass Balance (%)	99.3	99.1	99.7	98.8	98.4	97.9	98.3	99.4	97.8	99.1	99.0	97.8	99.2	99.5	99.1
Test Result (ESS>50mg/l)	Fail	Fail	Fail	Fail	Fail	Fail	Fail	Fail	Fail	Fail	Fail	Fail	Fail	Fail	Fail
ACTUAL TEST INFLUENT FLOW															
Influent Flow ( $m^3/h$ ) for 1 SST	475.1	622.8	788.9	781.5	784.2	785.3	933.8	782.6	1017.8	733.5	1021.4	1095.2	1022.5	1022.8	1009.6
% of IDFT maximum $Q_i$	41.2	52.5	87.7	69.5	59.4	60.1	68.2	51.4	71.2	63.3	88.3	76.7	71.8	68.8	60.7
Overflow Rate ( $m/h$ )	0.72	0.95	1.20	1.19	1.19	1.19	1.42	1.19	1.54	1.17	1.55	1.66	1.55	1.55	1.53
Recycle Flow ( $m^3/h$ )	397.5	398.0	239.9	396.9	397.7	475.7	397.7	552.8	397.7	397.7	397.2	397.7	555.6	714.0	753.5
Underflow Rate ( $m/h$ )	0.60	0.60	0.36	0.60	0.60	0.72	0.60	0.84	0.60	0.60	0.60	0.60	0.84	1.08	1.14
Recycle Ratio	0.837	0.639	0.304	0.508	0.507	0.606	0.426	0.706	0.391	0.514	0.389	0.363	0.543	0.698	0.746
Applied Flux ( $kgSS/(m^2 \cdot h)$ )	5.37	6.15	5.94	7.39	6.57	7.65	7.20	7.68	7.40	6.91	8.71	7.80	9.55	10.50	9.68
% of IDFT maximum flux	56.2	64.4	90.3	77.5	68.8	70.7	75.4	64.3	77.5	72.3	91.3	81.7	79.7	78.9	73.0
Actual Retention Time (h)	3.0	2.6	2.5	2.2	2.2	2.1	2.0	2.0	1.8	2.2	1.8	1.8	1.7	1.5	1.5
Duration of Run (min)	6000	6000	6000	6000	6000	6000	6000	6000	6000	6000	6000	6000	6000	6000	6000
Duration of Run (# of $R_{90}$ )	33.3	39.0	39.3	45.0	45.2	48.2	50.9	51.0	54.1	44.7	54.2	57.0	60.3	66.3	67.4
Sim time Step (min)	2.5	2.5	2.5	2.5	2.5	2.5	2.5	2.5	2.5	2.5	2.5	2.5	2.5	2.5	2.5
Sim time Step (% $R_{90}$ )	1.39	1.62	1.64	1.88	1.88	2.01	2.12	2.13	2.25	1.86	2.26	2.38	2.51	2.76	2.81
Effluent SS ( $mg/l$ )*	3.9	5.0	484.3	5.7	5.8	5.7	6.8	6.1	17.9	5.3	479.9	238.0	66.9	9.9	7.5
Recycle Conc ( $mg/l$ )*	8891.9	10200.2	13268.3	12236.7	10879.7	10577.1	11900.8	9137.8	12205.3	11430.0	12150.5	11792.4	11078.1	9672.4	8453.7
Mass Balance (%)	100.0	100.2	91.2	99.9	100.0	100.0	100.0	100.0	100.0	100.0	92.7	96.3	98.9	100.0	100.0
Test Result (ESS>50mg/l)	Safe	Safe	Fail	Safe	Safe	Safe	Safe	Safe	Safe	Safe	Fail	Fail	Fail	Safe	Safe
Observed Result	Safe	Safe	Safe	Safe	Safe	Safe	Safe	Safe	Safe	Safe	Fail	Fail	Fail	Fail	Fail

\*Mean over the last 2  $R_{90}$  values.



Figs 10 a and b: Calculated 1DFT maximum SLR versus test applied SLR (Fig 10a, left) and test applied to 1DFT calculated maximum SLR ratios (Fig 10b, right) for the 15 Watts stress test on the Kanapaha SST.



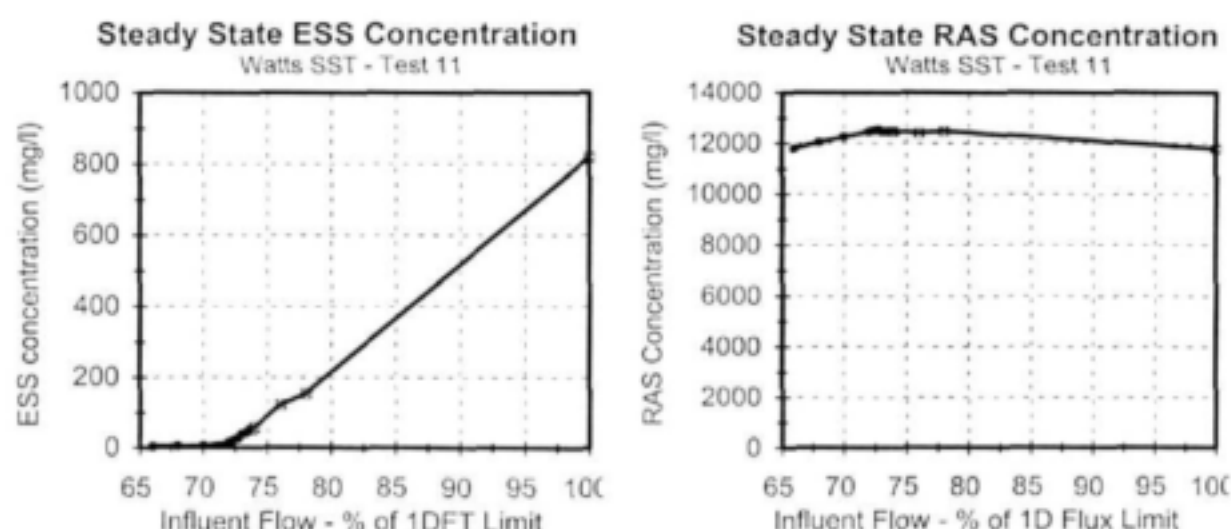
Figs 11a and b: 1DFT calculated maximum SLR versus SettlerCAD predicted maximum SLR (Fig 11a, left) and SettlerCAD predicted to 1DFT calculated maximum SLR ratios (Fig 11b, right) for the 15 Watts SLR stress tests on the Kanapaha SSTs.

## 5.2 Finding the SettlerCAD maximum SOR and SLR for the Watts SSTs

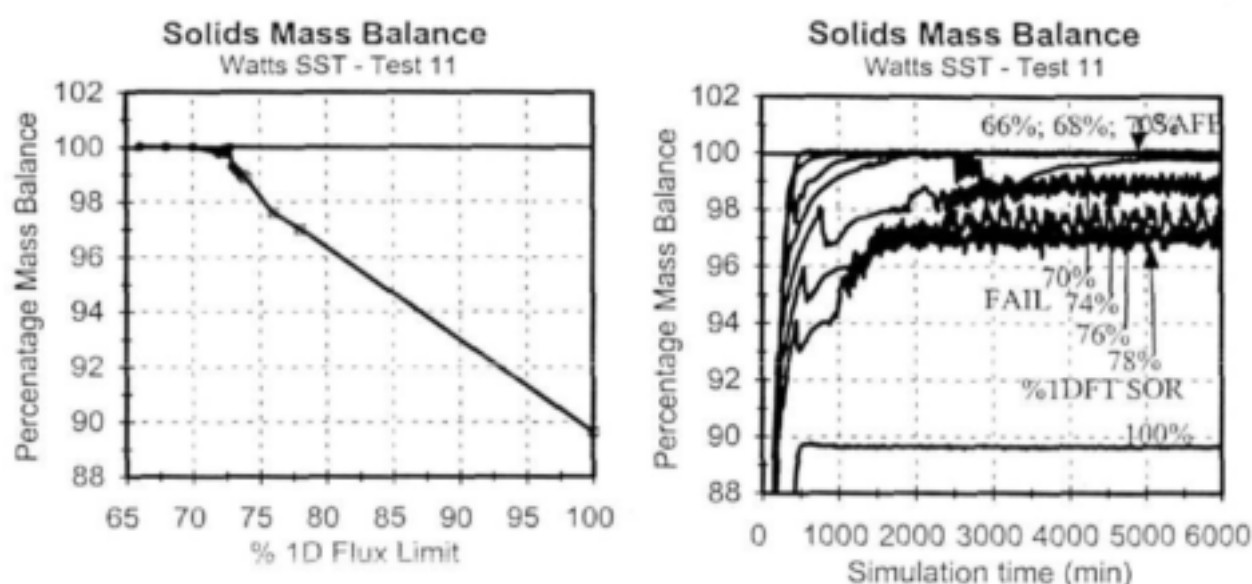
The data given in Table 7 was given as input to SettlerCAD. For each of the 15 tests, 16 SettlerCAD runs were setup. Runs 1 to 7 were at  $Q_i$  from 66 to 78% of the 1DFT SOR in 2% increments and an 8<sup>th</sup> run at 100%. Runs 9 to 15 were setup between consecutive safe and fail runs at 0.25% increments and the 16<sup>th</sup> run was at the actual test  $Q_i$ . The first run with ESS > 50 mg/l was accepted as the SettlerCAD predicted influent flow rate limit. The SettlerCAD flux

limit was calculated from the  $Q_i$  limit and the test  $Q_R$  and  $X_F$  values. The SettlerCAD predicted results of the first failure runs are given in Table 8 and are shown plotted in Figs 11a and b as 1DFT versus SettlerCAD predicted maximum SLR (Fig 11a) and SettlerCAD/1DFT maximum SLR ratio i.e. flux rating (Fig 11b). The results from the runs at the actual test influent flow rate are also given in Table 8. In Figs 11a and b, it can be seen that the SettlerCAD predicted flux rating of the Watts SST ranges between 0.777 (Test 9) and 0.825 (Test 15). Fig 11a shows the SettlerCAD maximum predicted SLR (flux rating) of the 15 tests fall very close to the 0.80 flux rating line. The SettlerCAD predicted maximum SOR (as % of the 1DFT maximum) ranged between 70.0% (Test 8) and 74.5% (Test 15).

In the simulation runs, a simulation time of 6000 min was selected which was more than 35x the actual hydraulic retention time ( $35 \times R_{ha}$ ) for all the runs (see Table 8). As for the Darvill SST runs, these run times were sufficiently long to establish a final steady state condition and the final ESS ( $X_E$ ) and RAS ( $X_R$ ) concentrations accepted for each run were the averages of the predicted values over the last  $2 \times R_{ha}$ . The solids mass balance was based on these final average ESS and RAS concentrations (which are listed in Table 8). The same pattern regarding the mass balance was observed - provided the run did not end in the failure ( $ESS < 50 \text{ mg/l}$ ), the run yielded a solids mass balance within 0.5% of 100% and runs that ended in failure ( $ESS > 50 \text{ mg/l}$ ) yielded a lower than 99.5% solids mass balance; the greater the SST overload (i.e. the higher the ESS concentration), the lower the solids mass balance below 99.5%. The ESS, RAS and % mass balance versus influent flow (as% of the 1DFT limit  $Q_i$ ) for Test 11, which had the highest Test/1DFT SOR and SLR ratios, are shown in Figs 12a to c. In Fig 12d, the % mass balance versus simulation time for runs 1 to 8 of Test 11 at 66 to 78% of the 1DFT maximum overflow rate are shown - it can be seen that for the failed runs (i) even though a final steady state is achieved, this steady state does not yield a mass balance.



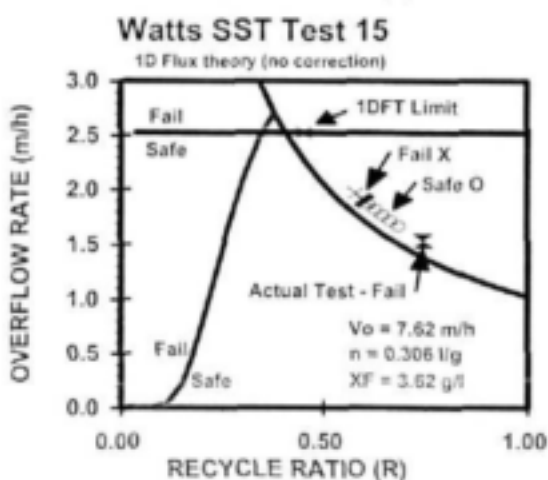
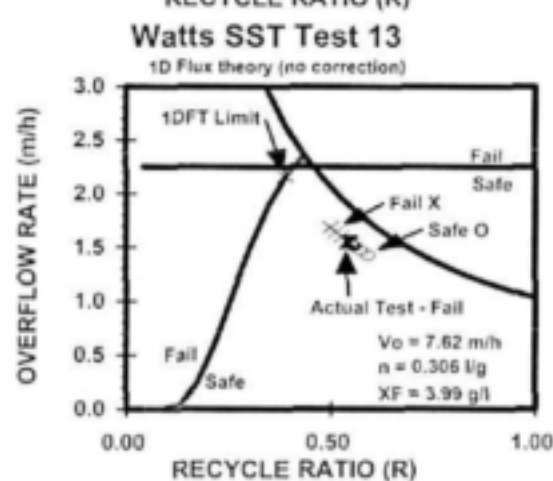
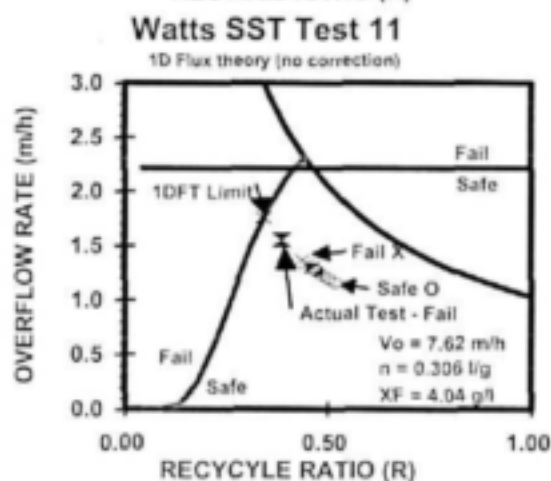
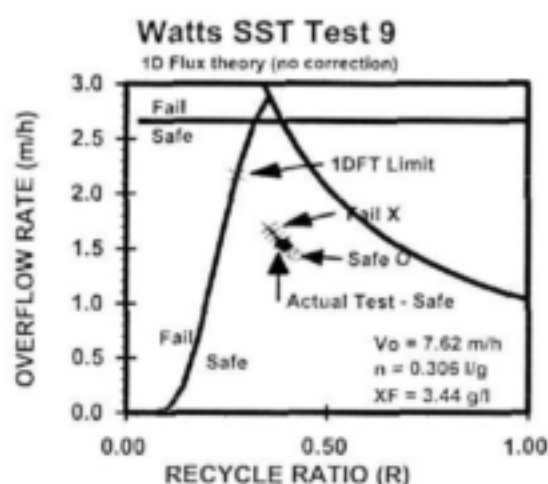
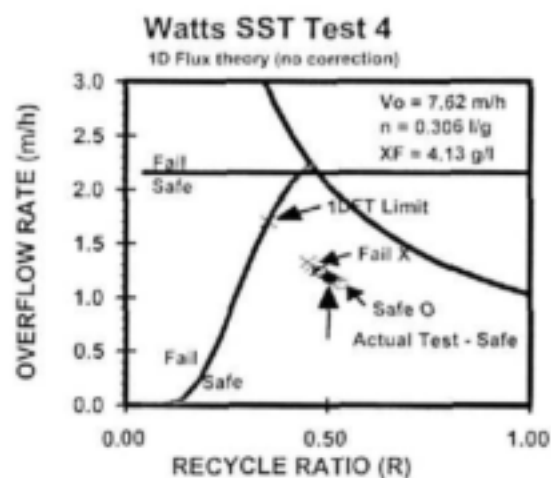
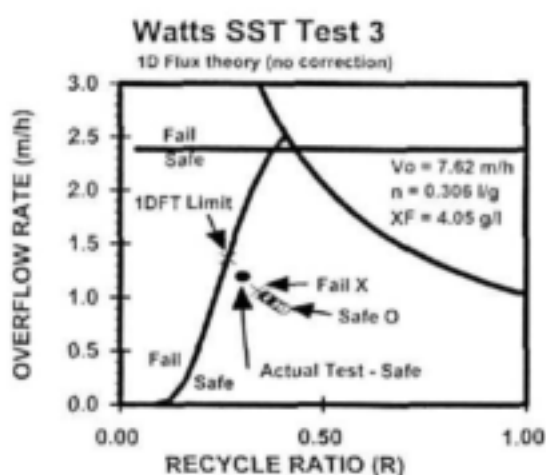
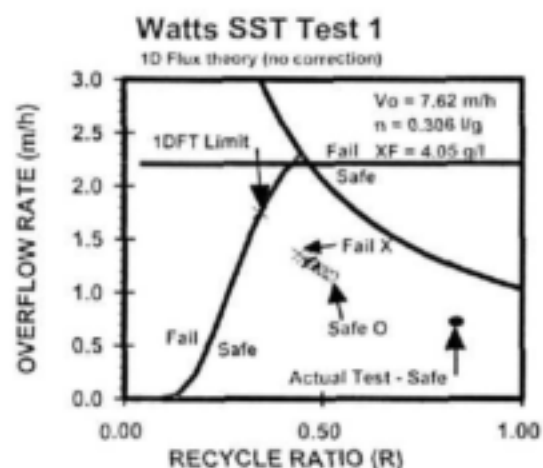
**Figs 12a and b:** Final ESS and RAS concentrations (Figs 12a, left and Fig 12b, right) versus influent flow as % 1DFT limit showing runs ended safe (●) and fail (⋈) for the Test 11 SettlerCAD runs on the Watts SSTs.



*Figs 12c and d: % Mass balance versus influent flow as % 1DFT limit (Fig 12c, left) showing runs ended safe (●) and fail (✕) and versus simulation time (Fig 12d, right) for the Test 11 SettlerCAD runs on the Watts SSTs.*

The position and result (safe O, fail X) of the SettlerCAD simulation runs for Tests 1, 3, 4, 9, 11, 13, and 15 are shown in the D&O charts in Figs 13a to g. The actual test position and result (safe ● or fail ✕) also is indicated. In the charts, the SettlerCAD predicted SOR limit is given at the transition from the safe to the fail positions. If the actual test position (●) is within the safe (O) runs, then SettlerCAD correctly predicted a safe result for the actual test, and if the actual test position (✕) is within the fail (X) runs, then SettlerCAD correctly predicted a fail result for the actual test. The 7 tests in Fig 13 were selected to demonstrate the following:

- Test 1: Lowest test/1DFT SOR (0.412) and SLR (0.562) ratios with SHC I governing capacity; Test ended safe and SettlerCAD predicted result correctly.
- Test 3: Second highest test/1DFT SOR (0.877) and SLR (0.903) ratios with SHC I governing capacity; Test ended safe but SettlerCAD predicted result incorrectly as fail.
- Test 4: Lowest flux load factor  $V_0/(nX_F) = 6.04$  m/h with SHC I governing capacity; Test ended safe and SettlerCAD predicted result correctly.
- Test 9: Highest flux load factor  $V_0/(nX_F) = 7.24$  m/h with SHC I governing capacity; Test ended safe and SettlerCAD predicted result correctly.
- Test 11: Highest test/1DFT SOR (0.883) and SLR (0.913) ratios with SHC I governing capacity; Test ended fail and SettlerCAD predicted result correctly.
- Test 13: Test/1DFT SOR (0.718) and SLR (0.797) ratios very close to SettlerCAD/1DFT SOR (1.01) and SLR (1.01) ratios with SHC II governing capacity; Test ended fail and SettlerCAD predicted result correctly.
- Test 15: Low test/1DFT SOR (0.607) and SLR (0.703) ratios with SHC II governing capacity; Test ended fail but SettlerCAD predicted result incorrectly.

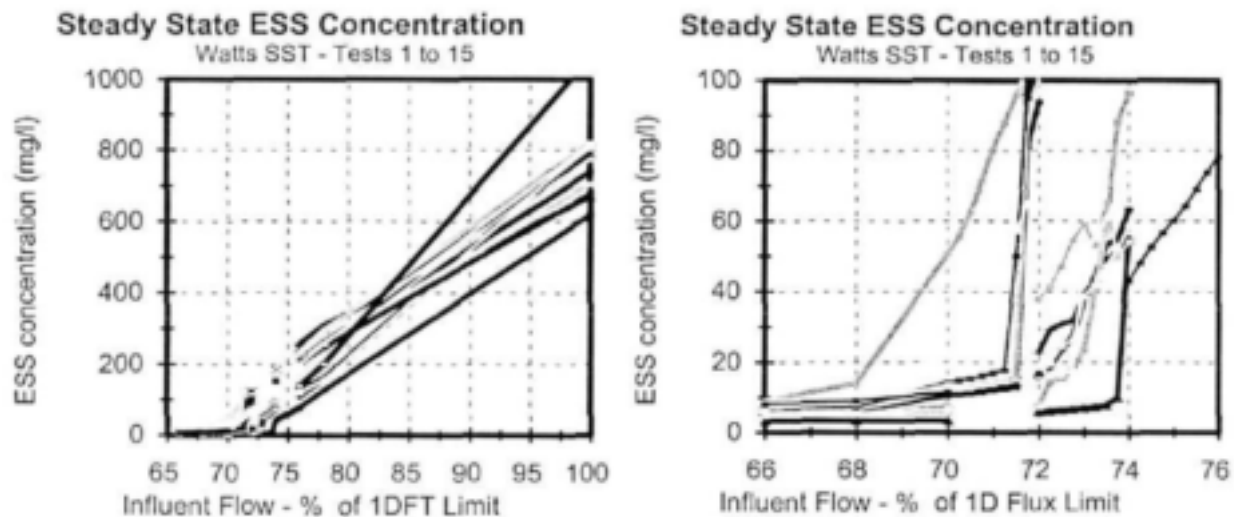


**Figs 13 a to i:** 1DFT D&O charts showing the SST operating positions and result (safe O, fail X) of the SettlerCAD runs and actual tests (safe ●, fail X) for Tests 1, 3, 4, 9, 11, 13 and 15 on the Watts SST.



From all 15 D&O charts, SettlerCAD correctly predicted the result for 12 tests, i.e. Tests 1, 2 and 4 to 10 (safe) and 11 to 13 (fail) but incorrectly predicted the result for 3 tests, i.e. Tests 3 (actual test safe, SettlerCAD fail) and 14 and 15 (actual test fail, SettlerCAD safe). This aspect is discussed further below.

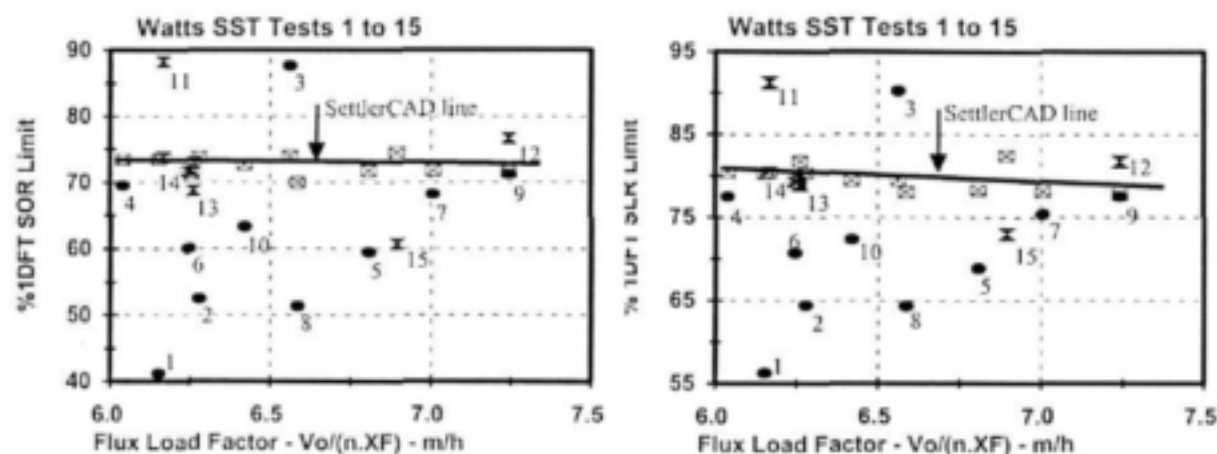
The ESS concentration versus  $Q_i$  (as a % of the 1DFT limit) for all the runs are shown in Fig 14. It can be seen that the ESS concentration increases gradually above 50 mg/l in the narrow range between 70 and 74% of the 1DFT limit influent flow. The precipitous increase in ESS concentration observed with the new (deep) Darvill SST is not apparent, the increase in ESS of the Watts SST resembles more the gradual increase in ESS of the old (shallow) Darvill SST. However, the Watts SST geometry resembles more the new Darvill SST with a 3.66m SWD and 1:15.4 sloping bottom compared with a 4.1m SWD and a 1:10 sloping bottom.



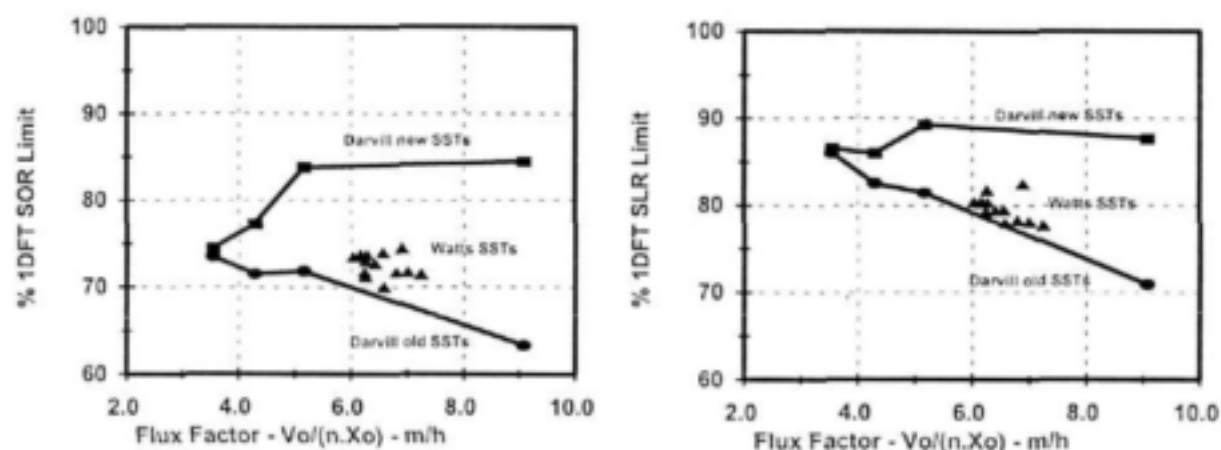
**Figs 14a and b:** SettlerCAD predicted steady state ESS concentration versus influent flow (as % of 1DFT limit) showing the whole field (Fig 14a, left) and zoomed in detail (Fig 14b, right).

The SettlerCAD predicted maximum SOR and SLR, as a % of the 1DFT limits, are plotted versus the flux factor  $V_0/(nX_F)$  in Figs 13a and b. Also shown are the 15 actual test points (safe ●, fail ☒). In these figures, the actual tests that ended safe (●) and fail (☒) which plot *below* and *above* the SettlerCAD predicted SOR and SLR limits (☒), are tests the result of which SettlerCAD predicted correctly; the actual tests that ended safe (●) and fail (☒) which plot *above* and *below* the SettlerCAD predicted SOR and SLR limits (☒), are tests the result of which SettlerCAD predicted incorrectly. Table 9 gives more detail on this listing the actual test SOR as a % of the SettlerCAD predicted maximum SOR, and the SettlerCAD predicted and observed result of the tests. From this, the test results which SettlerCAD predicts incorrectly are Tests 3 (observed safe but SettlerCAD predicts fail) and 14 and 15 (observed fail but SettlerCAD predicts safe). Of these 3 tests, only Tests 3 and 15 plot far from the SettlerCAD predicted maximum SOR and SLR results and therefore are definitely incorrectly predicated. However, Tests 4, 14, 13, 7, 9 and 12 all plot very close to the SettlerCAD predicted limits and are all

correctly predicted. This indicates that apart from Tests 3 and 15, SettlerCAD accurately identifies the SOR and SLR capacity of the Watts SST.



**Figs 15a and b:** SettlerCAD predicted maximum SOR (Fig 15a, left) and SLR (Fig 15b, right) as % of the 1DFT maximum limits versus flux load factor. Also shown are the positions and result (safe ●, fail ⚡) of the 15 actual tests identified by number.



**Figs 16a and b:** SettlerCAD predicted maximum SOR (Fig 16a, left) and SLR (Fig 16b, right) as % of the 1DFT maximum limits versus flux load factor for the Watts (3.66 m SWD, ▲) and Darvill new (4.1m SWD, ■) and old (2.5m SWD, ●) SSTs.

Figures 15a and b show a small decreasing trend in SettlerCAD predicted SOR and SLR (⊗) as the flux load factor increases - for the SOR (⊗, Fig 15a) from 74% (Test 4) to 71% (Tests 9 and 12) and for the SLR (⊗, Fig 15b) from 81% (Test 4) to 79% (Tests 9 and 12). This seems to suggest that the Watts SST is as insensitive to HLR as the Darvill new SST (Figs 9a and b). However, the flux factor range for the Watts tests is very narrow - only from 6.0 to 7.2 m/h, whereas for the Darvill tests the flux load factor range was from 3.5 to 9.0 m/h, leading to a much greater range in 1DFT SORs and SLRs. To place the Watts SettlerCAD simulation results in context of the Darvill simulation results, the Darvill and Watts simulation results are plotted together in Figs 16a and b. The Watts SettlerCAD predicted SOR and SLR limit results (▲) lie between the old (●) and new (■) Darvill SST lines, but closer to the old SST line. Considering



between the old (●) and new (■) Darvill SST lines, but closer to the old SST line. Considering that with respect to external SST geometry, the Watts SST (3.66m SWD and 1:15.4 sloping bottom) is closer in likeness to the new Darvill SST (4.1m SWD and 1:10 sloping bottom) than to the old Darvill SST (2.5m SWD and flat bottom), the expectation was that the Watts results should fall closer to the new Darvill SST results than those of the old SST, but this did not happen. However, a relatively consistent pattern does seem to be emerging because at least the Watts SST results fall between the Darvill new and old SST results and show a similar decreasing trend in capacity as the flux load factor increases. Greater clarity may be obtained from simulating some of the 45 SLR stress tests done on the Dutch shallow (1.5 to 2.5m SWD) SSTs by Stofkoper and Trentelman (1982) and reported by STOWa (1981). Also, in Section 7 below, additional Watts SST runs (i) with a Stamford baffle and (ii) with a 6.0 m SWD are discussed to evaluate the effect of baffles and SWD on the flux rating.

## 6 SIMULATING THE DUTCH STOWa SSTs WITH SettlerCAD

### 6.1 The STOWa SST SLR stress tests.

Stofkoper and Trentelmann (1982) conducted 47 SLR stress tests on 25 different circular SSTs with 30 to 46m diameter ( $\phi$ ), 1.5 to 2.5m SWD and 1:12 sloping bottoms with scraper sludge collection to a central hopper. Details of these tests are reported by STOWa (1981a,b,c). The larger SSTs had double sided inset ( $<1 \times \text{SWD}$  from periphery) effluent launders but the outer edge was blocked off so that effluent flowed only over the inner edge of the launder (see Ekama *et al.*, 1997 pg 173). The first 14 tests were done on the 45.5m  $\phi$ , 2.25m SWD Rijen SST (STOWa Tests 1 to 14, Rijen Tests 1 to 6a, 6b and 7 to 13), the second 10 tests on the 41.8m  $\phi$ , 2.0m SWD Oss SST (STOWa Tests 15 to 24, Oss Tests 1 to 10), and the final 23 tests on 23 different SSTs. In the tests, influent to the plant was shut off and accumulated in the sewer. At the same time, sludge return flow was set to the required rate and while the influent was withheld, most of the sludge in the SST was transferred to the biological reactor. The test was commenced when the influent pumps were started and set at the required rate to give a selected SOR. The influent and recycle flows were kept constant until test led to (i) sludge loss with the effluent, in which case the test ended in fail (F), (ii) a steady state in which the sludge blanket height (SBH) remained constant, in which case the test ended safe (S), or (iii) an inability to maintain the influent flow at the required rate due to insufficient sewage, in which case the test result was inferred from SBH measurements - if this was not possible with reasonable accuracy, the test was deemed inconclusive (NE, no equilibrium). During each test the following were measured at regular intervals (i) influent and recycle flows, (ii) sludge settleability with the SSVI and DSVI tests, (iii) SBH, (iv) feed, RAS and ESS concentrations and (v) concentration - depth profiles at various radial distances from the centre. Multiple batch zone settling velocity tests, from which the  $V_0$  and  $n$  values could be calculated, were also measured. However, these results could not be used for defining the sludge settleability because these tests were conducted over too narrow a concentration range (1.0 to 4.5 g/l). Hence for this investigation, the  $V_0$  and  $n$  values for the different tests were calculated from the measured SSVI or DSVI with the relationships reported by Ekama and Marais (1986) (see Ozinsky and Ekama, 1995; Ekama *et al.*, 1997).

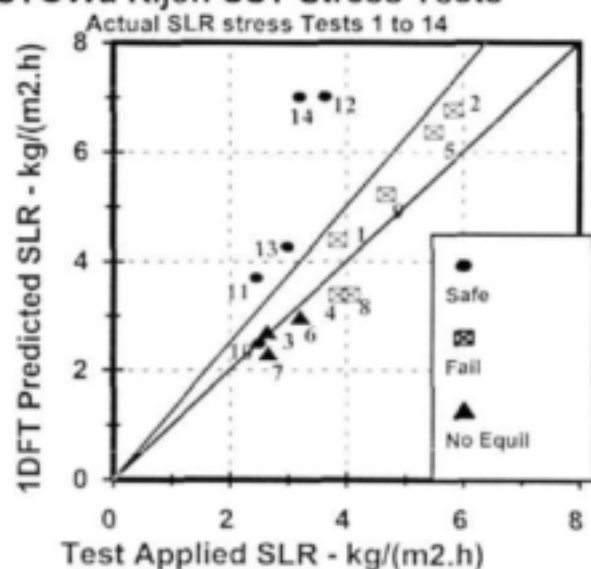
Internal feature detail such as the dimensions of the feedwell skirt diameter ( $\phi_{FS}$ ) and depth ( $h_{FS}$ ) and the inlet feedwell diameter ( $\phi_{IF}$ ) and depth ( $h_{IF}$ ) required as input by SettlerCAD were not available for all the SSTs stress tested. The detailed reports of the SST evaluation project (STOWa, 1981a,b,c) cite some internal feature detail of 22 SSTs surveyed in Holland. However, only 7 of these 22 SSTs were among the 25 SSTs stress tested. From the information of the 22 SSTs surveyed, the feedwell skirt diameter ( $\phi_{FS}$ ), as a fraction of the SST diameter ( $\phi_{ST}$ ) i.e.  $\phi_{FS}/\phi_{ST}$  varied from 0.05 to 0.16 with a mean of 0.10 and the feedwell skirt depth ( $h_{FS}$ ), as a fraction of the SST depth at the radius of the feedwell skirt ( $h_{ST}$ ) i.e.  $h_{FS}/h_{ST}$  varied from 0.27 to 0.55 with a mean of 0.42. So for the STOWa SSTs simulated, the feedwell skirt diameter ( $\phi_{FS}$ )

and depth ( $h_{FS}$ ) were set at these mean values. No information was given on the inlet feedwell diameter ( $\phi_{IF}$ ) and depth ( $h_{IF}$ ) so these dimensions were fixed at a 2.0m diameter and a depth 0.3m less than the feedwell skirt depth. To check the sensitivity of the simulations on the inlet dimensions, 16 SettlerCAD runs were set up for the Rijen SST under Rijen Test 1 conditions. The first 8 runs had the same inlet arrangement as defined above but had increasing influent flow rate to determine the SettlerCAD SOR and SLR capacity. The last 8 runs had a constant SOR and SLR of the first fail run but different inlet dimensions, i.e. feedwell skirt diameters ( $\phi_{FS}$ ) and depths ( $h_{FS}$ ) (in m) of 2.8 and 1.1, 4.6 and 1.7, and 6.0 and 2.1m in combination with inlet feedwell diameter ( $\phi_{IF}$ ) and depths ( $h_{IF}$ ) (in m) 1.0 and 1.0, 1.0 and 1.4, and 2.0 and 1.4. It was found that the runs with the large and deep inlet feedwell in combination with the 4.6 m  $\phi$  ( $\phi_{FS}/\phi_{ST} = 0.10$ ) and 6.0 m  $\phi$  ( $\phi_{FS}/\phi_{ST} = 0.13$ ) and 1.7 deep ( $h_{FS}/h_{ST} = 0.42$ ) feedwell skirt ended safe whereas the other runs ended fail. This confirmed the selection of the feedwell skirt of  $\phi_{FS}/\phi_{ST} = 0.10$  and  $h_{FS}/h_{ST} = 0.42$  with fixed inlet feedwell diameter of 2.0m and a depth 0.3m less than the feed well skirt.

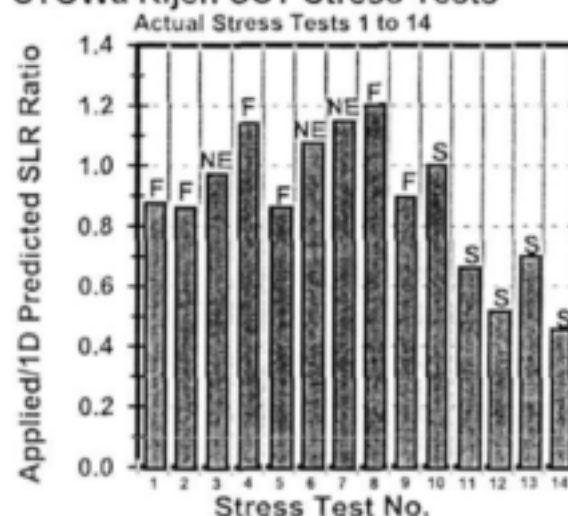
## 6.2 Simulating the Rijen SST SLR stress tests with SettlerCAD

From the  $V_0$ ,  $n$  and  $X_F$ , the 1DFT predicted maximum SOR and SLR were calculated for the 14 Rijen SLR tests with the method described in Section 3.2 above and are listed in Table 10. The 1DFT predicted and test applied SLRs and the Test/1DFT SLR ratio from Table 10 are plotted in Figs 17a and b.

**STOWa Rijen SST Stress Tests**



**STOWa Rijen SST Stress Tests**



*Figs 17a and b: 1DFT maximum SLR versus test applied SLR (Fig 17a, left) and Test/1DFT maximum SLR ratio (Fig 17b, right) for the 14 Stress tests reported by STOWa (1981) on the Rijen SST.*

Of the 14 tests, 6 tests ended fail (F, ∞, Tests 1, 2, 4, 5, 8 and 9), 5 ended safe (S, ●, Tests 10 to 14) and 3 inconclusive (NE, Tests 3, 6 and 7). From Fig 17b, the Test/1DFT maximum SLR ratio for the 14 tests are between 0.457 (Test 14) and 1.322 (Test 8). Tests 1 to 9 all have Test/1DFT SLR ratios >0.80 and therefore can be expected to fail and do. It is quite likely that had the inconclusive Tests 3, 6 and 7 been run for longer that these would have ended fail because they have Test/1DFT maximum SLR ratios > 0.85. Of the 5 safe tests, it is expected that the 4 Tests 11 to 14 ended safe (●) because they have low (<0.65) Test/1DFT maximum SLR ratios. The only odd test of the 14 is Test 10, which at a Test/1DFT maximum SLR ratio of 1.00 ended safe (●); in Fig 17a it plots near the 3 inconclusive tests (▲). In Fig 17a, the 2 safe Tests 11 and 13 and the 4 fail Tests 1, 9, 5 and 2 define the measured capacity of the Rijen SST to be between 0.75 and 0.85 of the 1DFT SLR maximum.

### 6.3 Finding the SettlerCAD maximum SOR and SLR for the Rijen SST.

The data given in Table 10 was given as input to SettlerCAD. For 6 of the 14 tests, 16 SettlerCAD runs per test were setup. The 6 tests selected were the 2 tests with the highest flux load factor  $V_0/(nX_F)$  (Tests 1 and 3), the 2 tests with the lowest flux load factor (Tests 4 and 8) and the 2 tests nearest the average flux load factor (Tests 2 and 11). SettlerCAD runs 1 to 7 for each of the 6 tests simulated were at  $Q_i$  from 60 to 72% of the 1DFT SOR in 2% increments and an 8<sup>th</sup> run at 100%. Runs 9 to 15 were setup between consecutive safe and fail runs at 0.25% increments and the 16<sup>th</sup> run was at the actual test  $Q_i$ . The first run with ESS > 50 mg/l was accepted as the SettlerCAD predicted maximum influent flow rate limit. The SettlerCAD SLR limit was calculated from the  $Q_i$  limit and the test  $Q_R$  and  $X_F$  values. The SettlerCAD predicted results of the first failure runs are given in Table 11 and are shown plotted in Figs 18a and b as 1DFT versus SettlerCAD predicted maximum SLR (Fig 18a) and SettlerCAD/1DFT maximum SLR ratio i.e. flux rating (Fig 18b). The results from the runs at the actual test influent flow rate are also given in Table 11.

**Table 10: Summary of the 14 SLR stress test results on the STOWA Rijen WWTP SSTs.**

Parameter		STOWa Test #	Test 1	Test 2	Test 3	Test 4	Test 5	Test 6	Test 7	Test 8	Test 9	Test 10	Test 11	Test 12	Test 13	Test 14
		Rijen Test #	Test 1	Test 2	Test 3	Test 4	Test 5	Test 6a	Test 6b	Test 7	Test 8	Test 9	Test 10	Test 11	Test 12	Test 13
SST	Number of SSTs		1	1	1	1	1	1	1	1	1	1	1	1	1	1
	Surface area (m <sup>2</sup> )		1626	1626	1626	1626	1626	1626	1626	1626	1626	1626	1626	1626	1626	1626
Actual test loading conditions	Influent flow (Ml/d)		42.5	42.5	34.3	34.3	34.3	28.9	28.9	28.9	28.9	24.6	24.6	24.6	20.3	20.3
	Overflow rate SUR (m/h)		1.09	1.09	0.88	0.88	0.88	0.74	0.74	0.74	0.74	0.63	0.63	0.63	0.52	0.52
	Recycle flow (Ml/d)		12.8	24.2	6.9	12.7	24.4	6.9	6.9	12.7	24.3	6.9	12.8	24.4	12.8	24.4
	Underflow rate (m/h)		0.327	0.621	0.176	0.326	0.625	0.178	0.178	0.326	0.622	0.176	0.328	0.624	0.328	0.624
	Recycle ratio		0.300	0.570	0.200	0.370	0.710	0.241	0.241	0.441	0.841	0.279	0.521	0.990	0.631	1.200
	Feed Concentration (g/l)		2.720	3.410	2.500	3.200	3.650	3.500	2.900	3.820	3.440	3.100	2.560	2.900	3.530	2.800
	Applied SLR [kgSS/(m <sup>2</sup> .h)]		3.85	5.83	2.64	3.86	5.49	3.21	2.66	4.07	4.69	2.50	2.45	3.64	2.99	3.20
	Weir loading rate [m <sup>3</sup> /(h.m)]		12.40	12.40	10.01	10.01	10.01	8.42	8.42	8.42	8.42	7.17	7.17	7.17	5.92	5.92
	HLR [(qA+qR), m/h]		1.417	1.711	1.056	1.206	1.505	0.918	0.918	1.066	1.362	0.806	0.958	1.254	0.848	1.144
Sludge settleability	V <sub>0</sub> (m/h)		6.53	6.33	6.53	4.86	5.94	7.15	5.38	4.86	4.86	5.94	5.38	6.53	6.33	6.53
	n (t/g)		0.406	0.415	0.406	0.488	0.433	0.379	0.460	0.488	0.488	0.433	0.460	0.406	0.415	0.406
	SSVI (DSVI) (ml/g)*		90	(140)	90	120	100	80	110	120	120	100	110	90	(140)	90
1DFT <sup>†</sup> predicted limits	Maximum SLR [kg/(m <sup>2</sup> .h)]		4.39	6.77	2.71	3.38	6.37	2.98	2.32	3.38	5.23	2.49	3.70	7.01	4.28	7.01
	Overflow rate (m/h)		1.289	1.363	0.908	0.731	1.121	0.675	0.621	0.560	0.898	0.628	1.117	1.794	0.884	1.880
	Influent Q <sub>i</sub> (excl Q <sub>R</sub> ) (m <sup>3</sup> /h)		2095.8	2217.3	1476.5	1189.0	1822.2	1097.0	1009.4	910.3	1459.7	1021.0	1816.4	2917.8	1437.1	3057.9
Flux ratings	Flux load factor [V <sub>0</sub> /(nX <sub>r</sub> ), m/h]		5.91	4.47	6.43	3.11	3.76	5.39	4.03	2.61	2.89	4.42	4.56	5.55	4.32	5.75
	Test/1DFT SLR ratio		87.7	86.2	97.4	114.1	86.2	107.7	114.9	120.3	89.6	100.3	66.3	51.9	70.0	45.7
	Test/1DFT overflow rate ratio		84.6	79.9	96.9	120.4	78.5	109.7	119.2	132.2	82.4	100.3	56.4	35.1	58.8	27.7

**Table 12: Comparison of SettlerCAD predicted result with the actual Tests 1 to 14 on the STOWa Rijen SSTs.**

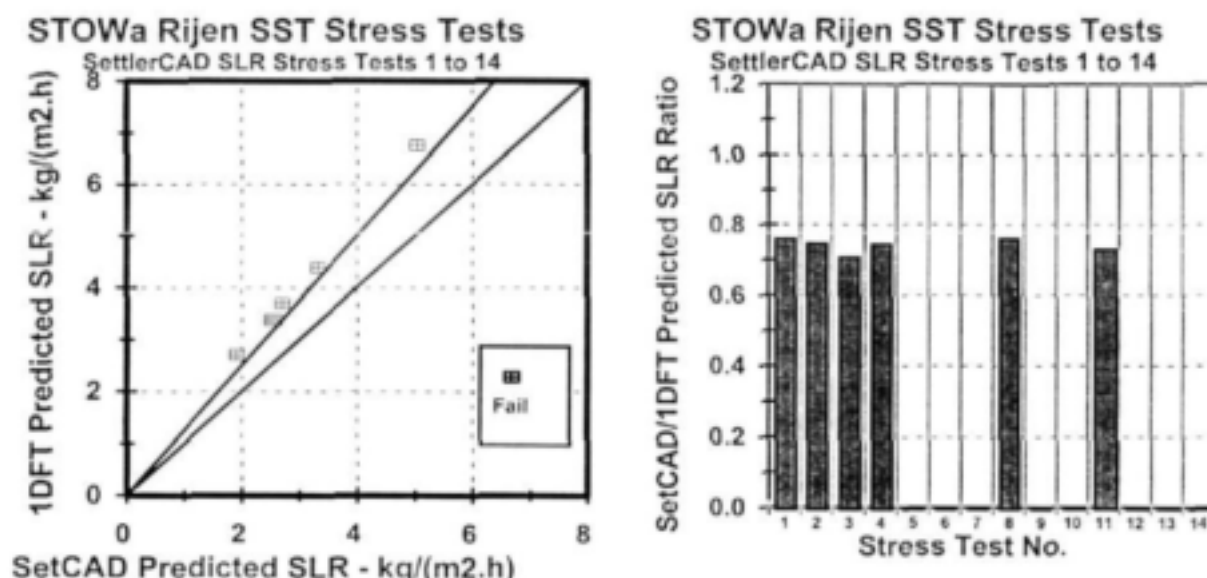
PARAMETER		STOWa Test #	Test 1	Test 2	Test 3	Test 4	Test 5	Test 6	Test 7	Test 8	Test 9	Test 10	Test 11	Test 12	Test 13	Test 14
		Q <sub>i</sub> = Influent flow (excl Q <sub>R</sub> ) Rijen #	Test 1	Test 2	Test 3	Test 4	Test 5	Test 6a	Test 6b	Test 7	Test 8	Test 9	Test 10	Test 11	Test 12	Test 13
Test Q <sub>i</sub> for 1 SST (m <sup>3</sup> /h)			1772.5	1772.5	1431.0	1431.0	1431.0	1203.4	1203.4	1203.4	1203.4	1024.5	1024.5	1024.5	845.6	845.6
% of 1DFT maximum Q <sub>i</sub>			84.6	79.9	96.9	120.4	78.5	109.7	119.2	132.2	82.4	100.3	56.4	35.1	58.8	27.7
1DFT predicted outcome			Safe	Safe	Safe	Fail	Safe	Fail	Fail	Fail	Safe	Fail	Safe	Safe	Safe	Safe
SettlerCAD predicted max Q <sub>i</sub> (m <sup>3</sup> /h)			1461.8	1396.9	959.7	749.1				564.4			1180.7			
% of SettlerCAD predicted max Q <sub>i</sub>			121.3	126.9	149.1	191.0				213.2			86.8			
SettlerCAD predicted outcome			Fail	Fail	Fail	Fail				Fail			Safe			
Observed test result			Fail	Fail	No Equil	Fail	Fail	No Equil	No Equil	Fail	Fail	Safe	Safe	Safe	Safe	Safe

**Table 11: Summary of the SettlerCAD simulation results for the SettlerCAD influent flow limit (top) and actual test influent flow (bottom) for the 14 SLR tests on the STOWa Rijen SST ( $Q_i$  = Influent flow in  $m^3/h$ ).**

SettlerCAD $Q_i$ LIMIT STOWa # Rijen Test #	Test 1 Test 1	Test 2 Test 2	Test 3 Test 3	Test 4 Test 4	Test 5 Test 5	Test 6 Test 6a	Test 7 Test 6b	Test 8 Test 7	Test 9 Test 8	Test 10 Test 9	Test 11 Test 10	Test 12 Test 11	Test 13 Test 12	Test 14 Test 13
Flux factor $V_d/(nX_f)$ - $m/h$	5.91	4.47	6.43	3.11	3.76	5.39	4.03	2.61	2.89	4.42	4.56	5.55	4.32	5.75
Influent Flow ( $m^3/h$ ) for 1 SST	1461.8	1396.9	959.7	749.1				564.4			1180.7			
% of IDFT maximum $Q_i$	69.75	63.00	65.00	63.00				62.00			65.00			
Overflow Rate ( $m/h$ )	0.90	0.86	0.59	0.46				0.35			0.73			
Recycle Flow ( $m^3/h$ )	531.8	1009.9	186.2	530.1				530.1			533.4			
Underflow Rate ( $m/h$ )	0.327	0.621	0.176	0.326				0.326			0.328			
Recycle Ratio	0.36	0.72	0.30	0.71				0.94			0.45			
Applied Flux ( $kgSS/(m^2 \cdot h)$ )	3.33	5.05	1.92	2.52				2.57			2.70			
% of IDFT maximum flux	75.9	74.6	70.7	74.4				76.0			72.9			
Actual Retention Time (h)	2.4	1.9	3.8	3.7				4.3			2.7			
Duration of Run (min)	4000	4000	4000	4000				4000			4000			
Duration of Run (# of $R_{90}$ )	28.4	34.2	17.7	18.2				15.6			24.4			
Sim time Step (min)	2.5	2.5	2.5	2.5				2.5			2.5			
Sim time Step (% $R_{90}$ )	1.77	2.14	1.11	1.14				0.97			1.52			
Effluent SS ( $mg/l$ )*	63.8	50.9	52.7	50.7				85.8			54.7			
Recycle Conc ( $mg/l$ )*	9494	8037	9942	7551				7672			7989.7			
Mass Balance (%)	94.8	99.8	93.0	98.7				98.4			98.6			
Test Result (ESS > 50 $mg/l$ )	Fail	Fail	Fail	Fail				Fail			Fail			
<b>ACTUAL TEST INFLUENT FLOW</b>														
Influent Flow ( $m^3/h$ ) for 1 SST	1772.5	1772.5	1431.0	1431.0	1431.0	1203.4	1203.4	1203.4	1203.4	1024.5	1024.5	1024.5	845.6	845.6
% of IDFT maximum $Q_i$	84.6	79.9	96.9	120.4	78.5	109.7	119.2	132.2	82.4	100.3	56.4	35.1	58.8	27.7
Overflow Rate ( $m/h$ )	1.09	1.09	0.88	0.88	0.88	0.74	0.74	0.74	0.74	0.63	0.63	0.63	0.52	0.52
Recycle Flow ( $m^3/h$ )	12.8	24.2	6.9	12.7	24.4	6.9	6.9	12.7	24.3	6.9	12.8	24.4	12.8	24.4
Underflow Rate ( $m/h$ )	0.327	0.621	0.176	0.326	0.625	0.178	0.178	0.326	0.622	0.176	0.328	0.624	0.328	0.624
Recycle Ratio	0.300	0.570	0.200	0.370	0.710	0.241	0.241	0.441	0.841	0.279	0.521	0.990	0.631	1.200
Applied Flux ( $kgSS/(m^2 \cdot h)$ )	3.85	5.83	2.64	3.86	5.49	3.21	2.66	4.07	4.69	2.50	2.45	3.64	2.99	3.20
% of IDFT maximum flux	87.7	86.2	97.4	114.1	86.2	107.7	114.9	120.3	89.6	100.3	66.3	51.9	70.0	45.7
Actual Retention Time (h)	2.0	1.7	2.7	2.4	1.9	3.1	3.1	2.7	2.1	3.6	3.0	2.3	3.4	2.5
Duration of Run (min)	4000	4000	4000	4000				4000			4000			
Duration of Run (# of $R_{90}$ )	32.8	39.6	24.4	27.9				24.7			22.2			
Sim time Step (min)	2.5	2.5	2.5	2.5				2.5			2.5			
Sim time Step (% $R_{90}$ )	2.05	2.47	1.53	1.74				1.54			1.39			
Effluent SS ( $mg/l$ )*	503.5	399.0	581.4	1271.3				1761.2			3.7			
Recycle Conc ( $mg/l$ )*	9258.9	8317.2	10591.5	7369.1				7500.5			7472			
Mass Balance (%)	92.8	96.0	90.0	91.2				60.7			100.0			
Test Result (ESS > 50 $mg/l$ )	Fail	Fail	Fail	Fail				Fail			Safe			
Observed Result	Fail	Fail	No Equil	Fail	Fail	No Equil	No Equil	Fail	Fail	Safe	Safe	Safe	Safe	Safe

\* Mean over the last 2  $R_{90}$  values.

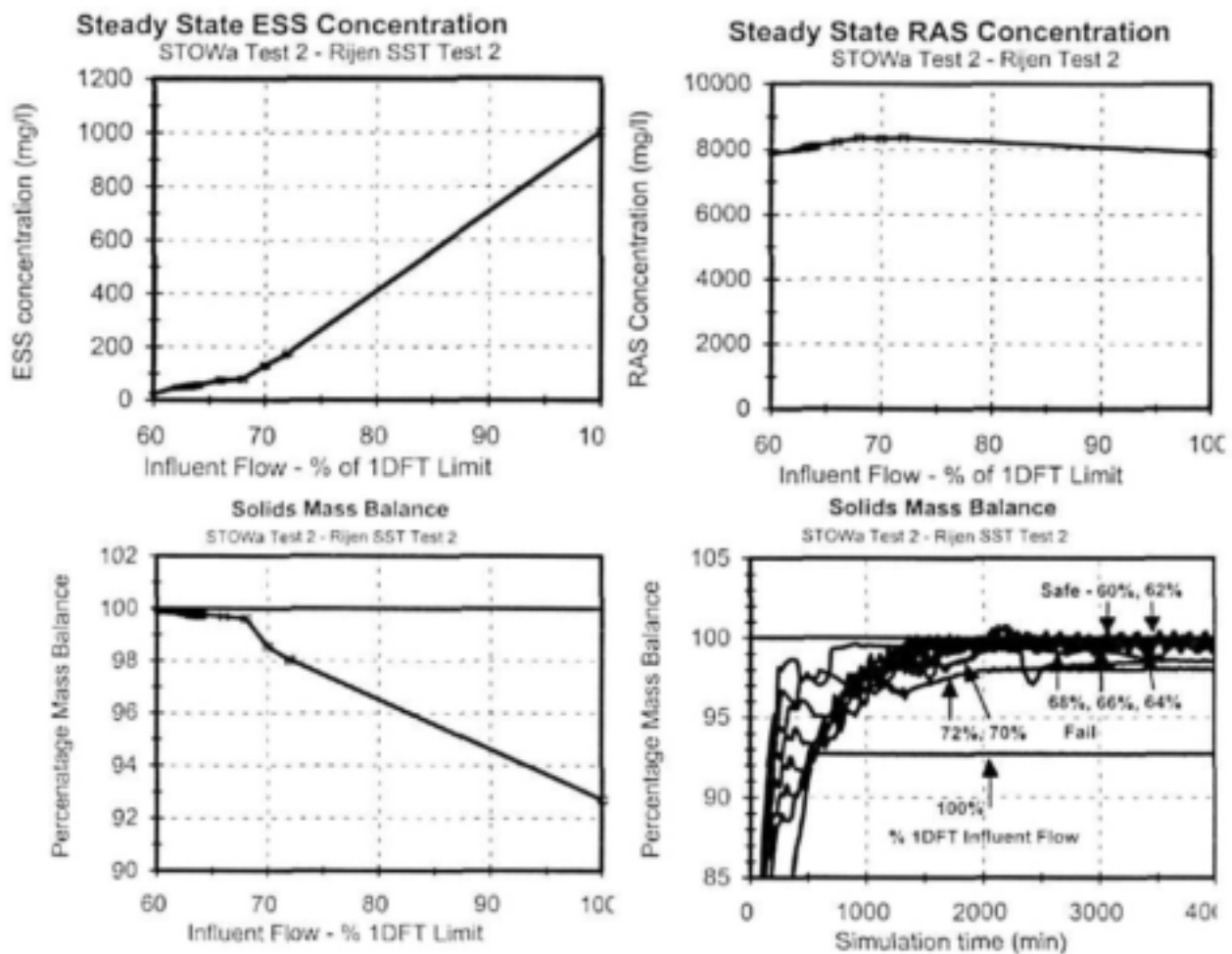
In Figs 18a and b (or Table 10) it can be seen that the SettlerCAD predicted flux rating of the Rijen SST ranges between 0.707 (Test 3) and 0.760 (Test 8). Fig 18a shows the SettlerCAD maximum predicted SLR (flux rating) of the 6 tests all fall above the 0.80 flux rating line indicating that the SettlerCAD maximum SLR is around 0.74 of the 1DFT maximum. The SettlerCAD predicted maximum SOR (as % of the 1DFT maximum) ranged between 62.0% (Test 8) and 69.7% (Test 1).



**Figs 18a and b:** 1DFT calculated maximum SLR versus SettlerCAD predicted maximum SLR (Fig 18a, left) and SettlerCAD predicted to 1DFT calculated maximum SLR ratios (Fig 18b, right) for SLR stress Tests 1, 2, 3, 4, 8 and 11 on the Rijen SST.

In the simulation runs, a simulation time of 4000 min was selected which was 18 to 34 times the actual hydraulic retention time ( $R_{ha}$ ) for all the SettlerCAD runs for determining the SettlerCAD predicted SOR and SLR limits (see Table 11) and 21 to 40 times  $R_{ha}$  of the actual tests. As for the Darvill and Watts SST runs, these run times were sufficiently long to establish a final steady state condition and the final ESS and RAS ( $X_R$ ) concentrations accepted for each run were the averages of the predicted values over the last  $2 \times R_{ha}$ . The solids mass balance was based on these final average ESS and RAS concentrations (which are listed in Table 11). The same pattern regarding the mass balance was observed - provided the run did not in the failure ( $ESS < 50$  mg/l), the run yielded a solids mass balance within 0.5% of 100% and runs that ended in failure ( $ESS > 50$  mg/l) yielded a lower than 99.5% solids mass balance; the greater the SST overload (i.e. the higher the ESS concentration), the lower the solids mass balance below 99.5%. The ESS, RAS and % mass balance versus influent flow (as% of the 1DFT limit  $Q_i$ ) for Test 2, which had the highest Test applied SLR and SOR, are shown in Figs 19a to c. In Fig 19d, the % mass balance versus simulation time for runs 1 to 8 of Test 2 at 60 to 72% of the 1DFT maximum influent flow are shown - it can be seen that for the failed runs, even though a final steady state is achieved, this steady state does not yield a mass balance.





**Figs 19a to d:** Final ESS and RAS concentrations (Figs 19a, top left and Fig 19b, top right) and % mass balance (Fig 19c, bottom left) versus influent flow as % 1DFT limit showing runs ended safe (●) and fail (⊗) and % mass balance versus simulation time (Fig 19d, bottom right) for the SettlerCAD runs on the Rijen SST Test 2.

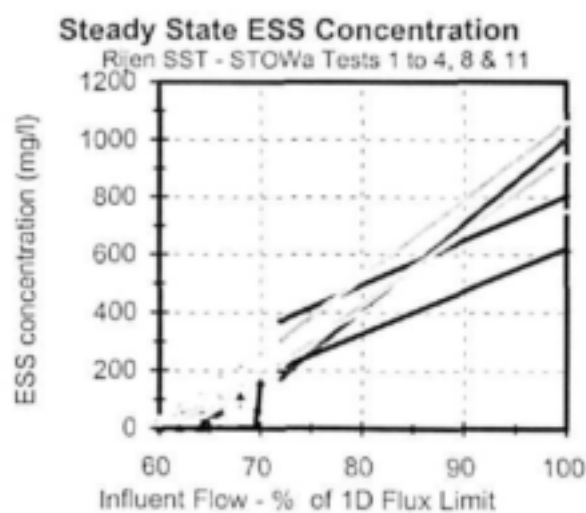
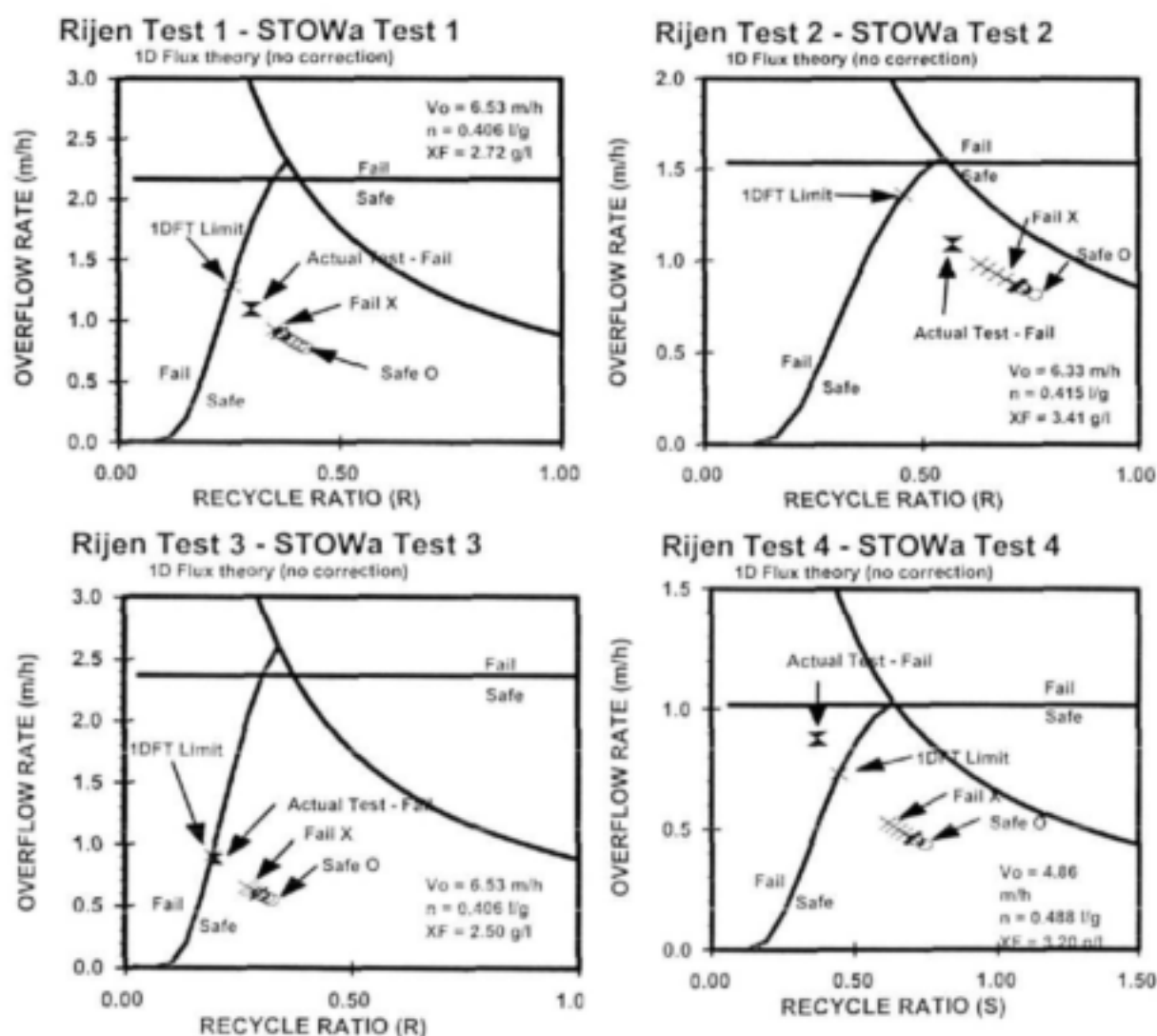


**Fig 20:** Final steady state ESS concentration versus influent flow as a % of the 1DFT SOR limit for the 6 Rijen SST tests simulated.

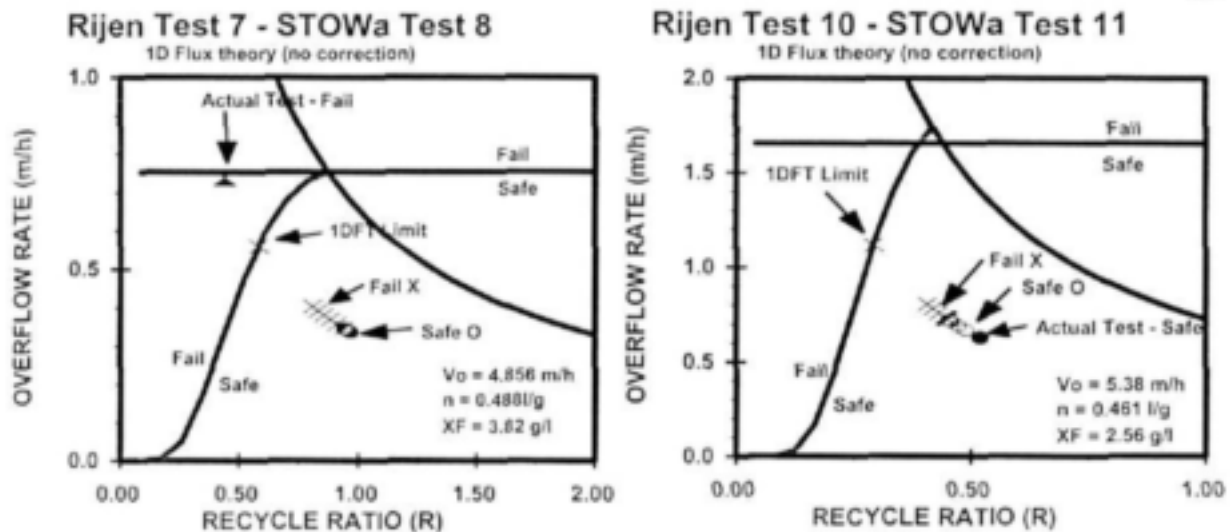
The final average ESS concentration versus  $Q_i$  (as a % of the 1DFT limit) for the 6 Rijen tests simulated are shown in Fig 20. It can be seen that the ESS concentration increases gradually above 50 mg/l in the range between 60 and 70% of the 1DFT limit influent flow. The gradual increase in ESS concentration of the shallow (2.25m SWD) Rijen resembles the gradual increase in ESS of the old (2.5m flat) Darvill SST. Compared with this SST, even though shallower, considerable extra volume exists in the Rijen SST from its 1:12 bottom slope and larger diameter ( $H_{ave} = 2.88\text{m}$ ).



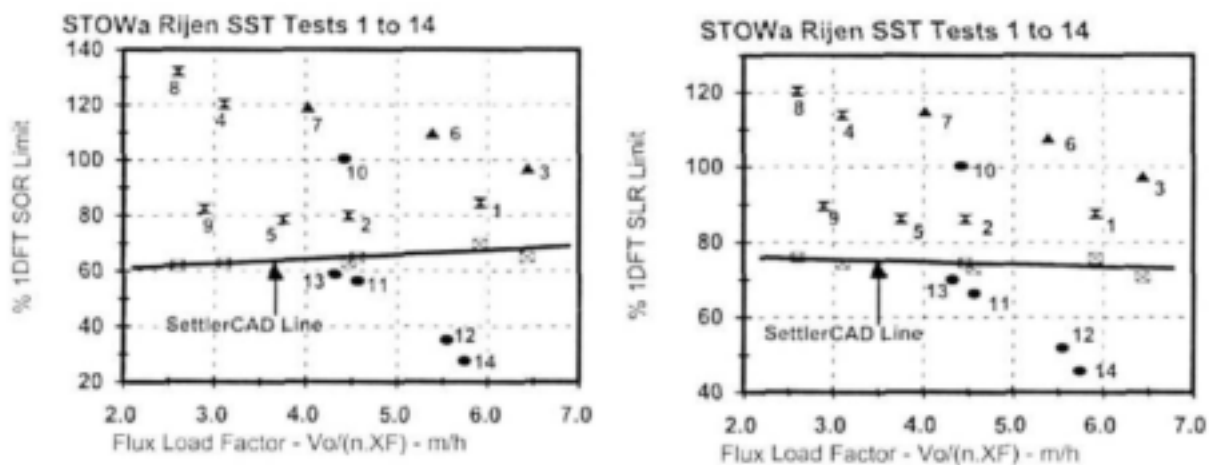
The position and result (safe O, fail X) of the SettlerCAD simulation runs for the 6 simulated Tests 1, 2, 3, 4, 8 and 11 are shown in the D&O charts in Figs 21a to f. The actual test position and result (safe ● or fail X) also is indicated. In the charts, the SettlerCAD predicted SOR limit is given at the transition from the safe to the fail positions. If the actual test position of the safe runs (●) is within or below the safe (O) runs, then SettlerCAD correctly predicted a safe result for the actual test. Similarly, if the actual test position of the fail tests (X) is within or above the fail (X) runs, then SettlerCAD correctly predicted a fail result for the actual test. From the six D&O charts, SettlerCAD correctly predicted the result for the 6 tests simulated if it is assumed that Test 3, which ended No Equilibrium (NE, ▲ in Fig 17a), ended fail. From Fig 17a, this is a reasonable assumption because it had Test/1DFT SLR ratio = 0.97 (this applies also to Tests 6 and 7 which ended NE because these had Test/1DFT SLR ratios of 1.08 and 1.15 respectively). In fact, had all 14 Rijen tests been simulated, SettlerCAD would have predicted the test result correctly of all the tests except Test 10. This can be seen in Fig 22a and b, which plot the SettlerCAD predicted maximum SOR and SLR versus the flux load factor.



*Figs 21a to d: 1DFT D&O charts showing the SST operating positions and result (Safe O, Fail X) of the SettlerCAD runs and actual tests (safe ●, fail X) for Tests 1 to 4 on the Rijen SST.*



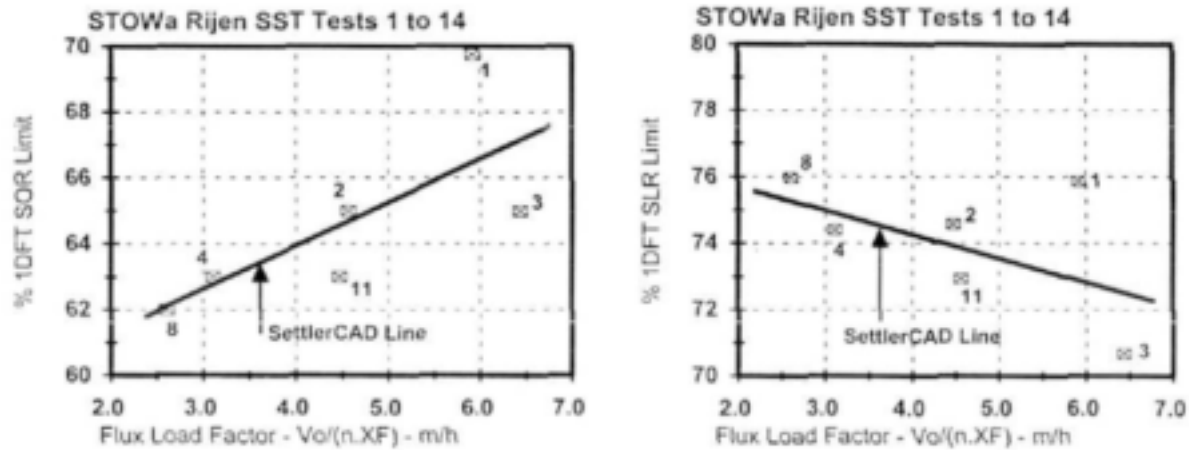
Figs 21e and f: 1DFT D&O charts showing the SST operating positions and result (safe O, fail X) of the SettlerCAD runs and actual tests (safe ●, fail X) for Tests 7 and 10 on the Rijen SST.



Figs 22a and b: SettlerCAD predicted maximum SOR (●) (Fig 22a, left) and SLR (▲) (Fig 22b, right), as a % of the 1DFT limit values versus flux load factor  $V_o/(nX_F)$ . Also shown are the 14 actual test points (safe ●, fail X or No Equil ▲) identified by test number.

Also shown in Figs 22a and b are the 14 actual test points (safe ●, fail X and no equil ▲). In these figures, the actual tests that ended safe (●) and fail (X, ▲) which plot *below* and *above* the SettlerCAD predicted SOR and SLR limits (line through ●) respectively, are the tests that SettlerCAD would predict correctly. Similarly, the actual tests that ended safe (●) and fail (X, ▲) which plot *above* and *below* the SettlerCAD predicted SOR and SLR limits (line through ●), are tests which SettlerCAD would predict incorrectly. Table 12 gives more detail on this listing the actual test SOR as a % of the SettlerCAD predicted maximum SOR, and the SettlerCAD predicted and observed result of the tests. From this, the only test which SettlerCAD would predict incorrectly is Test 10 (observed safe but SettlerCAD would predict fail). In Figs 22a and b, Tests 9, 5, 2 and 1 (all fail) plot at around 80% and 88% respectively of the 1DFT SOR and SLR limits above the "SettlerCAD lines" and Tests 13 and 11 (both safe) plot at around 60% and 70% of the 1DFT SOR and SLR limits below the "SettlerCAD lines". The gap between the safe

and fail tests therefore is quite large 15%. This means the SettlerCAD lines can plot in a 15% range and still predict 13 out of 14 test results correctly. Therefore unlike the Watts tests, the Rijen tests are therefore not very useful for checking the accuracy with which SettlerCAD predicts SST capacity.

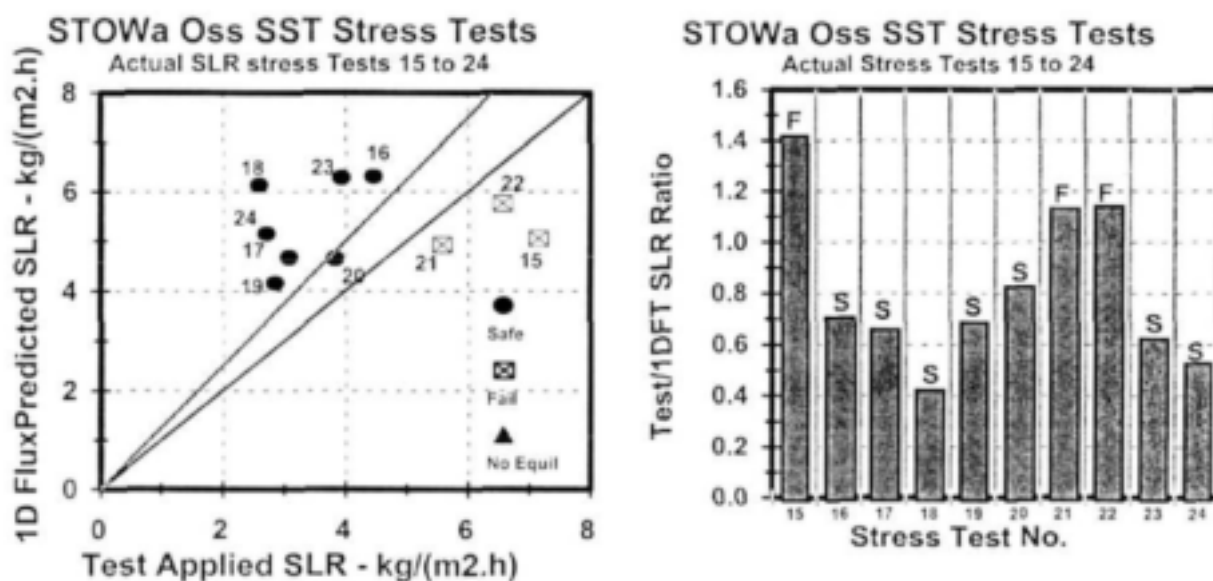


**Figs 23a and b:** SettlerCAD predicted maximum SOR (⊗) (Fig 23a, left) and SLR (⊗) (Fig 23b, right), as a % of the 1DFT limit values versus flux load factor  $V_d/(nX_F)$  for the six test simulated with SettlerCAD identified by test number.

Figures 23a and b, which are the same as Figs 22a and b but with a vertical scale range of only 10% of 1DFT limit SOR and SLR, show a small increasing and decreasing trend respectively in the SettlerCAD predicted SOR (⊗) and SLR (⊗) as the flux load factor increases for the 6 tests simulated - for the SOR (⊗, Fig 23a) from 62% (Test 8) to 67% (between Tests 1 and 3) and for the SLR (⊗, Fig 23b) from 76% (Test 8) to 74% (between Tests 1 and 3). This indicates that the Rijen SST has a low flux rating of around 74% of the 1DFT SLR limit (or a hydraulic capacity 64% of the 1DFT SOR limit) but it appears to be relatively insensitive to HLR variation arising from a wide range in flux load factor from 2.5 to 6.4 m/h.

#### 6.4 Simulating the Oss SST SLR stress tests with SettlerCAD

From the  $V_{0,n}$  and  $X_{F,n}$ , the 1DFT predicted maximum SOR and SLR were calculated for the 10 Oss SLR tests with the method described earlier in Section 3.2 and are listed in Table 13. The 1DFT predicted and test applied SLRs and the Test/1DFT SLR ratio from Table 13 are plotted in Figs 24a and b. Of the 10 tests, 3 tests ended fail (F,  $\square$ , Tests 15, 21 and 23) and 7 ended safe (S,  $\bullet$ , Tests 16 to 20, 22 and 24). From Fig 24b, the Test/1DFT maximum SLR ratios for the 10 tests are between 0.422 (Test 18) and 1.417 (Test 15). Tests 5, 21 and 22 all have Test/1DFT SLR ratios  $>1.10$  and therefore can be expected to fail and do. Of the 7 safe tests, it is expected that the 3 Tests 18, 23 and 24 end safe ( $\bullet$ ) because they have low ( $<0.65$ ) Test/1DFT maximum SLR ratios. The only possibly odd test of the 10 is Test 20, which at a Test/1DFT maximum SLR ratio of 0.823 ended safe ( $\bullet$ ). There are no incorrectly placed tests in Fig 24a - all safe tests plot above the diagonal and all fail tests below the diagonal. The safe test with the highest Test/1DFT maximum SLR ratio is Test 20 at 0.823, which is possibly close or slightly over the SettlerCAD predicted maximum SLR. The fail test with the lowest Test/1DFT maximum SLR ratio is Test 21 at 1.13. This makes the range between the highest safe and lowest fail tests very large (30%), with the result that the Oss tests are not useful to check the accuracy with which SettlerCAD predicts SST capacity.



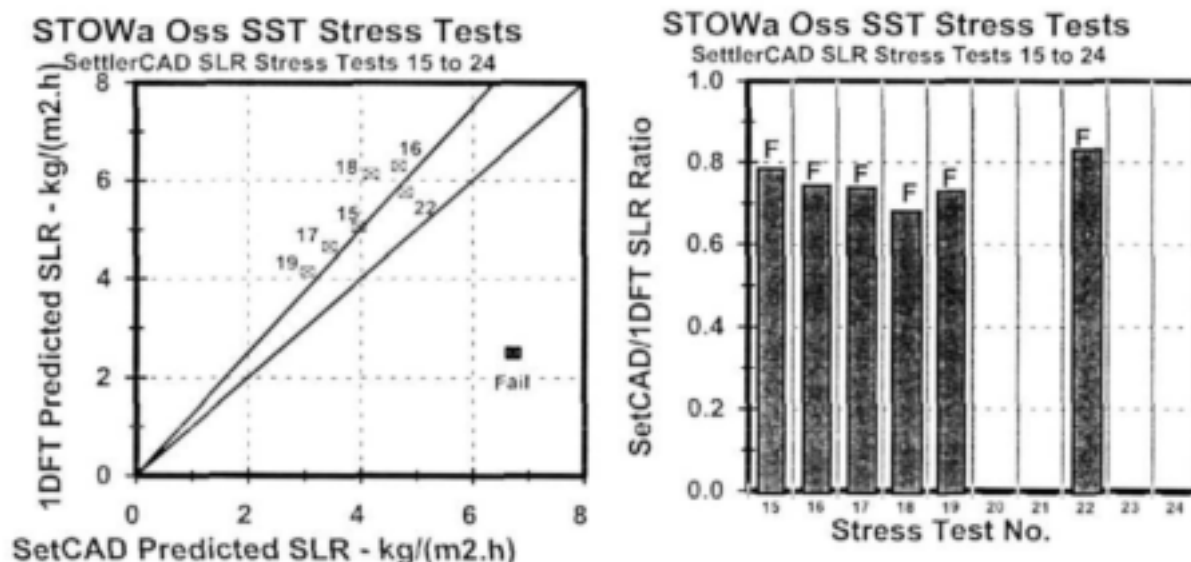
Figs 24a and b: 1DFT maximum SLR versus test applied SLR (Fig 24a, left) and Test/1DFT maximum SLR ratio (Fig 24b, right) for the 10 stress tests reported by STOWa (1981) on the Oss SST.

#### 6.5 Finding the SettlerCAD maximum SOR and SLR for the Oss SST.

The data given in Table 13 was given as input to SettlerCAD. Like for the Rijen tests, for 6 of the 10 Oss tests, 16 SettlerCAD runs per test were setup. The 6 tests selected were the 2 tests with the highest (Tests 18 and 17), the 2 tests with the lowest (Tests 22 and 15) and the 2 tests nearest the average flux load factor (Tests 16 and 19). SettlerCAD runs 1 to 7 for each of the 6

tests simulated were at  $Q_i$  from 60 to 72% of the 1DFT SOR in 2% increments and an 8<sup>th</sup> run at 100%. Runs 9 to 15 were setup between consecutive safe and fail runs at 0.25% increments and the 16<sup>th</sup> run was at the actual test  $Q_i$ . The first run with  $ESS > 50$  mg/l was accepted as the SettlerCAD predicted maximum influent flow rate limit. The SettlerCAD SLR limit was calculated from the  $Q_i$  limit and the test  $Q_R$  and  $X_F$  values. The SettlerCAD predicted results of the first failure runs are given in Table 14 and are shown plotted in Fig 25a and b. The results from the runs at the actual test influent flow rate are also given in Table 14.

In Fig 25a and b (or Table 14) it can be seen that the SettlerCAD predicted flux rating of the Oss SST ranges between 0.730 (Test 19) and 0.832 (Test 22). Fig 25a shows the SettlerCAD maximum predicted SLR (flux rating) of 5 of the 6 tests (not Test 22) fall above the 0.80 flux rating line indicating that the SettlerCAD maximum SLR is around 0.74 of the 1DFT maximum. The SettlerCAD predicted maximum SOR (as % of the 1DFT maximum) ranged between 60.2% (Test 15) and 63.5% (Test 19).



*Figs 25a and b: 1DFT calculated maximum SLR versus SettlerCAD predicted maximum SLR (Fig 25a, left) and SettlerCAD predicted to 1DFT calculated maximum SLR ratios (Fig 25b, right) for STOWa SLR stress Tests 15 to 19 and 22 on the Oss SST.*

**Table 13: Summary of the 10 SLR stress test results on the STOWA Oss SST.**

Parameter STOWa Test # Oss Test #		Test 15 Test 1	Test 16 Test 2	Test 17 Test 3	Test 18 Test 4	Test 19 Test 5	Test 20 Test 6	Test 21 Test 7	Test 22 Test 8	Test 23 Test 9	Test 24 Test 10
SST	Number of SSTs	1	1	1	1	1	1	1	1	1	1
	Surface area (m <sup>2</sup> )	1372	1372	1372	1372	1372	1372	1372	1372	1372	1372
Actual test loading conditions	Influent flow (M/d)	27.0	27.0	24.4	24.4	22.4	22.4	21.1	21.1	16.8	15.2
	Overflow rate (m/h)	0.82	0.82	0.74	0.74	0.68	0.68	0.64	0.64	0.51	0.46
	Recycle flow (M/d)	13.0	20.3	13.2	20.5	13.2	20.4	13.1	20.5	20.2	20.6
	Underflow rate (m/h)	0.394	0.615	0.400	0.622	0.401	0.619	0.397	0.621	0.612	0.626
	Recycle ratio	0.48	0.75	0.541	0.841	0.590	0.910	0.620	0.970	1.200	1.361
	Feed Concentration (g/l)	5.900	3.100	2.700	1.900	2.640	2.950	5.380	5.210	3.500	2.500
	Applied SLR [kgSS/(m <sup>2</sup> .h)]	7.16	4.45	3.08	2.59	2.85	3.83	5.58	6.57	3.93	2.72
	Weir loading rate [m <sup>3</sup> /(h.m)]	8.57	8.57	7.73	7.73	7.11	7.11	6.69	6.69	5.33	4.81
	HLR [(qA+qR), m/h]	1.214	1.435	1.140	1.362	1.081	1.299	1.037	1.261	1.122	1.086
Sludge settleability	V <sub>90</sub> (m/h)	6.53	5.94	5.94	5.94	5.20	4.37	6.33	5.38	5.94	4.86
	n (l/g)	0.406	0.433	0.433	0.433	0.470	0.515	0.415	0.460	0.433	0.488
	SSVI (DSVI) (m/g)*	90	100	100	100	(170)	130	(140)	110	100	120
IDFT predicted limits	Maximum SLR [kg/(m <sup>2</sup> .h)]	5.06	6.31	4.67	6.14	4.16	4.65	4.93	5.76	6.28	5.15
	Overflow rate (m/h)	0.463	1.419	1.330	2.607	1.174	0.956	0.520	0.485	1.184	1.434
	Influent Q <sub>i</sub> (excl Q <sub>R</sub> ) (m <sup>3</sup> /h)	653.3	1947.4	1825.5	3578.7	1611.5	1312.2	713.4	665.3	1624.5	1968.6
Flux ratings	Flux load factor [V <sub>90</sub> /(nX <sub>90</sub> ), m/h]	2.73	4.42	5.08	7.22	4.20	2.88	2.83	2.24	3.92	3.98
	Test/IDFT flux ratio	141.7	70.6	65.9	42.2	68.6	82.5	113.1	114.0	62.5	52.7
	Test/IDFT overflow rate ratio	177.2	57.8	55.6	28.4	57.9	71.1	123.1	132.0	43.1	32.1

**Table 15: Comparison of SettlerCAD predicted result with the actual Tests 1 to 10 on the STOWa Oss SST.**

PARAMETER STOWa Test # Q <sub>i</sub> = Influent flow (excl Q <sub>R</sub> ) Oss #		Test 15 Test 1	Test 16 Test 2	Test 17 Test 3	Test 18 Test 4	Test 19 Test 5	Test 20 Test 6	Test 21 Test 7	Test 22 Test 8	Test 23 Test 9	Test 24 Test 10
Test Q <sub>i</sub> for 1 SST (m <sup>3</sup> /h)		1125.4	1125.4	1015.6	1015.6	933.3	933.3	878.4	878.4	700.0	631.3
% of IDFT maximum Q <sub>i</sub>		177.2	57.8	55.6	28.4	57.9	71.1	123.1	132.0	43.1	32.1
IDFT predicted outcome		Fail	Safe	Safe	Safe	Safe	Safe	Fail	Fail	Safe	Safe
SettlerCAD predicted max Q <sub>i</sub> (m <sup>3</sup> /h)		382.7	1226.9	1204.8	2165.1	1027.3			410.8		
% of SettlerCAD predicted max Q <sub>i</sub>		294.0	91.7	84.3	46.9	90.8			213.8		
SettlerCAD predicted outcome		Fail	Safe	Safe	Safe	Safe			Fail		
Observed test result		Fail	Safe	Safe	Safe	Safe	Safe	Fail	Fail	Safe	Safe

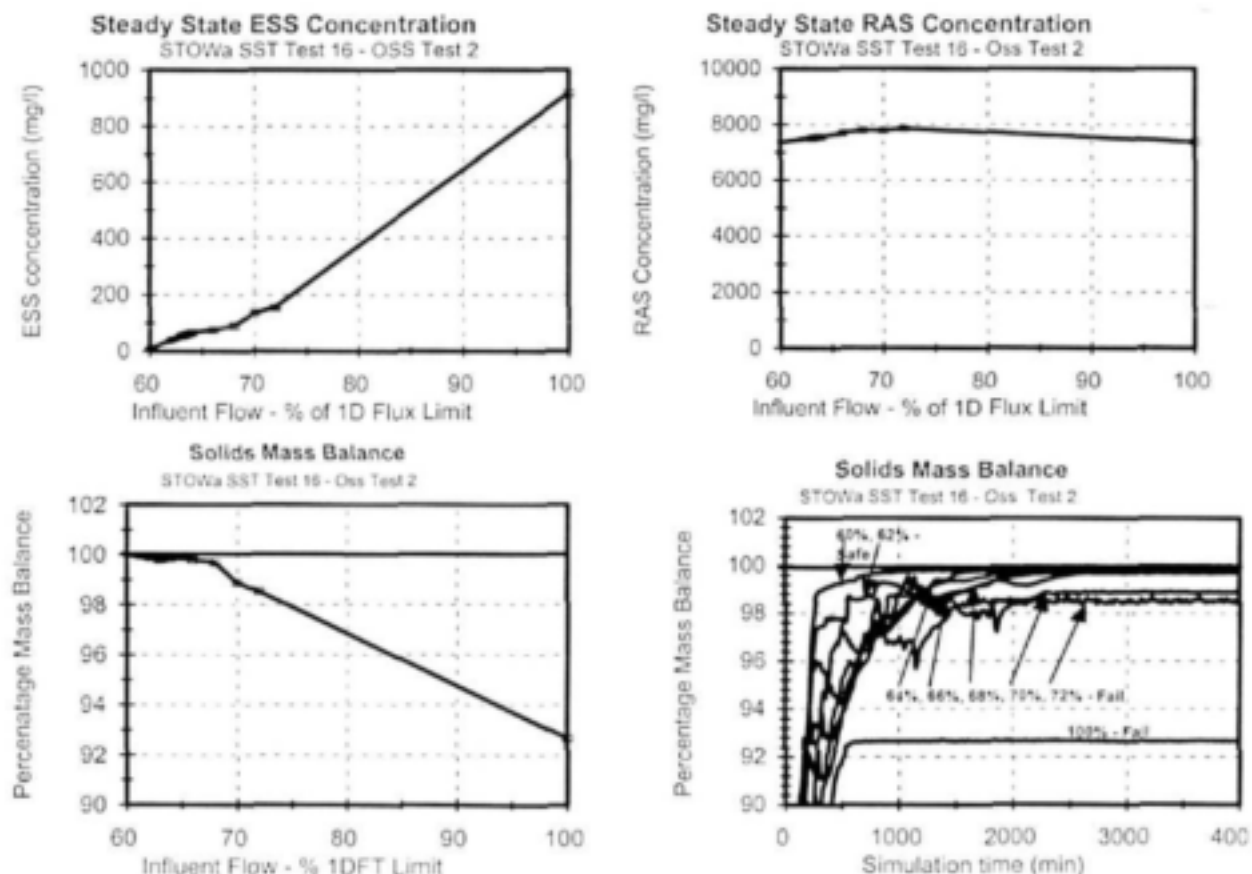
**Table 14:** Summary of the SettlerCAD simulation results for the SettlerCAD influent flow limit (top) and actual test influent flow (bottom) for the 10 SLR tests on the STOWa Oss SST ( $Q_i$  = Influent flow in  $m^3/h$ ).

SettlerCAD $Q_i$ LIMIT STOWa # Oss Test #	Test 15 Test 1	Test 16 Test 2	Test 17 Test 3	Test 18 Test 4	Test 19 Test 5	Test 20 Test 6	Test 21 Test 7	Test 22 Test 8	Test 23 Test 9	Test 24 Test 10
Flux factor $V_0/(nX_r)$ - $m/h$	2.73	4.42	5.08	7.22	4.20	2.88	2.83	2.24	3.92	3.98
Influent Flow ( $m^3/h$ ) for 1 SST	382.7	1226.9	1204.8	2165.1	1027.3			410.8		
% of 1DFT maximum $Q_i$	60.25	63.00	66.00	60.50	63.75			61.75		
Overflow Rate ( $m/h$ )	0.28	0.89	0.88	1.58	0.75			0.30		
Recycle Flow ( $m^3/h$ )	540.7	844.1	549.0	853.7	550.4			852.3		
Underflow Rate ( $m/h$ )	0.395	0.615	0.400	0.622	0.401			0.621		
Recycle Ratio	1.41	0.69	0.46	0.39	0.54			2.07		
Applied Flux ( $kgSS/(m^2 \cdot h)$ )	3.97	4.68	3.45	4.18	3.03			4.79		
% of 1DFT maximum flux	78.5	74.2	73.9	68.1	73.0			83.2		
Actual Retention Time (h)	3.8	1.7	2.0	1.2	2.2			2.8		
Duration of Run (min)	4000	4000	4000	4000	4000			4000		
Duration of Run (# of $R_{hd}$ )	17.4	39.0	33.0	56.8	29.7			23.8		
Sim time Step (min)	2.5	2.5	2.5	2.5	2.5			2.5		
Sim time Step (% $R_{hd}$ )	1.09	2.44	2.06	3.55	1.86			1.49		
Effluent SS ( $mg/l$ )*	64.8	54.9	63.6	50.1	50.9			52.1		
Recycle Conc ( $mg/l$ )*	9949	7510	8350	6585	7456			7670		
Mass Balance (%)*	99.2	99.8	98.4	99.9	99.8			99.7		
Test Result (ESS>50mg/l)	Fail	Fail	Fail	Fail	Fail			Fail		
ACTUAL TEST INFLUENT FLOW										
Influent Flow ( $m^3/h$ ) for 1 SST	1125.4	1125.4	1015.6	1015.6	933.3	933.3	878.4	878.4	700.0	631.3
% of 1DFT maximum $Q_i$	177.2	57.8	55.6	28.4	57.9	71.1	123.1	132.0	43.1	32.1
Overflow Rate ( $m/h$ )	0.82	0.82	0.74	0.74	0.68	0.68	0.64	0.64	0.51	0.46
Recycle Flow ( $m^3/h$ )	13.0	20.3	13.2	20.5	13.2	20.4	13.1	20.5	20.2	20.6
Underflow Rate ( $m/h$ )	0.394	0.615	0.400	0.622	0.401	0.619	0.397	0.621	0.612	0.626
Recycle Ratio	0.480	0.750	0.541	0.841	0.590	0.910	0.620	0.970	1.200	1.361
Applied Flux ( $kgSS/(m^2 \cdot h)$ )	7.16	4.45	3.08	2.59	2.85	3.83	5.58	6.57	3.93	2.72
% of 1DFT maximum flux	141.7	70.6	65.9	42.2	68.6	82.5	113.1	114.0	62.5	52.7
Actual Retention Time (h)	2.1	1.8	2.3	1.9	2.4	2.0	2.5	2.0	2.3	2.4
Duration of Run (min)	4000	4000	4000	4000	4000	4000	4000	4000	4000	4000
Duration of Run (# of $R_{hd}$ )	31.4	37.1	29.5	35.2	27.9	33.6	26.8	32.6	29.0	28.1
Sim time Step (min)	2.5	2.5	2.5	2.5	2.5	2.5	2.5	2.5	2.5	2.5
Sim time Step (% $R_{hd}$ )	1.96	2.32	1.84	2.20	1.75	2.10	1.67	2.04	1.81	1.75
Effluent SS ( $mg/l$ )*	2768.1	6.3	2.8	0.9	7.0			2036.3		
Recycle Conc ( $mg/l$ )*	10929.8	7224	7691.0	4159.4	7105.6			7926.0		
Mass Balance (%)*	91.8	100.0	100.0	100.0	100.0			94.8		
Test Result (ESS>50mg/l)	Fail	Safe	Safe	Safe	Safe			Fail		
Observed Result	Fail	Safe	Safe	Safe	Safe	Safe	Fail	Fail	Safe	Safe

\*Mean over the last 2  $R_{hd}$  values.



In the simulation runs, a simulation time of 4000 min was selected which was 18 to 57 times the actual hydraulic retention time ( $R_{ha}$ ) for all the SettlerCAD runs for determining the SettlerCAD predicted SOR and SLR limits (see Table 14) and 27 to 37 times  $R_{ha}$  of the actual tests. As for the the previous SST runs, these run times were sufficiently long to establish a final steady state condition and the final ESS ( $X_E$ ) and RAS ( $X_R$ ) concentrations accepted for each run were the averages of the predicted values over the last  $2 \times R_{ha}$ . The solids mass balance was based on these final average ESS and RAS concentrations (which are listed in Table 14). The same pattern regarding the mass balance was observed - provided the run did not in the failure ( $ESS < 50$  mg/l), the run yielded a solids mass balance within 0.5% of 100% and runs that ended in failure ( $ESS > 50$  mg/l) yielded a lower than 99.5% solids mass balance; the greater the SST overload (i.e. the higher the ESS concentration), the lower the solids mass balance below 99.5%. The ESS, RAS and % mass balance versus influent flow (as% of the 1DFT limit  $Q_i$ ) for Test 16, which is one of the safe tests, are shown in Figs 26a to c. In Fig 26d, the % mass balance versus simulation time for runs 1 to 8 of Test 16 at 60 to 72% of the 1DFT maximum influent flow are shown - it can be seen that for the failed runs, even though a final steady state is achieved, this steady state does not yield a mass balance.



**Figs 26a to d:** Final ESS and RAS concentrations (Figs 26a, top left and Fig 26b, top right) and % mass balance (Fig 26c, bottom left) versus influent flow as % 1DFT limit showing runs ended safe (●) and fail (⊗) and % mass balance versus simulation time (Fig 26d, bottom right) for the SettlerCAD runs on the STOWa Test 16 on the Oss SST.

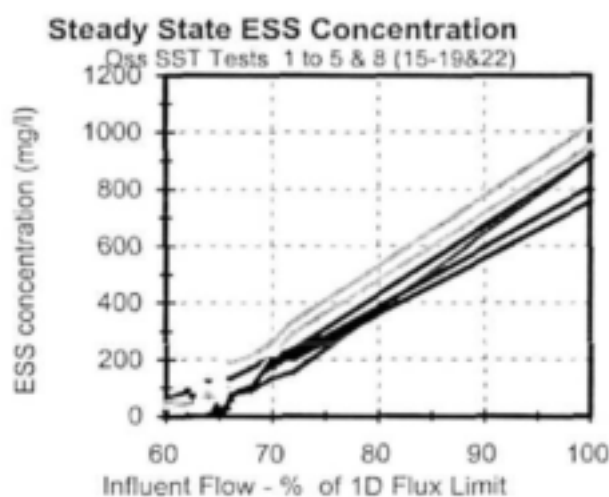
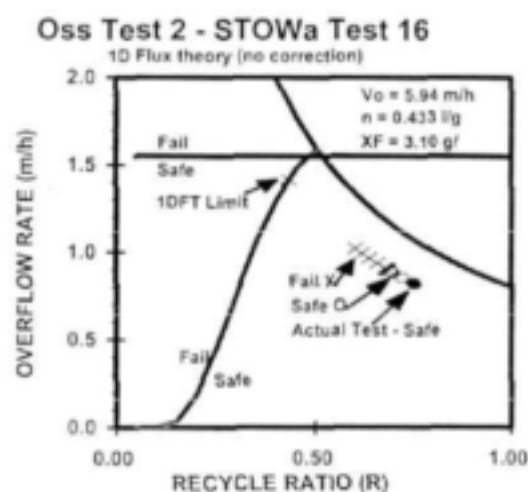
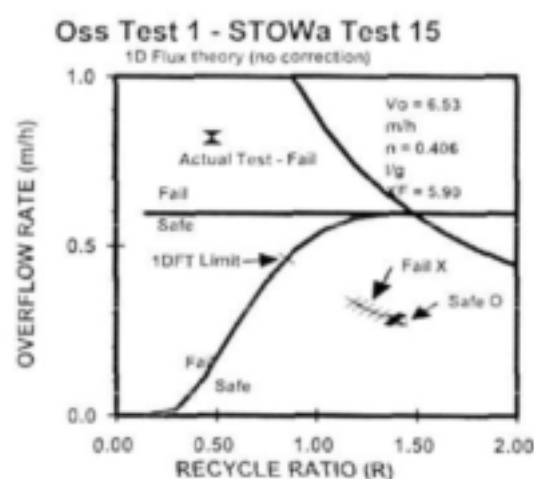


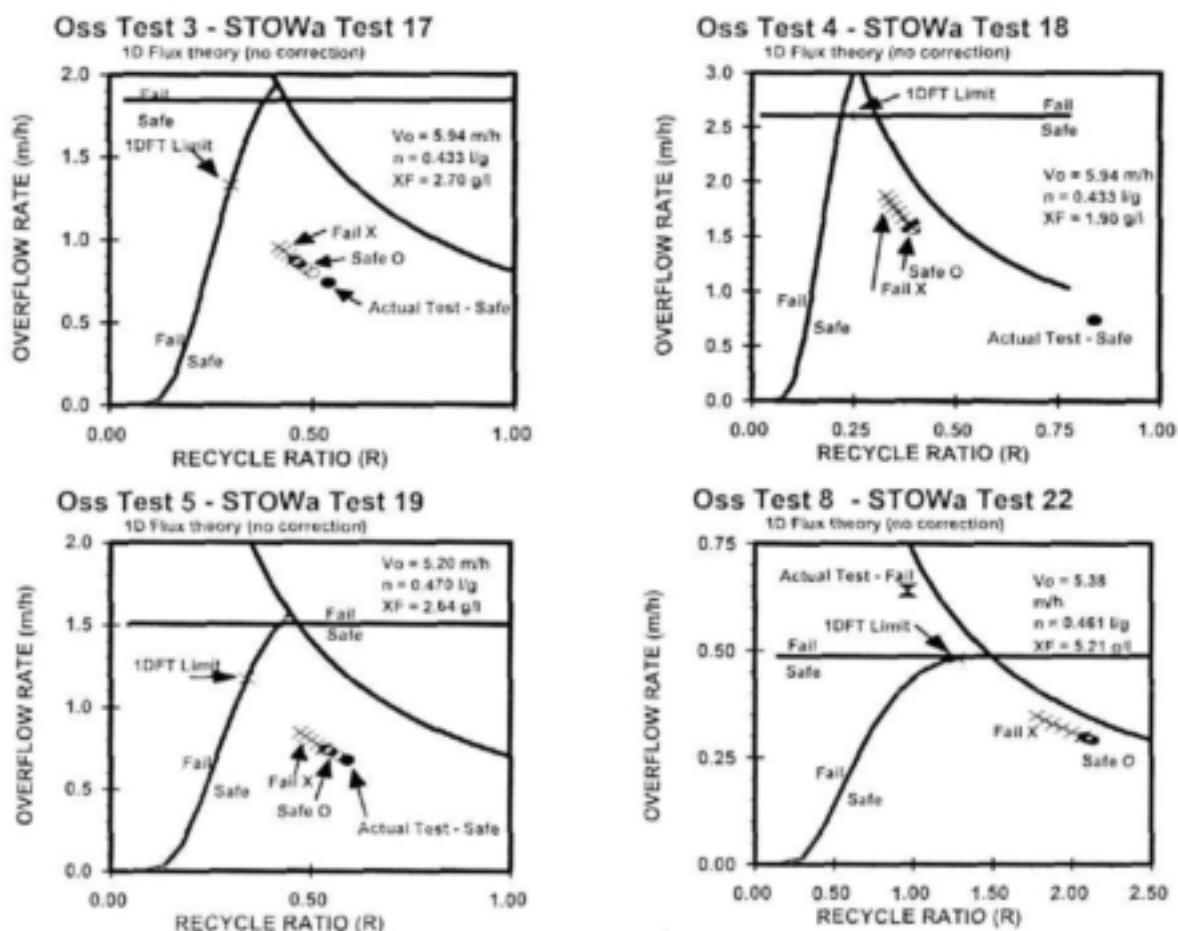
**Fig 27:** Final steady state ESS concentration versus influent flow as a % of the 1DFT SOR limit for the 6 Oss SST tests simulated.

The final average ESS concentration versus  $Q_i$  (as a % of the 1DFT limit) for the 6 Oss tests simulated are shown in Fig 27. It can be seen that the ESS concentration increases gradually above 50 mg/l in the range between 60 and 66% of the 1DFT limit influent flow. The gradual increase in ESS concentration of the shallow (2.0m SWD) Oss SST resembles that of the Darvill old and Rijen SSTs. This appears consistent because the average depths (adding the volume of the bottom cone as equivalent SWD) of these SSTs are 2.50 and 2.88m respectively, while that of the Oss SST is 2.58m.

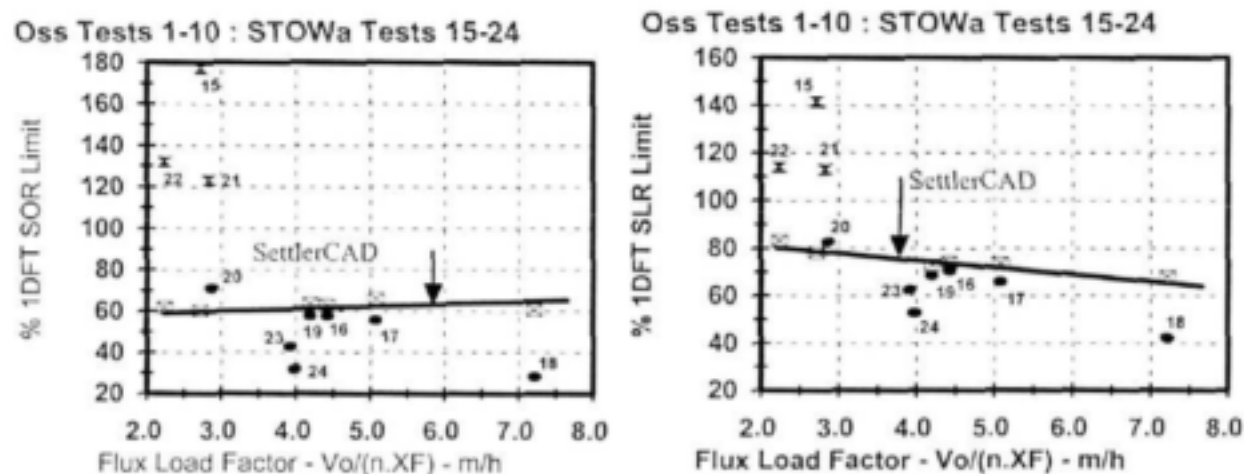
The position and result (safe O, fail X) of the SettlerCAD simulation runs for the simulated Tests 15 to 19 and 22 are shown in the D&O charts in Figs 28a to f. The actual test position and result (safe ● or fail X) also is indicated. In the charts, the SettlerCAD predicted SOR limit (for the test  $q_R$  and  $X_F$ ) is given at the transition from the safe to the fail positions. If the actual test position of the safe runs (●) is within or below the safe (O) runs, then SettlerCAD correctly predicted a safe result for the actual test. Similarly, if the actual test position of the fail tests (X) is within or above the fail (X) runs, then SettlerCAD correctly predicted a fail result for the actual test. From the 6 D&O charts, SettlerCAD correctly predicted the result for all 6 tests simulated. In fact, had all 10 Oss tests been simulated, SettlerCAD would have predicted the test result correctly of all the tests except possibly not Test 20. This is shown in Figs 29a and b, which plot the SettlerCAD predicted maximum SOR and SLR versus the flux load factor.



**Figs 28a and b:** 1DFT D&O charts showing the SST operating positions and result (safe O, fail X) of the SettlerCAD runs and actual tests (safe ●, fail X) for the STOWa Tests 15 and 16 on the OSS SST.



Figs 28c to f: 1DFT D&O charts showing the SST operating positions and result (safe O, fail X) of the SettlerCAD runs and actual tests (safe ●, fail X) for the STOWa Tests 17 to 19 and 22 on the OSS SST.

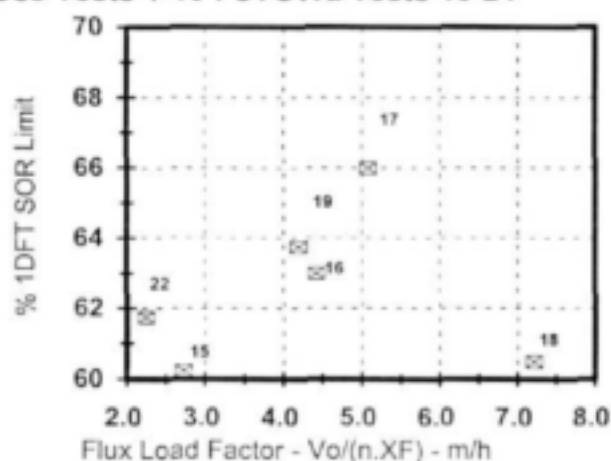


Figs 29a and b: SettlerCAD predicted maximum SOR (✂) (Fig 29a, left) and SLR (✂) (Fig 29b, right), as a % of the 1DFT limit values versus flux factor  $V_o/(n \cdot XF)$ . Also shown are the 14 actual test points (safe ●, fail X or No Equil ▲) identified by test number.

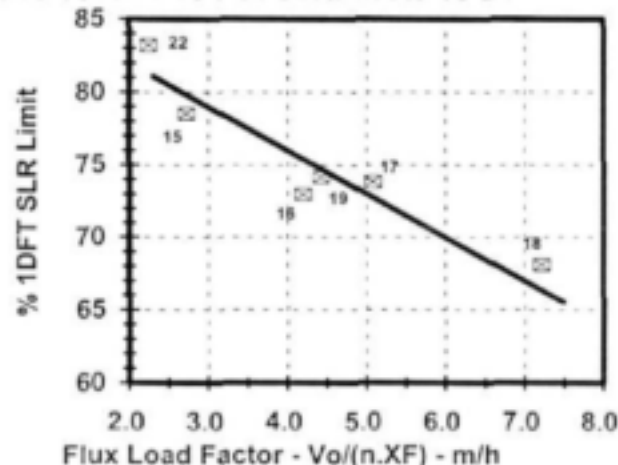
Also shown In Figs 29a and b are the 10 actual test points (safe ●, fail X). In these figures, the actual tests that ended safe (●) and fail (X) which plot below and above the SettlerCAD predicted SOR and SLR limits (line through ✂) respectively, are the tests that SettlerCAD would predict

correctly. Similarly, the actual tests that ended safe (●) and fail (✕) which plot *above* and *below* the SettlerCAD predicted SOR and SLR limits (line through ☼), are tests which SettlerCAD would predict incorrectly. Table 15 gives more detail on this listing the actual test SOR as a % of the SettlerCAD predicted maximum SOR, and the SettlerCAD predicted and observed result of the tests. From this, the only test which SettlerCAD would predict incorrectly is possibly Test 20, which ended safe but plots slightly above the SettlerCAD line. In Figs 29a and b, Tests 21 and 22 (both fail) plot at around 114% and 125% of the 1DFT SOR and SLR limits above the “SettlerCAD lines” and Tests 23, 19, 16 and 17 (all safe) plot at around 60% and 70% of the 1DFT SOR and SLR limits below the “SettlerCAD lines”. The gap between the safe and fail tests therefore is very large at 40%. This means the SettlerCAD lines can plot in a 40% range and still predict 10 out of 10 test results correctly. Therefore, like the Rijen tests but only worse so, the Oss tests are not useful for checking the accuracy with which SettlerCAD predicts SST capacity.

Oss Tests 1-10 : STOWa Tests 15-24



Oss Tests 1-10 : STOWa Tests 15-24

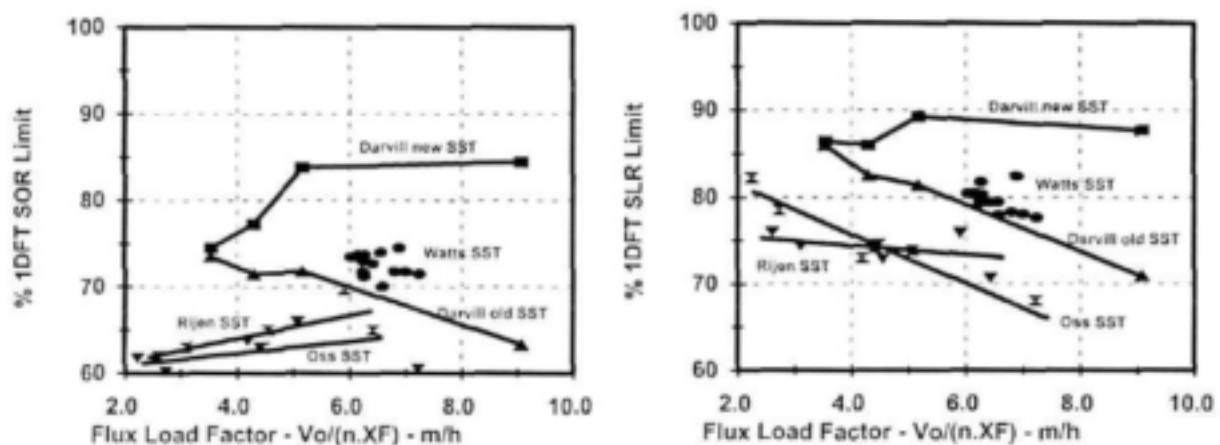


**Figs 30a and b:** SettlerCAD predicted maximum SOR (☼) (Fig 30a, left) and SLR (☼) (Fig 30b, right), as a % of the 1DFT limit values versus flux load factor  $V_d/(nX_p)$  for the six Oss SST tests simulated with SettlerCAD identified by test number.

Figures 30a and b, which are the same as Figs 29a and b but with a vertical scale range of only 10% and 25% of 1DFT limit SOR and SLR respectively, show a small increasing and decreasing trend respectively in the SettlerCAD predicted SOR (☼) and SLR (☼) as the flux factor increases for the 6 tests simulated - for the SOR (☼, Fig 30a) from 60% (Test 15) to 66% (Test 17) and for the SLR (☼, Fig 30b) from 82% (between Tests 15 and 22) to 68% (Test 18). This indicates that the Oss SST has a low hydraulic capacity of around 64% of the 1DFT SOR limit (or 74% of the 1DFT SLR limit) but appears to be relatively insensitive to hydraulic loading variation arising from a wide range in flux load factor from 2.5 to 6.4 m/h.

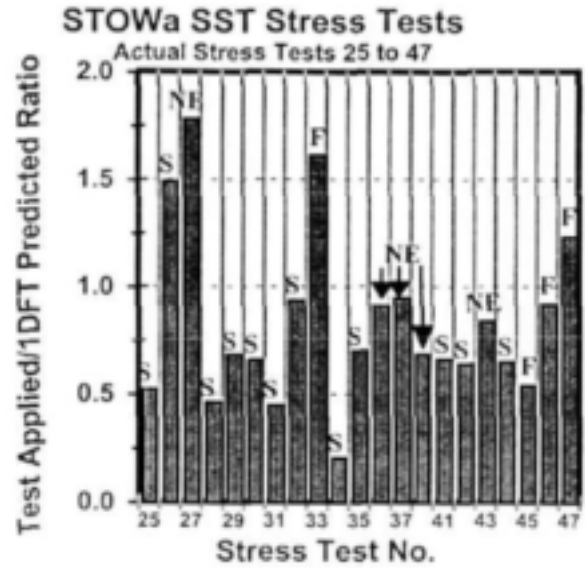
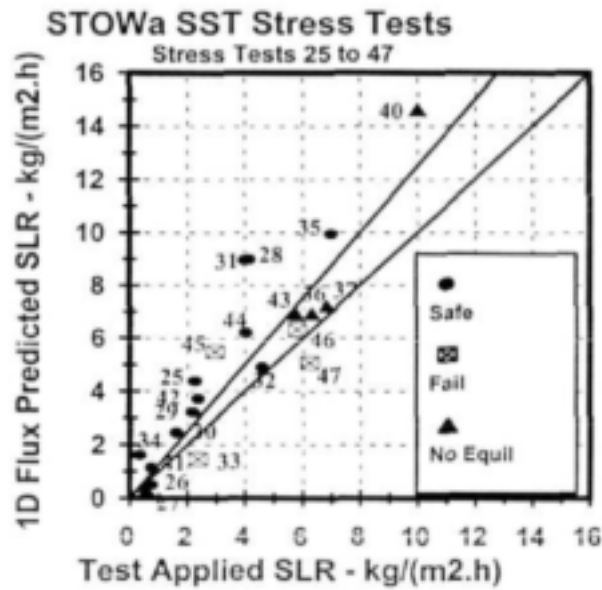
## 6.6 Conclusions from the Rijen and Oss SST simulations

To place the Rijen and Oss SettlerCAD simulation results in context of the Darvill and Watts simulation results, all the results are plotted together in Figs 27a and b. The Rijen (▼) and Oss (♠) SettlerCAD predicted SOR and SLR limit results lie below the Darvill old (▲) and new (■) and Watts (●) SST “lines”, but closer to the Darvill old SST line. Considering that with respect to external SST geometry, the Rijen (2.25 m SWD, 1:12 sloping bottom, 2.88m  $H_{ave}$ ) and Oss (2.0 m SWD, 1:12 sloping bottom, 2.58m  $H_{ave}$ ) SSTs are closer in likeness to the old Darvill SST (2.5m SWD and flat bottom) than the Darvill new (4.10 m SWD, 1:10 sloping bottom, 4.68m  $H_{ave}$ ) and Watts (3.66 m SWD, 1:15.4 sloping bottom, 3.97 m  $H_{ave}$ ), the expectation is that the Rijen and Oss results should fall near the old Darvill SST results, and this does indeed happen.



**Figs 31a and b:** SettlerCAD predicted maximum SOR (Fig 31a, left) and SLR (Fig 31b, right), as a % of the 1DFT limit values versus flux load factor  $V_d/(nX_p)$  for the 4 tests on the Darvill new (■) and old (▲) SSTs, 15 of the 15 tests on the Watts' SST (●), 6 each of the 14 and 10 tests on the Rijen (▼) and Oss (♠) SSTs.

The gap between the lowest loaded safe and highest loaded fail tests in the Rijen and Oss SST data sets is very wide, i.e. about 15% and 30% of the 1DFT SLR limit values respectively. These tests therefore do not help to provide additional validation of the accuracy with which SettlerCAD predicts SST failure. The same problem is apparent in the 23 remaining STOWa SST tests on the 23 different SSTs. In these 23 tests, the lowest and highest loaded safe tests are at 21 (Test 34) and 149% (Test 26) of the 1DFT SLR limit respectively, and the lowest and highest loaded fail tests are at 54 (Test 45) and 161% (Test 33) of the 1DFT SLR limit respectively. Eliminating the 7 tests with exceptionally high DSVIs (>400 mt/g) and/or low feed concentrations (< 0.6 g/l) (i.e. Tests 26, 27, 33, 34, 38, 39 and 41), reduces these gaps somewhat (i.e. for the safe tests from 45 to 94% and for the fail test from 54 to 123% of the 1DFT SLR limit) but not sufficiently to be able to provide additional validation of the accuracy with which SettlerCAD predicts SST failure (see Figs 32 a and b). Therefore none of these other 23 STOWa tests were simulated for this report. It was deemed more important to concentrate on evaluating the effect of SST depth and baffling on the flux rating. This is discussed in the next section.



*Figs 32a and b: 1DFT maximum SLR versus test applied SLR (Fig 32a, left) and Test/1DFT maximum SLR ratio (Fig 32b, right) for the 23 stress tests reported by STOWa (1981) on the 23 different SSTs.*

## 7 EFFECT OF BAFFLING AND DEPTH ON SST FLUX RATING (CAPACITY)

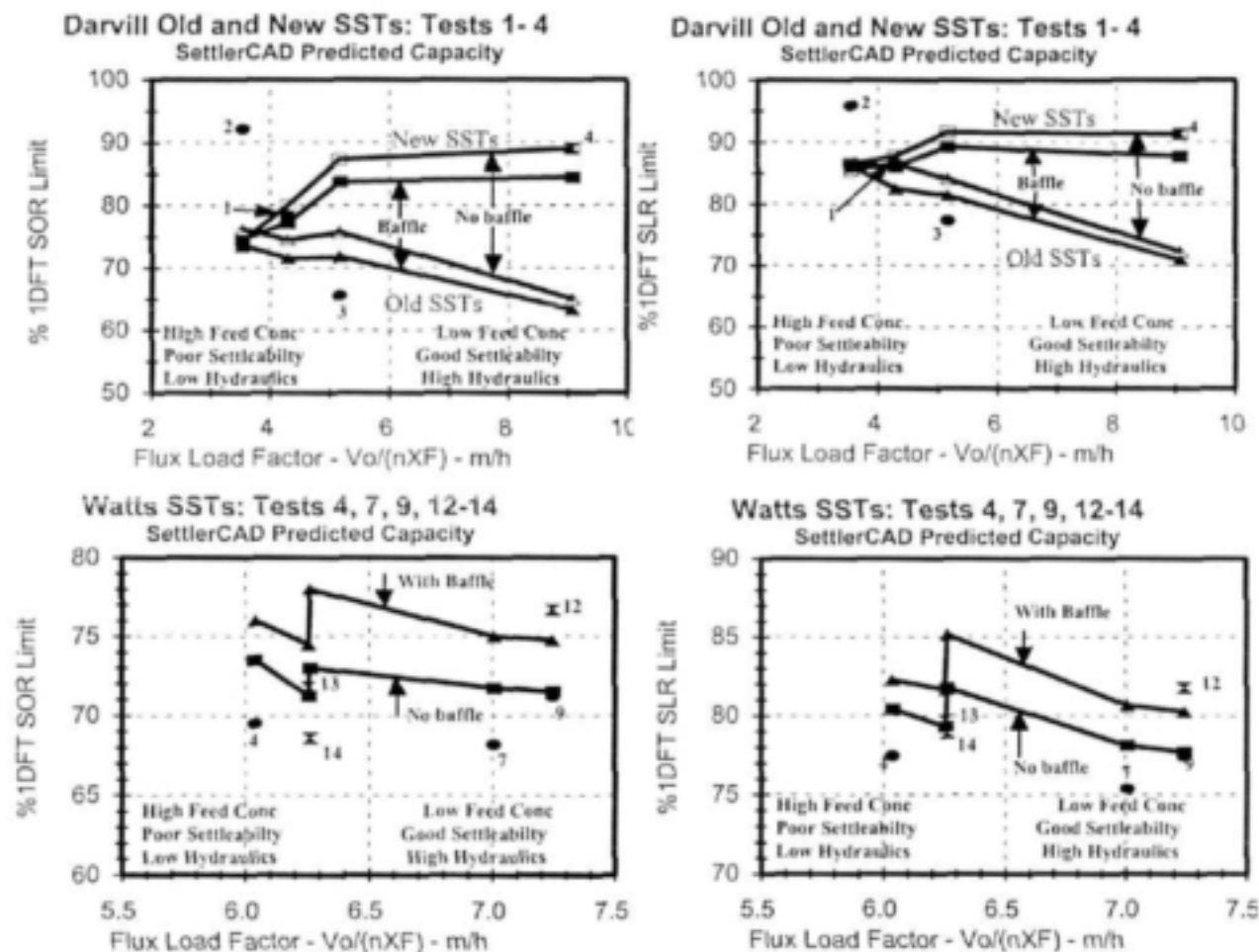
To evaluate the effect of the (i) Stamford baffle and (ii) SWD on the flux rating, the SettlerCAD predicted maximum SOR was determined for the 4 tests on the Darvill new and old SSTs (i) without Stamford baffles and (ii) with interchanged SWD. None of the other internal features were changed and were as listed in Table 1. The SettlerCAD predicted maximum SOR and associated SLR, HLR and actual retention time ( $R_{ta}$ ) are listed in Table 16 and compared with the results for the SSTs as built. Similarly, the SettlerCAD predicted maximum SOR was determined for the Watts SST (i) with a Stamford baffle extending 1.2 m from the side wall and 0.5 m below the water surface and (ii) with a 6.0 m SWD. None of the other internal features were changed. Not all 15 Watts tests were simulated. Six tests were selected that (i) represent the full range of flux load factor for all 15 tests (ii) lie closest to the previously predicted SettlerCAD line (Fig 15) and (iii) include both safe and fail tests. The SettlerCAD predicted maximum SOR and associated SLR, HLR and actual retention time ( $R_{ta}$ ) for the Watts SST are listed in Table 17 and compared with the results for the SSTs as built.

### 7.1 The Effect of baffling on SST flux rating (capacity)

The SettlerCAD predicted maximum SOR and associated SLR, HLR and actual retention time ( $R_{ta}$ ) for the Darvill new and old and Watts SSTs with and without Stamford baffles are shown in Figs 33a to d. For the Darvill SSTs, the flux rating (SLR, Fig 33b) of the new SST (4.1m SWD, 1:10 sloping bottom, scraper sludge collection) and old SST (2.5m SWD, flat bottom, suction sludge collection) is respectively 1.7 to 2.6% and 1.4 to 1.8% of the 1DFT limit SLR *higher* without the Stamford baffle. For the old SST, the increase in flux rating without the Stamford baffle decreases as the flux load factor (or HLR) increases, but for the new SST, increase appears insensitive to flux load factor. In contrast, for the Watts SST (3.66m SWD, 1:15.4 sloping bottom, suction sludge collection), the flux rating is about 2% of the 1DFT limit SLR *lower* without the Stamford baffle and is closely the same across the (narrow) flux load factor range.

From the above, it is concluded that while the Stamford baffle has a significant effect on the ESS concentration while the SST is underloaded, its influence on the flux rating (or capacity) is small and variable. With a Stamford baffle, the flux rating of the Darvill new and old SSTs is about 2% (of 1DFT SLR limit) *lower* while the flux rating of the Watts SST is about 2% (of 1DFT SLR limit) *higher*. This small influence of the Stamford baffle is in conformity with the expectation from Fig 1 - good internal feature design will keep ESS concentration lower while the SST is underloaded, (defined in this report as  $ESS < 50 \text{ mg/l}$ ) while the capacity is not significantly affected.

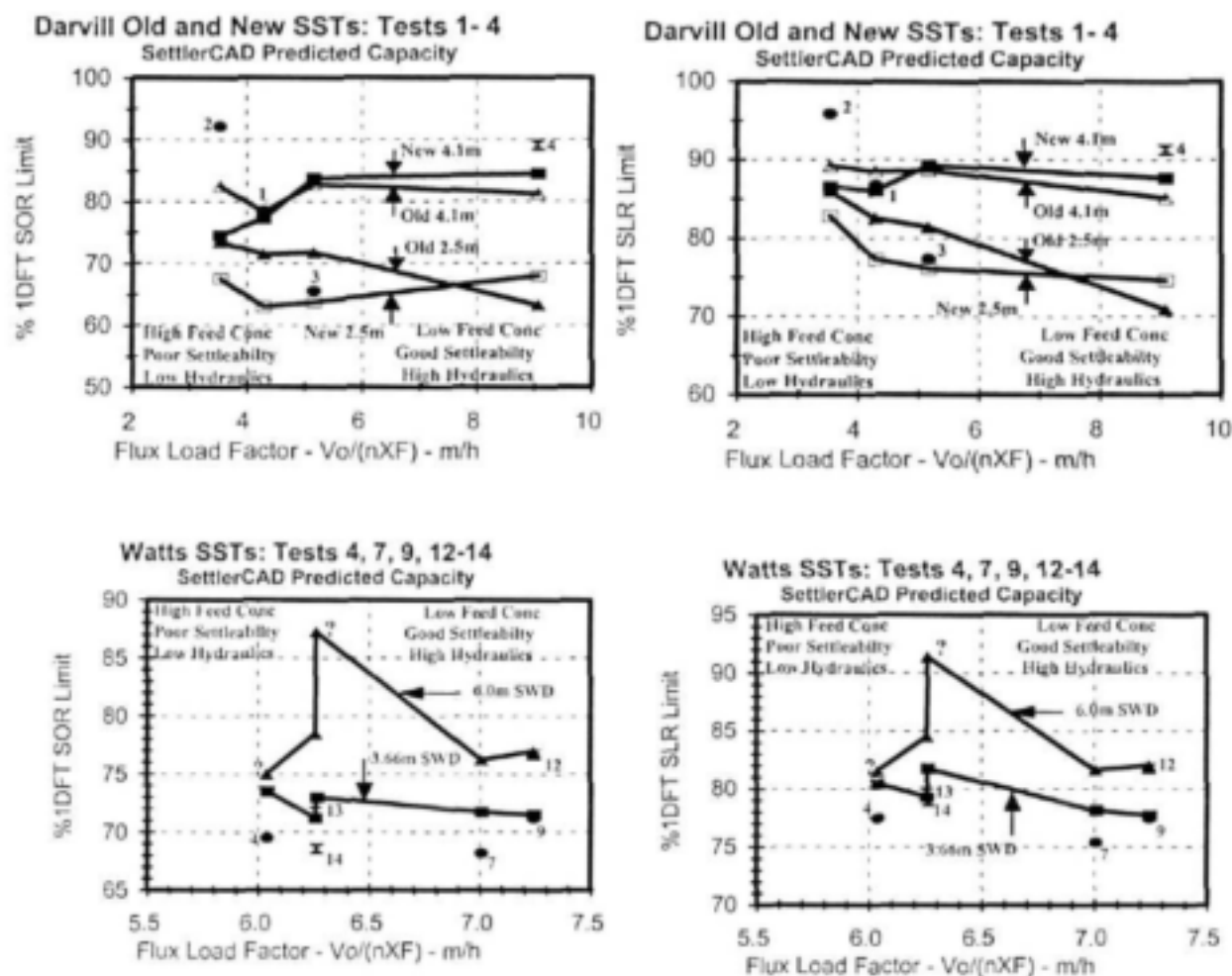




*Figs 33a to d: SettlerCAD predicted maximum SOR (Figs 33a and c, left) and SLR (Fig 33b and d, right) for the Darvill (top) and Watts (bottom) SSTs with and without baffles. The actual test values, identified by number and result (safe ●, fail ✕), are also shown.*

## 7.2 The Effect of depth on SST flux rating (capacity)

The SettlerCAD predicted maximum SOR and associated SLR, HLR and actual retention time ( $R_{10}$ ) for the Darvill new and old SSTs with interchanged depths (i.e. new 2.5 m SWD, 1: 10 sloping bottom and scraper sludge collection and old 4.1 m SWD, flat bottom and suction sludge collection) and the Watts SST with 6.0 m SWD are compared with that of the SSTs as built, (i.e. new 4.1 m SWD, 1: 10 sloping bottom and scraper sludge collection, old 2.5 m SWD, flat bottom and suction sludge collection and Watts with 3.66 m SWD, 1:15.4 sloping bottom and suction sludge collection) in Figs 34a to d.



**Figs 34a to d:** SettlerCAD predicted maximum SOR (Figs 34a and c, left) and SLR (Fig 34b and d, right) for the Darvill new and old SSTs (top) with interchanged SWD (old 4.1m and new 2.5m) and the Watts SST (bottom) with a SWD of 6.0 m compared with the SSTs as built (new 4.1m, old 2.5m and Watts 3.66m). The actual test values, identified by number and result (safe ●, fail ✕) are also shown.

The SettlerCAD predicted maximum SOR and SLR for the Darvill new and old SSTs with interchanged SWD are compared in Figs 34a and b, and for the Watts SST with SWD of 3.66 (as built) and 6.0 m in Figs 34c and d.

For the Darvill SSTs, the 4.1m SWD old SST has approximately the same flux rating (SLR) as the new 4.1 m SST (Fig 34b) and shows a small decrease from 89 to 85% of 1DFT SLR limit as flux load factor increases from 3 to 9 m/h. Likewise 2.5 m new SST has a similarly low flux rating as the 2.5 m old SST - the only difference is that the flux rating of the 2.5 m old SST decreases approximately linearly from 85 to 70% of 1DFT SLR limit as flux load factor increases from 3 to 9 m/h, whereas the flux rating of the new 2.5 m SST decreases from 82 to 78% of 1DFT SLR for flux load factor from 3.5 to 4.2 m/h and thereafter remains approximately constant at 76% of 1DFT SLR for flux load factor from 4.2 to 9 m/h. The differences in flux rating between

the new and old SSTs with the same SWD probably arise from the different SST bottoms and sludge collection systems, which for the old SST is flat and hydraulic suction and for the new SST is sloping 1:10 and scraper, differences which SettlerCAD can take into account, but the accuracy with which it simulates these is unknown.

For the Watts SST, 3.66 m SWD (as built) the 1DFT SLR limit (Fig 34d) shows a slight decreasing trend from 80 to 77% of 1DFT SLR as sludge load factor increases from 6.0 to 7.3 m/h. For Test 13 and 14 conditions ( $X_F$  and  $q_R$ ), the same flux load factor of 6.3 m/h leads to SettlerCAD predicted SLR predicted limits of 79 and 82% respectively. The feed concentration for Tests 13 and 14 are the same (3.98 g/l), but the underflow rate ( $q_R$ ) is significantly different at 0.84 m/h for Test 13 and 1.08 m/h for Test 14. However, the higher  $q_R$  of Test 14 does not give a significantly higher 1DFT SOR (Table 17) because the Test 13  $q_R$  value is already close to the SHC I one limit (see Fig 13f). So the higher HLR for Test 14 is mainly due to the higher  $q_R$ . Curiously, Test 13 with the lower HLR (2.38 m/h) has the lower SettlerCAD predicted SOR (71.25% of 1DFT SOR) compared with Test 14 (73.0% of 1DFT SOR) (Fig 34d). It was expected that this should be the other way around, i.e. Test 13 with the lower HLR should have the higher SettlerCAD predicted %1DFT SOR. The fact that this was not the case, indicated that low HLRs do not necessarily lead to high flux rating values. While no unusual features were observed in the flow field and velocity vectors of Test 14, its result was regarded spurious. With the 6.0 m SWD, the difference between Tests 13 and 14 is much greater - from 84 to 91% of 1DFT SLR (Fig 34d). It is not clear why Test 14 conditions lead to such an unusually a high flux rating of 91%. Moreover, in Fig 34d, for Test 4, there is a very little difference in the flux rating (SLR) of the 6.0 m and 3.66 m SWD SSTs - both are around 81%. For the 6.0 m SST, this is 10% of 1DFT SLR lower than for Test 14. Examining the flow field for Test 4, it was noticed that from around the middle of the simulation run time, the sludge blanket developed a seiche that persisted to the end of the run; also the velocity vectors were alternatively clockwise and anti-clockwise at successive simulation steps. It was concluded that for form of stable resonant oscillation developed in the SST that did not cause numerical instability. The results of Test 4 are therefore considered spurious and are marked ? in Figs 34c and d. Ignoring Tests 4 and 14, the Watts SST with a 6.0 m SWD has a flux rating of about 5% of 1DFT SLR higher than with a 3.66 m SWD.

From the above it is clear that the greater the SWD, the higher the flux rating. However, an increase in SWD from 3.66 to 6.0m represents a 60% increase in SST volume. For a 5% of 1DFT SLR increase in flux rating this volume increase is definitely not cost efficient - it would be better to select the shallower SWD (3.66m for the Watts SST) and increase the surface area to accommodate the lower flux rating.

**Table 16:** 1DFT calculated, test applied and SettlerCAD predicted SOR and associated SLR, HLR and actual retention time ( $R_{\text{act}}$ ) for the Darvill new and old SSTs (i) as built, (ii) without Stamford baffles and (iii) with interchanged SWD.

	Test 1		Test 2		Test 3		Test 4	
	New	Old	New	Old	New	Old	New	Old
<b>1DFT CALCULATED</b>								
1DFT SOR, m/h	1.104	1.104	0.775	0.775	1.503	1.503	2.796	2.796
1DFT SLR, kg/(m <sup>2</sup> h)	8.26	8.26	6.31	6.31	8.22	8.22	12.19	12.19
1DFT HLR, m/h	1.80	1.80	1.47	1.47	2.28	2.28	3.53	3.53
$V_o/(nX_p)$ , m/h	4.30	4.30	3.55	3.55	5.17	5.17	9.08	9.08
$q_R$ , m/h	0.693	0.693	0.693	0.693	0.779	0.779	0.736	0.736
$H_{\text{ave}}$ , m	4.68	2.50	4.68	2.50	4.68	2.50	4.68	2.50
$X_R$ , g/l	4.60	4.60	4.30	4.30	3.60	3.60	3.45	3.45
<b>TEST APPLIED</b>								
%1DFT SOR	78.5	78.5	92.1	92.1	65.6	65.6	89.1	89.1
%1DFT SLR	86.79	86.79	95.83	95.83	77.35	77.35	91.37	91.37
HLR, m/h	1.56	1.56	1.41	1.41	1.76	1.76	3.23	3.23
Act Ret Time, $R_{\text{act}}$ , h	3.00	1.60	3.33	1.78	2.65	1.42	1.45	0.77
<b>(i) SETTLERCAD PREDICTED RESULTS FOR SSTs AS BUILT</b>								
%1DFT SOR	77.25	71.50	74.50	73.50	83.75	71.75	84.50	63.25
%1DFT SLR	86.02	82.49	86.53	86.00	89.30	81.40	87.73	70.91
HLR, m/h	1.55	1.48	1.27	1.26	2.04	1.86	3.10	2.50
Act Ret Time, $R_{\text{act}}$ , h	3.03	1.69	3.69	1.98	2.30	1.35	1.51	1.00
<b>(ii) SETTLERCAD PREDICTED RESULTS FOR SSTs WITH SWITCHED DEPTHS</b>								
%1DFT SOR	63.00	78.25	67.50	82.50	63.75	82.75	78.50	81.25
%1DFT SLR	77.27	86.64	82.84	90.76	76.13	88.64	82.98	85.16
HLR, m/h	1.39	1.56	1.22	1.33	1.74	2.02	2.93	3.01
Act Ret Time, $R_{\text{act}}$ , h	3.37	1.61	3.85	1.88	2.70	1.24	1.60	0.83
<b>(iii) SETTLERCAD PREDICTED RESULTS FOR SSTs WITH NO STAMFORD BAFFLES</b>								
%1DFT SOR	80.00	74.50	74.30	76.25	87.30	75.80	89.00	65.00
%1DFT SLR	87.71	84.33	86.43	87.46	91.64	84.06	91.29	72.29
HLR, m/h	1.58	1.51	1.27	1.28	2.09	1.92	3.22	2.55
Act Ret Time, $R_{\text{act}}$ , h	2.97	1.65	3.69	1.95	2.24	1.30	1.45	0.98

**Table 17:** 1DFT calculated, test applied and SettlerCAD predicted SOR and associated SLR, HLR and actual retention time ( $R_{ha}$ ) for the Watts SSTs (i) as built, (ii) with Stamford baffle and (iii) with 6.0 m SWD.

	Test 4	Test 7	Test 9	Test 12	Test 13	Test 14
<b>1DFT CALCULATED</b>						
1DFT SOR, m/h	1.71	2.08	2.17	2.17	2.16	2.26
1DFT SLR, kg/(m <sup>2</sup> h)	9.54	9.55	9.55	9.55	11.98	13.31
1DFT HLR, m/h	2.31	2.68	2.77	2.77	3.00	3.34
$V_0/(nX_F)$ , m/h	6.04	7.01	7.24	7.24	6.26	6.26
Underflow rate, $q_R$ , m/h	0.603	0.604	0.604	0.604	0.843	1.084
Average depth, $H_{ave}$ , m	3.97	3.97	3.97	3.97	3.97	3.97
Feed Conc, $X_F$ , g/l	4 130	3 560	3 444	3 444	3 987	3 983
<b>TEST APPLIED</b>						
%1DFT SOR	69.52	68.21	71.25	76.67	71.83	68.78
%1DFT SLR	77.47	75.36	77.51	81.75	79.73	78.91
HLR, m/h	1.79	2.02	2.15	2.27	2.40	2.64
Act Ret Time, $R_{ha}$ , h	2.22	1.97	1.85	1.75	1.66	1.51
<b>(i) SETTLERCAD PREDICTED RESULTS FOR SSTs AS BUILT</b>						
%1DFT SOR	73.50	71.75	71.50	71.50	71.25	73.00
%1DFT SLR	80.41	78.11	77.71	77.71	79.32	81.76
HLR, m/h	1.86	2.09	2.15	2.15	2.38	2.73
Act Ret Time, $R_{ha}$ , h	2.14	1.90	1.84	1.84	1.67	1.45
<b>(ii) SETTLERCAD PREDICTED RESULTS FOR SSTs WITH 6.0 m SWD</b>						
%1DFT SOR	75.00	76.25	77.00	76.75	78.50	87.25
%1DFT SLR	84.52	81.60	82.01	81.81	84.54	91.39
HLR, m/h	1.88	2.19	2.27	2.27	2.54	3.05
Act Ret Time, $R_{ha}$ , h	2.11	1.81	1.75	1.75	1.56	1.30
<b>(iii) SETTLERCAD PREDICTED RESULTS FOR SSTs WITH STAMFORD BAFFLES</b>						
%1DFT SOR	76.00	75.00	74.75	74.75	74.50	78.00
%1DFT SLR	82.26	80.53	80.25	80.25	81.66	85.14
HLR, m/h	1.90	2.16	2.22	2.22	2.45	2.84
Act Ret Time, $R_{ha}$ , h	2.09	1.84	1.78	1.78	1.62	1.40

## 8 CONCLUSIONS AND RECOMMENDATIONS

### 8.1 Validation of SettlerCAD prediction accuracy

The only tests which were helpful to check the accuracy with which SettlerCAD simulated full scale SSTs were the Watts tests. Of all 15 Watts tests simulated, SettlerCAD correctly predicted the results of 12 tests, i.e. Tests 1, 2 and 4 to 10 (safe) and 11 to 13 (fail) but incorrectly predicted the results for 3 tests, i.e. Tests 3 (test safe, SettlerCAD fail) and 14 and 15 (test fail, SettlerCAD safe). Tests 4, 14, 13, 7, 9 and 12, which include 3 safe and 3 fail tests, fall in a very narrow %IDFT SOR (and SLR) range of 2% of 1DFT SOR from 71.5 to 73.5% and the SettlerCAD predicted SOR limit versus flux load factor line falls very close to these 6 tests. This narrow range, indicates that apart from Test 3 and 15, SettlerCAD accurately identifies the SOR and SLR capacity of the Watts SST. The SettlerCAD results of the Watts tests gives a good indication that the SettlerCAD predictions are valid for the simulation of full scale stress tests. SettlerCAD correctly predicted the result of 2 of the 4 Darvill tests and all 12 Rijen and Oss tests simulated. However, these tests were not helpful to validate the accuracy with which SettlerCAD predicted SST capacity, because, unlike the Watts tests, the range between the highest loaded safe and lowest loaded fail tests was too large (>10% of 1DFT SOR).

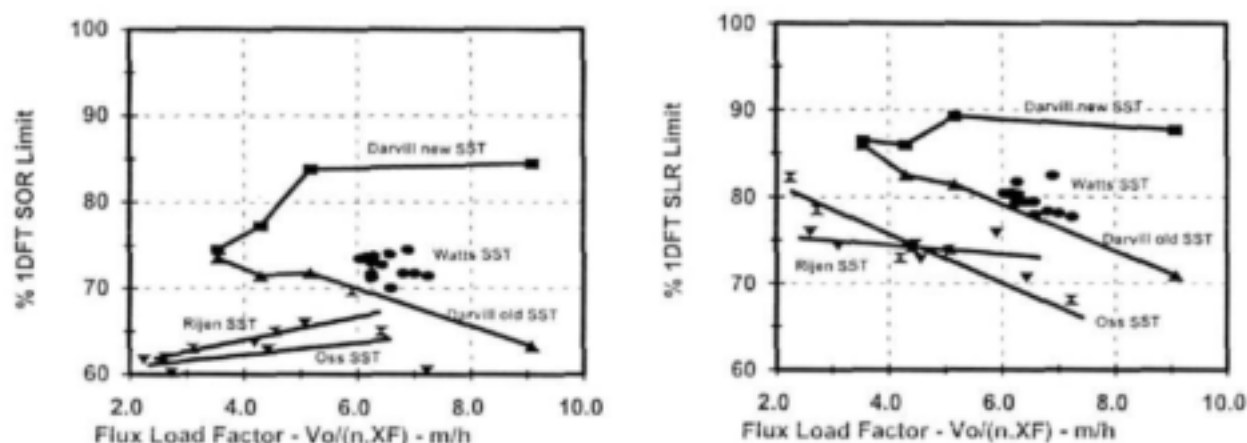
In all of the simulation runs, simulation times were selected which were >25 times the actual hydraulic retention time ( $25 \times R_{hd}$ ). These run times were sufficiently long to establish a final steady state condition towards the end of the simulation, which was checked from the solids mass balance calculated at each time step of the run. In the solids mass balance, the mass of solids exiting the SST via the underflow and overflow is calculated as a % of the inflow mass of sludge. Steady state was accepted to have been established when the % mass balance no longer changed.

The final ESS ( $X_E$ ) and RAS ( $X_R$ ) concentrations accepted for each run were the averages of the predicted values over the last  $2 \times R_{hd}$  of the run. Provided the run ended safe (ESS < 50 mg/l), the final concentrations yielded a solids mass balance within 0.5% of 100%. In contrast, runs that ended in failure (ESS > 50 mg/l) yielded a lower than 99.5 % solids mass balance and the greater the SST overload (i.e. higher the ESS concentration) the lower the solids mass balance below 99.5 %, even as low as 86 % for some runs at 100 % of the 1DFT SOR. Halving the simulation time steps and/or doubling the number of iterations per time step yielded identical simulation results and no improvement in % mass balance and therefore it was accepted that the low % mass balance was not due to numerical instability. It is suspected that the low mass balance for the failed runs is due to a simple logical error in SettlerCAD. It seems that the RAS concentration is "corrected" by subtracting from it the ESS concentration, because the higher the ESS concentration (or overload) the lower the RAS concentration. This is not consistent with the flux theory. Theoretically for increasing  $Q_I$  and constant  $Q_R$  and  $X_P$ , the RAS concentration

should remain constant (at  $X_R = j_L/q_R$ ) once the SLR capacity (failure) has been reached. This error does not influence the SettlerCAD predicted SOR and SLR limits because the ESS is still low at the transition from safe to fail.

## 8.2 Flux rating of the simulated SSTs.

The results of the SettlerCAD predicted SOR, as % of the 1DFT calculated maximum SOR, and associated SLR, also as % of the 1DFT calculated maximum SLR, of all the simulated tests on the Darvill new and old, Watts, Rijen and Oss SSTs are plotted together in Figs 35a and b. The Rijen (▼) and Oss (X) SettlerCAD predicted SOR and SLR limit results lie below the Darvill old (▲) and new (■) and Watts (●) SST “lines”, but closer to the Darvill old SST line. Considering that with respect to external SST geometry (Table 1), the Rijen and Oss SSTs are closer in likeness to the old Darvill SST than the Darvill new and Watts SSTs, the expectation is that the Rijen and Oss results should fall near the old Darvill SST results, and this does indeed happen.



*Figs 35a and b: SettlerCAD predicted maximum SOR (Fig 35a, left) and SLR (Fig 35b, right), as a % of the 1DFT limit values versus flux load factor  $V_d/(nX_F)$  for the 4 tests on the Darvill new (■) and old (▲) SSTs, 15 of the 15 tests on the Watts' SST (●), 6 each of the 14 and 10 tests on the Rijen (▼) and Oss (X) SSTs.*

The simulations of SST stress tests with the 2D hydrodynamic model SetterCAD indicate, as would be expected, that the SST hydraulic non-idealities are intrinsically part of the model and that SettlerCAD predicted maximum SOR and SLR were significantly below those calculated from the 1DFT. The simulations indicate that the *capacity*, or flux rating, of the 2.5m SWD flat bottom Darvill old SST decreases from 86% to 70% of the 1DFT maximum SLR as the flux load factor  $V_d/(nX_F)$  increases (which increases HLR due to an improvement in sludge settleability and/or decrease in feed concentration). The shallow Rijen and Oss SSTs have a lower flux rating (SLR) than the Darvill old SST which decreases from 80% to 67% as flux load factor increases. The 4.1m SWD 1:10 sloping bottom Darvill new SST does not show this sensitivity of capacity (or flux rating) to the flux load factor (or HLR) and the flux rating remained approximately

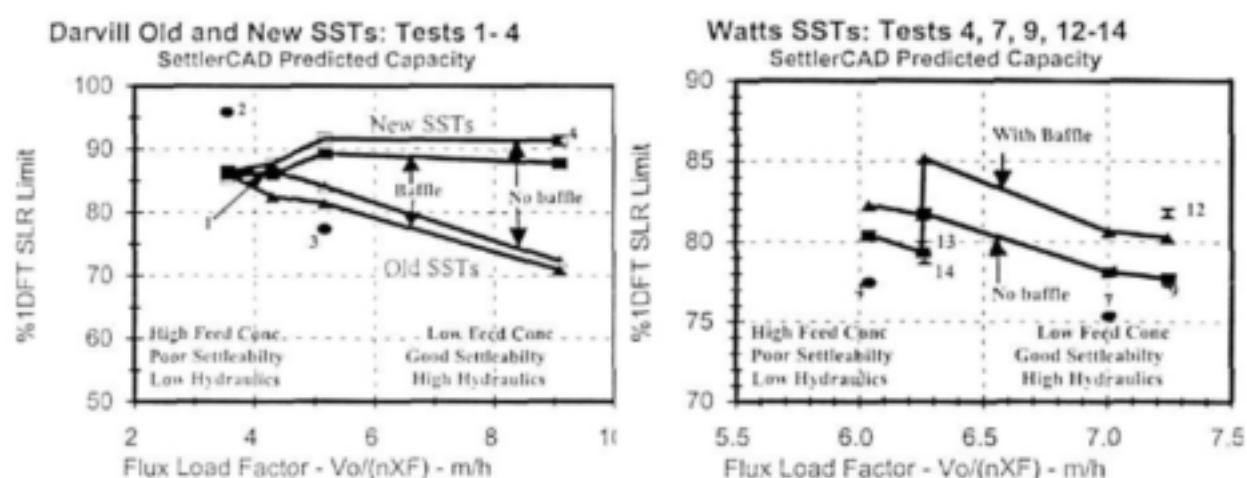


constant at around 87% of the 1DFT maximum SLR. The simulations show that the magnitude of the flux rating is not a constant value, and seems to be dependent on SST depth and HLR - the deeper the SST and the lower the HLR, the higher the flux rating. To determine the effect of the Stamford baffle and SWD on the flux rating, additional simulation runs were done on the Darvill SST (i) without the Stamford baffles and (ii) with interchanged SWD between the new and old SSTs and on the Watts SST (i) with a Stamford baffle and (ii) with 6.0m SWD.

### 8.3 The effect of the Stamford baffle on SST flux rating (capacity)

The SettlerCAD predicted maximum SLR (or flux rating) for the Darvill new and old and Watts SSTs with and without Stamford baffles are shown in Figs 36a and b.

For the Darvill SSTs, the SLR flux rating (Fig 36a) is about 2% of the 1DFT limit SLR *higher* without the Stamford baffle. In contrast, for the Watts SST (Fig 36b), the flux rating is about 2% of the 1DFT limit SLR *lower* without the Stamford baffle. From this, it is concluded that while the Stamford baffle has a significant effect on the ESS concentration while the SST is underloaded, its influence on the flux rating (or capacity) of the SST is small.



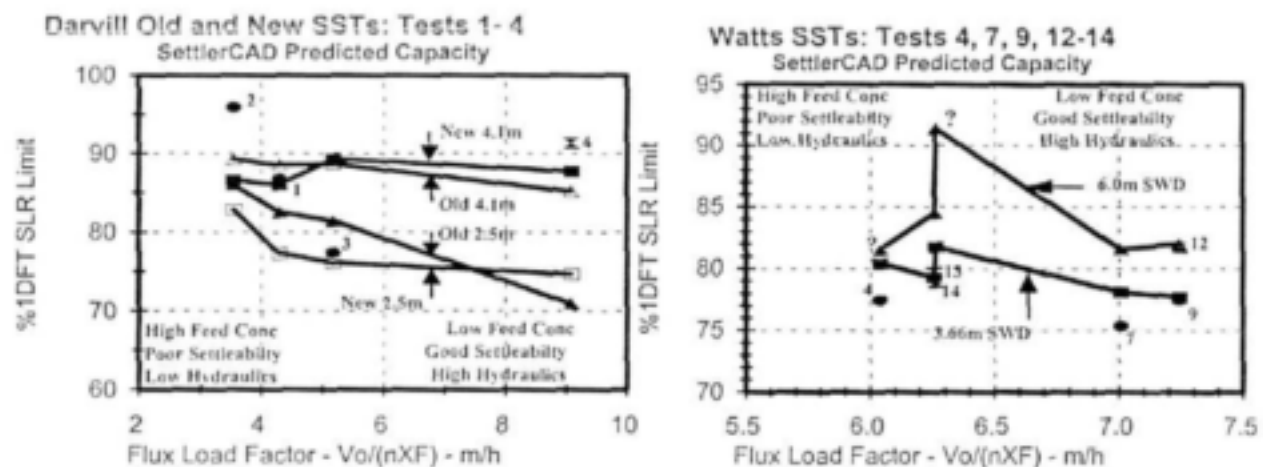
**36a and b:** SettlerCAD predicted maximum SLR for the Darvill (Fig 36a, left) and Watts (Fig 36b, right) SSTs with and without baffles. The actual test values, identified by number and result (safe ●, fail ⚡), are also shown.

### 8.4 The Effect of depth on SST flux rating (capacity)

The SettlerCAD predicted maximum SLR for the Darvill new and old SSTs with interchanged depths (i.e. new 2.5 m SWD, 1: 10 sloping bottom and scraper sludge collection and old 4.1 m SWD, flat bottom and suction sludge collection ) and the Watts SST with 6.0 m SWD are compared with that of the SSTs as built, (i.e. new 4.1 m SWD, 1: 10 sloping bottom and scraper sludge collection, old 2.5 m SWD, flat bottom and suction sludge collection and Watts with 3.66 m SWD, 1:15.4 sloping bottom and suction sludge collection) are plotted versus flux load factor

in Figs 37a and b.

For the Darvill SSTs, the 4.1m SWD old SST has approximately the same flux rating (SLR) as the new 4.1 m SST (Fig 37a) and shows a small decrease from 89 to 85% of 1DFT SLR limit as flux load factor increases from 3 to 9 m/h. Likewise 2.5 m new SST has a similarly low flux rating as the 2.5 m old SST. The differences in flux rating between the new and old SSTs with the same SWD probably arise from the different SST bottoms and sludge collection systems, which for the old SST is flat and hydraulic suction and for the new SST is sloping 1:10 and scraper. While SettlerCAD can accommodate these differences, the accuracy with which simulates then is unknown.



**Figs 37a and b:** SettlerCAD predicted maximum SLR for the Darvill new and old SSTs (Fig 37a, left) with interchanged SWD (old 4.1m and new 2.5m) and the Watts SST (Fig 37b, right) with a SWD of 6.0 m compared with the SSTs as built (new 4.1m, old 2.5m and Watts 3.66m). The actual test values, identified by number and result (safe ●, fail ⚡) are also shown.

For the Watts SST, 3.66 m SWD (as built) the 1DFT SLR limit (Fig 37b) shows a slight decreasing trend from 80 to 77% of 1DFT SLR as sludge load factor increases from 6.0 to 7.3 m/h. For Test 13 and 14 conditions ( $X_F$  and  $q_R$ ), the same flux load factor of 6.3 m/h leads to SettlerCAD predicted SLR predicted limits of 79 and 82% respectively. Ignoring Tests 4 and 14 (marked ?) for reasons detailed in Section 7.2 of the report, the Watts SST with a 6.0 m SWD has a flux rating of about 5% of 1DFT SLR higher than with a 3.66 m SWD.

From the above it is clear that the greater the SWD, the higher the flux rating. For the Watts SST, an increase in SWD from 3.66 to 6.0m represents a 60% increase in SST volume. For a 5% of 1DFT SLR increase in flux rating this volume increase is definitely not cost efficient - it would be better to select the shallower SWD (3.66m for the Watts SST) and increase the surface area to accommodate the lower flux rating.

## 8.5 Closure

The simulations of the full-scale SST SLR stress tests with the 2D hydrodynamic model SettlerCAD indicate, as would be expected, that the SST hydraulic non-idealities are intrinsically part of the model and that appropriate flux ratings for the full scale SSTs are reproduced “automatically” in the model. The simulations therefore provide further convincing evidence that the 1DFT cannot be applied to the design of full-scale SSTs without an appropriate reduction factor. The SettlerCAD simulations of the Darvill 35 m Ø SSTs indicated that the *capacity*, or flux rating, of the old flat bottom shallow (2.5 m SWD) SSTs decreased from 86 to 70% of the 1DFT maximum SLR as the flux load factor (or HLR) increased from an improvement in sludge settleability and/or decrease in feed concentration. The new sloping bottom deep (4.1m SWD) SSTs did not show this sensitivity of capacity (or flux rating) to flux load factor (or HLR) and the flux rating remained approximately constant at around 87% of the 1DFT maximum SLR. The magnitude of the flux rating therefore is not a constant value, and is shown to be dependent on SST depth and HLR; the deeper the SST, the higher the flux rating and the less sensitive the flux rating to flux load factor. Simulations of the Darvill new and old SSTs with inter-changed SWD and the Watts SST with 6.0m SWD, confirmed the sensitivity of the flux rating to depth and HLR. Furthermore, although the Stamford baffle can significantly reduce effluent suspended solids (ESS) concentration while the SST is underloaded, it does not increase the flux rating (or capacity) of the SST.

## 8.6 Recommendations

From the simulations the flux rating of 80% of the 1DFT maximum SLR recommendation by Ekama and Marais (1986) remains a reasonable value to apply in the design of full scale SSTs – for deep SSTs (4m SWD) the flux rating could be increased to 85% and for shallow SSTs (2.5m SWD) decreased to 75%. It is recommended that (i) while the apparent interrelationship between SST flux rating and depth suggests some optimization of the volume of the SST, that this be avoided and that (ii) the depth of the SST be designed independently of the surface area as is usually the practice and once selected, the appropriate flux rating is applied to the 1DFT estimate of the surface area.

## 9 REFERENCES

- de Haas DW, Wentzel MC, Gaydon P and Ekama GA (1998) Use of simultaneous chemical precipitation in modified activated sludge systems exhibiting enhanced biological phosphorus removal. Research Report W98, Dept. of Civil Eng., Univ. of Cape Town.
- Ekama G.A. and Marais G.vR. (1986) Sludge settleability and secondary settling tank design procedures. *Water Pollution Control*, **85**(1), 101-113.
- Ekama GA, Barnard JL, Günthert FW, Krebs P, McCorquodale JA, Parker DS and Wahlberg EJ (1997) *Secondary settling tanks: Theory, design, modelling and operation*. IAWQ STR No 6, pp216, International Association on Water Quality, London.
- Göhle F., Finnson A. and Hultman B. (1996) Dynamic simulation of sludge blanket movements in a full-scale rectangular sedimentation basin. *Water Sci. Technol.*, **33**(1), 89-99.
- Krebs P (1995) Success and shortcomings of clarifier modelling. *Wat. Sci. Technol.* **31**(2) 181-191.
- Ozinsky A E, Ekama G A and Reddy B D (1994). Mathematical simulation of dynamic behaviour of secondary settling tanks. Research Report W85, Dept. of Civil Eng., Univ. of Cape Town, Rondebosch, 7701, Cape, RSA.
- Ozinsky A.E. and Ekama G.A. (1995b) Secondary settling tank modelling and design Part 2: Linking sludge settleability measures. *Water SA*, **21**(4), 333-349.
- Stofkoper J.A. and Trentelman C.C.M. (1982) Richtlijnen voor het dimensioneren van ronde nabezinktanks voor actiefslibinstallaties. *H<sub>2</sub>O*, **15**(14), 344-354.
- STOWa (Stichting Toegepast Onderzoek Waterbeheer. Formerly STORA - Stichting Toegepast Onderzoek Reiniging Afvalwater ) Hydraulische en technologische aspecten van het nabezink-proces.  
 (1981a) Rapport 1 - Literatuur  
 (1981b) Rapport 2 - Ronde nabezinktanks (Praktijkonderzoek)  
 (1981c) Rapport 2 - Ronde nabezinktanks (Ontwerpgegevens en bedrijfservaring)  
 (1983) Rapport 3 - Rechthoekige nabezinktanks (Inventarisatie en praktijkonderzoek). Postbus 8090, RB 3505, Utrecht, Holland.
- Takács I., Patry G. G. and Nolasco D. (1991) A dynamic model for clarification-thickening process. *Water Research*, **25**(10), 1263-1271.
- Wahlberg E.J. and Keinath T.M. (1988) Development of settling flux curves using SVI. *Journal WPCF*, **60**(12), 2095-2100.
- Wahlberg E.J., Augustus M., Chapman D.T., Chen C-L., Esler J.K., Keinath T.M., Parker D.S., Tekippe R.J. and Wilson T.E. (1994b) Evaluating activated sludge secondary clarifier performance using the CRTC protocol: Four case studies. *Procs. 67th Annual WEF Conference and Exposition, Chicago*, **I**, 1-12.
- Wahlberg E.J., Gerges H.Z., Gharagozian and Stenstrom M.K. (1998) Discussion on "Secondary clarifier analysis using data from the Clarifier Research Technical Committee protocol" by Vitasovic Z.C., Zhou S., McCorquodale J.A. and Lingren K (1997) *Water Environment Research*, **69**(5), 999-1007, *Water Environment Research*, **70**(2), 249-253.
- Watts RW, Svoronos SA and Koopman B (1996). One dimensional modelling of secondary clarifiers using a concentration feed velocity dependent dispersion coefficient. *Water Research*, **30**(9), 2112-2124.
- Zhou S, Pfeil R, Strand E, Ji Z and Vitasovic C (1998) SettlerCAD (formerly Clarity) Release 1.1 - A 2D hydrodynamic model for secondary clarifiers. Reid Crowther Consulting, Seattle, WA.

## APPENDIX 1

## ESTIMATION OF SECONDARY SETTLING TANK CAPACITY WITH THE ONE DIMENSIONAL IDEALIZED FLUX THEORY (1DFT)

## 1. INTRODUCTION

Biological sludges usually show a strong flocculating tendency even at low concentrations ( $\sim 1000 \text{ mgTSS/l}$ ). This gives rise to a zone settling behaviour if a batch of mixed liquor is allowed to settle under quiescent conditions (Fig A1). In zone settling, the particles, irrespective of their size, all settle at the same rate throughout the zone depth. The rate of settlement is controlled by the rate at which the particles subside through the water and this rate is inversely related to the sludge concentration. Although the sludge blanket settles with a well-defined clear supernatant/mixed liquor interface, the sludge particles are suspended by the water between the particles; the upper particles are not mechanically supported by the lower ones.

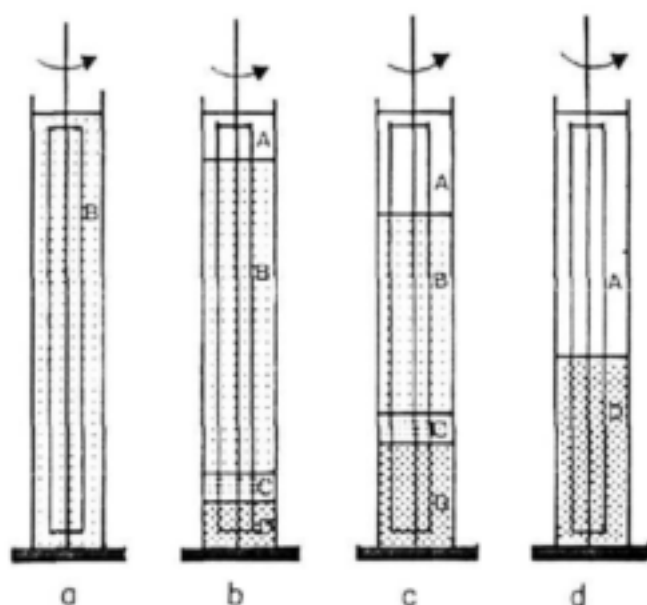


*Fig A1: Chronological progress of a stirred batch settling test showing the four different settling regimes in the column at different stages of settling from the start: Fig A1(a) lag stage - column filled with sludge at concentration  $X$  represented by  $B$  before settling commences; Figs A1 (b) and (c) at some time during settling, showing an increasing volume of clear supernatant ( $A$ ) appearing at the top and three regimes of settling viz, (i) zone settling ( $B$ ) at concentration  $X$  below*

*the clear supernatant, (ii) a transition zone ( $C$ ) in which zone settling still takes place but the concentration increases with depth and (iii) a compaction zone ( $D$ ) at the bottom of the column; and Fig A1(d) towards the end of the settling test when zone settling regimes  $B$  and  $C$  have subsided into the bottommost compaction regime ( $D$ ) and only thickening by compression takes place.*

Sludge flocs reaching the bottom of the batch cylinder build up as a compression layer (Fig A1). Compression is distinctly different to zone settling. In the compression region, each layer of particles provides mechanical support for the layers above it. Particle movement no longer is

governed only by the hydraulic frictional forces and the linkage between the particles, as in the zone settling region, but instead the net force downward of each floc is transmitted to the particles below by mechanical contact. This causes water to be squeezed out from the compressing particles and the settling behaviour in the compression stage is governed by the interstitial pressure, compressibility and permeability of the sludge.

## 2. MEASUREMENT OF THE FLUX CONSTANTS $V_0$ AND $n$

During zone settling, the subsidence rate of the solid/liquid interface is called the zone settling velocity; if the column is stirred, it is called the stirred zone settling velocity (SZSV). Because the sludge concentration of the zone settling region remains constant during this stage and is equal to the concentration of the mixed liquor with which the column was filled, the SZSV is defined as the stirred settling velocity of the sludge  $V_{zs}$ , at a concentration equal to the mixed liquor concentration  $X$ . Standard Methods No. 213 D (1985) recommends that a column at least 1 m tall and 100 mm in diameter be used for the SZSV test.

The SZSV ( $V_{zs}$ ) of the sludge is obtained from a solid/liquid interface depth versus time plot (Fig A2) and is given by the slope of the straight line part of the interface height versus time curve. The  $V_{zs}$  decreases as the concentration ( $X$ ) increases (Fig A2). By conducting a number of stirred settling tests at different concentrations ranging between 1 to 12 gMLSS/l (at least 6), the  $V_{zs}$  at different concentrations ( $X$ ) is obtained.

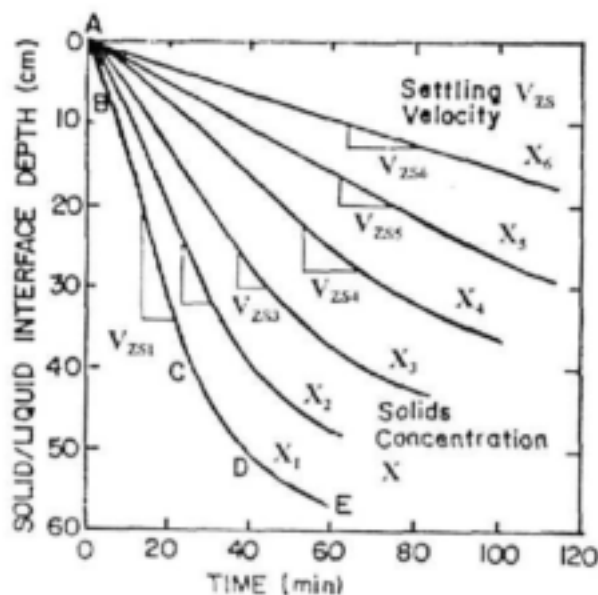


*Fig A2: Solid-liquid interface height versus time observed in stirred batch settling tests at different initial solids concentrations. Slope of straight line section gives the zone settling velocity ( $V_{zs}$ ) which decreases from  $V_{zs1}$  to  $V_{zs6}$  as concentration ( $X$ ) increases from  $X_1$  to  $X_6$ .*

### 3. RELATIONSHIP BETWEEN ZONE SETTLING VELOCITY AND CONCENTRATION

Considerable research has been undertaken to establish the form of the relationship between the  $V_{zs}$  and  $X$  and a number of mathematical expressions have been proposed, e.g. hyperbolic, logarithmic, power and exponential. Of these, the two most popular forms are exponential (by Vesilind, 1968a,b) and logarithmic (by Dick and Young, 1972). The exponential form

$$V_{zs} = V_o \exp(-nX) \quad (\text{m/h}) \quad \text{A1}$$

appears to have been accepted over the years for the following reasons: (i) The WRC design procedure is based on it (White, 1975, 1976); (ii) Rachwal *et al.* (1982) present a large number of full scale plant data (733) showing that it gives the best correlation over the other three forms cited above; (iii) Smollen and Ekama (1984) and Ekama *et al.* (1984) show that unlike the logarithmic, the exponential form gives (a) a theoretically consistent description of the settling flux curve (for  $X > 1$  g/t) with defined turning and inflection points, (b) a more internally consistent SST model and (c) a better correlation with their own full scale plant data set, the extensive data set of Pitman's (1980, 1984) from full scale plants accumulated over a number of years, and the pilot scale data set of Tunttoolavest *et al.* (1983) ( $R^2$  for all  $>0.96$ ).

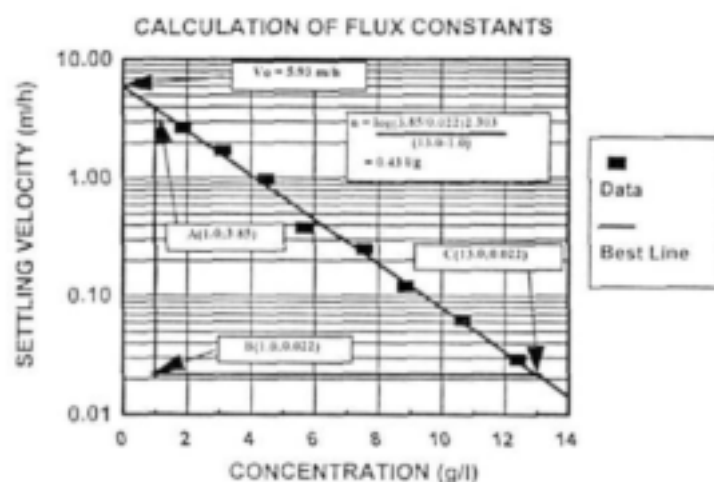


*Fig A3: Determination of flux theory settling constants  $V_o$  and  $n$  from multiple batch stirred settling tests over a range of concentrations.*

The constants  $V_o$  and  $n$  in the exponential equation, Eq A1 are obtained by linear least squares regression of natural logarithm  $\ln V_{zs}$  versus  $X$  over a range of concentrations from 1 to 12 g/l (Fig A3). These constants (which have units m/h and  $\text{m}^3/\text{kgMLSS}$  or  $\text{t/g}$  respectively) reflect the settling characteristics of the sludge. Generally, good settling sludges have high  $V_o$  values around 13 m/h and low  $n$  values around 0.25  $\text{m}^3/\text{kg}$ , whereas poor settling sludges have low  $V_o$  values around 5 m/h and high  $n$  values around 0.5  $\text{m}^3/\text{kg}$ . The relatively consistent changes in the  $V_o$  and  $n$  values from good to poor settling sludges led Pitman (1984) (see also Ekama *et al.*, 1984, 1997) to propose that the parameter  $V_o/n$  [i.e.  $V_o$  divided by  $n$ , which has the same units as flux



kg/(m<sup>2</sup>h)] defines numerically the sludge settleability for the flux theory. Once the values of the constants  $V_0$  and  $n$  are known, no further information is required to apply the flux theory to SSTs (Vesilind, 1968b; Pitman, 1984; Ekama *et al.*, 1984, 1997; Daigger and Roper, 1985). Application of the steady state 1D idealized flux theory (1DFT) to the design of SSTs is discussed in this Appendix.

Unfortunately, there are three problems associated with measuring the flux theory constants  $V_0$  and  $n$ . (1) It is labour intensive in that at least 6 to 10 settling velocity tests are required over a concentration range up to at least 12 g/l; at the higher concentrations (>6 g/l) the test is tedious and time consuming, requiring 2 to 3 hours settlement to properly identify the SZSV. Such extended periods of settlement with nitrifying sludges often lead to the second problem viz. (2) denitrification in the settling column, which causes severe retardation of the SZSV (and sometimes flotation!). Denitrification can be detected by the escape of gas bubbles from settling sludge and generally causes a poor correlation with Eq A1, i.e.  $R^2 < 0.90$  or very high  $n$  values (> 0.5 l/g) for poor settling sludges (low  $V_0$ ). These problems can be overcome with careful and vigilant work making the test acceptable for practical research. However, the effort is such that measurement of  $V_0$  and  $n$  at activated sludge plants is unlikely to be adopted in routine practice. (3) The results are variable and some scatter in  $V_0$  and  $n$  values is obtained with repeated tests. As a result of (1) and (2) above, the simpler sludge settleability parameters Sludge Volume Index (SVI), Diluted SVI (DSVI) or Stirred Specific Volume Index (SSVI) are preferred. However, with these, the benefits of the flux theory cannot be utilized. This problem has been overcome by developing empirical relationships between the simpler sludge settleability measures and the  $V_0$  and  $n$ . These empirical relationships allow "indirect" access to the flux theory. The different empirical relationships that have been developed are compared by Ozinsky *et al.* (1995) and summarized by Ekama *et al.* (1997).

#### 4. FLUX DUE TO GRAVITY SETTLING

The solids transport through a unit area per unit time, or flux ( $j$ ), due to settling induced by gravity ( $j_s$ ), is defined as the product of zone settling velocity  $V_{zs}$  (m/h) and the solids concentration  $X$  (kgSS/m<sup>3</sup>), i.e

$$j_s = V_{zs} X \quad \text{kgSS/(m}^2\text{h)} \quad \text{A2}$$

where

$j_s$	= gravity flux	kgSS/(m <sup>2</sup> h)
$V_{zs}$	= zone settling velocity	m/h and
$X$	= solids concentration	kg/m <sup>3</sup>

A graph of the gravity flux versus concentration is given in Fig A4. When the concentration  $X$  is very low, the gravity flux  $j_s$  is very low, but the gravity flux quickly increases with concentration reaching a maximum flux at around 2 to 3 g/l. For concentrations greater than around 4 to 5 g/l, the gravity flux decreases rapidly due to the reduction in the zone settling velocity  $V_{zs}$  with concentration.

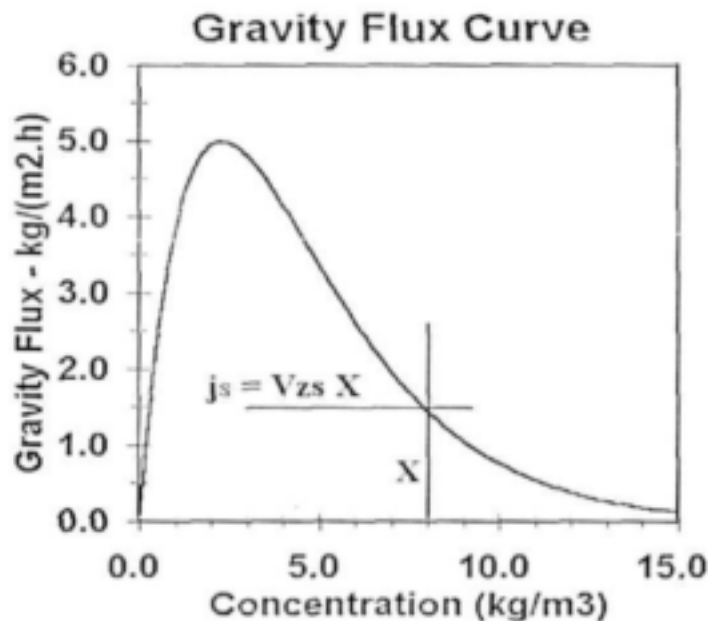


*Fig A4: The gravity flux versus sludge concentration curve. The gravity flux is the transport of sludge to the bottom of the SST due to gravity settling of the sludge with respect to the water.*

The above definition of the gravity flux forms the basis of the flux theory and is implemented as such in various SST models from the simple steady state 1D idealized flux theory (1DFT), through the more complex dynamic 1D SST models, to the very sophisticated 2D hydrodynamic models for SSTs such as SettlerCAD (Zhou *et al.*, 1998). In these models the settlement of the solids are essentially modelled in the same way via the gravity flux defined by Eqs A1 and A2. Essentially, it is only the water movement that is modelled differently in the different models from the very simple to the very complex. In the steady state 1DFT model, this is in the vertical direction only, in the dynamic non-steady state 1D models, such as those by Ozinsky *et al.* (1994), Grijspeert *et al.* (1995) and Watts *et al.* (1996), this is also in the vertical direction only, but turbulent diffusion/dispersion is included, creating mixing between the stacked horizontal layers making up the depth of the SST to represent the hydraulic non-idealities, and in the 2D hydrodynamic models such as SettlerCAD, this is modelled hydrodynamically in the more realistic vertical and horizontal directions.

## 5. 1D IDEALIZED FLUX THEORY - GRAPHICAL APPLICATION

The graphical design procedure for the 1DFT is outlined first to give a visual representation of what is done mathematically in the analytical design procedure with the design and operating chart discussed later. It must be remembered that this graphical procedure was developed by

Yoshioka *et al.* (1957) and others a decade before the empirical relationships between  $V_{zs}$  and  $X$  were developed which allowed a mathematical approach to be followed. However, most of the basic principles of the 1DFT were established with the graphical approach.

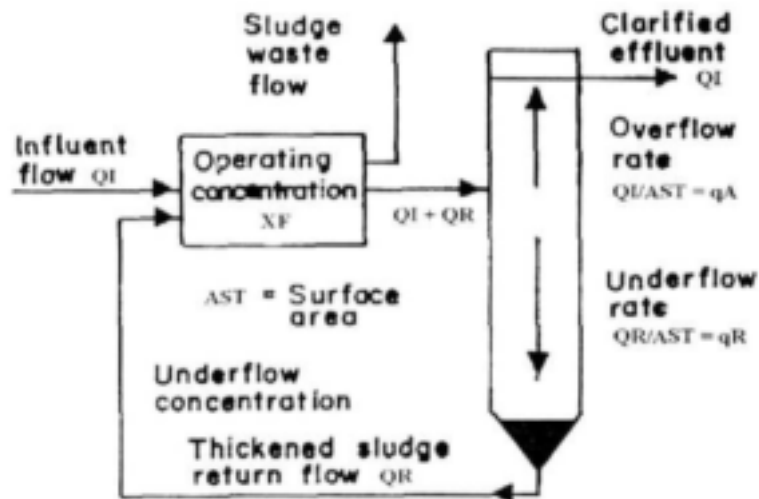


*Fig A5: Idealized 1D secondary settling tank in the activated sludge system showing water and sludge movement in the vertical direction only and perfect separation of the influent ( $Q_I$ ) and recycle ( $Q_R$ ) flows at the feed point leading to an upward overflow rate ( $q_A$ ) by the influent flow and a downward underflow rate ( $q_R$ ) by the recycle flow.*

In the idealised one dimensional (1D) continuously operating settling tank (shown schematically in Fig A5), water and solids move in a vertical direction only. The feed flow entering the SST, which comprises the influent flow to the treatment plant ( $Q_I$ ) and the sludge return flow ( $Q_R$ ) is perfectly separated at the feed point into the influent flow moving vertically upwards and the recycle flow moving vertically downwards. The upward water velocity from the influent flow is called the overflow rate  $q_A (=Q_I/A_{ST})$  and the downward water velocity from the recycle flow is called the underflow rate  $q_R (=Q_R/A_{ST})$ . The solids entering the settling tank with the feed flow  $Q_F (=Q_I+Q_R)$  is transferred to the bottom of the SST by two flux components: (1) the gravity flux ( $j_s$ ), which results from the settlement of the solids with respect to the water and (2) the bulk flux ( $j_B$ ), which results from the downward movement of the water with respect to the bottom of the SST due to the underflow rate. The gravity flux  $j_s$  is given by Eq A2. The bulk flux  $j_B$  is the product of the local sludge concentration ( $X$ ) and the underflow rate ( $q_R$ ), viz.

$$j_B = X q_R \quad \text{m/h} \quad \text{A3}$$

where

$q_R$	= underflow rate	m/h
	= $Q_R/A_{ST}$	
$A_{ST}$	= surface area settling tank	m <sup>2</sup>
$Q_R$	= sludge return flow	m <sup>3</sup> /h

For a fixed underflow rate ( $q_R$ ), the bulk flux  $j_B$  is proportional to sludge concentration  $X$ . This is shown graphically in Fig A6.

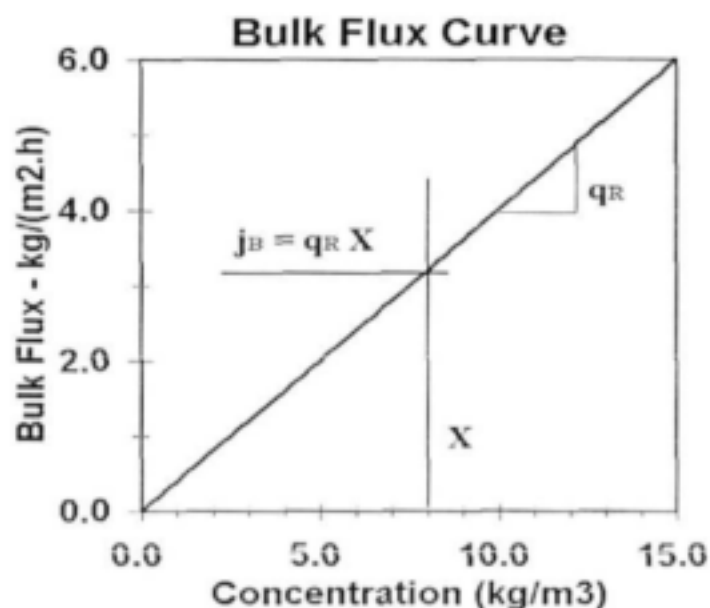


*Fig A6: The bulk flux curve versus sludge concentration for constant underflow rate  $q_R$ . Bulk flux is the transport of sludge due to downward movement of the water with respect to the SST bottom.*

The total solids transport or flux to the bottom to SST ( $j_T$ ) is the sum of the gravity ( $j_s$ ) and bulk ( $j_B$ ) fluxes i.e.

$$\begin{aligned}
 j_T &= j_s + j_B && \text{kg/(m}^2\text{h)} \\
 &= X (V_{zs} + q_R) && \text{kg/(m}^2\text{h)} \quad \text{A4}
 \end{aligned}$$

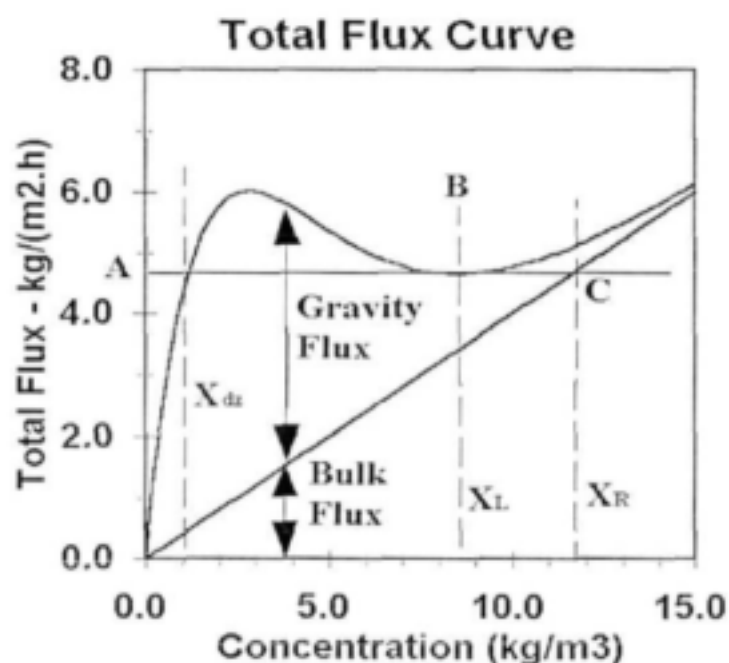


*Fig A7: Total downward flux to the SST bottom versus concentration, which is the sum of the gravity and bulk fluxes.*

For the design of the SST, the maximum influent flow ( $Q_i$ ) is usually the peak wet weather flow (PWWF)  $Q_{i,PWWF}$ . For a selected value of the underflow rate ( $q_R$ ), the two flux components can be added graphically which is shown in Fig A7. For the particular choice of underflow rate, the total flux ( $j_T$ ) attains a minimum value ( $j_L$ , Point B in Fig A7) at a certain concentration called the limiting concentration  $X_L$ . This concentration  $X_L$  has the minimum flux or solids transport

to the bottom of the SST of all the other concentrations that can arise between a very low concentration (say half of the feed concentration,  $X_F$ ) and the high underflow concentration ( $X_R$ ). This means that for the selected underflow rate, all solids concentrations in the SST higher or lower than  $X_L$  have fluxes greater than that of the concentration  $X_L$  and would be transported faster to the bottom of the SST than  $X_L$  concentration. Because a concentration of  $X_L$  can realistically exist in the SST in a particular concentration layer between the feed point and the SST bottom, this concentration layer limits the solids transport rate, or flux, to the bottom of the tank. This situation could also be visualized as follows; all the sludge entering the SST and exiting via the underflow, passes through a range of concentrations as it settles and concentrates from say half the feed concentration up to the underflow concentration  $X_R$ , one of which is the  $X_L$  concentration. This  $X_L$  concentration is the bottle-neck concentration because it has the lowest flux of all the concentrations that can exist in the SST. Hence, to insure that all the solids entering the SST can reach the bottom, the sludge mass applied to the SST at the feed point per unit surface area and time (called the applied flux,  $j_{AP}$ ) must be less than or at most equal to the limiting flux ( $j_L$ ), which is the flux of the layer with the  $X_L$  concentration. Now the applied flux ( $j_{AP}$ ) on the SST is given by the product of the feed (or reactor) concentration  $X_F$  and the total hydraulic loading rate (HLR =  $Q_F/A_{ST}$ ), which is the combined underflow  $q_R$  ( $=Q_R/A_{ST}$ ) and overflow  $q_A$  ( $=Q_{LPWWF}/A_{ST}$ ) rates (see Fig A5). Therefore, for safe or underloaded operation of the SST

$$j_{AP} < j_L \quad \text{kg/(m}^2\text{h)} \quad \text{A5}$$

where

$$j_{AP} = X_F (Q_L + Q_R) / A_{ST} \text{ or } X_F (q_A + q_R) \quad \text{kg/(m}^2\text{h)} \quad \text{A6}$$

and

$$j_L = X_L (V_{SXL} + q_R) \quad \text{kg/(m}^2\text{h)} \quad \text{A7}$$

where

$$V_{SXL} = \text{zone settling velocity of the } X_L \text{ concentration} \quad \text{m/h}$$

and the SST is critically loaded, i.e. at the point of failure, when

$$j_{AP} = j_L \quad \text{kg/(m}^2\text{h)} \quad \text{A8}$$

Equation A8 therefore fixes the capacity of the SST and hence the surface area  $A_{ST}$  for the selected underflow rate  $q_R$ , is found from Eqs A6 and A7, viz.

$$A_{ST} = Q_{LPWWF} / q_A \quad \text{m}^2 \quad \text{A9}$$

where

$$q_A = j_L / X_F - q_R \quad \text{m/h} \quad \text{A10}$$

From the above, to determine  $A_{ST}$  requires  $X_L$  to be known. The  $X_L$  concentration and its associated limiting flux  $j_L$  is determined graphically from a plot like Fig A7. A horizontal line (ABC) tangential to the minimum total flux  $j_L$  (Point B) sets  $j_{AP} = j_L$  and gives the maximum applied flux  $j_{AP}$ , which can be read off the vertical axis at Point A.

For the selected  $q_R$ , which fixes also the recycle flow ( $Q_R$ ) and recycle ratio ( $R$ ), the underflow concentration  $X_R$  is determined from the solids mass balance around the SST, i.e.

$$\begin{aligned} X_R Q_R + X_E Q_I &= X_F (Q_I + Q_R) \text{ or} & \text{kg/h} \\ X_R q_R + X_E q_A &= X_F (q_A + q_R) = j_{AP} & \text{kg/(m}^2\text{h)} \end{aligned} \quad A11$$

For safe operating conditions, i.e. where  $j_{AP} \leq j_L$ , all the solids entering the SST exit it via the sludge underflow, i.e.  $X_E = 0$  and hence from Eq A11, the underflow concentration  $X_R$  is given by,

$$X_R = X_F (Q_I + Q_R) / Q_R \quad \text{kgSS/m}^3 \quad A12a$$

$$= X_F (1+R)/R \quad \text{kgSS/m}^3 \quad A12b$$

$$= j_{AP} / q_R \quad \text{kgSS/m}^3 \quad A12c$$

where

$$X_R = \text{solids concentration in the underflow recycle} \quad \text{kgSS/m}^3$$

The underflow concentration  $X_R$  can also be determined graphically from Fig A7. The  $X$  value where the horizontal line representing  $j_{AP} = j_L$  cuts the bulk flux line (at Point C) is  $X_R$ , which is the concentration at which the bulk flux ( $j_B$ ) equals the applied flux for zero gravity flux ( $j_S = 0$ ), i.e.  $j_B = j_{AP} = q_R X_R$ , from which  $X_R = j_{AP} / q_R$  and is the same as Eq 12c. In Fig A7, it can be seen that the slope of the bulk flux line is given by  $j_{AP} / X_R = q_R$  m/h.

For the specified reactor concentration ( $X_F$ ) and maximum influent flow rate ( $Q_{I,PWWF}$ ), the required area of the settling tank ( $A_{ST}$ ) is found by repeating the graphical procedure outlined above for different underflow rates ( $q_R$ ), which requires the construction of a new  $j_T$  versus  $X$  plot like Fig A7 for each  $q_R$ . If this is done, it will be found that as  $q_R$  increases (which concomitantly increases  $Q_R$  and  $R$ ), the overflow rate ( $q_A$ ) increases and the area of the SST ( $A_{ST}$ ) decreases. The required  $A_{ST}$  will be the largest area obtained for the anticipated range of  $q_R$  to be applied on the SST, which generally will be for the lowest  $q_R$  (and hence lowest  $Q_R$  and  $R$ ) selected. This can be seen in Fig A8, which shows  $q_A$  increasing for increasing  $q_R$ . From Fig A8, in order to minimize the area of the SST, the largest possible underflow rate  $q_R$  needs to be selected. When constructing the total flux ( $j_T$ ) versus concentration ( $X$ ) plot like Fig A7 for incremental increases in  $q_R$ , it will be noticed that for  $q_R$  values greater than a certain critical one, called  $q_{R,crit}$ , a minimum in the total flux ( $j_T$ ) line no longer exists. A value for  $X_L$  therefore cannot be

determined for  $q_R > q_{R,crit}$  and the limiting flux concept of the flux theory therefore no longer applies. The highest underflow rate for which a  $X_L$  can be determined, and therefore for which the limiting flux concept applies, is  $q_{R,crit}$ , which in turn gives the critical recycle flow,  $Q_{R,crit}$  ( $= q_{R,crit} \times A_{ST}$ ) and a critical recycle ratio,  $R_{crit}$  ( $= Q_{R,crit} / Q_{LPWWF}$ ). The critical underflow rate  $q_{R,crit}$  is the  $q_R$  value which makes a point on the  $j_T$  line exactly horizontal without the existence of a minimum (see Fig A9). The  $X$  value of the horizontal point along the  $j_T$  line for  $q_R = q_{R,crit}$  is the last valid  $X_L$  that can be determined and is the minimum valid  $X_L$  value and therefore is named  $X_{L,min}$ . This  $X_{L,min}$  gives the highest  $j_L$  value and so this maximum  $j_L$  value is called  $j_{L,max}$ , which in turn gives the maximum overflow rate  $q_A$  and hence the minimum surface area (see Fig A8). For  $q_R \leq q_{R,crit}$ , the  $j_T$  line will always have a horizontal point and a minimum  $j_L$  so for  $q_R \leq q_{R,crit}$  there will always be a  $X_L$  and so the limiting flux concept of the flux theory applies. This limiting flux concept criterion of the flux theory is called solids handling criterion (SHC) I.

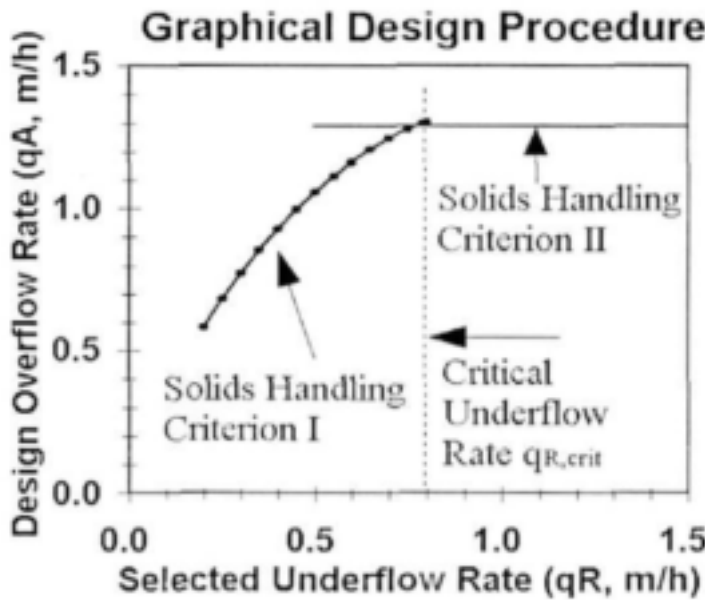


*Fig A8: Design overflow rate ( $q_A$ ) versus selected underflow rate ( $q_R$ ) obtained from the graphical design procedure for incremental increases in underflow rate, showing the maximum overflow rate of solids handling criterion (SHC) I slightly above that for SHC II.*

When  $q_R > q_{R,crit}$ , the slope of the  $j_T$  versus  $X$  line is always positive, i.e.  $j_T$  increases for all  $X$  and so the limiting flux concept or SHC I no longer applies. When  $q_R > q_{R,crit}$ , solids handling criterion (SHC) II governs the maximum flux and hence the surface area of the SST. White (1975) and Merkel (1974) independently suggested that when SHC I no longer applies, the limiting flux  $j_L$  of the SST is given by the flux of the feed concentration  $X_F$ . Mathematically this is expressed as follows

$$X_F (Q_{LPWWF} + Q_R) / A_{ST} = j_{AP} \leq j_L = X_F (V_{ZSNF} + q_R) \quad \text{kgSS}/(\text{m}^2\text{h}) \quad \text{A13a}$$

which simplifies to

$$q_{A,LPWWF} = Q_{LPWWF} / A_{ST} \leq V_{ZSNF} \quad \text{m/h} \quad \text{A13b}$$



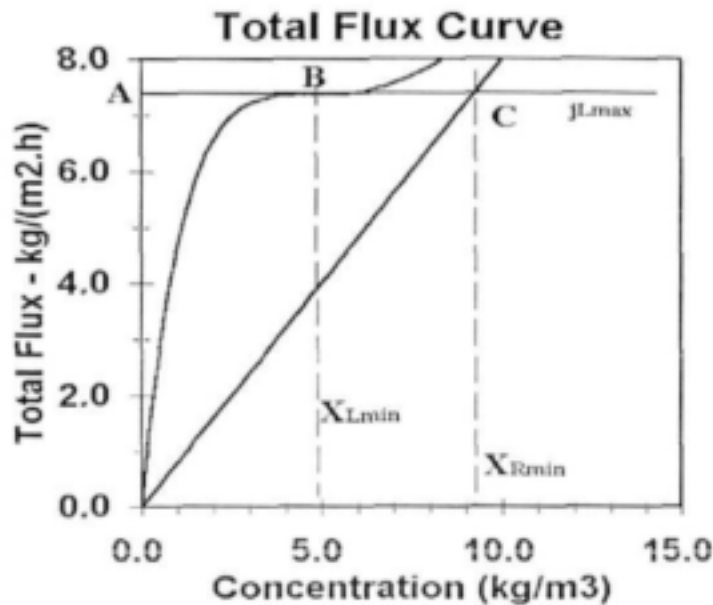


**Fig A9:** Total flux versus sludge concentration for the critical underflow rate ( $q_{R,cri}$ ) giving the maximum limiting flux  $j_{Lmax}$  and the minimum limiting concentration  $X_{Lmin}$  which is the upper limit for SHC I. For underflow rates greater than  $q_{R,cri}$  a minimum in the total flux versus concentration curve no longer appears and a different criterion is required to determine the SST area i.e. SHC II.

Equation A13 is SHC II, which states that the overflow rate at PWWF must not exceed the settling velocity of the sludge at the feed concentration ( $V_{ZSXF}$ , m/h). This conclusion is confirmed theoretically from the state point approach of Yoshioka *et al.* (1957) which is discussed below. Equation A13 shows that SHC II is independent of recycle flow ( $Q_R$ ) and therefore the area of the SST remains constant for  $q_R > q_{R,cri}$  and plots as a horizontal line in Fig A8 at a value  $q_A$  slightly lower than the minimum value found from SHC I (see Fig A8).

Yoshioka *et al.* (1957) simplified the graphical method for determining  $X_L$  and introduced the SST steady state operating position or state point into the graphical method (Fig A10). In Fig A7, they rotated line ABC clockwise about Point A on the vertical axis (which represents  $j_{AP} = j_L$ ), until Point C (which represents  $X_R$ ) was on the horizontal axis. This in effect changes the slope of the bulk flux line (which represents  $q_R$ ) to zero, and restores the total flux  $j_T$  line back to the gravity flux ( $j_s$ ) curve. This rotation does not change the  $X_L$  value of Point B and geometrically, from similar triangles, the slope of the bulk flux line in Fig A7 is numerically equal to the slope of line ABC in Fig A10, except that in Fig A7 it has a +ve slope whereas in Fig A10 it has a -ve slope. The line ABC in Fig A10 therefore represents the underflow and its slope is equal to the underflow rate ( $q_R$ , m/h). Hence, in Fig A10, a whole range of  $q_R$  values can be tested in the same gravity flux curve where the  $q_R$  values are represented by underflow lines similar to line ABC, with different slopes equal to the selected  $q_R$ , each touching tangentially on the inside of the downward leg of the gravity flux curve. The  $X$  value of the tangent Point B is  $X_L$  and the intersection points of the underflow line with the vertical and horizontal axes at Points A and C respectively are the limiting flux  $j_L$  and underflow concentration  $X_R$  respectively. This graphical construction is clearly much more convenient than constructing the total flux curve like Fig A7 for each selected  $q_R$ .

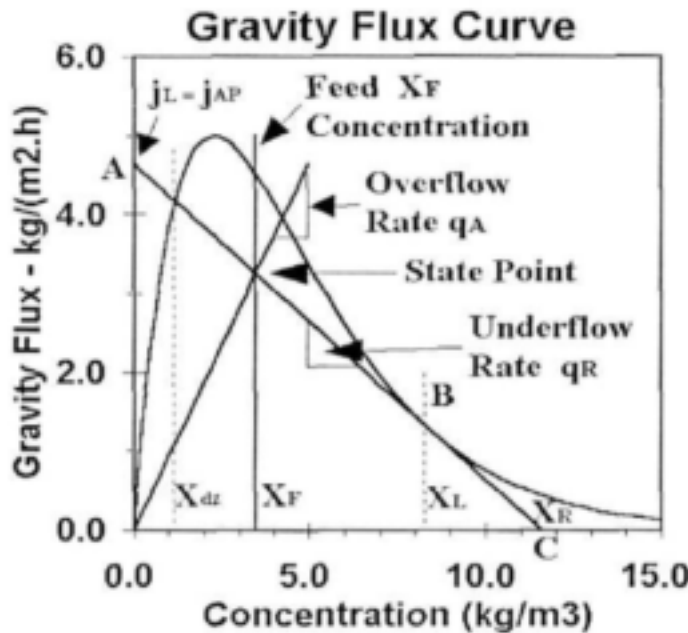


**Fig A10:** The Yoshioka *et al.* (1957) simplified graphical procedure and state point, which superimposes the operating condition of the SST onto the gravity flux curve. The state point defines the loading state of the SST and the underflow rate ( $q_R$ ), overflow rate ( $q_A$ ) and feed concentration lines intersect at the state point. When the underflow line makes a tangent to the gravity flux curve (as shown), the SST is critically loaded.

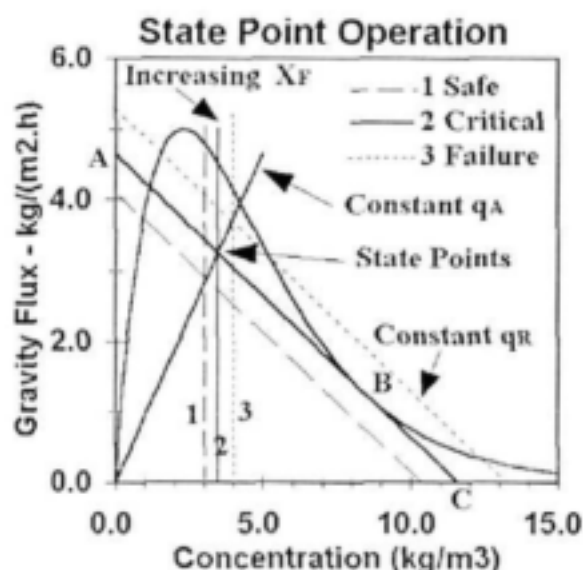
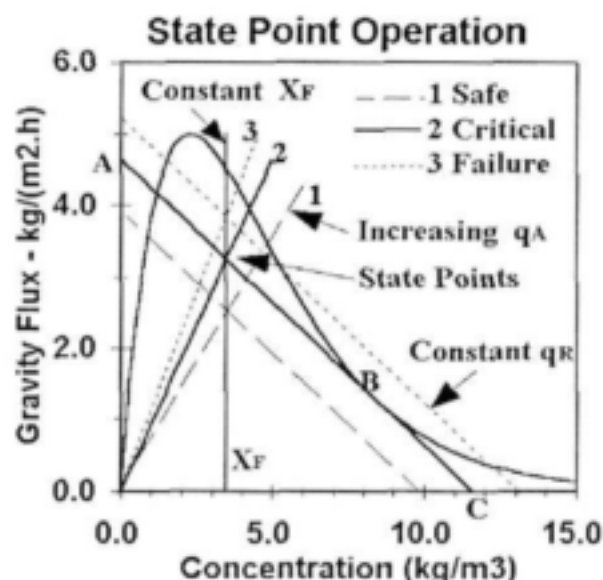
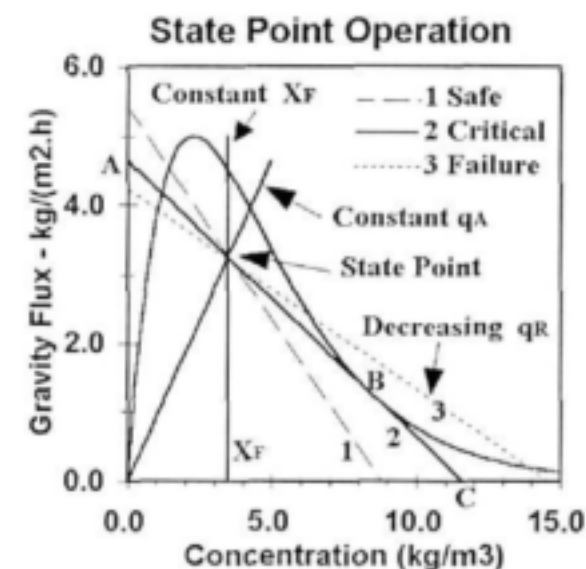
The graphical method of Yoshioka *et al.* (1957) allows the SST steady state operating point, or state point, to be superimposed on the gravity flux graph. The feed concentration ( $X_F$ ) is represented by a vertical line at  $X = X_F$ . The state point is the intersection point of the feed concentration and underflow lines. This slope of a line drawn from the origin of the graph to the state point is the overflow rate ( $q_A$ ). Hence, the underflow, feed concentration and overflow lines intersect at the state point which represents the steady state operating conditions of the SST, where the slopes of the underflow and overflow lines are the underflow ( $q_R$ ) and overflow ( $q_A$ ) rates respectively. Note that these lines have opposite slopes, i.e.  $q_R$  is -ve and  $q_A$  is +ve, which is consistent because in the idealised 1D SST (Fig A5), these two flows move in opposite directions.

For a given  $X_F$ , and selected  $q_R$  and  $q_A$ , if the underflow line is within the gravity flux curve and does not touch the downward leg of the gravity flux curve, the SST is underloaded and  $j_{AP} < j_L$ . When the underflow line touches the gravity flux curve as a tangent, then the SST is critically loaded and  $j_{AP} = j_L$ . When the underflow line cuts the gravity flux curve in three places, i.e. once on the rising leg (at very low  $X$ ) and twice on the downward leg (at higher  $X$ ), the SST is overloaded and  $j_{AP} > j_L$ . The feed concentration, underflow and overflow lines intersecting at the state point therefore superimpose the steady state operating condition of the SST onto the gravity flux curve (which is fixed by the sludge settleability parameters  $V_0$  and  $n$ ). When the underflow line is within or tangential to the gravity flux curve, then the operating conditions of the SST fit within the envelope of the gravity flux curve and the SST is under- ( $j_{AP} < j_L$ ) or critically- ( $j_{AP} = j_L$ ) loaded for the selected  $q_R$  and accepted sludge settleability.

From the above, the graphical design procedure of Yoshioka *et al.* (1957) is as follows (Fig A10): For a given gravity flux curve (which requires only  $V_0$  and  $n$  to be known) and a chosen  $X_F$  and  $q_R$ , (i) draw the underflow line at a slope of  $q_R$  m/h so that it touches the gravity flux

curve in a tangent on the inside of the curve, (ii) draw the vertical feed concentration line at  $X = X_F$  and (iii) draw the overflow line from origin to the state point, which is the intersection point of the feed concentration and underflow lines. The slope of the overflow line is the maximum overflow rate for the selected  $q_R$ , from which the area of the SST ( $A_{ST}$ ) is calculated with Eq A9. The applied flux ( $j_{AP}$ ), underflow concentration ( $X_R$ ) and the limiting concentration ( $X_L$ ) are given by the underflow line intersection points on the vertical axis (Point A) and horizontal axis (Point C), and  $X$  value of tangent point on the gravity flux curve (Point B) respectively. With the  $A_{ST}$ ,  $q_R$  and  $q_A$  known, the recycle flow  $Q_R$  and ratio  $R$  are found from  $Q_R = A_{ST} q_R$  and  $R = q_R / q_A$ . By selecting increasing  $q_R$  values, the identical  $q_A$  versus  $q_R$  plot as in Fig A8 will be obtained for SHC I.

From the curvature of the gravity flux curve (Fig A4), for  $X > X$  for which  $j = j_{max}$ , i.e.  $> 2$  to  $3$  g/l, there is an inflection point on the downward leg of the gravity flux curve. To the right of  $j_{max}$  but near it, the curvature is +ve (convex) but further beyond  $j_{max}$  (higher  $X$ ) the curvature is -ve (concave). The point at which the curvature changes from +ve to -ve is the inflection point. Now, tangential underflow lines can only be drawn on the inside of the gravity flux curve with -ve curvature, i.e. for  $X$  values greater than the  $X$  value of the inflection point, i.e. to the right of the inflection point. Therefore, the steepest tangential underflow line that can be drawn to the gravity flux curve, is one with a slope equal to the slope of the gravity flux curve at the inflection point. This is  $q_{R,cris}$ , which gives this steepest sloping overflow rate line and hence the highest overflow rate in terms of SHC I. An underflow line tangential to the gravity flux curve at the inflection point is therefore represented in Fig A8 at  $q_{R,cris}$ , which gives the minimum surface area ( $A_{STmin}$ ) and is the limit of SHC I. When the underflow line is steeper than  $Q_{R,cris}$ , the curvature of the gravity flux curve (now +ve) is such that the state point now can be on the gravity flux curve and the underflow line only cut it once, with the result that the feed concentration, overflow and underflow lines now intersect on the gravity flux curve. With the state point on the gravity flux curve the slope of the underflow line is now not governed by the slope of the gravity flux curve but dependent only on the position of the  $X_F$  line. The lower the  $X_F$ , the steeper the overflow line and the higher the overflow rate. By definition, with the state point on the gravity flux curve, the slope of the overflow line  $q_A$  is  $j_S / X_F$ , hence  $q_A = V_{ZSXF} X_F / X_F = V_{ZSXF}$ . This is the theoretical basis for SHC II (Eq A14b). The overflow rate for SHC II is independent of  $q_R$  and dependent only on the feed concentration  $X_F$  through  $V_{ZSXF}$ . The convenience of the Yoshioka *et al.* (1957) graphical method is that the complete design for the range of underflow rates can be done on the same gravity flux curve.



*Figs A11 a, b, c: Graphical representation of the SST operating conditions on the gravity flux curve showing the effect of incremental (i) decreases in underflow rate (Fig A11a, top left), (ii) increases in overflow rate (Fig A11b, top right) and (iii) increases in feed concentration (Fig A11c, left) from 1 - safe, 2 - critically to 3 - failed loading conditions.*

The state point defines the operating conditions of the SST, and operating changes in underflow rate ( $q_R$ ), overflow rate ( $q_A$ ) and feed concentration ( $X_F$ ) are reflected on the gravity flux curve as follows: (i) a decrease in the underflow rate rotates the underflow line about the state point in an anti-clockwise direction, but the state point remains in position (see Fig A11a); (ii) an increase in overflow rate rotates the overflow line about the origin in an anti-clockwise direction and moves the state point upwards along the feed concentration line, while the underflow line slope remains constant but intersects the state point (see Fig A11b), (iii) and increase in feed concentration moves the vertical feed concentration line to the right and because the slopes of the overflow and underflow rates remains unchanged, the state point moves along the overflow line while the underflow line continues to pass through the state point (see Fig A11c).

Because the state point defines the operating condition of the SST, the state point position in the

gravity flux graph defines the loading condition on the SST, i.e. whether under-, critically- or overloaded, and whether SHC I or II governs the capacity of the SST. Referring to Figs 11a, b and c:

- (1) When the state point is within the envelope of, and not on, the gravity flux curve, SHC II is met and SHC I governs the capacity of the SST. When the underflow line
  - (i) cuts the gravity flux curve in one point only, i.e. through the rising leg of the gravity flux curve, safe operating conditions prevail,
  - (ii) cuts the gravity flux curve at one point only, i.e. through the rising leg of the gravity flux curve and is tangential on the inside of the gravity flux curve at high  $X$ , critical loading conditions prevail,
  - (iii) cuts the gravity flux curve in three points, i.e. once through the rising leg of the gravity flux curve and twice through the descending leg of the gravity flux curve, overloaded conditions prevail;
- (2) when the state point is on the gravity flux curve, critically loaded conditions with respect to SHC II prevail; if the feed concentration  $X_f$  is greater than the concentration  $X$  of the inflection point, the underflow line has to be tangential to the gravity flux curve and hence the loading condition also is critical with respect to SHC I, but if  $X_f$  is less the  $X$  of the inflection point, SHC I does not apply.
- (3) If the state point is outside the envelope of the gravity flux curve, the SST is overloaded with respect to both SHC II and SHC I; SHC I also is not met because conditions 1(i) and 1(ii) above are not met.

The above conditions can be readily applied to design for given peak influent flow ( $Q_{I,PWWF}$ ) and feed concentration ( $X_f$ ) to find the minimum surface area  $A_{STmin}$ , viz: (1) Identify the inflection point on the gravity flux curve and draw a tangent underflow line to it. (2) Draw in the vertical feed concentration line and the intersection point of this line with the underflow line is the state point. (3) Draw the overflow line from the origin to the state point. The slope of this line gives the maximum overflow rate  $q_{Amax}$  for SHC I. (4) Determine the settling velocity of the sludge at the feed concentration  $V_{ZSXF}$ , which is equal to the maximum overflow rate for SHC II. (5) Select the lower of  $q_{Amax}$  and  $V_{ZSXF}$  and  $A_{STmin} = Q_{I,PWWF} / (q_{Amax} \text{ or } V_{ZSXF})$ . With  $A_{ST}$  known, the recycle flow  $Q_R$  is found from  $Q_R = q_R A_{ST}$  and the recycle ratio  $R$  from  $R = Q_R / Q_{I,PWWF}$ . It will be found that usually  $V_{ZSXF} < q_{Amax}$  of SHC I and hence usually  $A_{STmin} = Q_{I,PWWF} / (V_{ZSXF})$ . Any underflow rate  $q_R$  lower than the slope of the inflection point of the gravity flux curve will lead to a greater  $A_{ST}$ . For  $q_R$  lower than that of the slope of the inflection point, the design procedure is the same except now the underflow line is drawn tangentially to the gravity flux curve at a value of  $X$  greater than the inflection point  $X$  value.

Although the above graphical procedure is still a "trial and error" one in that repeated selection

of the underflow rate  $q_R$  is made and the corresponding  $q_A$ ,  $A_{ST}$ ,  $Q_R$  and  $R$  determined for safe operation, it is far simpler than the total flux curve method because each selected  $q_R$  can be analysed on the same gravity flux curve, thereby obviating the need for constructing different total flux curves like Fig A7 for each  $q_R$ . Note that the two graphical methods give identical results because the condition described the horizontal line at  $j_L$  in Fig A7 is identical to that described by the underflow line tangential to the gravity flux curve in Fig A10.

## 6. DYNAMIC CONDITIONS

Under normal dry weather daily operation of the SST, the feed concentration ( $X_F$ ) and underflow rate ( $q_R$ ) can be taken as remaining approximately constant. However, the influent flow, and hence the overflow rate ( $q_A$ ) and recycle ratio ( $R$ ), change cyclically over the day causing the state point to move (Fig A11b). This results in temporary sludge storage in the SST from two causes: (1) With diurnal variation in  $q_A$  and  $R$ , the underflow concentration  $X_R$ , varies over the day (see Eq A12a). At high influent flow,  $R$  is low and hence  $X_R$  is high. To obtain higher  $X_R$  in the recycle flow requires longer thickening times on the SST bottom. Hence, even if the SST is underloaded throughout the 24 hour day, the sludge blanket height will increase and decrease over the day in phase with the increasing and decreasing influent flow due to the changing compaction times required to achieve the required  $X_R$ . Depending on the magnitude of  $Q_R$  and the settleability of the sludge, the diurnal movement in sludge blanket height in the bottom compaction zone of the SST is around 0.75 to 1.0 m. (2) It may happen that during the peak dry weather flow (PDWF) period overloaded conditions develop in the SST, in which event a rising sludge blanket (theoretically at a concentration of  $X_U$ ) will develop. The overload, depending on its severity, may persist for a few hours without sludge loss, because the SST has sufficient depth to accommodate the sludge accumulating in it, thereby avoiding the sludge blanket to rise up to within 1 m of the effluent launders. Consequently, the continuously changing sludge loading rate and different compaction times over the day cause the sludge blanket to move up and down in the SST, which may even be temporarily overloaded, without significant sludge loss with the effluent.

The principal factor that prevents sludge loss during a temporary overload is the sludge storage capacity of the SST, which once the area has been fixed, is directly proportional to the depth. Generally, the deeper the SST, the higher (if short) or longer (if small) the temporary overload that can be sustained without sludge loss. Unfortunately no guidance regarding the depth of the SST can be derived from the 1DFT and depth design is based on primarily practical experience. The Abwassertechnischen Vereinigung (ATV, 1976, 1991) have developed empirical procedures based on the DSVI to calculate four different zone depths in the SST, viz. the clear water, separation, sludge storage and compaction depths (see Ekama *et al.*, 1997). An average depth of 3 to 4 m is common. Deep SSTs (>4m) have the advantage that ample allowance is made in



the SST for the various zones depths, thereby keeping the sludge blanket well below the effluent launders (>1m). Deep SSTs are also less prone to hydraulic disturbances from influent flow variations, density currents, inlet and outlet arrangements and sludge collection systems. 2D hydrodynamic modelling studies have indicated that the greater the SST depth, the greater the flux rating, i.e. the greater the percentage of the 1DFT theoretical maximum solids and hydraulic loading rates that can be applied to the SST (Ekama and Marias, 2001).

## 7. MATHEMATICAL APPLICATION OF THE 1D FLUX THEORY

Clearly the graphical approach to the 1DFT described above gives considerable insight into design and operation of SSTs taking due consideration of the sludge settling characteristics and feed concentration. However, despite the convenient developments in this graphical approach, the procedure remains rather tedious and time consuming because the design has to be executed manually. The biggest difficulty is that the shape of the gravity flux curve can only be approximated graphically between the measured concentrations and settling velocities, with the result that estimation of the position of the gravity flux curve is uncertain. This causes a significant measure of error and uncertainty in the estimations from the procedure.

In order to overcome the difficulties associated with the graphical approach, a mathematical approach was developed, which required defining a mathematical equation linking the zone settling velocity and sludge concentration. When this approach was developed around 1970, the form of this equation evoked significant debate (Smollen and Ekama, 1984, Ozinsky and Ekama, 1995) but today it seems that the exponential form is almost universally accepted (see Section 3 above). It should be noted that aside from the somewhat better correlation that the exponential form yields over the other forms for most of the experimental data, this form is just as empirical as the other forms. However, the properties of the exponential form are better suited to the 1DFT problem because it yields an more internally consistent model for the SST.

### 7.1 Mathematical properties of the theoretical flux equation

From the exponential equation linking settling velocity and concentration (Eq A1), the gravity flux is given by

$$j_s = X V_{zs} = X V_o \exp(-nX) \quad \text{kg/(m}^2\text{h)} \quad \text{A14}$$

The slope of the gravity flux curve is given by the derivative of Eq A14, viz.

$$\frac{dj_s}{dX} = V_o e^{-nX}(1 - nX) \quad \text{m/h} \quad \text{A15}$$



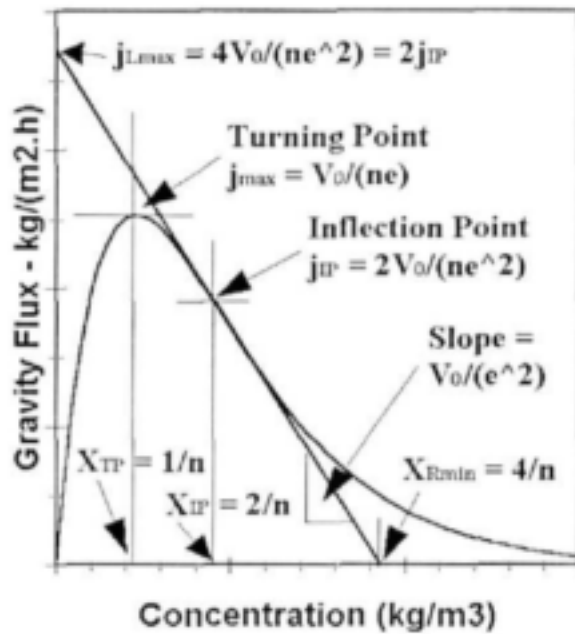


*Fig A12: Mathematical properties of the gravity flux curve based on the semi-log equation linking the zone settling velocity and sludge concentration (Eq A1).*

which, when set to 0, gives a turning point in the gravity flux curve at  $X = 1/n$  and a flux of  $V_0/(ne)$  (Fig A12). Differentiating Eq A15 with respect to  $X$  and substituting  $1/n$  for  $X$  shows that the turning point with coordinates  $+1/n, +V_0/(ne)$  is a maximum, giving the maximum flux  $j_{max} = V_0/(ne)$ . Setting the second derivative to zero shows that there is an inflection point on the gravity flux curve at coordinates  $+2/n, +2V_0/(ne^2)$ . This is the inflection point at which SHC I ceases to be valid in the graphical method because no steeper underflow line can make a tangent to the inside of the gravity flux curve (Fig A12). The slope of the gravity flux curve at the inflection point is found by substituting  $2/n$  for  $X$  into Eq A15 which yields  $-V_0/(e^2)$  m/h, which is the maximum underflow rate  $q_R$  for SHC I. The intercept of the underflow line tangential to the inflection point with the vertical and horizontal axes are respectively the maximum limiting flux ( $j_{Lmax}$ ) and the minimum underflow concentration ( $X_{Rmin}$ ) for the SHC I to govern the design of the SST, which, from the coordinates and slope of the inflection point are;

$$j_{Lmax} = \frac{4V_0}{ne^2} = \frac{4j_{max}}{e} = 2j_{IP} \quad \text{kg/(m}^2\text{h)} \quad \text{A16a}$$

$$X_{Rmin} = \frac{4}{n} = 4X_{TP} = 2X_{IP} \quad \text{kg/m}^3 \quad \text{A16b}$$

where subscripts IP and TP refer respectively to the inflection and turning points (see Fig A12).

## 7.2 Application of the exponential flux equation to SST

The overflow rate to satisfy the SHC I is found from Eqs A8 and A6 and is given by

$$q_A = \frac{j_L}{X_F(1+R)} = \frac{j_L}{X_R R} \quad \text{m/h} \quad \text{A17}$$

where

$$X_R = X_F(1+R)/R \quad \text{kg/m}^3 \quad \text{A12b}$$

Note that Eq A8 above, like the state point concept, is valid only under safe operating conditions as defined above, i.e. equal mass flow rates of sludge in the feed and recycle flows ( $X_E = 0$ ).

The general equation of the underflow line with a point of tangency to the gravity flux curve is

$$j = j_L (1 - X/X_R) \quad \text{kg/(m}^2\text{h)} \quad \text{A18}$$

and its slope is given by

$$dj/dX = -j_L/X_R \quad \text{m/h} \quad \text{A19}$$

At the point of tangency (see Fig A10), i.e. at  $X = X_L$ , both the fluxes and the slopes of the gravity flux curve and underflow line are equal, i.e. Eq A14 = Eq A18 and Eq A15 = Eq A19. Equating the slopes and fluxes of the gravity flux curve and underflow line yields two equations with two unknowns,  $X_L$  and  $j_L$ , viz.

$$j_L \left[ 1 - \frac{X_L}{X_R} \right] = X_L V_0 \exp(-nX_L) \quad \text{kg/(m}^2\text{h)} \quad \text{A20}$$

$$V_0 \exp(-nX_L)(1 - nX_L) = -j_L/X_R \quad \text{m/h} \quad \text{A21}$$

Making  $j_L$  the subject of Eq A20 and substituting this for  $j_L$  into Eq 21 eliminates  $j_L$  and yields a quadratic for  $X_L$ . Solving for  $X_L$  and ignoring the unrealistic solution<sup>1</sup> yields,

$$X_L = (X_R/2)[1 + \sqrt{1 - 4/(nX_R)}] \quad \text{kg/m}^3 \quad \text{A22}$$

Note that in Eq A22, no solutions for  $X_L$  are possible when the square root term is negative, i.e. for  $X_R > 4/n$ , which from Fig A12 is  $X_{Rmin}$ . Hence when  $X_R = 4/n$ ,  $X_L$  is a minimum and equal to the  $X$  value of the inflection point, i.e.  $X_{Lmin} = X_R/2 = 2/n$ .

Substituting Eq A22 for  $X_L$  into Eq A20 yields the limiting flux  $j_L$  associated with  $X_L$  in terms of  $X_R$ , i.e.

$$j_L = V_0 X_R \frac{(1 + \alpha)}{(1 - \alpha)} \exp \left[ \frac{-nX_R(1 + \alpha)}{2} \right] \quad \text{kg/(m}^2\text{h)} \quad \text{A23a}$$

---

<sup>1</sup>Because of the quadratic form of the equation, a  $\pm$  appears before the square root term of Eq 22. The unrealistic solution is the -ve one, i.e. the lower of the two  $X_L$  solutions. This unrealistic solution for  $X_L$  is mathematically possible but represents failure of the SST. It is the "underflow line" from the  $X_R$  concentration on the horizontal axis touching the gravity flux curve on the *outside* between the inflection and turning points i.e.  $X_L < X_{ip}$ . The realistic solution is the higher  $X_L$  value which has a point of tangency on the *inside* of the gravity flux curve at  $X_L$  values greater than the  $X$  value of the inflection point i.e.  $X_L > X_{ip}$ .

where

$$\alpha = \sqrt{1 - 4/(nX_R)} \quad \text{A23b}$$

If  $\alpha < 0$ , there is no solution for  $j_L$ . Setting  $\alpha = 0$  yields  $X_R = X_{Rmin} = 4/n$  and hence from Eq A23,  $j_L = 4V_0/(ne^2)$ , which is  $j_{Lmax}$  (Fig A12). No solution for  $j_L$  is possible for  $X_R < 4/n$  because the curvature of the gravity flux curve is such that no valid tangential underflow line can be constructed within the envelope of the gravity flux curve. From the graphical method, this is known to be the limit of SHC I.

Substituting Eq A12b for  $X_R$  into Eq A23 and substituting Eq A23 into Eq A17, yields the maximum overflow rate  $q_A$  versus  $R$  for SHC I to be met, viz.

$$q_A = \frac{V_0}{R} \frac{(1 + \alpha)}{(1 - \alpha)} \exp \left[ \frac{-n(1+R)X_F(1 + \alpha)}{2R} \right] \quad \text{m/h} \quad \text{A24a}$$

where

$$\alpha = \sqrt{1 - \frac{4R}{n(1+R)X_F}} \quad \text{A24b}$$

Equation A24 relates the overflow rate  $q_A$  to the recycle ratio  $R$  for specified values of feed concentration  $X_F$  and setting characteristics of the sludge  $V_0$  and  $n$  to meet SHC I. If  $\alpha = 0$ ,  $X_F = 4R/[(1+R)n]$ . Hence from Eq A24, if  $\alpha = 0$ ,

$$q_A = V_0/(e^2 R) \quad \text{m/h} \quad \text{A25}$$

Transferring the  $R$  in Eq A25 to the left hand side, gives underflow rate  $q_R = q_A R = V_0/e^2$ , which can be recognized as the slope of the tangential underflow line at the inflection point, i.e.

$$q_{R,crit} = q_{AmaxSHC I} R_{crit} = V_0/e^2 \quad \text{m/h} \quad \text{A26}$$

The  $q_A$  of Eq A25 is therefore the maximum overflow rate allowed in terms of SHC I,  $q_{AmaxSHC I}$  and represents the limit of this criterion (see Fig A8). The recycle ratio  $R$  at this point is  $R_{crit}$  and from Eqs A12 and 25, is given by

$$R_{crit} = \frac{X_F}{X_{Rmin} - X_F} = \frac{X_F}{4/n - X_F} \quad \text{A27}$$

As before in the graphical method, when the underflow rate is greater than the slope of the gravity flux curve at the inflection point, then SHC II governs the area design of the SST. From Eq A9, this is defined by

$$q_{AmaxSHC II} = V_0 e^{-nX_F} \quad \text{m/h} \quad \text{A28}$$

### 7.3 SST design and operating chart

By plotting  $q_A$  versus  $R$  from Eqs A24 and A28 for known values of  $V_0$  and  $n$  and selected  $X_F$ , the steady state design and operating (D&O) chart for the SST is obtained (Fig A13). The SHC I (Eq A24) is represented by the s-shaped line from the origin to point D and shows that as  $R$  increases so the permissible overflow rate increases. This line represents all the possible SST designs for underflow lines (rates) making tangents to the gravity flux curve from very low underflow rates (very low  $R$ ) up to the critical underflow rate  $q_{R,crit}$  ( $R_{crit}$ ). At point D,  $q_{R,crit}$  ( $= V_0/e^2$ ) is reached, SHC I stops and Eq A24 no longer gives solutions for  $q_A$  for  $R$  values greater than  $R_{crit}$  at Point D. The SST loading condition at Point D in the D&O chart is represented on the gravity flux curve at the inflection point. Hence at Point D,  $q_R = q_{R,crit}$ ,  $X_L = X_{Lmin}$ ,  $X_R = X_{Rmin} = 4/n$ ,  $j_L = j_{Lmax} = 4V_0/(ne^2)$ ,  $R_{crit} = X_F/(4/n - X_F)$  and  $q_{AmaxSHC I} = V_0/(e^2 R_{crit})$ . Point D in the D&O chart is identical to the maximum  $q_A$  point for SHC I (giving minimum  $A_{ST}$ ) in the  $q_A$  versus  $q_R$  plot of Fig A8. The SHC II (Eq A28), being independent of  $R$ , plots as a horizontal line in the D&O chart and cuts the SHC I line on or below Point D. Because both SHC I and II have to be met for  $R < R_{crit}$ , safe operation of the SST is represented in the D&O chart by  $q_A - R$  points below both the SHC I and II lines; for  $R > R_{crit}$ ,  $q_A - R$  points below the SHC II line only because SHC I does not apply. There are some instances where the  $q_{AmaxSHC I}$  is greater than  $q_{AmaxSHC II}$ . Therefore, in general, the design point for minimum area of the SST for PWWF is not Point D in the D&O chart, but the intersection point of the SHC I and II lines - for the cases where the  $q_{AmaxSHC I} > q_{AmaxSHC II}$ , the  $R$  value of the SHC I and II lines intersection point is less than  $R_{crit}$ . This is the same as the maximum overflow rate for SHC I being slightly higher than that for SHC II in the  $q_A$  versus  $q_R$  graph developed from the graphical procedure (Fig A8).

If, for the same  $V_0$  and  $n$ ,  $X_F$  is varied and the SHC I and II lines plotted in the same D&O chart, it will be found that the SHC I plots as a family of s-shaped lines from the origin to a hyperbola represented by  $q_{R,crit} = V_0/e^2$  (i.e. the slope of the inflection point) and the SHC II as a family of horizontal lines cutting the

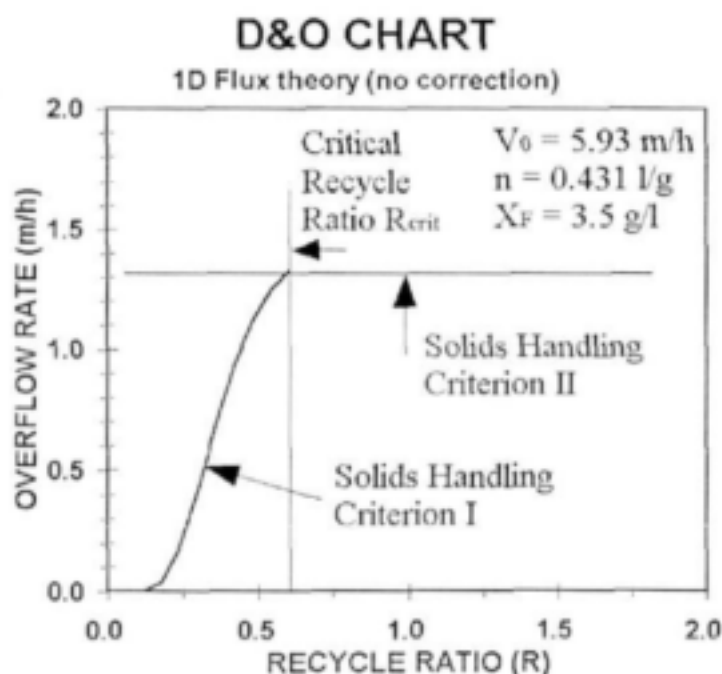


*Fig A13: Design and operating chart for fixed flux settleability constants  $V_0$  and  $n$  and selected feed concentration  $X_F$  showing Solids Handling Criteria I and II and the critical recycle ratio ( $R_{crit}$ ) where SHC I ceases. Note that the overflow rate for SHC II is slightly lower than that for SHC I.*

SHC I line near but always below the SHC I end point on the hyperbola (Fig A14). For design, in the region below the hyperbola, both SHC I and II have to be met and in the region above the hyperbola, only SHC II.

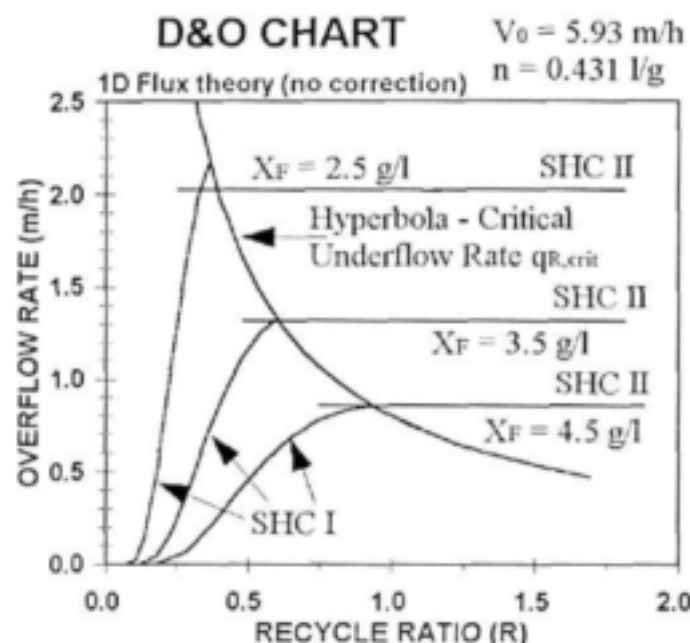


*Fig A14: D&O chart for fixed flux settleability constants  $V_0$  and  $n$  and varying feed concentration  $X_F$ . The line of the points where SHC I ceases at different  $X_F$  concentrations is the hyperbola critical underflow rate  $q_{R,crit} = q_{AmaxSHC I}$ ,  $R_{crit} = V_0 / e^2$  (Eq A25). The area below the hyperbola is where SHC I and II both need to be met and the area above the hyperbola is where SHC II only needs to be met for safe operating conditions.*

From the above mathematical development, it is clear that the inflection point on the gravity flux curve, or Point D in the D&O chart, plays a major role in the design of the SST - it in fact governs the maximum overflow rate for SHC I ( $q_{AmaxSHC I}$ ), which, in some instances (usually good settling sludges), is only slightly higher than that for SHC II ( $q_{AmaxSHC II}$ ). The advantage of the exponential equation linking  $V_{zs}$  and  $X$  is that it implicitly includes the definition of (i) a low flux at very low concentration (0.1 - 1.0 g/l), (ii) a turning point in the gravity flux curve and (iii) an inflection point when determining the  $V_0$  and  $n$  by means of semi-log least squares regression. For the logarithmic form, even though two settleability parameters are being determined with log-log least squares regression [i.e.  $a$  and  $b$  in  $V_{zs} = a(X)^b$ ], these three properties have to be manually drawn into the gravity flux versus concentration curve - these properties are not implicitly included in the log-log  $V_s = a(X)^b$  equation like in the semi-log  $V_s = V_0 e^{-nX}$  equation (Smollen and Ekama, 1984). Mathematically, the semi-log equation (Eq A1) therefore makes a much better 1DFT model than the log-log equation.

The D&O chart is also valid for diurnal flow conditions. For successful (safe) operation of the SST, the conditions prescribed by the D&O chart must be met at all times of the day. For example, for a fixed SST area, as the influent flow increases, so the recycle ratio decreases and the overflow rate increases. This moves the operating point, represented by the  $q_A$  -  $R$  value pairs in the D&O chart, upwards and to the left along a constant  $q_R$  line, represented by a hyperbola  $q_R = q_A R \text{ m/h}$ . At all times of the day, the  $q_A$  -  $R$  value pairs must be within the safe operating area, i.e. below the SHC II line for  $R > R_{crit}$  and below both the SHC I and II lines for  $R < R_{crit}$ .

This approach is of course conservative and assumes the SST has no depth and therefore no sludge storage, which is clearly not realistic. However, it does give a good guide to the design and operation of the SST under diurnal flow conditions. The 1DFT design procedure is demonstrated in a design example below.

## 8 DESIGN EXAMPLE

The MLSS concentration of an activated sludge reactor  $X_F$  is  $3.5 \text{ kgTSS/m}^3$ , and the flux constants  $V_0$  and  $n$  were measured to be  $5.93 \text{ m/h}$  and  $0.43 \text{ m}^3/\text{kgSS}$  respectively (see Fig A3). These constants give a SSVI and DSVI of about  $100 \text{ ml/g}$  and  $150 \text{ ml/g}$  respectively indicating that the sludge is of rather poor settleability and approaching a bulking sludge. The average dry weather flow ( $Q_{LADWF}$ ) is  $220 \text{ m}^3/\text{h}$  ( $5.28 \text{ Ml/d}$ ), and the dry weather flow varies in a cyclic pattern with a minimum  $Q_{LMDWF}$  of  $0.41Q_{LADWF}$  and a peak  $Q_{LPDWF}$  of  $1.59Q_{LADWF}$ . The peak wet weather flow ( $Q_{LPWWF}$ ) is  $2.39Q_{LADWF}$ .

For the  $V_0$ ,  $n$  and  $X_F$  values, the following are calculated for the design:

$X_{R,crit} = 4/n =$	9.28 g/l	Eq A16b
$R_{crit} = 3.5/(4/n-3.5) =$	0.605 -	Eq A27
$q_{R,crit} = V_0/c^2 =$	0.803 m/h	Eq A26
$X_{Lmin} = 2/n \text{ or } X_{R,crit}/2 =$	4.64 g/l	Eq A16b
$j_{Lmax} = 4V_0/(nc^2) = X_{R,crit} \times q_{R,crit} =$	7.46 kg/(m <sup>2</sup> h)	Eq A16a
$q_{AmaxSHC I} = q_{R,crit}/R_{crit} \text{ or } j_{Lmax}/X_F - q_{R,crit} =$	1.328 m/h	Eq A10
$q_{AmaxSHC II} = V_0 \exp(-n X_F) =$	1.314 m/h	Eq A28

For the  $V_0$  and  $n$  values, the D&O chart is constructed as set out above. At  $Q_{LPWWF}$ , SHC II must be met and because  $q_{AmaxSHC II} < q_{AmaxSHC I}$  (only slightly), the area is calculated on the basis of  $q_{AmaxSHC II}$  and SHC I is met by adjusting the recycle ratio  $R$  to the value where  $q_{AmaxSHC I} = q_{AmaxSHC II}$ . This  $R$  value, which is less than  $R_{crit}$  and found by trial and error, is the minimum  $R$  to satisfy SHC I and is called  $R_{min}$ . In this example,  $R_{min} = 0.588$ . For high  $X_F$  and/or poor sludge settleability there is usually a much larger difference between  $R_{min}$  and  $R_{crit}$ . The  $Q_{LPWWF}$  is  $2.39 \times 220 = 525 \text{ m}^3/\text{h}$ . From Eq A28 (Fig A14), the maximum overflow rate at  $X_F = 3.5 \text{ kg/m}^3$  is  $1.314 \text{ m/h}$  (given by horizontal SHC II line). Hence the minimum SST area is  $525/1.31 = 401 \text{ m}^2$ . In order that SHC I is met under PWWF conditions, the recycle ratio at PWWF with respect to PWWF ( $R_{PWWF}$ ) must be greater than  $R_{min} = 0.588$ , given by the  $R$  value of the intersection point of the SHC I and II lines which is slightly to the left of the hyperbola (see point D in Fig A14). Hence, at PWWF, the recycle flow  $Q_R$  should be equal to or greater than  $0.588 \times 525 = 309 \text{ m}^3/\text{h}$  or  $1.40$  times  $Q_{LADWF}$ , otherwise failure (gross sludge loss) will occur, i.e. for  $R_{PWWF} < 0.588$ , the  $q_A - R$  intersection point falls above the SHC I line in Fig A14.

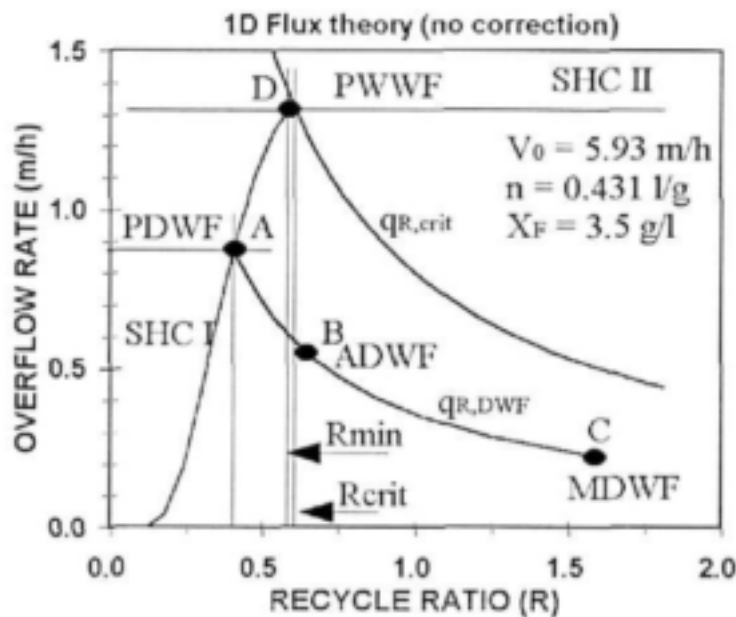
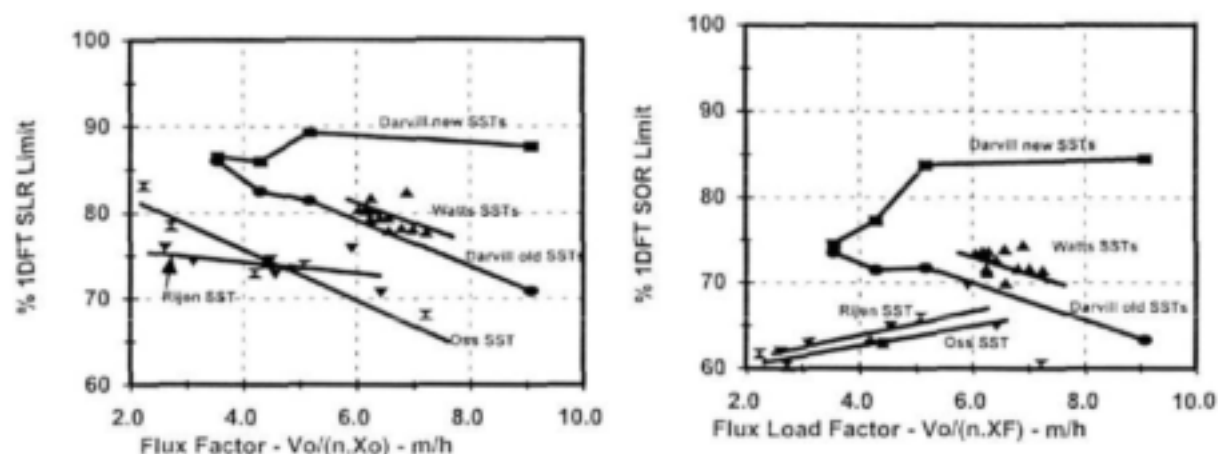


*Fig A14: D&O chart for the design example showing the showing the SST PWWF capacity defining Point D and the diurnal DWF operating positions at constant recycle flow for Peak DWF (Point A), Average DWF (Point B) and Minimum DWF (point C).*

The overflow rate at PDWF is  $1.59 \times 220 / 401 = 0.872$  m/h. This is well below the SHC II limit of 1.314 m/h. In order that SHC I is met at PDWF, the underflow recycle ratio  $R$  with respect to PDWF must be at least 0.405, given by the  $R$  value of the intersection point of the horizontal  $q_A = 0.876$  m/h line and the SHC I line for  $X_F = 3.5$  kg/m<sup>3</sup> (see point A in Fig A14). Hence the recycle flow  $Q_R$  at PDWF should be at least  $0.405 \times 1.59 \times 220 = 142$  m<sup>3</sup>/h or approximately 0.645 with respect to  $Q_{LADWF}$ . Accepting the SST area of 401 m<sup>2</sup> and fixing the recycle flow  $Q_R$  at a constant 142 m<sup>3</sup>/h, the overflow rate ( $q_A$ ) and recycle ratio ( $R$ ) at ADWF are 0.548 m/h and 0.645:1 with respect to  $Q_{LADWF}$  respectively (see point B in Fig A14). The overflow rate and recycle ratio at minimum dry weather flow (MDWF) are 0.225 m/h and 1.571:1 with respect to  $Q_{LADWF}$  respectively (see point C in Fig A14). Hence in the D&O chart, the locus of the points defining the PDWF, ADWF and MDWF operating conditions moves between points A and C through B in Fig A14, falling on the hyperbola  $q_R = 142 / 401 = 0.354$  m/h. All these points represent safe operating conditions with respect to the two sludge handling capacity criteria. Hence, under dry weather conditions, the SST should operate satisfactorily. Provision for wet weather flow is made up to a PWWF of  $2.39 Q_{LADWF}$ , but the recycle flow  $Q_R$  needs to be increased from 142 to 308 m<sup>3</sup>/h to accommodate this. For lower WWFs than this peak, the recycle flow need not be increased so high. The required recycle flow can be determined from the D&O chart along the SHC I line as was done for the PDWF.

The applicability of the 1D idealized flux theory (1DFT) for design of SST was evaluated by Marais *et al.* (2000, 2001) and Ekama and Marais (2001) by comparing its predicted maximum surface overflow (SOR) and solids loading (SLR) rates with that calculated from the 2D hydrodynamic model SettlerCAD using as a basis 35 full scale SST stress tests conducted on different SSTs with diameters from 30 to 45m and 2.25 to 4.1m side water depth, with and without Stamford baffles. The results of some simulations are summarized in Fig A15a and b.





Figs 15a and b: SettlerCAD predicted maximum SOR (Fig 1a, left) and SLR (Fig 1b, right), as a % of the 1DFT limit values, versus flux load factor  $V_d/(nX_F)$  for the 4 tests on the Darvill new (■) and old (●) SSTs, 15 of the 15 tests on the Watts' SST (▲), 6 of the 14 tests on the Rijen SST (▼) and 6 of the 10 tests on the Oss SST (×).

From the simulations, a relatively consistent pattern appeared, i.e. that the 1DFT can be used for design but its predicted maximum SLR needs to be reduced by an appropriate flux rating, the magnitude of which depends mainly on SST depth and hydraulic loading rate (HLR). Simulations of the Watts *et al.* (1996) SST with 6.0m SWD, and the Darvill new (4.1m SWD) and old (2.5m SWD) SSTs with interchanged SWD, were run to confirm the sensitivity of the flux rating to depth and HLR. Simulations with and without Stamford and/or Crosby baffles were also done. While the design of the internal features of the SST, such as baffling, have a marked influence on the effluent SS concentration, these features appeared to have only a small influence on the flux rating, i.e. capacity, of the SST.

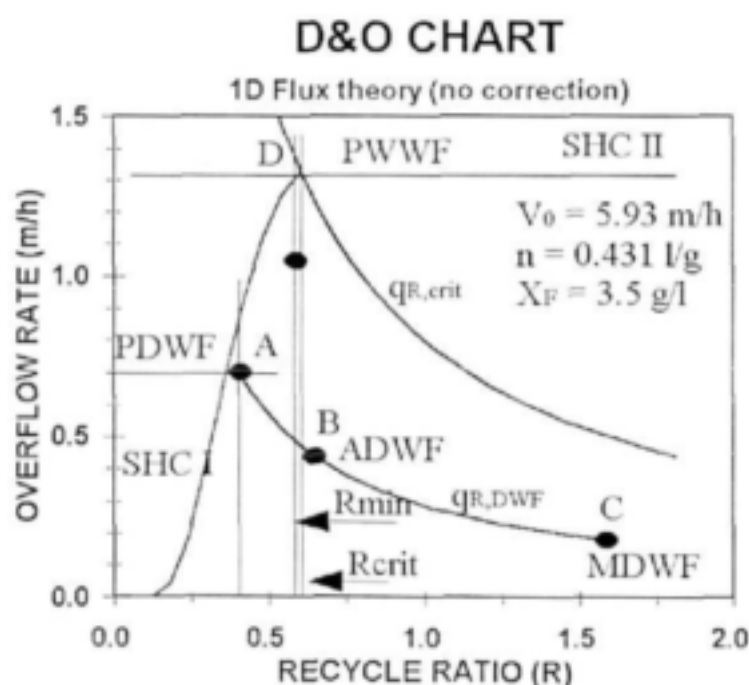


Fig A16: D&O chart for the design example with the SST area increased by 25%. Note that the PWWF PDWF, ADWF and MDWF operating positions have moved vertically downwards (i.e. recycle ratios have not changed) and fall well below the SHC I and II lines to account for the non idealities in full scale SSTs.

As a consequence of the reduced capacity of full scale SSTs compared with that calculated from the 1DFT, the 1DFT calculated maximum SOR and SLR need to be reduced. Until more information is obtained, it would appear that from the simulations that the flux rating of 0.80 of the 1DFT maximum SLR recommended by Ekama and Marais (1986) remains a reasonable value to apply in the design of full scale SSTs - for deep SSTs (4m SWD) the flux rating could be increased to 0.85 and for shallow SSTs (2.5m SWD) decreased to 0.75 (Fig A16b, left).

Reducing the 1DFT SLR to 80% of the calculated value is equivalent to increasing the SST surface area by 25% ( $1/0.80 = 1.25$ ). Increasing the area by 25% gives a  $400 \times 1.25 = 500 \text{ m}^2$  SST for this design example. This increased area changes the PWWF, PDWF, ADWF and MDWF operating positions in the D&O chart, which are shown in Fig A16. Increasing the SST area moves the operating positions vertically downward in the D&O chart, i.e. the recycle ratio values do not change because the design influent and recycle flows have not changed; however, the overflow and underflow rates have decreased to 80% of the 1DFT values.

## 9 REFERENCES

- ATV - Abwassertechnische Vereinigung (1976) Erläuterungen und Ergänzungen zum Arbeitsbericht des ATV-Fachausschusses 2.5 Absetzverfahren. Die Bemessung der Nachklärbecken von Belebungsanlagen. *Korrespondenz Abwasser*, **23**(8), 231-235.
- ATV - Abwassertechnische Vereinigung (1991) Dimensioning of single stage activated sludge plants upwards from 5000 total inhabitants and population equivalents. *ATV Rules and Standards*. Wastewater- waste, UDC 628.356:628.32.001.2(083), Issue No. 11/92.
- Daigger G.T. and Roper R.E. (1985) The relationship between SVI and activated sludge settling characteristics. *Journal WPCF*, **57**(8), 859-866.
- Dick R.I. and Young K.W. (1972) Analysis of thickener performance of final settling tanks. Presented at 27th Purdue Industrial Waste Conference, Lafayette, Indiana.
- Ekama G.A., Pitman A.R., Smollen M. and Marais G.vR. (1984) Secondary settling tanks - Chapter 8 in *Theory design and operation of nutrient removal activated sludge processes*. Water Research Commission, P O Box 824, Pretoria, 0001, RSA.
- Ekama G.A. and Marais G.vR. (1986) Sludge settleability and secondary settling tank design procedures. *Water Pollut. Control*, **5**(1), 101-113.
- Ekama GA, Barnard JL, Günthert FW, Krebs P, McCorquodale JA, Parker DS, Wahlberg EJ (1997) *Secondary settling tanks: Theory, design, modelling and operation*. IAWQ STR No 6, pp216, International Association on Water Quality, London.
- Ekama GA and Marais P (2001) Hydrodynamic modelling of secondary settling tanks - Final report to the Water Research Commission on contract K5/835. WRC Report 835/1/01, Water Research commission, PO Box 824 , Pretoria, 0001, RSA.
- Grijpspeerdt K, Vanrolleghem P, and Verstraete W (1991) Selection of one dimensional models for online use. *Wat. Sci. Technol.* **31**(2), 193-204.
- Marais P, Ekama GA and de Haas DW (2000) Comparison of the 1D idealized flux theory and a 2D hydrodynamic model with full-scale secondary settling tank performance data. *Procs. 6<sup>th</sup> biennial Water Institute of Southern Africa conference and exhibition*, Suncity,

- 28/5 to 1/6/2000. CD-ROM ISBN 0-620-25661-3.
- Marais P and Ekama GA (2001) Comparison of the 1D idealized flux theory and a 2D hydrodynamic model with full scale secondary settling tank performance data. Research report W111, Dept. of Civil Eng., Univ. of Cape Town, Rondebosch, 7701, Cape, RSA.
- Marais PM, Ekama GA and de Haas DW (2001) Assessing the applicability of the 1D flux theory to full-scale secondary settling tank design with a 2D hydrodynamic model. *Procs. 74<sup>th</sup> Water Environment Federation Conference and Exhibition*, Atlanta, 13-17 Oct. (2)
- Merkel W. (1974) Die Bemessung horizontal durchströmter Nachklärbecken von Belebungsanlagen. *gwf-Wasser/Abwasser*, **115** H(6), 272-282.
- Ozinsky A.E. and Ekama G.A. (1995) Secondary settling tank modelling and design Part 2: Linking sludge settleability measures. *Water SA*, **21**(4), 333-349.
- Pitman A.R. (1980) Settling properties of extended aeration sludges. *Journal WPCF*, **52**(3), 524-536.
- Pitman A.R. (1984) Settling of nutrient removal activated sludges. *Water Sci. Technol.*, **17**(Amsterdam), 493-504.
- Rachwal A.J., Johnstone D.W.M., Hanbury M.J. and Critchard D.J. (1982) The application of settleability tests for control of activated sludge plants. Chapter 13 in *Bulking of activated sludge - Preventative and remedial methods*, Eds: Chamber B. and Tomlinson E. J., Ellis-Hopwood Publishers, Chichester, UK, 224-242.
- Smollen M. and Ekama G.A. (1984) Comparison of empirical settling velocity equations in flux theory for secondary settling tanks. *Water SA*, **10**(4), 175-184.
- Standard Methods (1985) *Standard Methods for the examination of water and wastewater*, 16th Edn., AWWA, WEF, APHA, 1015 Fifteenth St. NW, Washington, DC 20005.
- STOWa (1981) (Stichting Toegepast Onderzoek Waterbeheer. Formerly STORA - Stichting Toegepast Onderzoek Reiniging Afvalwater) *Hydraulische en technologische aspecten van het nabezink-proces. Rapport 2 - Ronde nabezinktanks - Praktijkonderzoek, Ontwerpgegevens en Bedrijfservaring*. Postbus 8090, RB 3505, Utrecht, Holland.
- Tuntoolavest M., Miller E. and Grady CPL Jr. (1983) Factors affecting the clarification performance of activated sludge final settlers. *Journal WPCF*, **55**(3), 234-248.
- Vesilind P.A. (1968a) Discussion of 'Evaluation of activated sludge thickening theories' by Dick R.I. and Ewing B.B. in *J. San. Eng. Div., ASCE*, **93**(SA4), 9-29, *J. San. Eng. Div., ASCE*, **94**(SA1), 185-191
- Vesilind P.A. (1968) Design of prototype thickeners from batch settling tests. *Water and Sewage Works*, **115**(July), 302-307.
- Watts RW, Svoronos SA and Koopman B (1996). One dimensional modelling of secondary clarifiers using a concentration feed velocity dependent dispersion coefficient. *Water Research*, **30**(9), 2112-2124.
- White M.J.D. (1975) Settling of activated sludge. Technical Report TR11, *Water Research Centre*, England.
- White M.J.D. (1976) Design and control of secondary settlement tanks. *Water Pollut. Control*, **75**(4), 459-467.
- Yoshioka N., Hotta Y., Tanaka S., Naito S. and Tsugami S. (1957) Continuous thickening of homogenous flocculated slurries. *Chem. Eng. (Kagaku Kogaku)*, Tokyo, **21**, 66-74.
- Zhou S, Pfeil R, Strand E, Ji Z and Vitasovic C (1998) SettlerCAD (formerly Clarity) Release 1.1 - A 2D hydrodynamic model for secondary clarifiers. Reid Crowther Consulting, Seattle, WA.

## APPENDIX 2

## LIST OF ABBREVIATIONS FOR PART 1

ADWF	Average Dry Weather Flow	mm	millimetres
ASCE	American Society of Civil Engineers	PDWF	Peak Dry Weather Flow
ATV	Abwassertechnischen Vereinigung	PWWF	Peak Wet Weather Flow
CFD	Computational Fluid Dynamics	RAS	Return Activated Sludge
CRTC	Clarifier Research Technical Committee of the ASCE	RSA	Republic of South Africa
d	day	SBH	Sludge Blanket Height
D&O	Design and Operating chart	SHC	Solids Handling Criterion
DSVI	Diluted Sludge Volume Index	SLR	Solids Loading Rate
DWF	Dry Weather Flow	SOR	Surface Overflow Rate
e.g.	For example	SS	Suspended Solids concentration
Eq	Equation	SST	Secondary Settling Tank
ESS	Effluent Suspended Solids	SSVI	Stirred Specific Volume Index
<i>et al.</i>	and others	STOWa	Stichting Toegepast Reiniging Waterbeheer (Holland)
exp	exponent	STR	Scientific and Technical Report
Fig	Figure	SVI	Sludge Volume Index
g	gram	SWD	Side Water Depth of SST
h	hour	SZSV	Stirred Zone Settling Velocity
HLR	Hydraulic Loading Rate	TP	Turning Point
HRT	Hydraulic Retention Time	TSS	Total Suspended Solids
i.e.	that is	UCT	University of Cape Town
IAWQ	International Association for Water Quality	USA	United States of America
IP	Inflexion point	viz.	that is to say (videlicet)
kg	kilogram	WAS	Waste Activated Sludge
L	Length	WLR	Weir Loading Rate
ℓ	litres	WRC	Water Research Commission (South Africa)
ln	logarithm to the base <i>e</i>	WW	Wastewater
log	logarithm to the base 10	WWF	Wet Weather Flow
M	Mass	WWTP	Wastewater Treatment Plant
m	metre	ZSV	Zone Settling Velocity
max	maximum	1D	One Dimensional
MDWF	Minimum Dry Weather Flow	1DFT	One dimensional steady state idealized flux theory
mg	milligrams	2D	Two Dimensional
mg/ℓ	milligrams per litre		
min	minutes		
ml	millilitres		
Mℓ	Megalitres (10 <sup>6</sup> l) (=0.264 million US gallons)		
Mℓ/d	Megalitres per day (=0.264 mgd)		
ml/g	millilitres per gram		
MLSS	Mixed Liquor Suspended Solids		

## LIST OF SYMBOLS FOR PART 1

$\alpha$	Square root term in overflow rate - recycle ratio Equation A24	-
$\Delta$	General symbol denoting change or difference	-
$\phi$	Diameter	L
$\phi_{IF}$	Diameter of inlet feedwell	L
$\phi_{FS}$	Diameter of feedwell skirt baffle	L
$\phi_{ST}$	Diameter of SST	L
$a$	Constant in log-log zone settling velocity equation	-
$A_{ST}$	Surface area of SST	L <sup>2</sup>
$A_{STmin}$	Minimum surface area of SST	L <sup>2</sup>
$b$	Constant in log-log zone settling velocity equation	-
$e$	Base number of the natural logarithm scale ( $e = 2.713..$ )	-
$f_{ns}$	fraction of non-settling particles in the feed solids concentration ( $X_F$ )	-
$h_{IF}$	Depth of inlet feedwell	L
$h_{FS}$	Depth of feedwell skirt baffle	L
$h_{ST}$	Depth of SST at feedwell skirt baffle	L
$H$	General symbol for water depth in SST	L
$H_{ave}$	Average water depth	L
$H_{swd}$	Side water depth	L
$j$	General symbol for flux [kgSS/(m <sup>2</sup> .h)]	M/(L <sup>2</sup> T)
$j_{AP}$	Applied flux to SST	M/(L <sup>2</sup> T)
$j_B$	Flux due to the movement of water relative to SST wall (bulk flux)	M/(L <sup>2</sup> T)
$j_L$	Limiting flux	M/(L <sup>2</sup> T)
$j_{Lmax}$	Maximum limiting flux	M/(L <sup>2</sup> T)
$j_{max}$	Maximum flux	M/(L <sup>2</sup> T)
$j_s$	Flux of the settling SS with respect to the water (gravity settling flux)	M/(L <sup>2</sup> T)
$j_T$	Total flux of SS with respect to SST wall (gravity flux + bulk flux)	M/(L <sup>2</sup> T)
$m$	Slope of SST floor (m:1)	-
$k_2$	Constant in Takács double exponential settleability Equation 2	L <sup>3</sup> /M
$n$	Flux theory constant in semi-log $V_{25} - X$ Equation 1	L <sup>3</sup> /M
$n$	Constant in Takács double exponential settleability Equation 2	L <sup>3</sup> /M
$N_{TS}$	Number of steps in simulation run time	-
$Q$	General symbol for volumetric flow rate (m <sup>3</sup> /h)	L <sup>3</sup> /T
$Q_E$	Effluent flow rate from SST ( $= Q_i - Q_w$ )	L <sup>3</sup> /T
$Q_F$	Feed flow rate to SST ( $= Q_i + Q_R - Q_w$ )	L <sup>3</sup> /T
$Q_i$	Influent flow rate to wastewater treatment plant	L <sup>3</sup> /T
$Q_{I,ADWF}$	Influent flow rate at Average DWF	L <sup>3</sup> /T
$Q_{I,MDWF}$	Influent flow rate at Minimum DWF	L <sup>3</sup> /T
$Q_{I,PDWF}$	Influent flow rate at Peak DWF	L <sup>3</sup> /T
$Q_{I,PWWF}$	Influent flow rate at Peak WWF	L <sup>3</sup> /T
$Q_R$	Return activated sludge (RAS) flow rate (before underflow WAS abstraction)	L <sup>3</sup> /T
$Q_{R,ADWF}$	RAS flow rate at ADWF with respect to ADWF	L <sup>3</sup> /T
$Q_{R,crit}$	Critical RAS flow rate	L <sup>3</sup> /T
$Q_{R,PWWF}$	RAS flow rate at PWWF with respect to PWWF	L <sup>3</sup> /T
$Q_w$	Waste activated sludge (WAS) flow rate	L <sup>3</sup> /T
$q_A$	Surface overflow rate ( $Q_i/A_{ST}$ )	L/T
$q_{A,ADWF}$	Overflow rate at DWF	L/T

$q_{A,PWWF}$	Overflow rate at WWF	L/T
$q_{Amax}$	Maximum surface overflow rate	L/T
$q_{AmaxSHC\ I}$	Solids Handling Criterion I maximum surface overflow rate	L/T
$q_{AmaxSHC\ II}$	Solids Handling Criterion II maximum surface overflow rate	L/T
$q_R$	Underflow rate ( $Q_R/A_{ST}$ , m/h)	L/T
$q_{R,crit}$	Critical underflow rate in flux theory (i.e. $q_R = V_o/e^2$ m/h)	L/T
$q_w$	Weir loading rate [ $m^3/(h.m)$ ]	$L^3/(LT)$
$R$	Underflow recycle ratio ( $= Q_R/Q_I$ )	-
$R_{crit}$	Critical underflow rate	-
$R_{ADWF}$	Underflow recycle ratio with respect to ADWF	-
$R_{ha}$	Actual hydraulic retention time	T
$R_{PWWF}$	Underflow recycle ratio with respect to PWWF	-
$t$	Time	T
$T$	Time	T
$T_{sim}$	Simulation run time	T
$V_o$	Flux theory constant in semi-log $V_{zs} - X$ relationship	L/T
$V_{ST}$	Volume of SST	$L^3$
$V_s$	Settling velocity of the sludge ( $= V_{zs}$ )	L/T
$V_{SXF}$	Settling velocity of the feed concentration ( $X_f$ )	L/T
$V_{SXL}$	Settling velocity of the limiting concentration ( $X_L$ )	L/T
$V_{ZS}$	Stirred zone settling velocity of the sludge	L/T
$X$	Suspended solids concentration (mgSS/l)	$M/L^3$
$X_E$	Effluent suspended solids concentration	$M/L^3$
$X_F$	Feed SS concentration to SST	$M/L^3$
$X_L$	Limiting solids concentration of the flux theory	$M/L^3$
$X_{Lmin}$	Minimum limiting solids concentration of the flux theory	$M/L^3$
$X_R$	Underflow sludge concentration	$M/L^3$
$X_{Rmin}$	Minimum underflow sludge concentration	$M/L^3$
$X_{R,crit}$	Critical underflow concentration ( $= X_{Rmin}$ )	$M/L^3$
$X_t$	Total suspended solids concentration	$M/L^3$
$X_w$	Wasteflow suspended solids concentration	$M/L^3$

**UNIVERSITY OF CAPE TOWN**  
**Department of Civil Engineering**  
*Water Research Group*

**FINAL REPORT**  
**to the Water Research Commission for the task**

**DEVELOPMENT OF A FINITE ELEMENT 2D HYDRODYNAMIC MODEL FOR  
SECONDARY SETTLING TANKS**

**in the contract K5/835**  
**HYDRODYNAMIC MODELLING OF SECONDARY SETTLING TANKS**

**by**

**Dorothee Kleine and Daya Reddy**

## **1 INTRODUCTION**

Secondary settling tanks (SSTs) form a crucial part of wastewater treatment plants. Besides having to produce the separation of suspended solids and clarified effluent the final settling tank is used to concentrate and recycle the settled sludge to the biological reactor. The efficiency of the biological reactor in the wastewater treatment system is determined by the efficiency of this final clarifying process. Problems arise due to the dominating two-phase flow in the settling tanks. The lack of knowledge regarding this complex flow often leads to false estimations with regard to the design of the inlet and outlet structure, and to oversizing during the renovation and construction of new plants. One way of promoting improved design and of resolving the bottleneck of existing settling tank is through the use of Computational Fluid Dynamics modelling of final settling tanks. The degree of flow and solids maldistribution can be qualified and suggestions can be made concerning improvements. This could lead to lower operating costs, higher capacities and to delayed investment expenditures.

Hydrodynamic models have been developed for simulating secondary settling tanks to get a better understanding of the complex flow patterns in these tanks and to make design and optimization of the SST internal features possible. These models use mainly the finite volume method (FVM) as numerical method (McCorquodale and Zhou, 1993; Lakehal *et al.*, 1999).



The purpose of this work is to develop and implement a finite element analysis of SSTs. Although this method is originated in stress analysis, applications of the finite element method in heat transfer and fluid flow are now widespread.

Both numerical methods, the FEM and the FVM, have their pros and cons. The power of the finite element method lies in its ability to treat problems on irregular domains, and to provide local grid refinement. The flexible geometry of the FEM supports the description and adaptation of complex internal features of SSTs like inlet and outlet arrangements.

The hydrodynamic SST model solves the continuity, momentum and the solids transport equations, as well as the  $k$ - $\epsilon$ -turbulence equations that are described in Chapter 5 of the book "Secondary Settling Tanks: Theory, Modelling, Design and Operation", IAWQ STR 6 (Ekama *et al.*, 1997).

The physical and mathematical extension requires efficient and robust solution schemes for the coupled system of equations describing the problem. The characteristically complex and highly unstable flow in SSTs imposes great challenges on the numerical and computational approaches.

The treatment of the convection terms and the gravity-density term in the Navier-Stokes equations is an important issue to be addressed. The flow pattern in SSTs strongly depends on the viscosity and on buoyancy forces. Furthermore, at high concentration range the settling velocity of the sludge approaches the magnitude of the turbulent diffusivity, which makes the settling motion difficult or even impossible to obtain. Questions arise as to what extent the settling motion in the high concentration range is hindered by diffusion or its turbulent part, and what influence the turbulence has particularly in stable stratification of SSTs. Since the velocities in the main section of SSTs are very small, it is difficult to carry out measurements that can give suitable data to describe the rheology of sludge in the high concentration range.

The problems that arise in the numerical treatment of these partial differential equations arise from the strong nonlinearity of the system of equations, the incompressibility constraint, local changes of the problem character in space and time, and the temporarily stiff systems of differential equations.

The main goal of this project is to compile a working finite element package for 2D hydrodynamic modelling of SSTs that is capable of simulating the benchmark results available in the literature.

## 2 SECONDARY SETTLING TANKS

### 2.1 Function of Secondary Settling Tanks

Secondary settling tanks form a crucial part of wastewater treatment plants based on activated sludge. Activated sludge is biological mass (flocs) produced in the treatment of wastewater by the growth of suspended bacteria. The activity of these living organisms results in the biodegradation of wastewater or sludge components. In the secondary settling tank the activated sludge is subsequently separated from the treated wastewater by gravity sedimentation and is returned to the process (Fig 1).

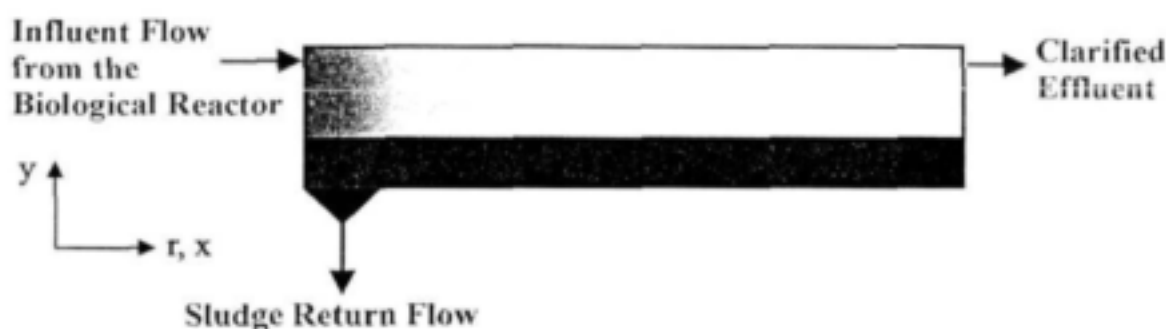


*Fig 1: Secondary Settling Tank*

### 2.2 Hydrodynamic Modelling of SSTs

Fluid dynamics problems must obey the two governing equations of continuity and momentum. In addition, the flow in a sedimentation tank is characterized by the simultaneous flow of two phases. This two-phase system is a suspension of particles in a fluid, which comprises suspended solids and water. In settling tanks the sludge particles have different shapes and forms. Due to these different forms and shapes the sludge particles enclose the surrounding fluid. As a result the solids influence the liquid and vice versa, and with that the flow distribution can completely change.

The dynamics of sedimentation are determined by the interaction between buoyancy and drag forces. Due to their higher density the suspended solids have a tendency towards sedimentation and to accumulation at the bottom of the tank, leading to a stratified flow field. The sedimentation process involves a relative velocity of the solids with respect to the fluid phase. In the low concentration range the activated sludge is flocculent, which means that particle diameter and hence the settling velocity increase with concentration. At a certain concentration the difference between the velocities of the two phases decreases with increasing particle concentration due to increasing cohesive forces. This is the concentration range of hindered settling.

Many complications arise due to factors such as the wide variety of sizes and shapes of the particles, nonuniform flow patterns, agglomeration, and interparticle forces.

Different mathematical models have been developed to describe two-phase flows (Gidaspow, 1994). In these models each phase is calculated by a separate momentum equation. The coupling of the two phases takes place over interphase-friction forces, the pressure, and the requirement that over the entire flow domain, the volume of the two phases forms a continuum.

Due to the strong interlink between the activated sludge and the water it is assumed that the two phases react as a fluid mixture with variable density. In the mathematical model this fluid mixture of water and suspended solids is calculated by a momentum equation that includes a source term to represent the forces due to change in the density of the fluid mixture. The local density of this fluid mixture depends on the local concentration of the sludge particles, which is solved by a particulate mass conservation equation. This equation involves the relative velocity between the two phases due to their different densities. A density-state equation then gives the local density of the fluid mixture with respect to the solid concentration. The coupling between the momentum equation and the solids transport equation / density-state-equation is achieved through the gravity-density term in the momentum equation (Fig 2).

### Fluid Mixture = Pure Water + Suspended Solids

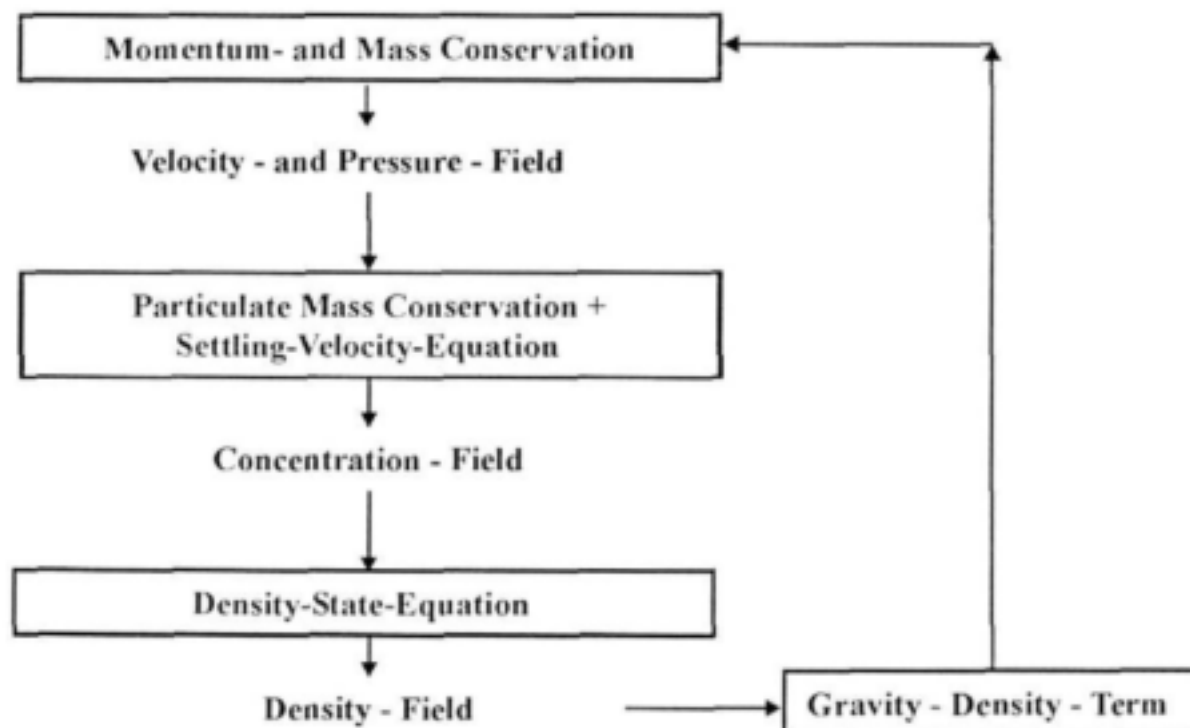


*Fig 2: Modelling of fluid-solid flow in SSTs*

### 3 FUNDAMENTAL EQUATIONS

As described in the above chapter the distribution of mean flow quantities in settling tanks is governed by the conservation equations for mass, momentum and solid concentration. For the modelling of two-dimensional unsteady, turbulent, density stratified flow in secondary settling tanks the following system of equations is required (Ekama *et al.*, 1997):

#### 3.1 Conservation of Fluid Mass: Continuity Equation

The continuity equation describes the physical principle of mass conservation. In the case of settling tanks the fluid mixture is treated as if it were a single phase fluid, and the equation is

$$\frac{\partial r^m U}{\partial r} + \frac{\partial r^m V}{\partial y} = 0 \quad (1)$$

The variables  $U$  and  $V$  are the temporal mean velocity components in the  $r$  and  $y$  directions,  $m = 1$  for the cylindrical coordinates and  $m = 0$  with  $r = x$  for the Cartesian coordinates.

In the above equation the use of the Boussinesq approximation has been made. The change of the fluid volume caused by the variable density of the fluid mixture is very small, so that the continuity equation for incompressible flow is assumed. With the Boussinesq approximation the influence of the variable density  $\rho$  appears only in the gravity-density term in the momentum equation.

#### 3.2 Conservation of Momentum: The Navier-Stokes Equations

The physical principle is described by Cauchy's equation of motion, which says that the total force on a body equals its change of momentum. In general, forces acting on a fluid system may be classified as body forces proportional to the volume or mass of the system, such as gravity, and surface forces proportional to the area of surface on which they act, such as pressure and viscous forces.

The set of momentum equations describing two-dimensional, unsteady, turbulent, flow in rectangular or circular settling tanks are:

*Conservation of Momentum in the Horizontal (x) resp. Radial Direction (r)*

$$\frac{\partial U}{\partial t} + U \frac{\partial U}{\partial r} + V \frac{\partial U}{\partial y} = - \frac{1}{\rho_r} \frac{\partial p}{\partial r} + \frac{1}{r^m} \frac{\partial}{\partial r} \left( r^m \nu_{eff} \frac{\partial U}{\partial r} \right) + \frac{1}{r^m} \frac{\partial}{\partial y} \left( r^m \nu_{eff} \frac{\partial U}{\partial y} \right) + S_U \quad (2)$$

### Conservation of Momentum in the Vertical Direction ( $y$ )

$$\frac{\partial V}{\partial t} + U \frac{\partial V}{\partial r} + V \frac{\partial V}{\partial y} = - \frac{1}{\rho_r} \frac{\partial p}{\partial y} + \frac{1}{r^m} \frac{1}{\partial r} \left( r^m v_{eff} \frac{\partial V}{\partial r} \right) + \frac{1}{r^m} \frac{1}{\partial y} \left( r^m v_{eff} \frac{\partial V}{\partial y} \right) + S_v \quad (3)$$

where

$$S_u = \frac{1}{r^m} \frac{\partial}{\partial r} \left( r^m v_{eff} \frac{\partial U}{\partial r} \right) + \frac{1}{r^m} \frac{\partial}{\partial y} \left( r^m v_{eff} \frac{\partial U}{\partial y} \right) - 2 \frac{v_{eff}}{r^2} U r \quad (4)$$

and

$$S_v = \frac{1}{r^m} \frac{\partial}{\partial r} \left( r^m v_{eff} \frac{\partial V}{\partial y} \right) + \frac{1}{r^m} \frac{\partial}{\partial y} \left( r^m v_{eff} \frac{\partial V}{\partial y} \right) - g \frac{\rho - \rho_r}{\rho_r} \quad (5)$$

The variables  $U$  and  $V$  are the temporal mean velocity components in the  $r$  (resp.  $x$ ) and  $y$  directions,  $p$  is the general pressure less the hydrostatic pressure at reference density  $\rho_r$ ,  $\rho$  is the fluid density and  $g$  is the component of gravitational acceleration in the vertical direction. The effective viscosity  $v_{eff}$  is the sum of the kinematic laminar and turbulent viscosity. The last term in Eq. 5 represents the force due to changes in the density of the fluid mixture.

### 3.3 Conservation of Particulate Mass: Concentration Equation

The equation for particulate mass equation consists of a convective part that is responsible for the particle movement in flow direction, and a diffusive part that distributes the solids in the direction of the concentration gradient. It describes the balance of the temporal and spatial rates of change of solid mass and the solid mass transport movement due to mixing and settling. The equation is

$$\frac{\partial C}{\partial t} + U \frac{\partial C}{\partial r} + V \frac{\partial C}{\partial y} = \frac{1}{r^m} \frac{\partial}{\partial r} \left( r^m v_{sr} \frac{\partial C}{\partial r} \right) + \frac{1}{r^m} \frac{\partial}{\partial y} \left( r^m v_{sy} \frac{\partial C}{\partial y} + r^m V_s C \right) \quad (6)$$

where

$$\begin{aligned} v_{sr} &= \frac{v_{eff}}{\sigma_{sr}} \text{ in horizontal direction} & [\text{m}^2/\text{s}], \\ v_{sy} &= \frac{v_{eff}}{\sigma_{sy}} \text{ in vertical direction} & [\text{m}^2/\text{s}] \end{aligned} \quad (7)$$

$C$  is the suspended solid concentration. The effective diffusivity of the solid concentration  $v_{sr}$  and  $v_{sy}$  is described with the use of the Reynolds analogy of mass transport and momentum transport involving the Schmidt numbers  $\sigma_{sr}$  in the  $r$ - or  $x$ -direction and  $\sigma_{sy}$  in the  $y$ -direction. Typical values

of the Schmidt number lie in the range of 0.5 to 1.0.  $V_s$  is the particle settling velocity, which is determined according to the local concentration by an approach described in the following chapter.

### 3.4 Solid Settling Equation

The settling equation by Takács *et al.* (1991) appears to be the best overall description of biological flocs in secondary clarifiers. The settling process is modelled using the double-exponential settling, which relates the solid settling velocity to the local concentration by

$$V_s = V_0 \left[ e^{-K(C-C_{min})} - e^{-K_1(C-C_{min})} \right] \quad (8)$$

Here  $V_0$  is a reference velocity (Stokes velocity),  $K$  and  $K_1$  are empirical coefficients for rapidly settling particles and for poorly settling particles respectively, and  $C_{min}$  is the non-settleable concentration. For the computation the second part of Eq. 8 is ignored, i.e. the poorly settling particles are not taken into account. Fig 3 shows the settling velocity against the concentration of the activated sludge for a set of parameters that is used for the simulation of the Darvill Old and New SST, as well for the Watts SST. For example, with a feed concentration of 3.6 g/l and a recycle concentration of 8.15 g/l for Darvill Test 3 the settling velocity decreases from 0.47 mm/s to 0.067 mm/s.

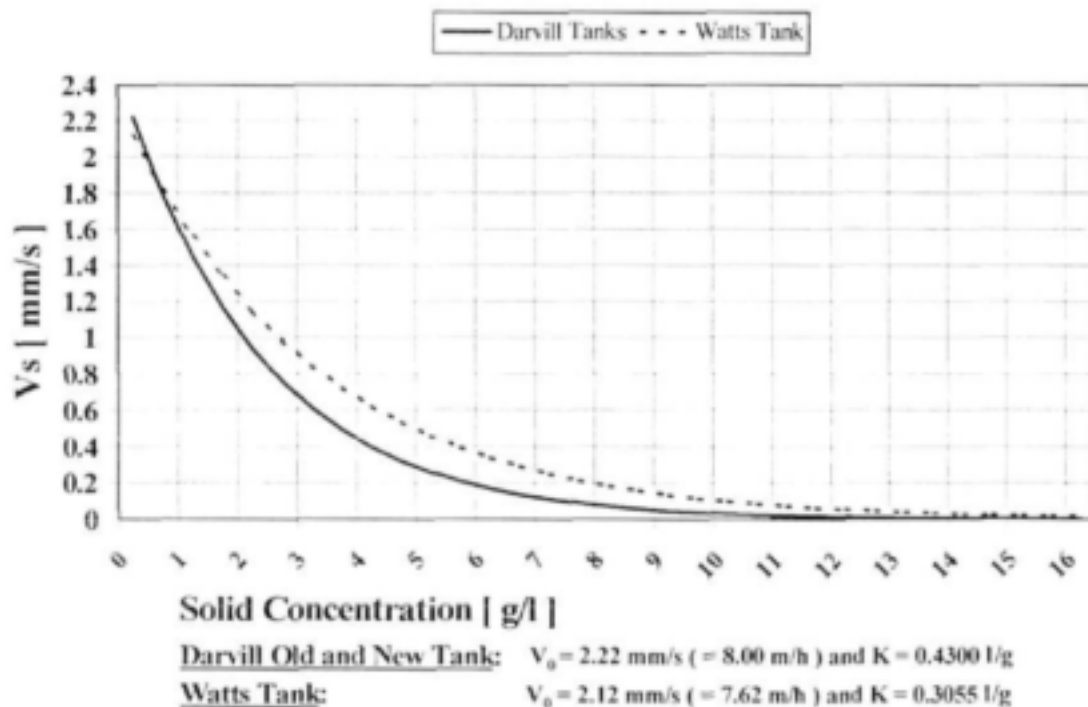


Fig 3: Modified settling function of Takács

### 3.5 Density-State Equation

The particulate mass conservation equation gives the concentration field, and with the density-state-equation the local density of the liquid-solid fluid mixture can be calculated according to

$$\rho = \rho_r + C \left( 1 - \frac{\rho_r}{\rho_s} \right) \quad (9)$$

Here  $\rho_s$  is the density of the dry particles solids,  $C$  the solids concentration in the same units as  $\rho$ , and  $\rho_r$  is the reference density (clear water). Fig 4 shows the density of the fluid mixture against the solid concentration. The small changes in the density of the fluid mixture have huge effects on the flow pattern in these SSTs, which is demonstrated in Chapter 5. For example, the liquid-solid density with a feed concentration of 3.6 g/l is with 1000.83 kg/m<sup>3</sup> only 0.83 ‰ higher than the reference density of clear water, and increases to 1001.88 kg/m<sup>3</sup> by a recycle sludge concentration of 8.15 g/l, which corresponds to less than 2 ‰ increase in the density of clear water.

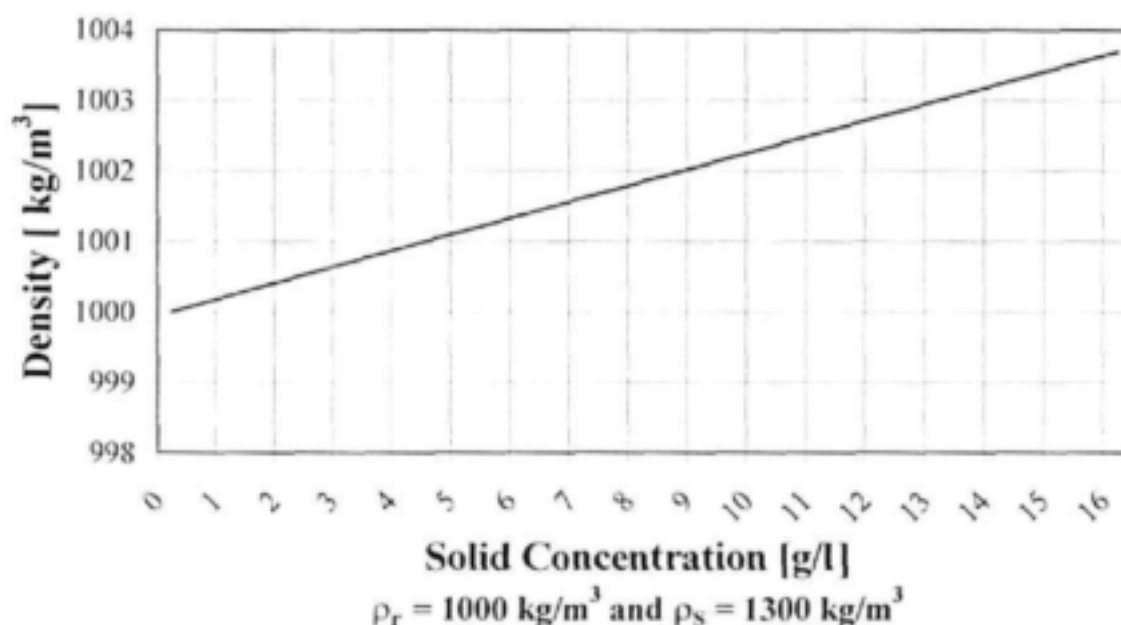


**Fig 4:** Density state equation

With the density-state equation the concentration of the solids is coupled to the hydrodynamics.



### 3.6 Turbulence Modelling

The flows of practical relevance are almost always turbulent. There is no unique definition for turbulent flow. In general turbulent fluid motion is irregular, random, unsteady and always 3D, in contrast to laminar flow, which can be 2D or 1D. The most accurate approach to turbulence simulation is to solve the Navier-Stokes equations. But the turbulent motion contains elements, which are much smaller than the extent of the flow domain.

In general turbulence is an eddying motion, which has a wide spectrum of eddy sizes. The eddies can be considered as vortex elements, which stretch each other, thereby passing energy on to smaller and smaller eddies until viscous forces become active and dissipate the energy. When buoyancy forces are present, there is also an exchange between potential energy of the mean flow and turbulent kinetic energy.

The engineer is not interested in the details of the fluctuating motion, but in the average character of real turbulence. Therefore the instantaneous values of the velocity, the pressure and the scalar quantity, in this context the solid concentration are separated into mean and fluctuating quantities. The turbulent velocity fluctuations act as a stress on the fluid as a result of the increased internal friction. Likewise the fluctuations of the solid concentration produce a turbulent mass flux. In most flow regions, the turbulent stresses and fluxes are much larger than their laminar counterparts.

Different mathematical approaches have been adopted to describe turbulence. They differ in their complexity and their numerical expense. The turbulence model should simulate the average character of real turbulence and together with the mean flow equations it forms a closed set.

Furthermore, turbulent transport is strongly affected by buoyancy effects. For instance, the stratified flow in settling tanks reduces turbulence, which means the turbulent viscosity and turbulent diffusivity are reduced. The characteristic of stable stratification permits the use of a constant turbulent or eddy viscosity / diffusivity in the whole tank (Krebs, 1989). One obvious disadvantage is the determination of suitable values for the turbulent sizes. Furthermore, regions of higher and lower turbulence are not distinguishable, as for example the inlet region and the main section of the settling tank.

The most commonly used turbulence model is the  $k$ - $\epsilon$ -turbulence model (Rodi, 1980) which determines the isotropic eddy viscosity  $\nu_t$  as a function of the turbulent kinetic energy  $k$  and its dissipation rate  $\epsilon$  by the formula

$$\nu_t = 0.09 \frac{k^2}{\epsilon} \quad . \quad (10)$$

The distribution of  $k$  and  $\varepsilon$  are determined from the semi-empirical transport equations

$$\frac{\partial k}{\partial t} + U \frac{\partial k}{\partial r} + V \frac{\partial k}{\partial y} = \frac{1}{r^m} \frac{\partial}{\partial r} \left( r^m \frac{\nu_t}{\sigma_k} \frac{\partial k}{\partial r} \right) + \frac{1}{r^m} \frac{\partial}{\partial y} \left( r^m \frac{\nu_t}{\sigma_k} \frac{\partial k}{\partial y} \right) + P_1 + P_2 - \varepsilon \quad (11)$$

and

$$\frac{\partial \varepsilon}{\partial t} + U \frac{\partial \varepsilon}{\partial r} + V \frac{\partial \varepsilon}{\partial y} = \frac{1}{r^m} \frac{\partial}{\partial r} \left( r^m \frac{\nu_t}{\sigma_\varepsilon} \frac{\partial \varepsilon}{\partial r} \right) + \frac{1}{r^m} \frac{\partial}{\partial y} \left( r^m \frac{\nu_t}{\sigma_\varepsilon} \frac{\partial \varepsilon}{\partial y} \right) + C_1 \frac{\varepsilon}{k} P_1 - C_2 \frac{\varepsilon^2}{k}, \quad (12)$$

where

$$P_1 = 2 \nu_t \left[ \left( \frac{\partial U}{\partial y} \right)^2 + \left( \frac{\partial V}{\partial r} \right)^2 + m \left( \frac{U}{r} \right)^2 + \frac{1}{2} \left( \frac{\partial U}{\partial y} + \frac{\partial V}{\partial r} \right)^2 \right] \quad (13)$$

represents the rate of production of turbulent kinetic energy resulting from the interaction of the turbulent stresses and velocity gradients, and

$$P_2 = \frac{g}{\rho_r} \cdot \frac{\nu_t}{\sigma_{sy}} \cdot \frac{\partial(\rho - \rho_r)}{\partial y} \quad (14)$$

the rate of production due to buoyancy effects.

The empirical constants  $C_\mu$ ,  $C_1$ , and  $C_2$ , as well as the turbulent Prandtl numbers for  $k$  and  $\varepsilon$ ,  $\sigma_k$  and  $\sigma_\varepsilon$  are given by Rodi (1980):  $C_\mu = 0.09$ ,  $C_1 = 1.44$ ,  $C_2 = 1.92$ ,  $\sigma_k = 1.0$  and  $\sigma_\varepsilon = 1.3$ .

In this work it is assumed that the eddy diffusivity that governs the solid mixing in the tank is proportional to the eddy viscosity, although this assumption has not yet been demonstrated (see Chapter 5.6.3 of the book "Secondary Settling Tanks: Theory, Modelling, Design and Operation", IAWQ STR 6 (Ekama *et al.*, 1997).

The buoyancy correction term  $P_2$  is often omitted as a first approximation (DeVantier and Larock, 1986; Zhou *et al.*, 1998).

## 4 NUMERICAL MODELLING

The modelling of this unsteady, multidensity, highly nonlinear fluid flow requires a very efficient and robust solution scheme. The following topics have to be taken into account:

- *Treatment of the incompressibility*
- *Treatment of the nonlinearity*
- *Complete inner and outer control*

The whole system of equations consists of six partial differential equations with six unknowns, namely the velocities in the horizontal and vertical direction, the pressure, and the solid concentration, as well as the turbulent kinetic energy and its dissipation. The system is solved by the finite element method and the fractional- $\theta$ -scheme in the spatial and temporal domains, respectively.

### 4.1 Spatial Discretization

Spatial approximation is achieved by the Galerkin weighted residual approach (Taylor and Hughes, 1981; Reddy, 1998). The finite element method subdivides the domain into a set of discrete volumes or finite elements, on which the solution is approximated by polynomials.

In the following the equations will be expressed in tensor notation in which indices  $i$  and  $j$  range over the dimension of the spatial domain. The usual summation convention on repeated indices is employed. In what follows,  $W$  is a test function.

For the continuity equation and the Navier-Stokes equations the residual formulations are

$$\int_{\Omega} W \frac{\partial r^m U_i}{\partial x_i} d\Omega = 0 \quad (15)$$

and

$$\int_{\Omega} W \left[ \frac{\partial U_i}{\partial t} + U_j \frac{\partial U_i}{\partial x_j} + \frac{1}{\rho_r} \frac{\partial p}{\partial x_j} + g \frac{\rho - \rho_r}{\rho_r} \delta_{i2} + 2 \frac{v_{eff}}{r^2} U_i \delta_{i1} + \right. \\ \left. - \frac{1}{r^m} \frac{\partial}{\partial x_j} \left( r^m v_{eff} \frac{\partial U_i}{\partial x_j} \right) - \frac{1}{r^m} \frac{\partial}{\partial x_j} \left( r^m v_{eff} \frac{\partial U_j}{\partial x_i} \right) \right] d\Omega = 0 \quad (16)$$

The scalar equations for the variables  $C$ ,  $k$  and  $\varepsilon$  are all similar in their formulation and we therefore show only the details of the concentration equation, for which

$$\int_{\Omega} W \left[ \frac{\partial C}{\partial t} + U_i \frac{\partial C}{\partial x_i} - \frac{1}{r^m} \frac{\partial}{\partial x_i} \left( r^m v_{si} \frac{\partial C}{\partial x_i} + r^m V_s C \right) \right] \partial \Omega = 0 \quad . \quad (17)$$

Integration by parts and use of the divergence theorem lead to the following expression

$$\int_{\Omega} \left[ W \left( \frac{\partial U_i}{\partial t} + U_j \frac{\partial U_i}{\partial x_j} + \frac{1}{\rho_r} \frac{\partial p}{\partial x_j} + g \frac{\rho^- - \rho_r}{\rho_r} \delta_{i2} + 2 \frac{v_{eff}}{r^2} U_i \delta_{i1} \right) + \frac{1}{r^m} \frac{\partial W}{\partial x_j} r^m v_{eff} \frac{\partial U_i}{\partial x_j} + \frac{1}{r^m} \frac{\partial W}{\partial x_j} r^m v_{eff} \frac{\partial U_j}{\partial x_i} \right] \partial \Omega = S \quad (18)$$

for the momentum equation, where

$$S = \oint_{\Gamma} W \left( v_{eff} \frac{\partial U_i}{\partial x_j} n_j + v_{eff} \frac{\partial U_j}{\partial x_i} n_i \right) \partial \Gamma \quad . \quad (19)$$

Here  $n_i$  is the  $i$ -component of the outward unit normal vector on the boundary  $\Gamma$ .

For the scalar equation of the concentration  $C$  we have

$$\int_{\Omega} \left[ W \left( \frac{\partial C}{\partial t} + U_i \frac{\partial C}{\partial x_i} - \frac{\partial (V_s C)}{\partial x_i} \right) + \frac{\partial W}{\partial x_i} \frac{v_{eff}}{\sigma_{si}} \frac{\partial C}{\partial x_i} \right] d\Omega = \oint_{\Gamma} W \frac{v_{eff}}{\sigma_{si}} \frac{\partial C}{\partial x_i} n_i d\Gamma \quad . \quad (20)$$

## 4.2 Weak Formulation of the Finite Element Equations

The discrete solution for the dependent variables ( $U$ ,  $V$ ,  $p$ ,  $C$ ,  $k$  and  $\varepsilon$ ) can be approximated within each element as a linear combination of appropriate interpolation function or basis (trial) function  $N$ . The approximate solutions of the variables  $U_i$  are

$$U_i = \sum_{m=1}^{N_e} (U_i(t))_m N_m \quad (21)$$

and for  $C$  (likewise for the other scalar variables  $p$ ,  $k$  and  $\varepsilon$ )

$$C = \sum_{m=1}^{N_p} (C(t))_m N_m, \quad (22)$$

where  $N_p$  is the total number of nodes on each element.

The classical Galerkin finite element method uses the same class of functions for the weighting function  $W$  and the basis function  $N$ . The approximate form (21) and (22) are substituted into the weighted residual formulations to obtain a set of equations for the unknowns  $(U)_m$ ,  $C_m$  and  $p_m$ , as well as for  $k_m$  and  $\varepsilon_m$ .

The nonlinear terms (convective flux and source term) are linearized using Picard iteration (Kelly, 1995). The transformation from Cartesian coordinates to the local coordinates is performed by the use of isoparametric finite elements. In this work a four noded isoparametric element is used. The piecewise bilinear interpolations for all variables are same in the formulation. The transformed integrals are then integrated numerically by 2 x 2 Gaussian Quadrature.

#### 4.3 Upwinding Technique - Streamline Upwind Petrov-Galerkin (SUPG) Method

It is well known that convective dominated cases lead to oscillating solutions. Those flows are characterised by a high Reynolds number or Peclet Number. The Galerkin method leads to central-difference type approximations of differential operators. At high Peclet numbers the central-differencing uncouples the unknowns, i.e. only variables with uneven or even indices are connected. This results in oscillations of the solution. One possible way of eliminating the oscillations is to severely refine the mesh, so that convection no longer dominates on an element. Another possibility is the use of upwinding techniques.

Upwind differencing amounts to approximating the convective derivatives with solution values at the upstream. The Streamline Upwind / Petrov-Galerkin method SUPG (Hughes and Brooks, 1982; Zienkiewicz and Taylor, 2000) is a modification of the classical Galerkin method to increase control over the advective / convective-derivative term. The weighting function for a typical node is modified to weight the element upwind of the node more heavily than the downwind element. The interpolation function  $N$  and the weighting function  $W$  are distinct. SUPG requires discontinuous weighting functions, which are the sum of the continuous weighting function used in the classical Galerkin method, and a discontinuous streamline upwind contribution. The modified weighting function is applied to all terms in the equation, resulting in a consistent residual formulation;  $W$  is given by

$$W = N + \frac{\alpha h / 2}{\sqrt{U_i U_i}} U_i \frac{\partial N}{\partial x_i} \quad , \quad (23)$$

where  $\alpha (= \coth(Pe) - 1/Pe)$  is the streamline upwind parameter, which depends on the element Peclet number  $Pe(=1/2h|u|/v)$ , and  $h$  is the characteristic length scale of the element (for detailed implementation see Zienkiewicz and Taylor, 2000).

From the mathematical point of view in this work the convergence problem is no longer a pure convective transport problem. In stratified flow fields, as in settling tanks, the gravity-production term can reduce the efficiency of the upwinding scheme.

#### 4.4 Temporal Discretization

The discretization in time can be performed by the usual methods such as Forward or Backward Euler-, the Crank-Nicolson or the Fractional-step- $\theta$ -scheme obtaining for each time step a sequence of generalised stationary problems, which is shown here, by way of example, for the Navier-Stokes equations

$$\frac{U_i^{t+\Delta t} - U_i^t}{\Delta t} + \theta[K]^{t+\Delta t} = -\frac{1}{\rho_r} \frac{\partial p^t}{\partial x_i} - g \frac{\rho^t - \rho_r}{\rho_r} \delta_{i2} - (1-\theta)[K]^t \quad (24)$$

with

$$K = U_j \frac{\partial U_i}{\partial x_j} - \frac{1}{r^m} \frac{\partial}{\partial x_j} \left( r^m v_{eff} \frac{\partial U_i}{\partial x_j} \right) - \frac{1}{r^m} \frac{\partial}{\partial x_j} \left( r^m v_{eff} \frac{\partial U_j}{\partial x_i} \right) + 2 \frac{v_{eff}}{r^2} U_i \delta_{i1} \quad (25)$$

By choosing suitably the value of  $\theta$  the mathematical model would be integrated either implicitly or explicitly in the temporal domain, e.g.  $\theta = 1$  for the implicit Euler scheme,  $\theta = 1/2$  for the Crank-Nicolson scheme, or  $\theta = 0$  for the explicit Euler scheme. These schemes have their advantages and deficiencies concerning accuracy and stability.

In this work the fractional-step- $\theta$ -scheme is adopted to integrate the time derivative (Turek, 1998). In this method the macro time step  $\Delta t$  is defined as a sequence of 3 time (sub-) steps  $\theta\Delta t$ ,  $\theta^*\Delta t$  and  $\theta\Delta t$ , and the corresponding implicit weighting factors are set to  $\alpha\theta$ ,  $\beta\theta^*$  and  $\alpha\theta$ , respectively, where  $\theta^* = 1 - 2\theta$ ,  $\alpha = (1 - 2\theta)/(1 - \theta)$  and  $\beta = \theta/(1 - \theta)$ . By choosing a special value for  $\theta$ , i.e.  $\theta = 1 - \sqrt{2}/2$ , the scheme is of second-order accuracy, strongly A-stable and physical oscillations are well preserved.

#### 4.5 Derivation of the Navier-Stokes Solver

The lack of an independent equation for the pressure complicates the solution of the Navier-Stokes equations. Furthermore mass conservation is a kinematic constraint on the velocity field in incompressible flows. One way to overcome this difficulty is to create a pressure field to satisfy the continuity equation.

There is a large variety of schemes all of which have been used in practice for several years. In this work a second-order accurate pressure-correction scheme by Van Kan (1986) is deployed to solve the unsteady, incompressible Navier-Stokes equations.

The treatment of incompressibility is taken into account by splitting the coupled problem of the Navier-Stokes-equations and the continuity equation and obtaining definite problems for the velocities as well as for the pressure, independently.

The solution at each time step  $\Delta t$  is obtained through three substeps:

Step 1:

$$\Delta U_i^* = U_i^* - U_i^t = \Delta t \left[ -\frac{1}{\rho_r} \frac{\partial p^t}{\partial x_i} - g \frac{\rho^t - \rho_r}{\rho_r} \delta_{i2} + K \right] \quad (26)$$

with

$$K = -U_j \frac{\partial U_i}{\partial x_j} + \frac{1}{r^m} \frac{\partial}{\partial x_j} \left( r^m v_{eff} \frac{\partial U_i}{\partial x_j} \right) + \frac{1}{r^m} \frac{\partial}{\partial x_j} \left( r^m v_{eff} \frac{\partial U_j}{\partial x_i} \right) - 2 \frac{v_{eff}}{r^2} U_i \delta_{i1} \quad (27)$$

In the first step starting at time  $t$  the linearized convection-diffusion equation for an intermediate velocity  $U_i^*$  is solved. The right hand side contains the gravity force and an "old" pressure approximation.

Step 2:

$$\frac{\partial^2 \Delta p}{\partial x_i^2} = \frac{1}{\Delta t} \left[ \frac{\partial r^m U_i^t}{\partial x_i} + \frac{\partial r^m \Delta U_i^*}{\partial x_i} \right] \quad (28)$$

An update equation for the pressure, a pressure-Poisson equation, is solved with the divergence of the intermediate velocity  $U_i^*$  and the velocity  $U_i$  of the previous time  $t$  on the right hand side.



Step 3:

In step 3 the new pressure  $p(t + \Delta t)$  and the new “discretely divergence-free” velocity  $U_i(t + \Delta t)$  will be updated.

$$p(t + \Delta t) = p(t) + \Delta p \quad (29), (30)$$

$$\Delta U_i = U_i(t + \Delta t) - U_i(t) = \Delta U_i^* - \Delta t \frac{\partial \Delta p}{\partial x_i}$$

The above-mentioned steps are repeated till a steady-state condition is reached. With the initial pressure  $p = 0$  for each time step the projection scheme is analogous to the scheme proposed by Chorin (1968).

#### 4.6 Equation Solution Technique

The numerical scheme for discretizing the mathematical model requires the solution of systems of linear equations to obtain the nodal solution. The whole equation system is coupled, i.e. the dominant variable of each equation occurs in some of the other equations. There are two approaches to solve such coupled systems: the simultaneous and the sequential approach.

In this work the whole equation system is decoupled through the use of an iterative scheme and linearisation of the system. Owing to the nonlinearity of these equations, an iterative process is required. The complete numerical solution process is split into two parts: the inner and the outer iterations. At each inner iteration the source terms and the coefficients that depend on the other variables are kept fixed. At the outer iterations the coefficient matrices and the source vector must be updated and the process repeated to obtain a solution that satisfies all of the equations. The right number of inner iterations per outer iteration has to be chosen carefully to optimize the solution process.

Nonstationary iteration methods are used to solve the system of equations (Barett *et al.* 1994; Kelly, 1995). In contrast to the stationary methods such as, the successive overrelaxation method, the computations involve information that changes at each iteration. The Conjugate Gradient (CG) method, is used to solve the symmetric positive definite system, i.e. the Pressure-Poisson equation. The CG proceeds by generating successive approximations to the solution. Two coupled recurrences are used, one that updates residuals using a search direction vector, and one that updates the search direction with a newly computed residual.

The Generalized Minimal Residual (GMRES) method is employed to solve the resulting non-symmetric nonlinear system of the discrete momentum and scalar equations (Saad *et al.* 1986). The GMRES method generates a sequence of orthogonal vectors, which are the residuals of the iterates. But in the absence of symmetry the previously computed vectors in the orthogonal sequence have to be retained. To avoid large storage requirement and work per iteration the restarted version of GMRES is adopted. The right decision of when to restart is one of the critical components for successful application of this method.

CG and GMRES are attractive as they provide a reference for checking the convergence of the inner iterations. At the same time they provide a measure of the convergence of the outer iterations.

## 5 EXAMPLE USE OF NUMERICAL MODEL AND EXPERIMENT

The performance of the model is analysed with tests done by de Haas *et al.* (1998) on SSTs of the Darvill wastewater treatment plant (Pietermaritzburg, South Africa), as well as with stress tests done by Watts *et al.* (1996) on one of the four SSTs at the Kanapaha Water Reclamation Facility (Florida, USA).

To take turbulence effects into account two different models were used. A constant turbulent viscosity was chosen for the Darvill Old and New Tank. This assumption is appropriate due to the fact that the turbulent inlet section of both tanks are small compared with the main section of the tank. This is not the case for the Watts Tank. The special construction of this SST makes it impossible to use a constant turbulent viscosity. The location of the skirt baffle divides the Watts Tank into two main sections of similar size: an inlet section of high turbulence, which acts as a mixing zone and the settling section of low turbulence, where settling takes place. Herewith the turbulence of the inlet section and its influence on the second section cannot be neglected. The use of the  $k-\varepsilon$  model was made for the simulation of the Watts Tank to take the different turbulence regions and their interaction into account. For the modelling of the diffusion coefficient in the concentration equation different modifications have been made. Best results could be reached by using Schmidt numbers higher than 1. Additional information is required in order to determine the extent to which the concentration distribution is affected by diffusion.

Furthermore the described mathematical model does not consider sludge compaction due to the hydrostatic pressure on the bottom of the tank. Those stress tests with very extreme loading conditions cannot verify the numerical model.

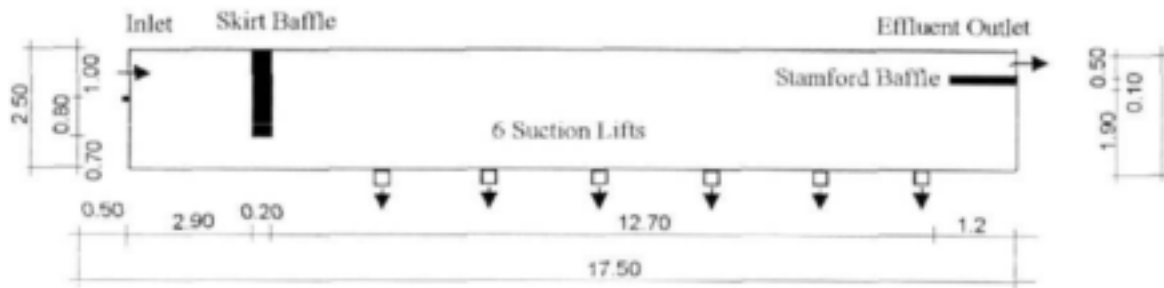
### 5.1 Geometry and Boundary Conditions for 2D-Model

The geometry and the boundaries of the simplified circular Darvill Old and New Tank as well as for the Watts Tank are shown in Fig 5.

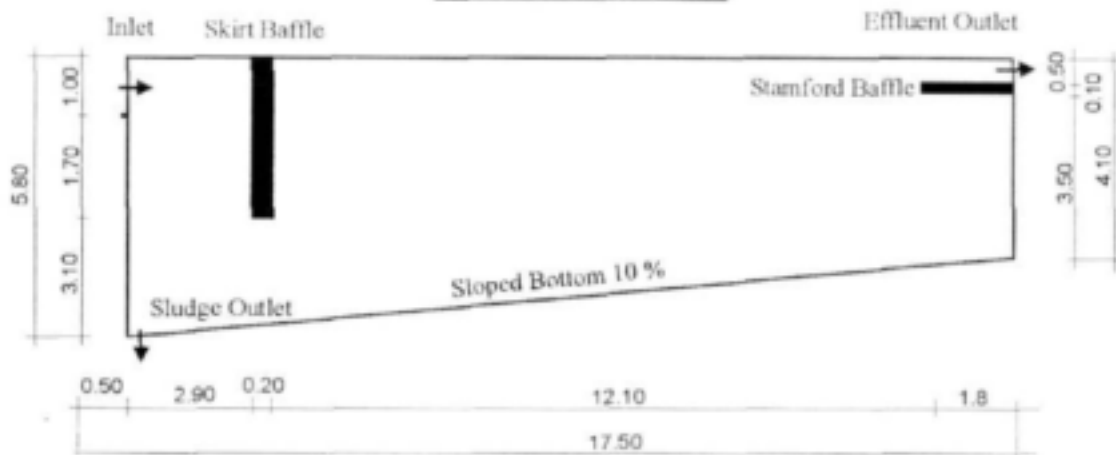
Both Darvill tanks have a diameter of 35 m. The side water depth of the Old Tank is 2.5 m and 4.1 m for the New Tank. The Old Tank has a flat floor and six suction lifts for the settled sludge. The New Tank has a 10 % sloping floor and the sludge is scraped to the central hopper. A 6.0 m diameter skirt baffle is acting as flocculator at the centre well to 1.8 m water depth and 2.7 m for the New Tank, respectively. A peripheral Stamford baffle at the effluent outlet extends 1.2 m respectively 1.7 m from the side wall.

The circular Watts Tank has a diameter of 29 m, a side water depth of 3.66 m and a centre feed, peripheral and radial effluent overflow and rotating multiple suction pipe sludge collection system (Fig 5).

### Darvill Old Tank



### Darvill New Tank



### Watts Tank

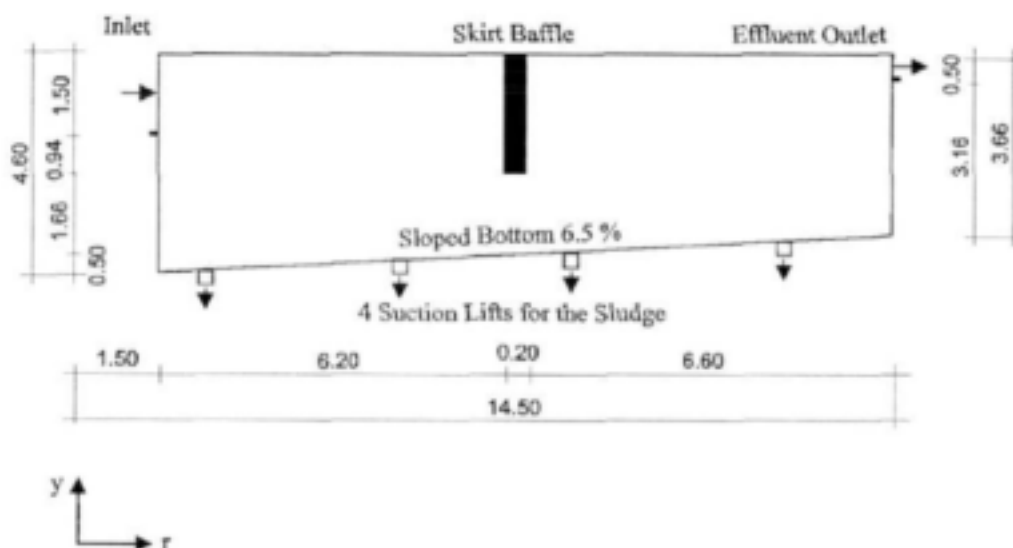


**Fig 5:** Geometry and boundaries for Darvill Old and New SST, as well as for the Watts SST

To complete the mathematical description for the model boundary conditions (BC) on all unknown problem variables have to be set. There are two prevalent boundary conditions:

- Essential (Dirichlet) BCs, where the value of the variable is prescribed.
- Natural (Neumann) BCs, where the first derivative is prescribed.

In the following the boundary conditions for the dependent variables are explained. In Fig 5 the boundaries of the simplified circular tank of the Darvill Old and New Tank, as well as one of the Watts SSTs are shown. There are six boundaries that have to be defined: inflow, effluent outlet, the outlet for the thickened sludge, the water surface, the bottom of the tank and the rigid walls. All loading conditions, parameters and results are listed in Table 1 at the end of Section 5.1.

### **Inlet Boundary**

In the model the inlet condition is idealized. The values of the variables  $U$ ,  $V$ ,  $k$ ,  $\varepsilon$  and  $C$  are assumed to be uniformly distributed at the inflow boundary. A uniform horizontal inflow is imposed, i.e. the radial velocity  $U = U_0$  and the vertical velocity  $V = 0$  and the inlet concentration  $C = C_0$ . The turbulent kinetic energy  $k$  is related to the inlet kinetic energy by  $k = KU_0^2$ , where  $K$  is 0.2. The inlet dissipation rate was approximated assuming equilibrium of turbulence production and dissipation by

$$\varepsilon_0 = C_\mu^{3/4} \frac{k^{3/2}}{l_m}, \quad (31)$$

where  $l_m = C_\mu (0.5 H_0)$  the mixing length,  $C_\mu = 0.09$  and  $H_0$  is the water depth of the settling tank inlet (Celik *et al.*, 1985).

### **Effluent Outlet Boundary**

The natural boundary conditions, which prescribe the gradients, are zero at the boundary of the effluent outlet. In order to have a well-posed problem the reference pressure is set to zero at the effluent outlet. The baffles and the effluent weir are treated as a reflecting boundary, where the natural boundary conditions of the sludge concentration  $C$  are zero.

### **Removal Boundary**

The velocity normal to the bottom is equal to the return activated flow divided by the bottom area affected. In practice the sludge in the Darvill Old Tank and Watts Tank is removed by rotating multiple suction pipe sludge collection system, which cannot be simulated with a 2D-model. The scraper of the Darvill New Tank, which exerts a shear force, is not included in the model. The turbulent kinetic energy  $k$  and its dissipation  $\varepsilon$  are treated like for the outflow boundary, their natural boundary conditions are set to zero.

### **Bottom and Water Surface Boundary for the Sludge Concentration**

At the bottom of the tank and at the water surface additional natural boundary conditions are necessary. For the prediction of the solid phase the settling velocity is added to the vertical velocity. As a result there are vertical velocities at the bottom of the tank and at the water surface. This corresponds to convective mass flux over the boundary of the domain. At the water surface there is a mass flux in the tank and at the bottom a mass flux out of the tank. In order to avoid this mass flux, an additional boundary condition has to be set. With that the sum of the convective and the mass transport due to diffusion must be zero. Taking the surface integral or line integral, the concentration gradient times the diffusion coefficient must be equal the settling velocity times the concentration as proposed by Imam *et al.* (1983):

$$n_y \left( \frac{v_{eff}}{\sigma_{sy}} \frac{\partial C}{\partial y} \right) = -V_s C \quad \text{at the water surface} \quad (32)$$

$$n_y \left( \frac{v_{eff}}{\sigma_{sy}} \frac{\partial C}{\partial y} \right) = V_s C \quad \text{at the bottom of the tank} \quad (33)$$

Here  $n_y$  is the unit outward normal at the bottom and at the surface of the tank.

### **Free Surface Boundary**

At the water surface, the rigid-lid approximation is made that assumes that there is negligible change in water surface elevation over the tank. The symmetry condition is applied that includes zero gradients and fluxes perpendicular to the boundary. The vertical velocity component is  $V = 0$  and the horizontal component  $U$  is assuming full slip, i.e. no shear stress at the surface. The turbulent kinetic energy  $k$  can be set to zero and for its dissipation  $\varepsilon$  the following empirical boundary condition (Celik and Rodi, 1988) is used

$$\varepsilon = \frac{k^{3/2}}{0.43H} \quad (34)$$

Here  $H$  is the depth of the tank.

### **Solid and Tank Bottom Boundaries**

At the rigid walls, the velocities are zero due to the no-slip condition and the log-law of the wall is used. The near-wall velocities are determined from a local application of the log-law, and the near-wall  $k$  and  $\varepsilon$  are derived in terms of wall shear stresses using the near-wall assumption that production equals dissipation. (Hill and Basharone, 1997).

Parameter		Darvill Old Tank Test 3	Darvill Old Tank Test 3 + 10%	Darvill New Tank Test 3 + 10%	Watts Test 1	Watts Test 4	Watts Test 12
SST	Surface Area (m <sup>2</sup> )	962	962	962	659	659	659
Loading Conditions	Influent Flow (m <sup>3</sup> /h)	948	1074	1074	475.1	788.9	1095.8
	Recycle Flow (m <sup>3</sup> /h)	750	750	750	397.5	397.5	397.5
	Recycle Ratio	0.79	0.7	0.7	0.84	0.51	0.36
	Feed Concentration (g/l)	3.600	3.600	3.600	4.053	4.130	3.444
Sludge Settleability	$V_0$ (m/h)	8.00	8.00	8.00	7.62	7.62	7.62
	$K$ (or $n$ )	0.430	0.430	0.430	0.3055	0.3055	0.3055
	DSVI <sup>1</sup> (ml/g)	62	62	62	94	94	94
Retention Time (h)		1.3	1.4	2.5	2.1	2.1	1.8
Observed Rest Result	Experiment	Safe	Not Tested	Not Tested	Safe	Safe	Fail
Test Result (ESS <sup>2</sup> > 50 mg/l)	SettlerCAD (Zhou, 1998) (see Part 1 of this report)	Safe	Fail	Safe	Safe	Safe	Fail

*Table 1: Summary of the loading conditions used for the simulation of the Darvill Old and New Tank, as well as for the Watts Tank*

<sup>1</sup>Diluted Sludge Volume Index

<sup>2</sup>Effluent Suspended Solids



## 5.2 Simulating the Darvill Old and New SSTs

The loading condition of Test 3 (see Part 1 of this report) is chosen such that both the Old and the New Tank are safe (Table 2). At a 10 % higher influent flow the sludge blanket in the Old Tank already reaches the effluent outlet while the New Tank is still in a stable and safe condition.

Parameter		Darvill Old Tank Test 3	Darvill Old Tank Test 3 + 10%	Darvill New Tank Test 3 + 10%
SST	Surface Area (m <sup>2</sup> )	962	962	962
Loading Conditions	Influent Flow (m <sup>3</sup> /h)	948	1074	1074
	Recycle Flow (m <sup>3</sup> /h)	750	750	750
	Recycle Ratio	0.79	0.7	0.7
	Feed Concentration (g/l)	3.600	3.600	3.600
Sludge Settleability	$V_0$ (m/h)	8.00	8.00	8.00
	$K$ (or $n$ )	0.430	0.430	0.430
	DSVI (ml/g)	62	62	62
Retention Time (h)		1.3	1.4	2.5
Time Step $\Delta t$ (s)		5.0	5.0	5.0
Turbulent Constant		0.0005	0.0005	0.0005
Viscosity $\nu_i$ (m <sup>2</sup> /s)				
Schmidt Number $\sigma_i$		5.0	5.0	5.0

**Table 2:** *Darvill Old and New Tank: Loading conditions and model parameter*

A mesh of 85 elements in the horizontal direction and 25 elements in the vertical direction for the Old Tank, and 58 elements for the New Tank in the vertical direction, is chosen (Fig 6). In Fig 7 the flow pattern of the neutral density case is shown for both tanks. These are the initial values for the computation of the Darvill SSTs.

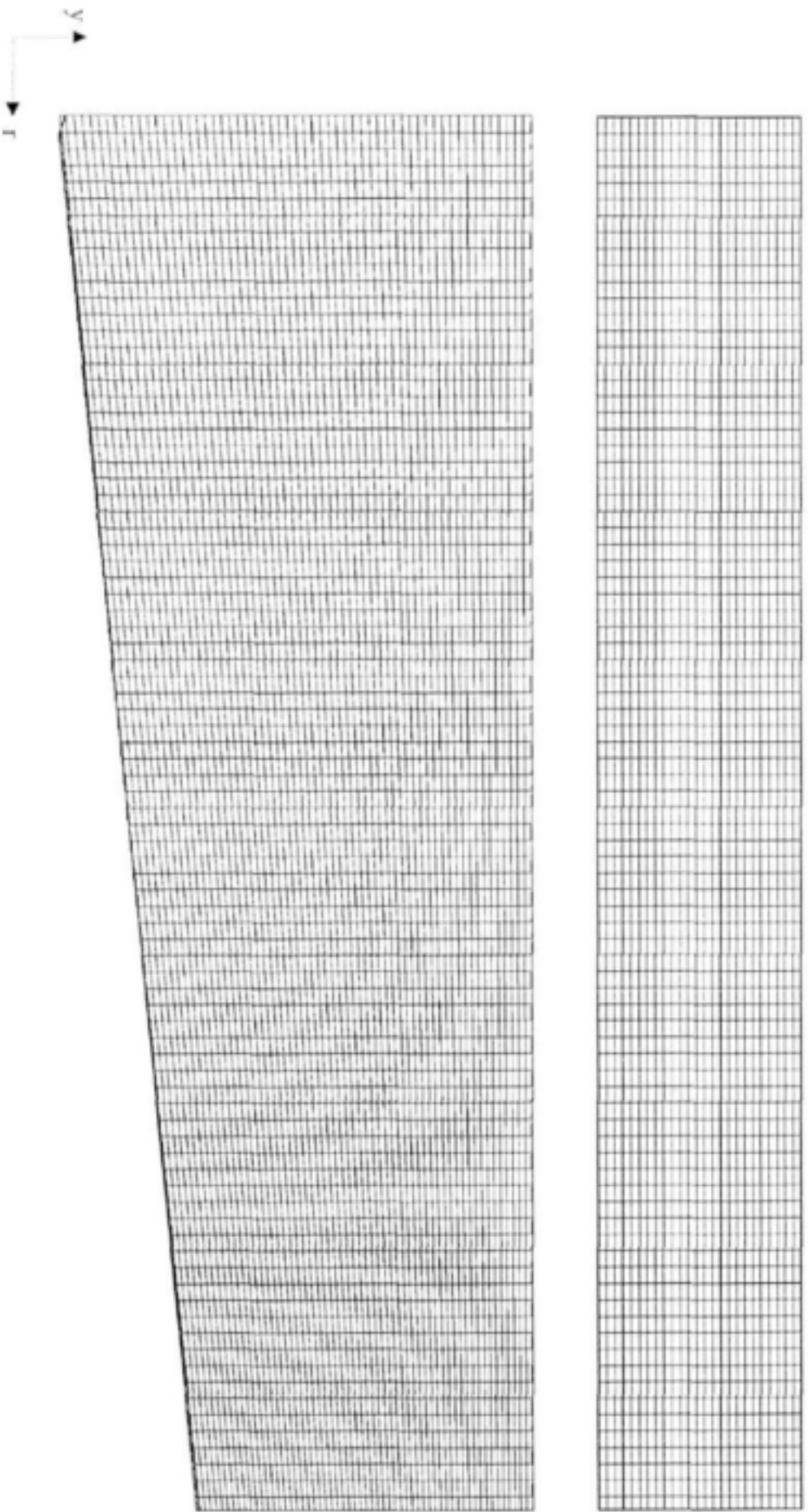


*Fig 6: Mesh of Darvill Old Tank (85 x 25) and New Tank (85 x 58)*

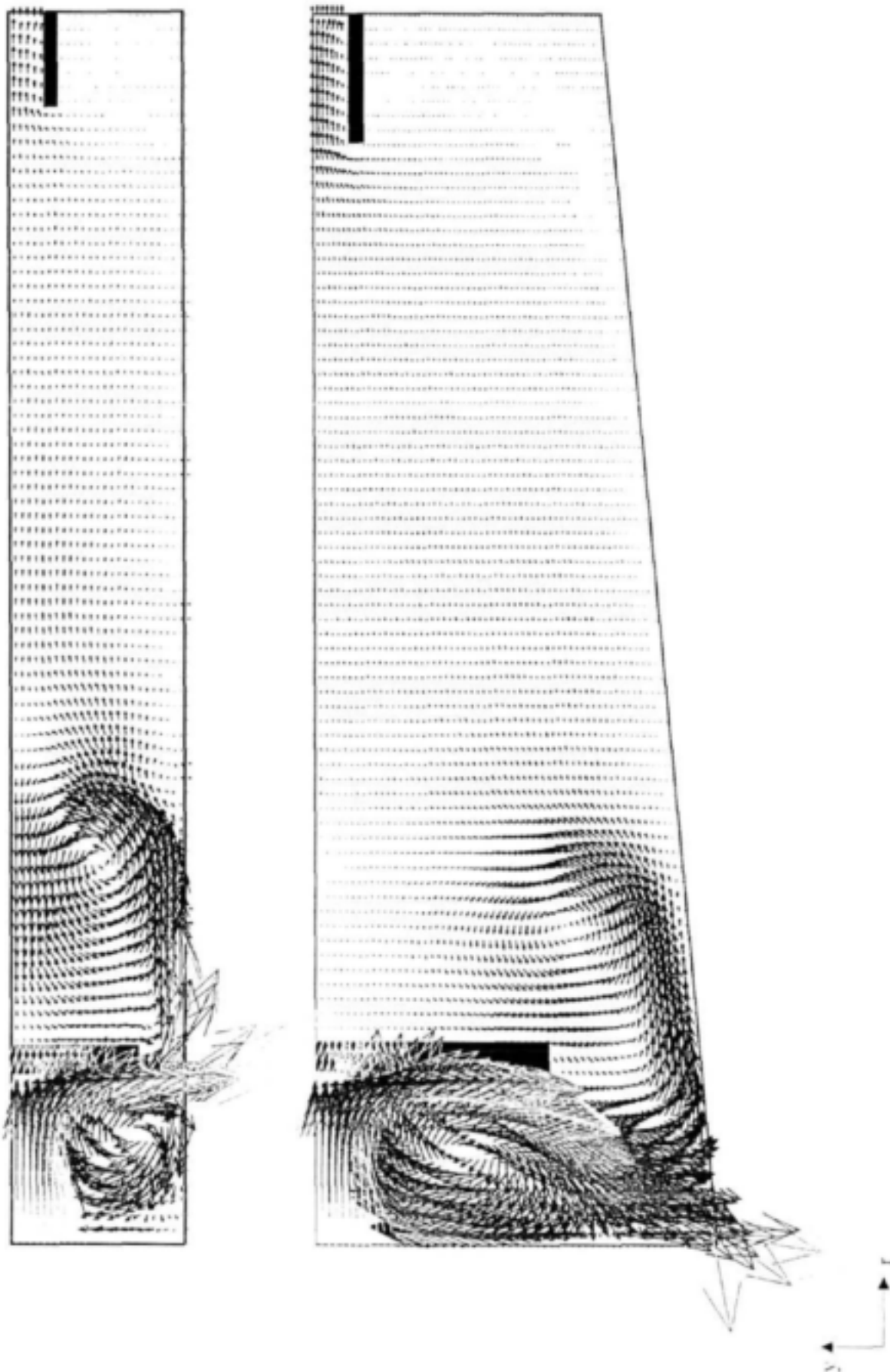
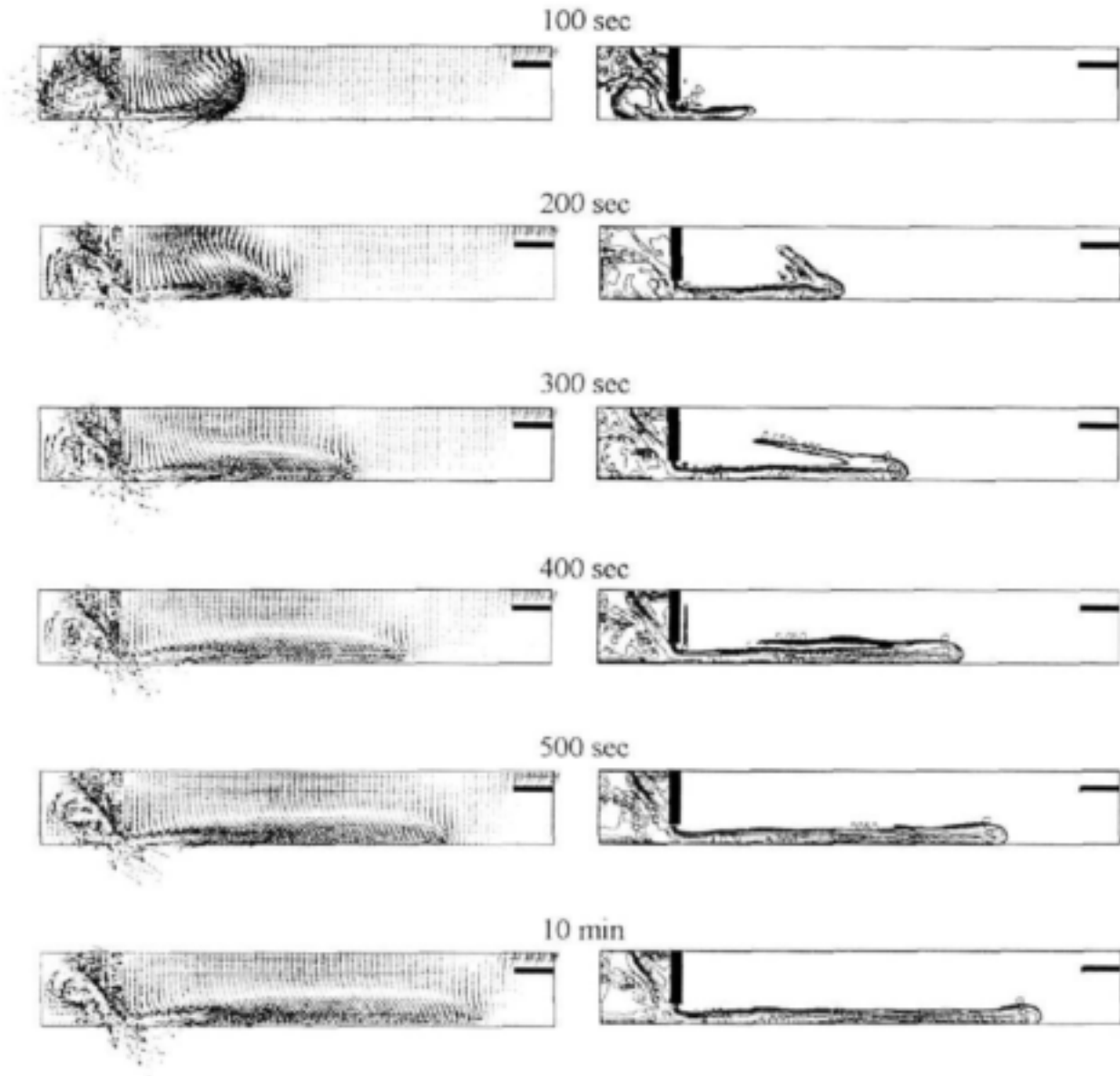


Fig 7: *Darvill Old and New Tank Neutral density case: Initial conditions*

### 5.2.1 Temporal and Steady State Result of Darvill Old SST

The temporal behaviour of the Old Tank is illustrated in Fig 8 and 9. The incoming jet from the inlet chamber moves along the bottom of the tank because of its higher density than the surrounding fluid. Mass conservation and viscous forces influences the flow pattern in the settling section, resulting in a complete flow circulation with a strong bottom forward current and a reverse current at the water surface.



**Fig 8:** *Darvill Old Tank Test3: After 100 sec to after 10 min  
Predicted flow pattern and sludge distribution  $C$  in g/l*

After 15 min the sludge current reaches the end of the tank, the region of the upward current to the effluent outlet. The sludge level is continuously rising, as is the sludge concentration. The jet coming from the inlet chamber with a smaller density is continuously lifted due to the increasing sludge concentration in the main section of the tank.

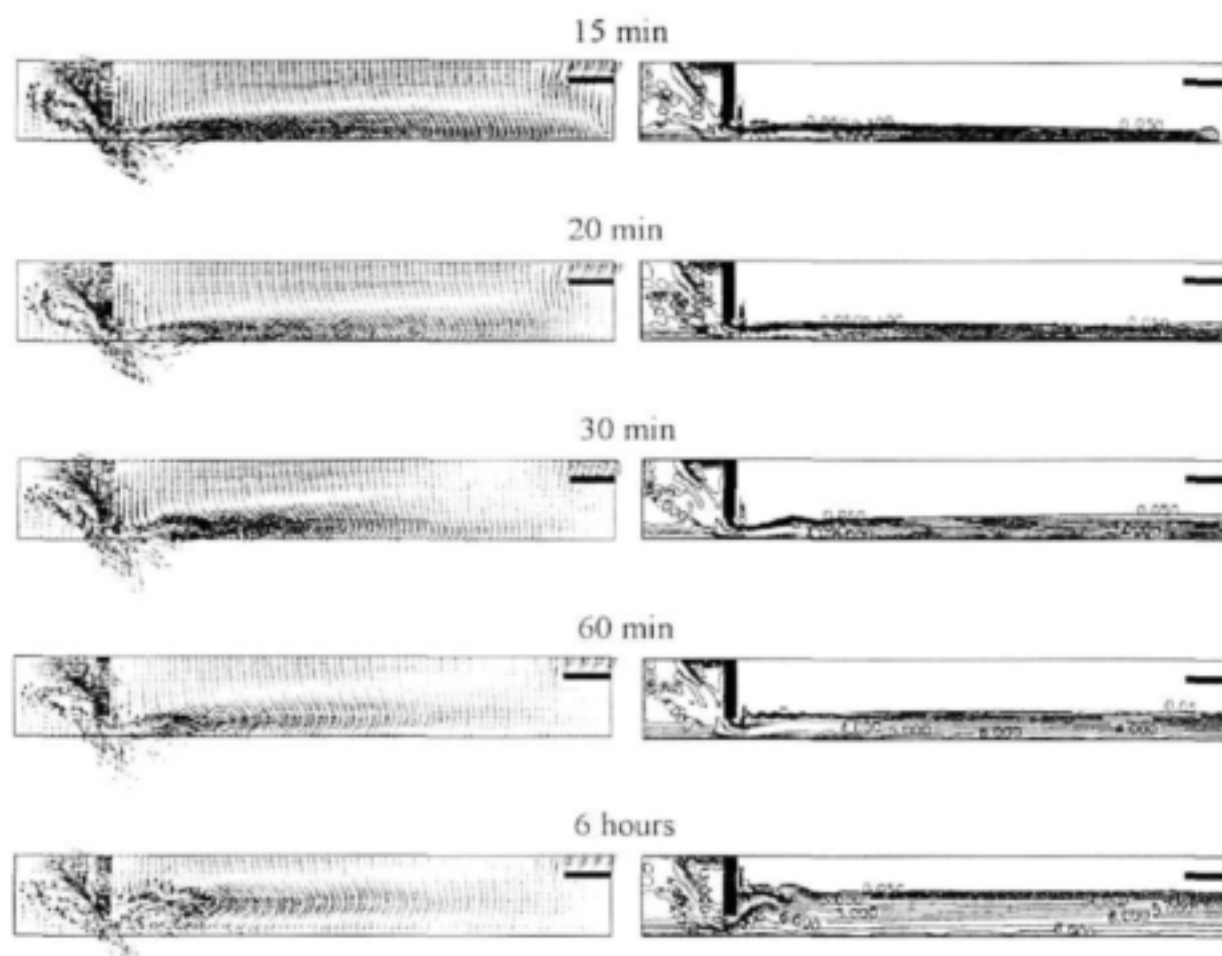


**Fig 9:** *Darvill Old Tank Test 3: After 15 min to after 6 hours  
Predicted flow pattern and sludge distribution  $C$  in g/l*

The steady state case illustrated in Fig 10 is reached when potential and kinetic energy have reached their balance. The loading conditions of Test 3 do not cause failure of the Old Tank. The sludge blanket reaches equilibrium and does not rise to the outlet for the clarified water. Fig 11 shows the steady state result with a 10% higher influent flow. Here the sludge blanket reaches the effluent outlet and the current coming from the inlet chamber is raised to the water surface.

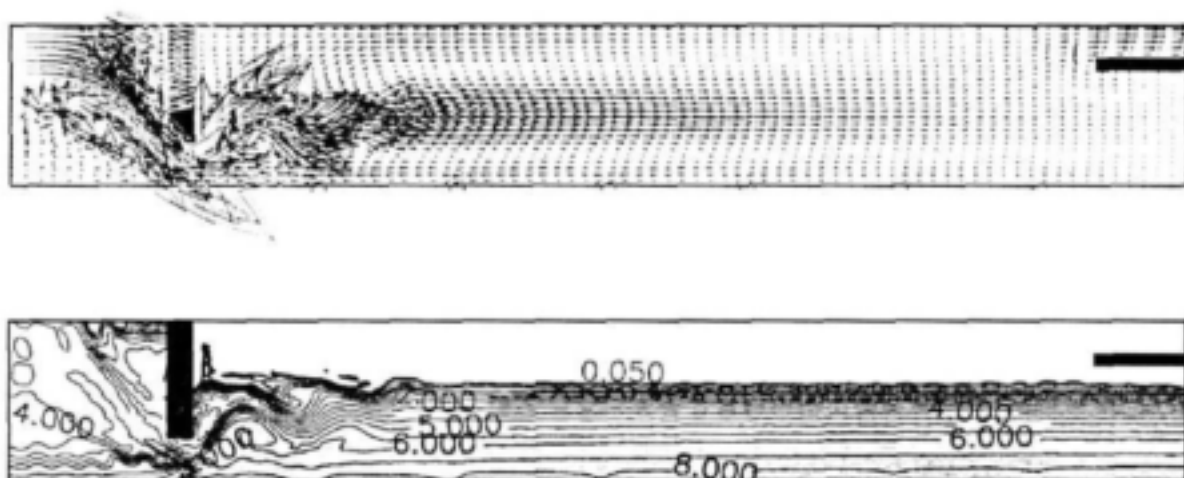


*Fig 10: Darvill Old Tank Test 3: Steady state case  
Predicted flow pattern and sludge distribution C in g/l*

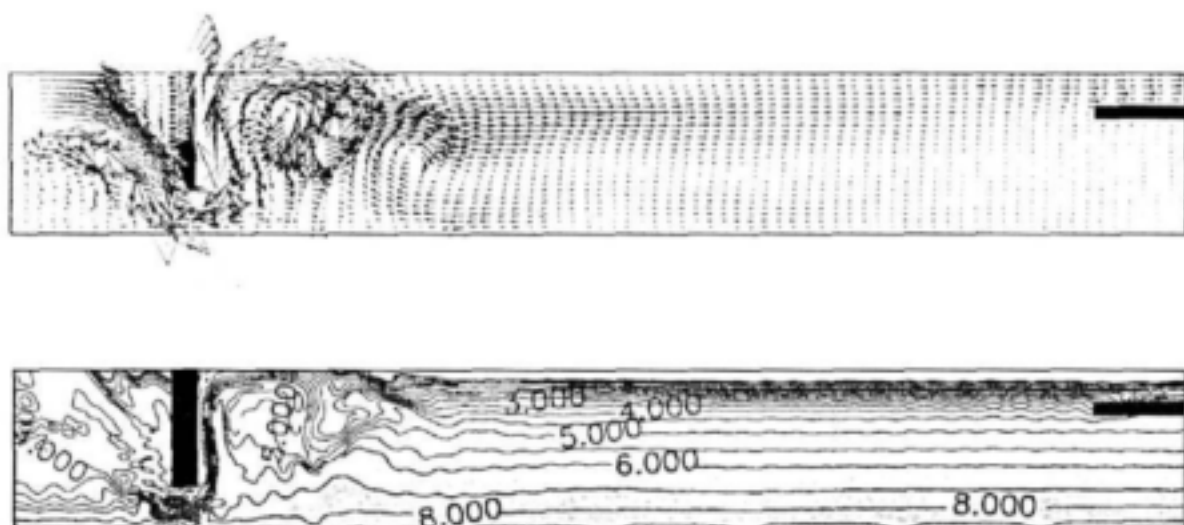


*Fig 11: Darvill Old Tank Test 3 with a 10 % higher influent flow:  
Steady state case  
Predicted flow pattern and sludge distribution C in g/l*

### 5.2.2 Temporal and Steady State Result of Darvill New SST

In Fig 12, 13 and 14 the computational results are shown for the New Tank under the 10 % higher influent flow than Test 3 (see Table 2).

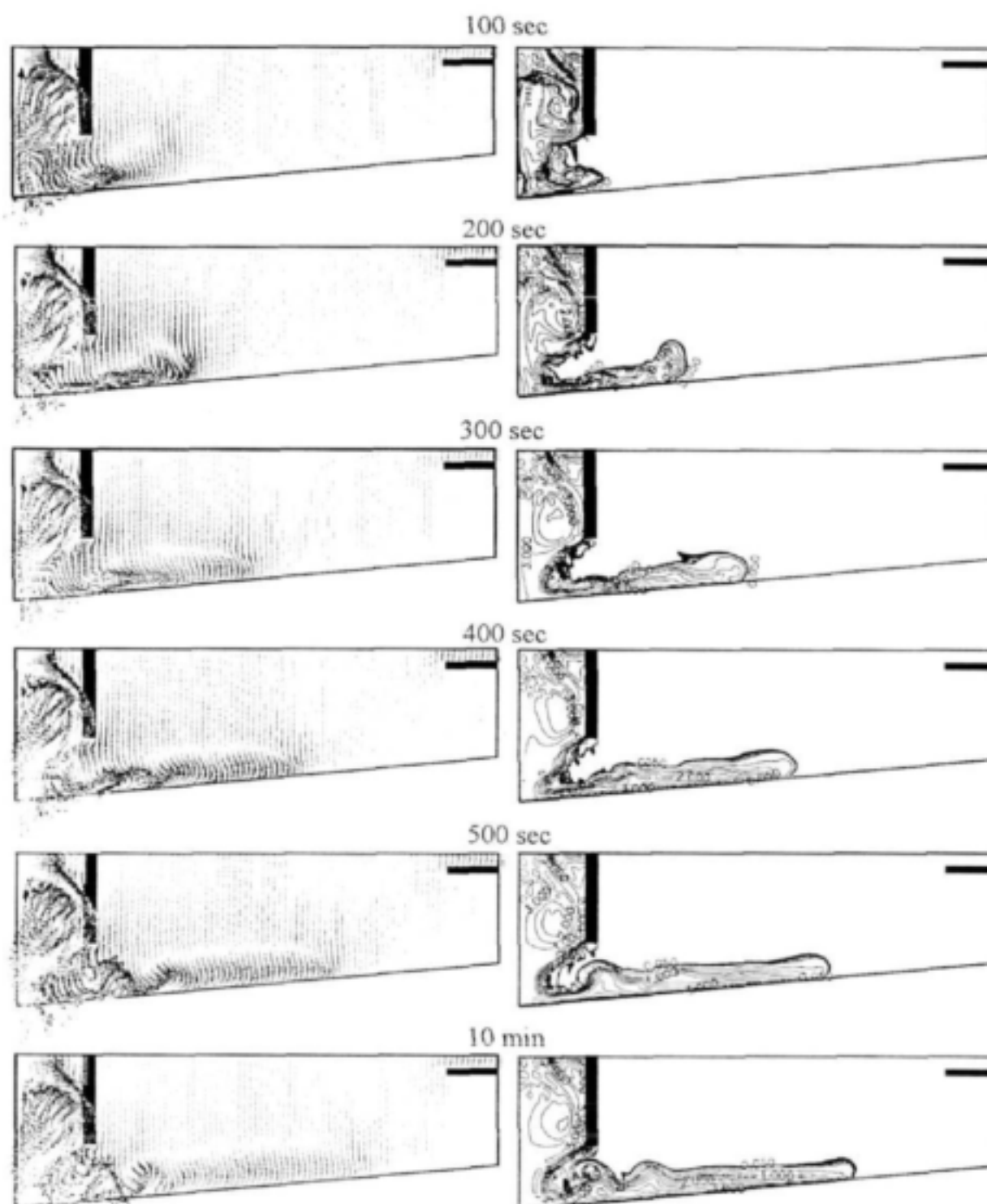


**Fig 12:** *Darvill New Tank* Test 3 with a 10% higher influent flow:  
After 100 sec to after 10 min  
Predicted flow pattern and sludge distribution  $C$  in  $g/l$



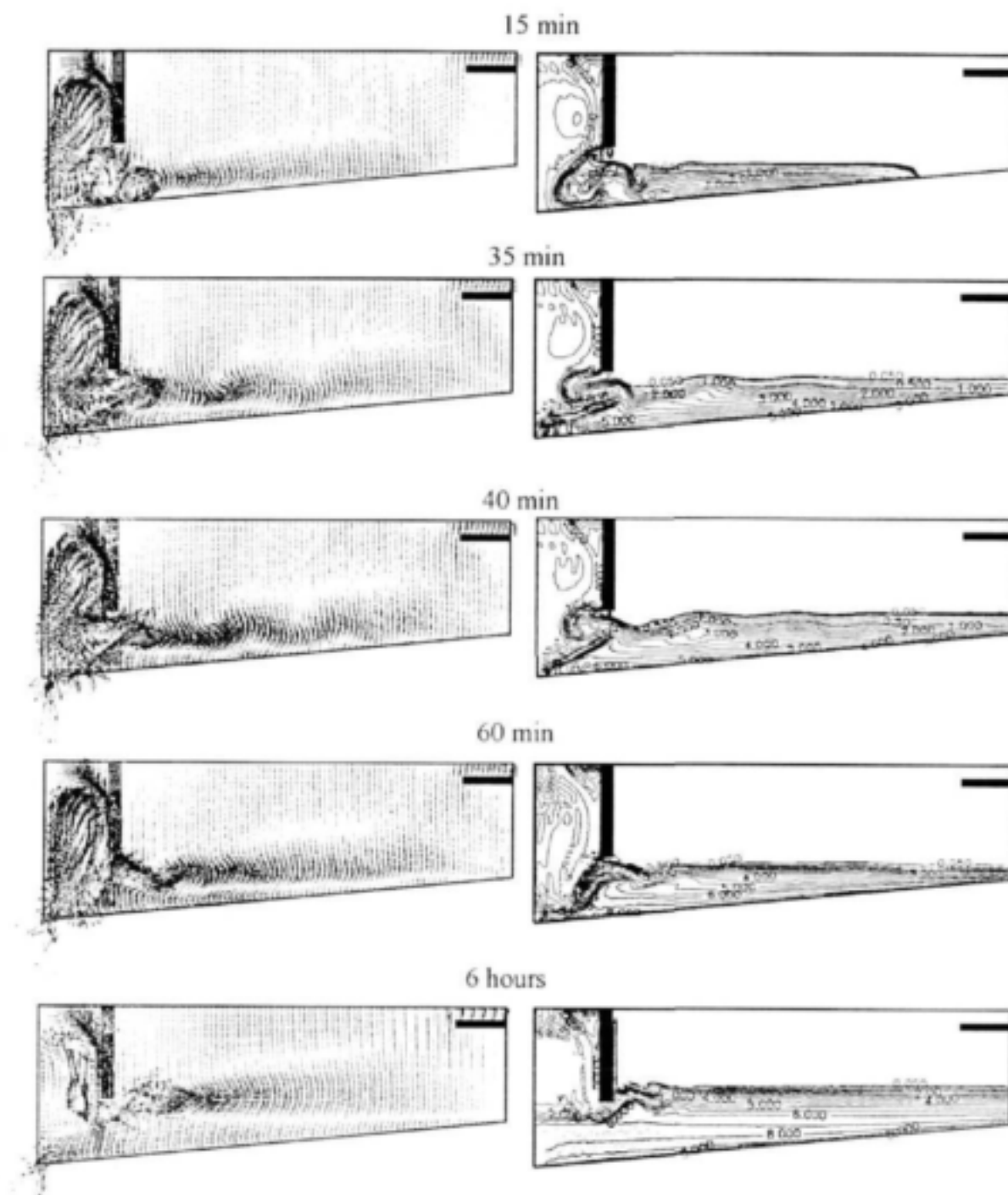


*Fig 13: Darvill New Tank Test 3 with a 10 % higher influent flow:  
After 15 min to after 6 hours  
Predicted flow pattern and sludge distribution C in g/l*

The incoming fluid mixture cascades down, in the process drawing in fluid from the settling section. Due to its higher density in connection with the height of 5.8 m the inflow contains a high potential energy that is changed into kinetic energy at the bottom. No particular construction guides the inflow into the settling section whirling up the hopper region as a result.

The sludge level rises continuously and the sludge current moves along the bottom to the end of the tank, also causing a complete flow circulation. The interaction between potential and kinetic energy results in waves that are clearly seen just behind the inlet chamber, first due to the impact with the bottom of the tank and then again due to the impact with the outside wall after 35 min (Fig 13).

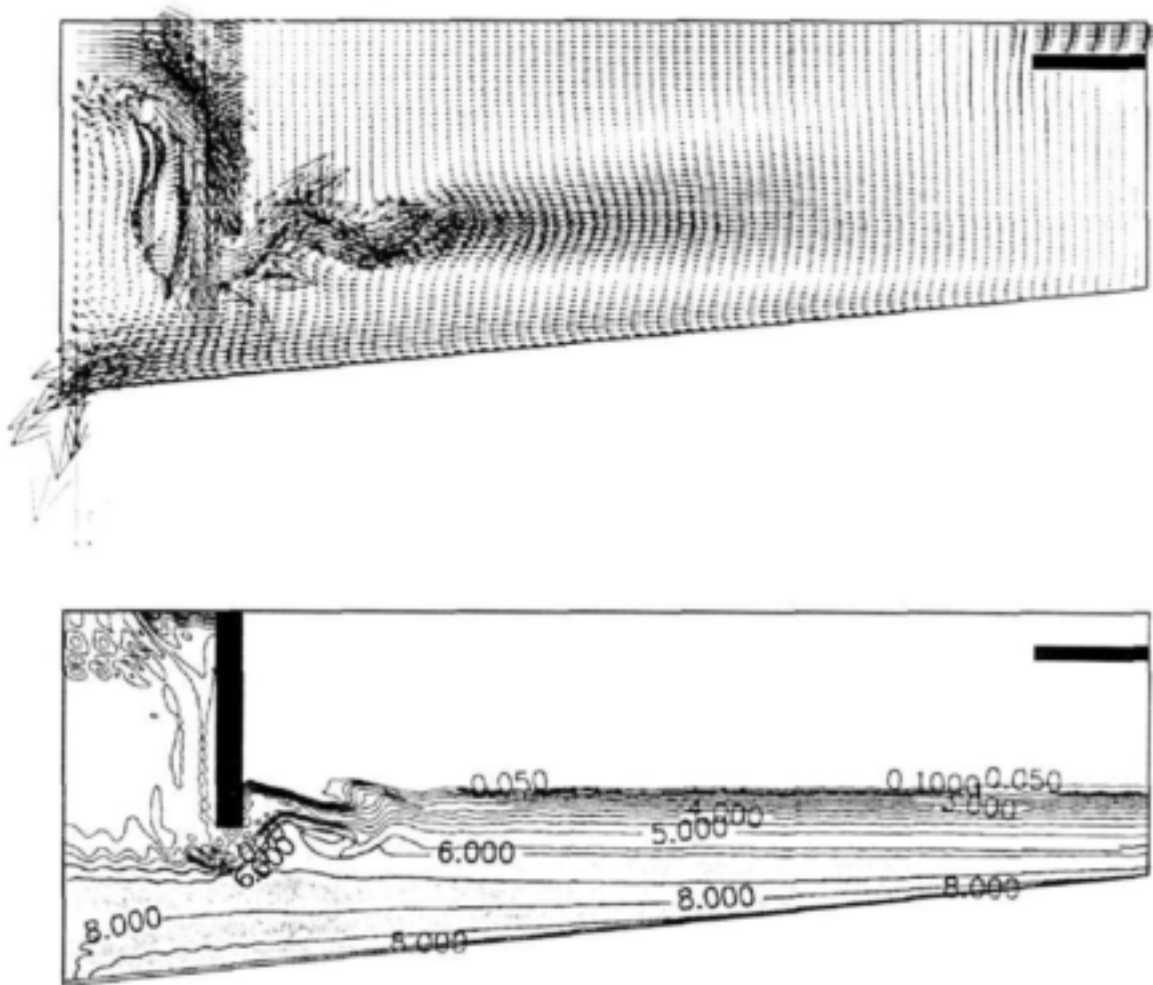


**Fig 14:** *Darvill New Tank Test 3 with a 10 % higher influent flow:  
Steady state case  
Predicted flow pattern and sludge distribution  $C$  in g/l*

The New Tank exhibits a safe behaviour, which is shown in Fig 14. This can be ascribed to the fact that this SST has a much bigger storage zone than the Old Tank, which leads to stable and constant behaviour over a wide range of loading conditions (see Part 1 of this report).

### 5.3 Simulating the Watts SSTs

#### 5.3.1 Watts Test 1

The simulation of Watts Test 1 pointed out that an adjustment of some 'free' parameters in the transport and sedimentation sub-model are required. Watts Test 1 is the safest stress test. Fig 15 shows the flow pattern and the sludge distribution by using a Schmidt number  $\sigma_s$  of 1. For this case the turbulent diffusivity is equivalent to the predicted turbulent viscosity field in Fig 15.

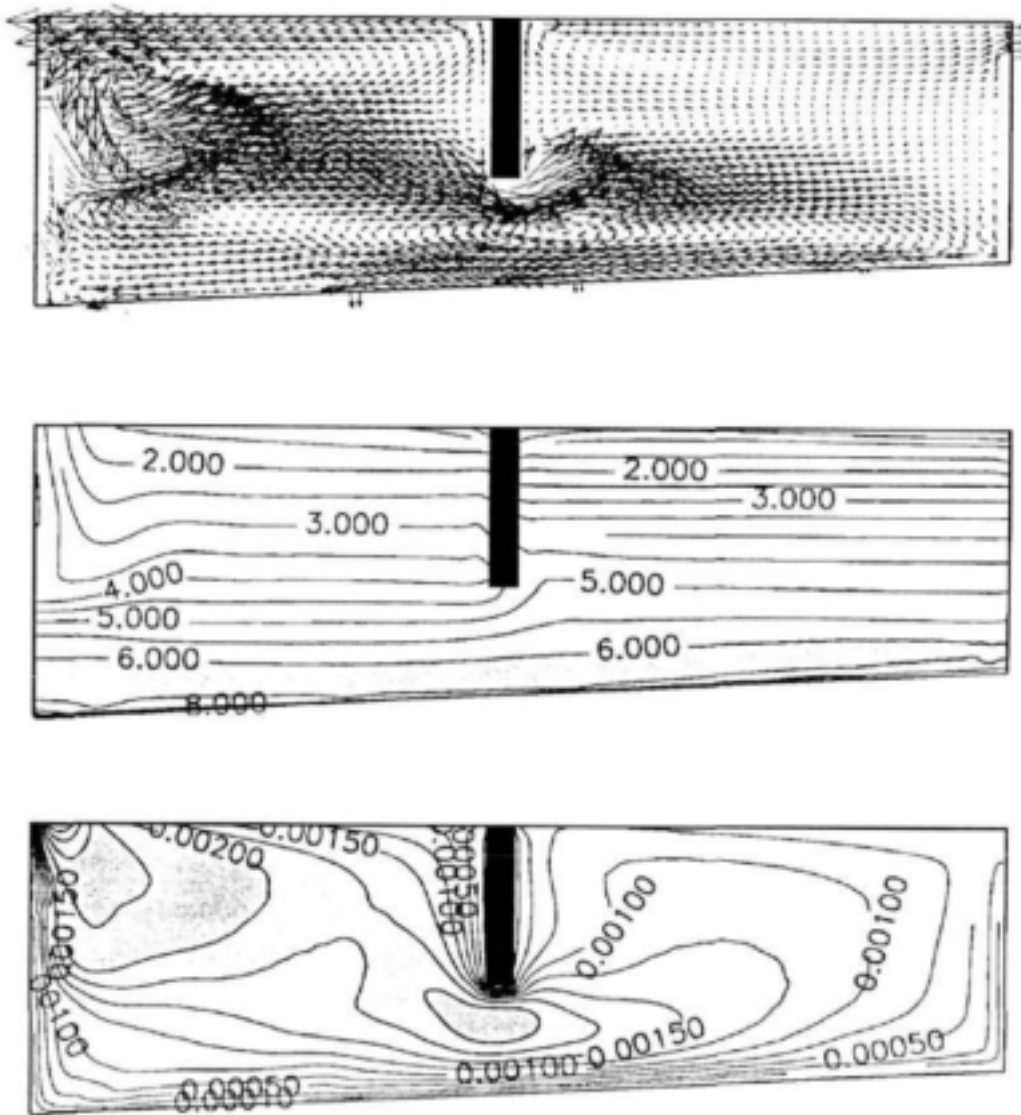


**Fig 15:** *Watts Tank Test 1: Predicted flow pattern and sludge distribution  $C$  in g/l, using a Schmidt number  $\sigma_s$  of 1.0, as well as the predicted turbulent viscosity field  $\nu_t$  in  $m^2/s$*

The simulation predicted failure for Test 1, which contradicts the observed test results. It prompts the question as to what extent the sludge particles are influenced by diffusion. Only the very small sludge particles will be influenced by turbulent diffusion. They can be related to the poorly settling particles and non-settleable particles, respectively.

The flux caused by turbulent diffusion is damped in the higher concentration environment, i.e. at the bottom of the tank, due to compaction and hindered movement of the sludge particles. On the other hand the viscosity of the fluid mixture increases with increasing sludge concentration, i.e. it cannot be assumed that the eddy diffusivity that governs the solid mixing in the tank is proportional to the viscosity of the fluid mixture, especially not in the high concentration range. Inclusion of the buoyancy correction term in the equation for the turbulent kinetic energy  $k$  leads to unsatisfactory results, in that the turbulence is reduced to zero. Additionally, stability problems result from negative values of the kinetic energy  $k$ .

Due to the lack of knowledge about the sludge behaviour in turbulent zones and in the high concentration environments, it became necessary to modify the ‘turbulent diffusion’ parameter. Those simulation results, which showed good agreement between the model output of SettlerCAD (Zhou *et al.*, 1998) and the measurements, were used to calibrate the solid distribution. The modification was made in such a way that the diffusion coefficient decreased with increasing concentration, i.e. for the Schmidt number  $\sigma_s$  the local concentration was chosen.

In Fig 16 the steady state computational result of the Watts Tank for Stress Test 1 is used to demonstrate the calibration of the Schmidt number  $\sigma_s$ . The Watts Tank is safe and the sludge blanket does not reach the outlet of the effluent. The different turbulence in the two sections is clearly seen. But this steady state does not yield a mass balance. The required concentration at the first ‘suction pipe’ cannot be reached. With an average concentration of 4.7 g/l the first suction pipe is drawing off parts from the incoming flow, which is also clearly seen in Fig 16 marked by the circle. This can be ascribed to the two facts: firstly, the 2D model cannot simulate a rotating suction lift, which the fluid will continuously be taken away at this point. In practice the suction lift has a revolution speed of one or two hours, for which the sludge has enough time to accumulate to the required recycle concentration. Secondly, the inflow is too small to achieve sufficient mixing and to create a thickening zone in this region below the inlet.

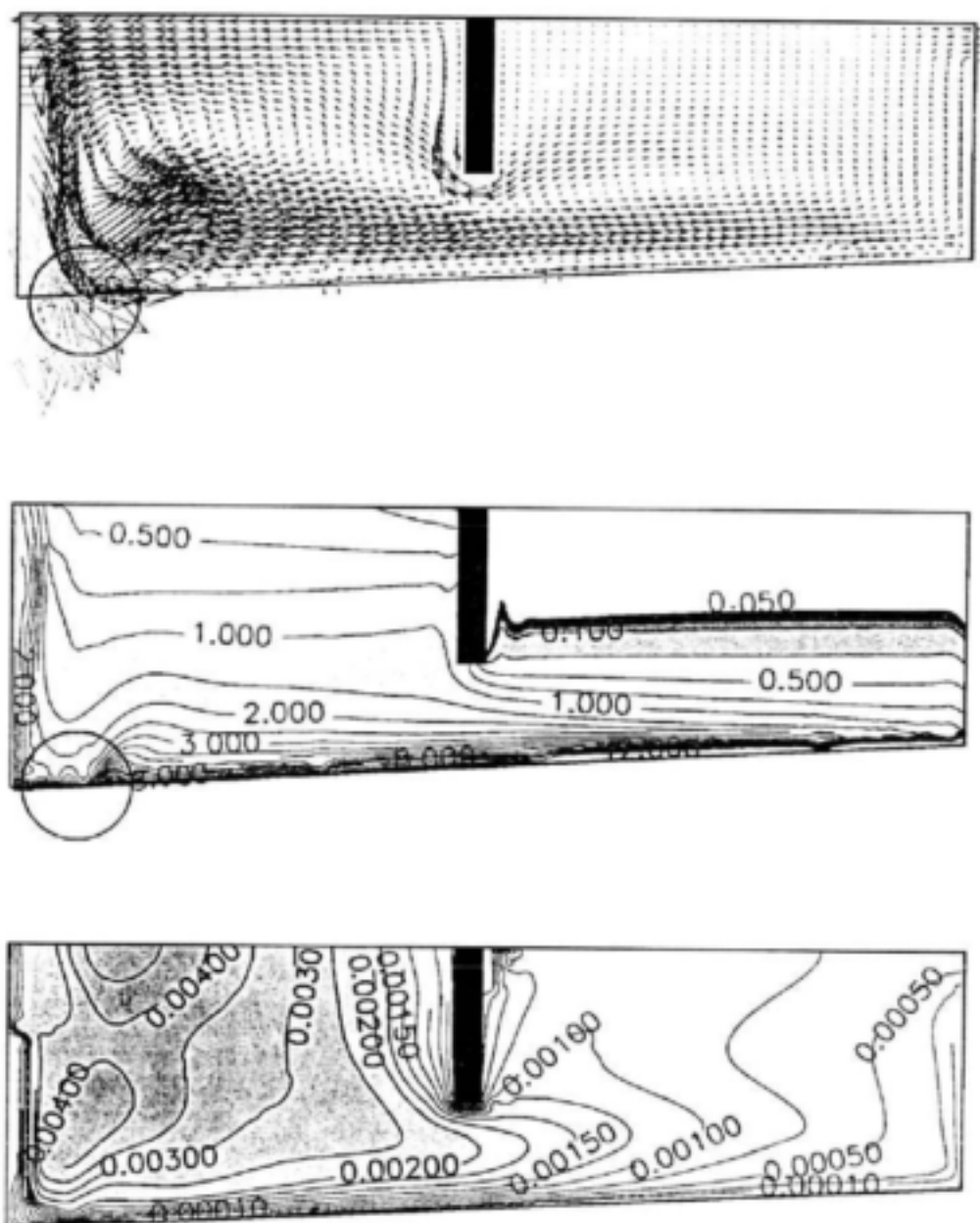


**Fig 16:** *Watts Tank Test 1: Predicted flow pattern and sludge distribution  $C$  in  $\text{g/l}$ , using the modified Schmidt number  $\sigma_*$ , as well as the predicted turbulent viscosity field  $v_t$  in  $\text{m}^2/\text{s}$*

### 5.3.2 Watts Test 12

The mesh used has 65 elements in the horizontal direction and 30 elements in the vertical direction (Fig 17). The predicted flow pattern and the turbulent viscosity field  $\nu_t$  of the neutral density case are shown in Fig 17 and Fig 18, respectively. These are the initial values for the simulation (Table 3).

Parameter		Watts Test 1	Watts Test 4	Watts Test 12
SST	Surface Area (m <sup>2</sup> )	659	659	659
Loading Conditions	Influent Flow (m <sup>3</sup> /h)	475.1	788.9	1095.8
	Recycle Flow (m <sup>3</sup> /h)	397.5	397.5	397.5
	Recycle Ratio	0.84	0.51	0.36
	Feed Concentration (g/l)	4.053	4.130	3.444
Sludge Settleability	$V_0$ (m/h)	7.62	7.62	7.62
	$K$ (resp. $n$ )	0.3055	0.3055	0.3055
	DSVI (ml/g)	94	94	94
Retention Time (h)		2.1	2.1	1.8
Time Step $\Delta t$ (s)		10	10	10
Turbulent Viscosity $\nu_t$ (m <sup>2</sup> /s)		$k-\varepsilon$ model	$k-\varepsilon$ model	$k-\varepsilon$ model
Schmidt Number $\sigma_s$	$C < 8$ g/l	1.0	1.0	1.0
	$1 \text{ g/l} < C < 8 \text{ g/l}$	$1.5 \times C$	$1.5 \times C$	$1.5 \times C$
	$8 \text{ g/l} < C$	$2.0 \times C$	$2.0 \times C$	$2.0 \times C$

**Table 3:** *Watts Tank: Loading conditions and model parameter*

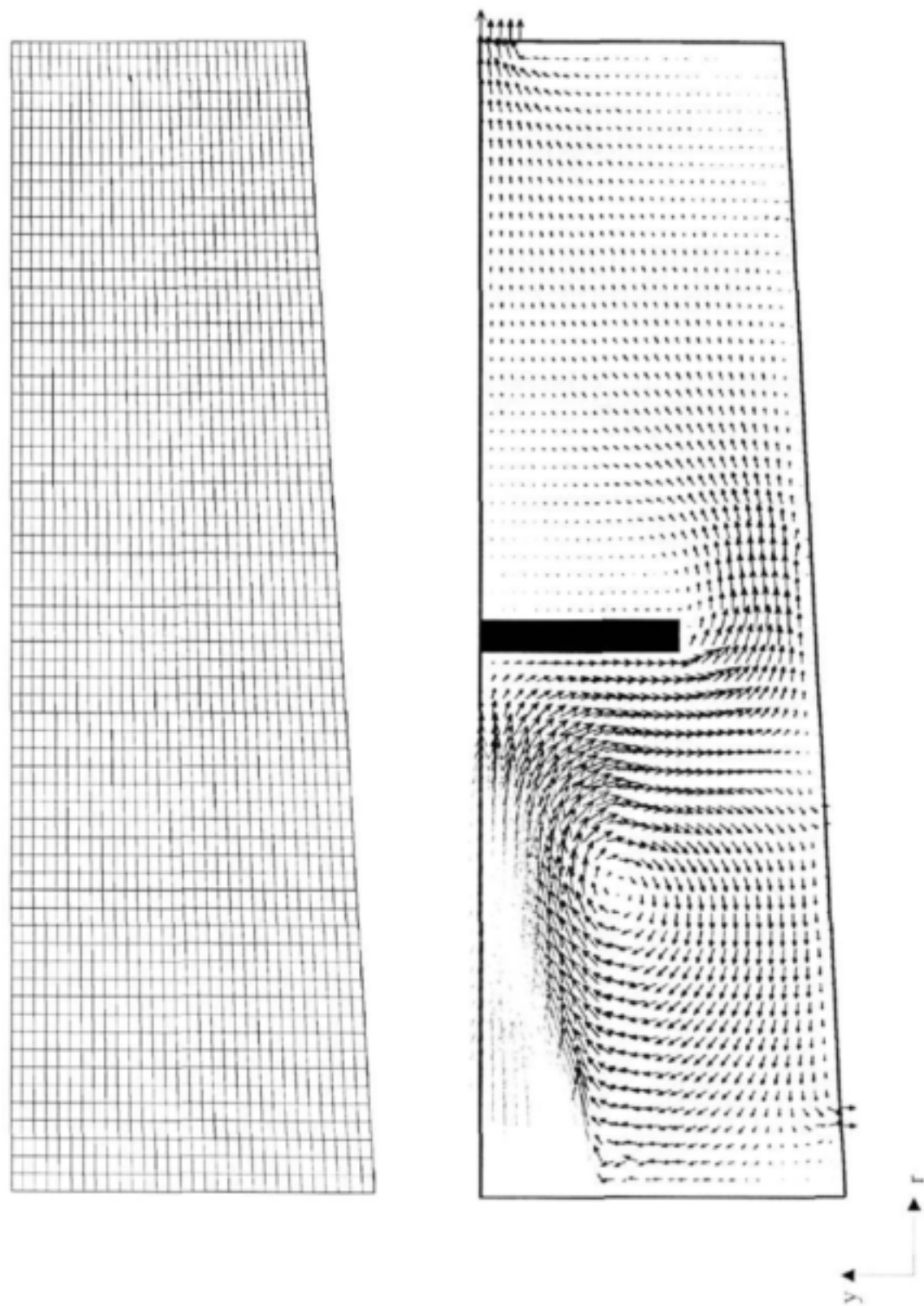
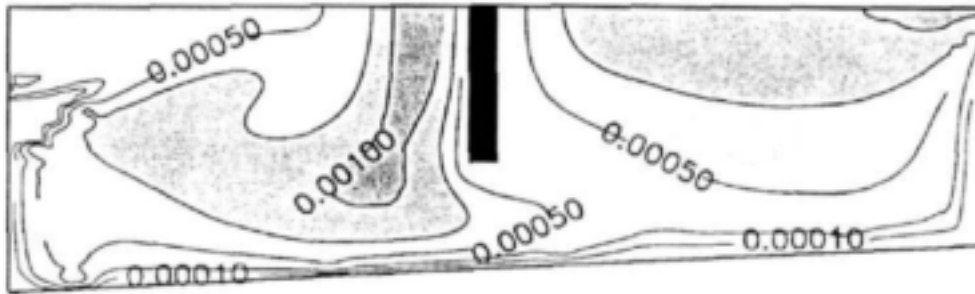


Fig 17: Watts Tank Test 12: Mesh of 65 x 30 elements and predicted flow pattern of the neutral density case





**Fig 18:** *Watts Tank Test 12: Neutral density case*  
*Predicted turbulent viscosity field  $v_t$  in  $m^2/s$*

The temporal behaviour before reaching the steady state case is illustrated in Fig 19 and 20. Already after 100 sec the “density waterfall”, which is clearly seen, causes a circulation opposite to the neutral density case, additionally drawing fluid from the settling section into the inlet section.

The flow pattern and sludge distribution make it clear that the first section acts as a mixing zone, absorbing kinetic energy caused by the density waterfall and guiding the inlet flow into the second section in which the actual sedimentation takes place.

A stable stratification develops with continuously rising sludge level in the second section. In both sections complete circulations of different intensity arise, this is also reflected in the different turbulence sizes (Fig 21).

The steady state case in which potential and kinetic energy have reached equilibrium is shown in Fig 21. Stress Test 12 causes failure of the Watts Tank. The sludge blanket reaches the outlet for the clarified water. The height of the thickening zone allows only a small gap below the skirt baffles for the inflow to reach the settling section. The incoming jet is raised due to the higher sludge concentration in the settling section.

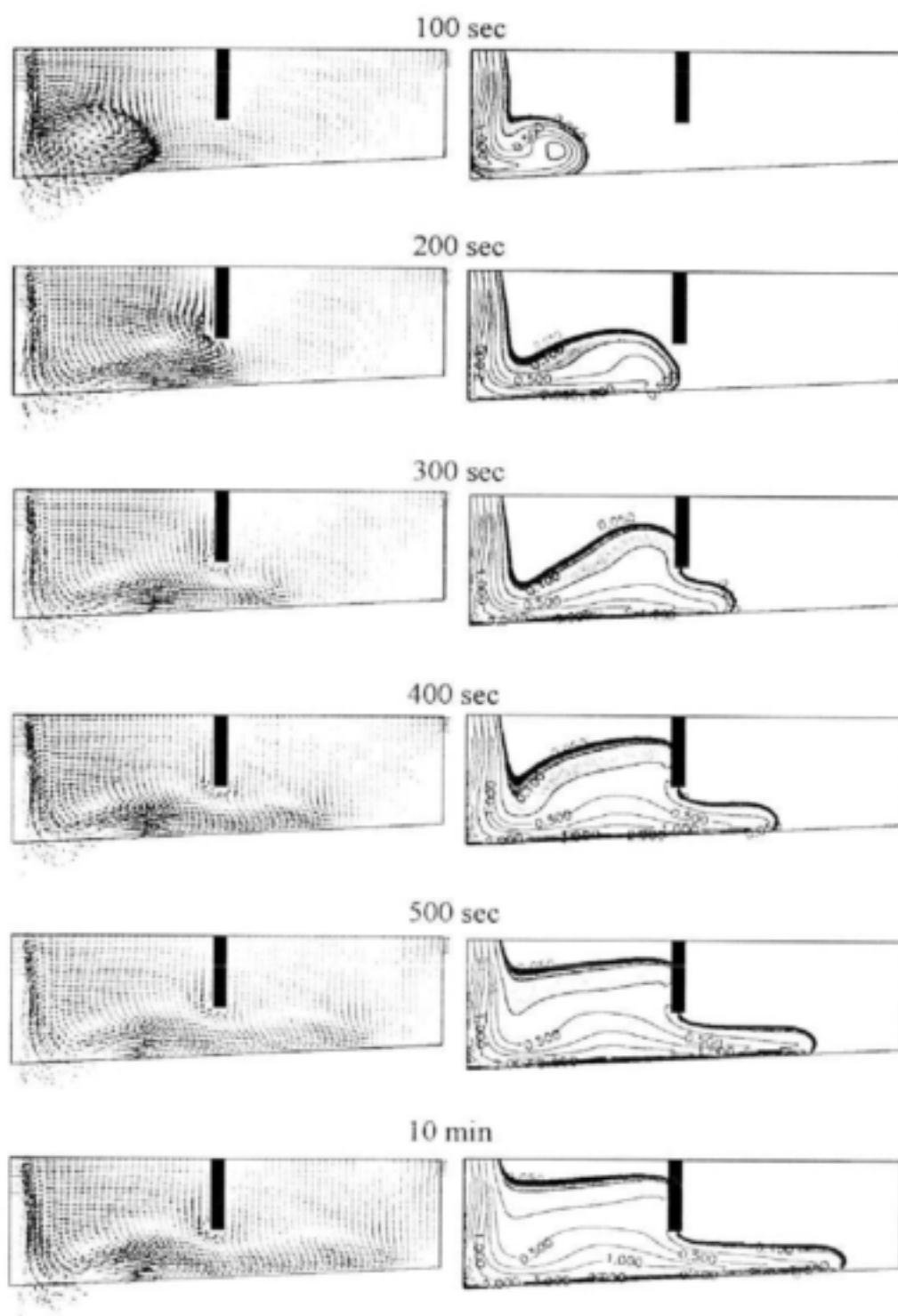


**Fig 19:** *Watts Tank Test 12: After 100 sec to after 10 min  
Predicted flow pattern and sludge distribution  $C$  in  $\text{g/l}$*

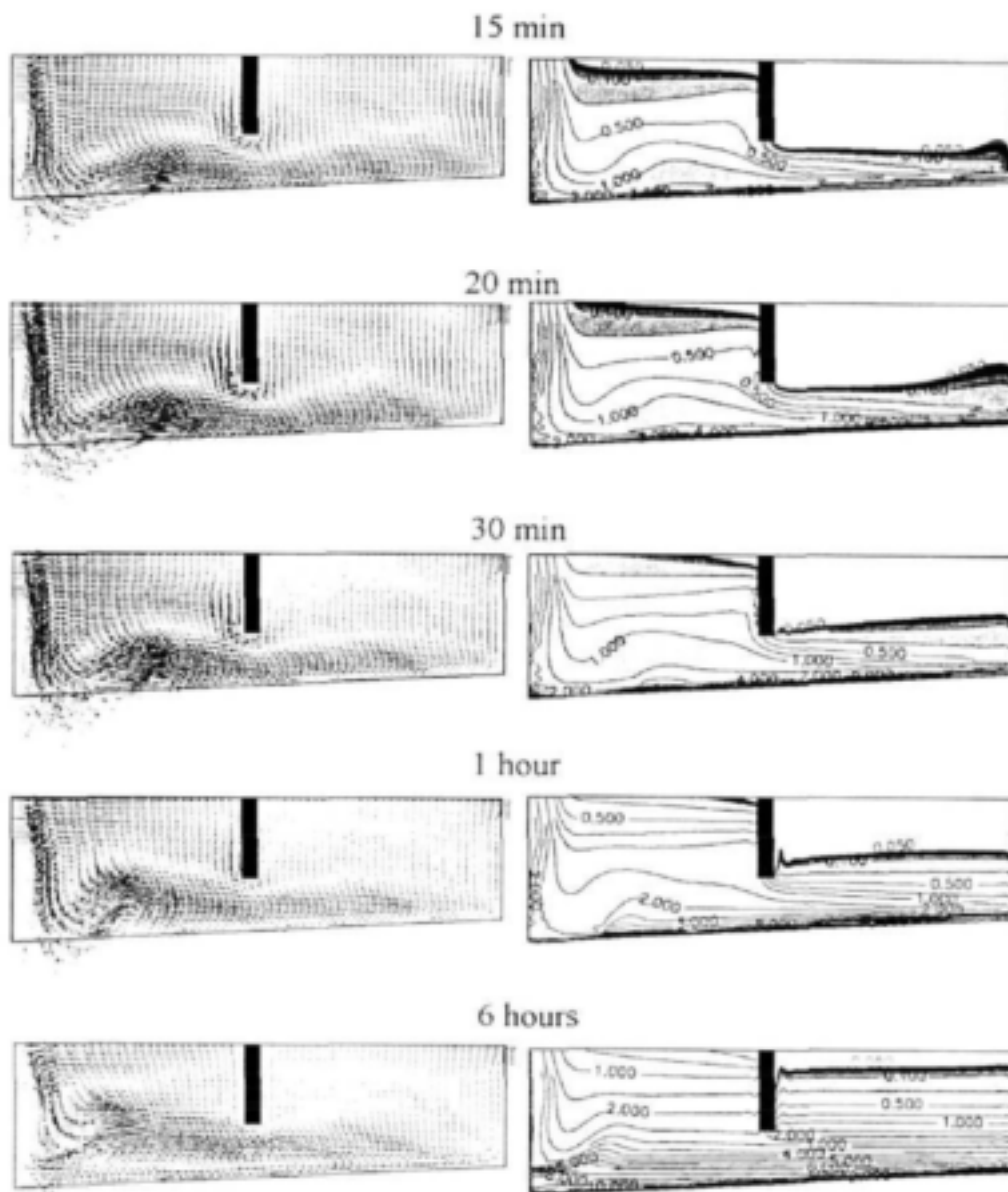


**Fig 20:** *Watts Tank Test 12: After 15 min to after 6 hours  
Predicted flow pattern and sludge distribution  $C$  in g/l*

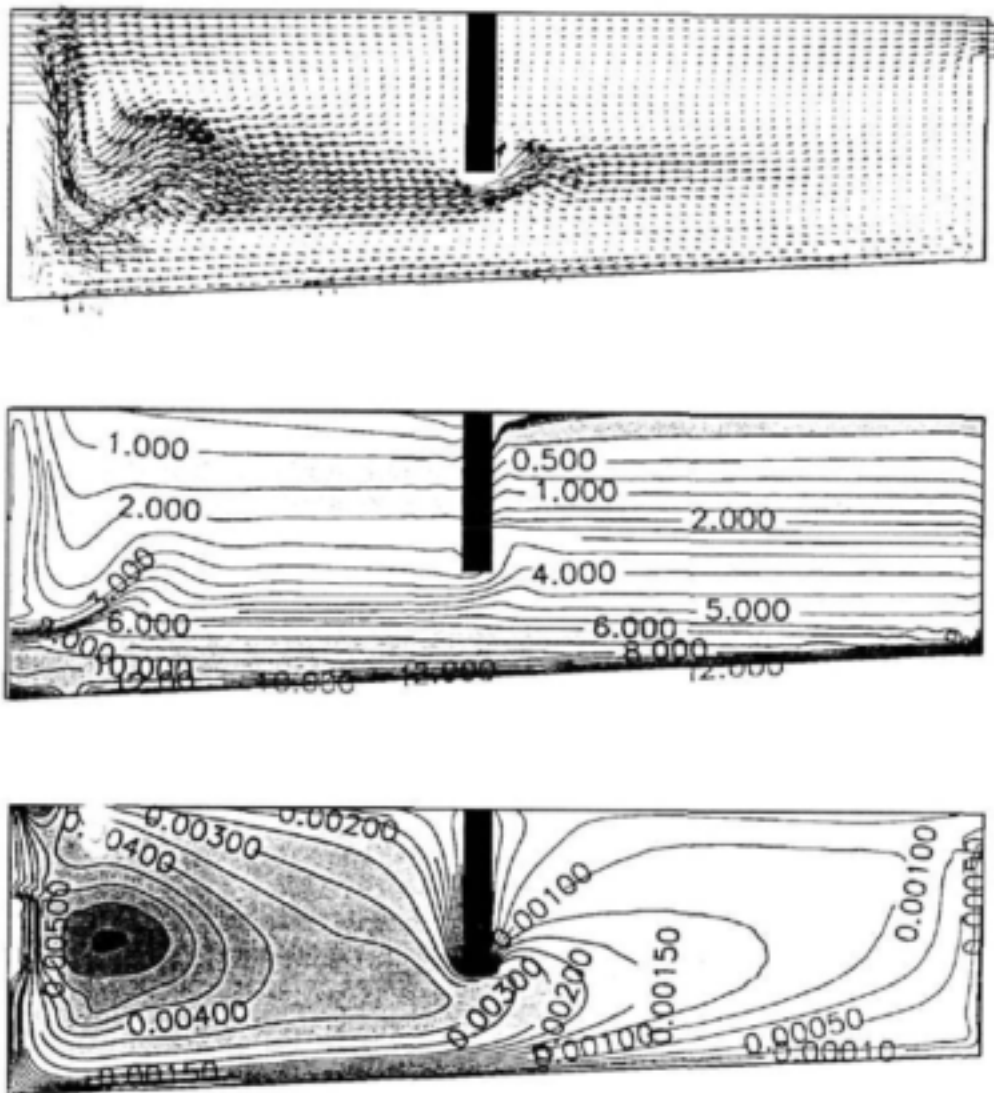


**Fig 21:** *Watts Tank Test 12: Steady state case*  
*Predicted flow pattern and sludge distribution  $C$  in g/l, as well as*  
*the predicted turbulent viscosity field  $v_t$  in  $m^2/s$*

The computational result of Test 4 is shown in Fig 22. With 97.5 % this steady state does not yield a mass balance, but the sludge blanket reaches equilibrium and does not rise to the effluent outlet.

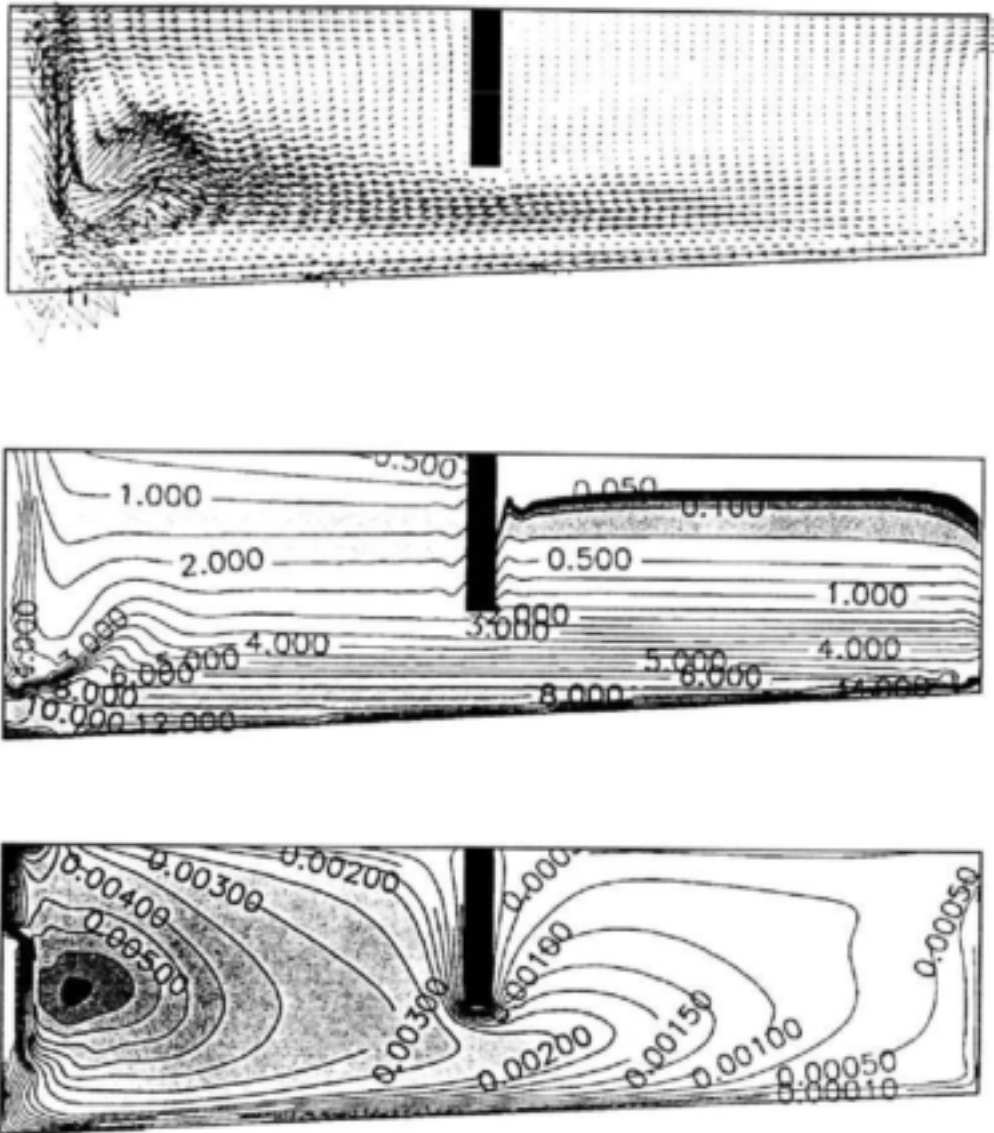


*Fig 22: Watts Tank Test 4: Steady state case  
 Predicted flow pattern and sludge distribution  $C$  in  $\text{g/l}$ , as well as  
 the predicted turbulent viscosity field  $v_t$  in  $\text{m}^2/\text{s}$*

## 6 CONCLUSION AND OUTLOOK

The main goal of this part of the project has been to compile a working finite element package for 2D hydrodynamic modelling of SSTs that is capable of simulating the benchmark results available in the literature. This "real life" application requires the design of "high-performance" solution tools, which have to fit together perfectly.

The finite element code produces reasonable results and is in good agreement with the benchmark results, as well as with the results obtained using SettlerCAD (Table 4). Good results could also be obtained by using a constant turbulent viscosity, provided that the construction of the tank allows it, i.e. an inlet region that is small compared to the main section of the tank. The use of the SUPG approach does not lead to an improvement, except for the neutral density case. On the other hand with SUPG the results and the convergence deteriorate with the presence of the gravity term.

The assumption that the eddy diffusivity, which governs the solids mixing in the tank, is proportional to the eddy viscosity, cannot be confirmed. Best computational results could be found by using a constant and small diffusion coefficient, i.e. the sludge is less influenced by diffusion than assumed by using the Reynolds analogy. Due to the uncertainty about the diffusion parameters and the sludge behaviour, especially in the high concentration environment, further investigation is needed to obtain reliable determination of the parameters describing the interaction between flow and settling of activated sludge.

Although the variation of the results is less an outcome of uncertainties within the numerical modelling procedure, they nevertheless demonstrate that the two phases, pure water and activated sludge, should be modelled separately by using a two-phase model in which each phase is calculated by a separate momentum equation. This highly nonlinear model would lead to a considerable number of unknowns and would require increased computation time.

The computation time and with it the computational efficiency can be improved with the use of numerical techniques (Turek, 1998), such as preconditioning, a more robust iterative treatment, the implementation of a multigrid technique or the choice of a more robust, accurate and efficient element pair. Furthermore, because of the progressive development of the program, it is somewhat inefficient in computer time, because numerous operations are repeated several times, instead of having their results stored once in the computer memory. To save on memory the matrix should be stored in a special way, for example using compressed sparse row storage. More efficient streamlining of the calculation procedure and routines can also reduce computation time. Finally, before the program can be released for general use, it is necessary to build up a user-friendly pre- and postprocessing procedure.

Parameter		Darvill OldTank Test3	Darvill OldTank Test 3 + 10%	Darvill NewTank Test 3 + 10%	Watts Test 1	Watts Test 4	Watts Test 12
Loading Conditions	Influent Flow (m <sup>3</sup> /h)	948	1074	1074	475.1	788.9	1095.8
	Recycle Flow (m <sup>3</sup> /h)	750	750	750	397.5	397.5	397.5
	Recycle Ratio	0.79	0.7	0.7	0.84	0.51	0.36
	Feed Concentration(g/l)	3.600	3.600	3.600	4.053	4.130	3.444
Sludge Settleability	DSVI (ml/g)	62	62	62	94	94	94
Retention Time (h)		1.3	1.4	2.5	2.1	1.8	1.8
Effluent SS <sup>1</sup> (mg/l)		0.0	44	0.0	0.0	20	253
Recycle Concentration (g/l)		8.2	8.8	8.76	8.2	11.9	11.6
Mass Balance (%)		101	101.5	100	92.7	97.5	100
Observed Test Result	Experiment	Safe	Not Tested	Not Tested	Safe	Safe	Fail
Test Result (ESS <sup>2</sup> > 50mg/l)	SettlerCAD (see Part 1)	Safe	Fail	Safe	Safe	Safe	Fail
Test Result (ESS > 50mg/l)	FEM - Program	Safe	Safe	Safe	Safe	Safe	Fail

**Table 4:** Summary and comparison of computational and benchmark results

<sup>1</sup>Suspended Solids concentration

<sup>2</sup>Effluent Suspended Solids



## 7 REFERENCES

- de Haas D.W. (1998) The use of simultaneous chemical precipitation in modified activated sludge systems exhibiting enhanced biological phosphate removal. PhD thesis, University of Cape Town, Rondebosch, Cape, 7701, RSA. (Chapter 6 - Fullscale plant trial).
- Barett R., Berry M., Chan T.F., Demmel J., Donato J.M., Dongarra J., Eijkhout V., Pozo R., Romine C. and Van der Vorst H. (1994) *Templates for the Solution of Linear Systems: Building Blocks for Iterative Methods*. SIAM
- Brooks A.N. and Hughes T.J.R. (1982) Streamline Upwind / Petrov - Galerkin Formulations for Convection Dominated Flows with Particular Emphasis on the Incompressible Navier-Stokes Equations. *Comp. Meth. Appl. Mech. Eng.*, **32**, 199-259.
- Celik I., Rodi W. and Stamou A. (1985) Prediction of Hydrodynamic Characteristics of Rectangular Settling Tanks. *Proc. Int. Symp. Refined Flow Modelling and Turbulence Measurements*, Iowa City, Iowa, USA.
- Celik I. and Rodi W. (1988) Modelling suspended sediment transport in nonequilibrium situations. *J. Hydraulics Engrg.*, ASCE, **114**(10), 1157-1188.
- Chorin A.J. (1968) Numerical solution of the Navier-Stokes equations. *Math. Comp.*, **22**, 745-762.
- DeVantier B.A. and Larock B.E. (1986) Modelling a recirculation density-driven turbulent flow. *Int. J. for Numerical Methods in Fluids*, **6**(4), 241-253.
- Ekama G.A., Barnard J.L., Günthert F.W., Krebs P., McCorquodale J.A., Parker D.S. and Wahlberg E.J., (1997) *Secondary Settling Tanks: Theory, Modelling, Design and Operation*. IAWQ STR No 6, International Association on Water Quality, London.
- Gidaspow D. (1994) *Multiphase Flow and Fluidization*. Academic Press, Inc., San Diego.
- Hill D.L. and Baskharone E.A. (1997) Development of a multiblock pressure-based algorithm using mixed interpolation for turbulent flows. *Int. J. Num. Meth. Fluids*, **25**, 615-631.
- Imam E. McCorquodale J.A. and Bewtra J.K. (1983) Numerical modelling of sedimentation tanks. *J. Hydraulics Engrg.*, ASCE, **109**(12), 1740-1754.
- Kelly C.T. (1995) *Iterative methods for linear and nonlinear equations*. SIAM Frontiers in Applied Mathematics.
- Krebs P. (1989) Modellierung von Strömungen in rechteckigen Nachklärbecken. *Gas-Wasser-Abwasser/Abwasser* **69** (11), 718-728.
- Lakhal D., Krebs P., Krijgsman J. and Rodi W. (1999). Computing shear flow and sludge blanket in secondary clarifiers. *J. Hydraulic Engrg.*, ASCE, **125**(3), 253-262.
- McCorquodale J.A. and Zhou S. (1993). Effects of hydraulics and solids loading on clarifier performance. *J. Hydraulic Res.*, **31**(4), 461-478.
- Reddy, B.D. (1998) *Introductory Functional Analysis with Applications to Boundary Value Problems and Finite Elements*. Texts in Applied Mathematics 27, Springer Verlag.

- Rodi W. (1980) *Turbulence models and their application in hydraulics; a state-of-the-art review*. Int. Association for Hydraulic Research, IAHR, Delft, The Netherlands.
- Saad Y. and Schultz M.H. (1986) GMRES: A generalized minimal residual method for solving nonsymmetric linear systems. *SIAM J. Sci. Statist. Comput.*, **7**, 856-869.
- Takács I., Patry G.G. and Nolasco D. (1991) A dynamic model of the clarification - thickening process. *Wat. Res.*, **25** (10), 1263-1271.
- Taylor C. and Hughes T.G (1981) *Finite Element Programming of the Navier-Stokes Equations*. Pineridge Press Swansea, U.K.
- Turek S. (1998) *Efficient solvers for incompressible flow problems: An algorithmic approach in view of computational aspects*. Springer Verlag
- Van Kan J. (1986) A second-order accurate pressure-correction scheme for viscous incompressible flow. *SIAM J. Sci. Stat. Comp.*, **7**, 870-891.
- Watts R.W., Svoronos S.A. and Koopman B. (1996) One dimensional modelling of secondary clarifiers using a concentration feed velocity dependent dispersion coefficient. *Water Research*, **30**(9), 2112-2124.
- Zhou S., Pfeil R., Strand E., Ji Z. and Vitasovic C. (1998) SettlerCAD (formerly Clarity) Release 1.1 - A 2D hydrodynamic model for secondary clarifiers. Reid Crowther Consulting, Seattle, WA., USA.
- Zienkiewicz O.C. and Taylor R.L. (2000) *The Finite Element Method*. Volume **3**, Fluid Dynamics, Butterworth-Heinemann

## APPENDIX 3

## LIST OF SYMBOLS FOR PART 2

$\alpha, \beta, \theta', \theta$	Parameters used in temporal discretization	[–]
$\delta_g$	Kronecker delta	[–]
$\Gamma$	Boundary of the spatial computation domain $\Omega$	[m]
$\gamma$	Streamline upwind parameter	[–]
$\Delta \rho$	Density difference between mixture and pure water	[m <sup>3</sup> /kg]
$\Delta t$	Change in time	[s]
$\varepsilon$	Turbulent dissipation rate	[m <sup>2</sup> /s <sup>3</sup> ]
$\varepsilon_0$	Inlet turbulent dissipation rate	[m <sup>2</sup> /s <sup>3</sup> ]
$\nu$	Kinematic viscosity	[m <sup>2</sup> /s]
$\nu_{sr}$	Eddy diffusivity of suspended solids in the $r$ (or $x$ ) direction ( $= \nu_t / \sigma_{sr}$ )	[m <sup>2</sup> /s]
$\nu_{sy}$	Eddy diffusivity of suspended solids in the $y$ direction ( $= \nu_t / \sigma_{sy}$ )	[m <sup>2</sup> /s]
$\nu_t$	Eddy viscosity	[m <sup>2</sup> /s]
$\rho$	Fluid density	[m <sup>3</sup> /kg]
$\rho_0$	Density of inflow	[m <sup>3</sup> /kg]
$\rho_s$	Density of dry solids	[m <sup>3</sup> /kg]
$\rho_r$	Reference density - density of pure water	[m <sup>3</sup> /kg]
$\sigma_k, \sigma_\varepsilon$	Prandtl numbers for $k$ and $\varepsilon$ constants	[–]
$\sigma_{sr}, \sigma_{sy}$	Schmidt numbers in $r$ ( $x$ ) and $y$ direction respectively	[–]
$\Omega$	Spatial computation domain	[m <sup>2</sup> ]
$C$	Suspended solids concentration	[kg/m <sup>3</sup> ]
$C_0$	Inlet suspended solids concentration	[kg/m <sup>3</sup> ]
$C\mu, C_1, C_2$	Constants used in $k$ - $\varepsilon$ model	[–]
$g$	Acceleration due to gravity (9.81 m/s <sup>2</sup> )	[m/s <sup>2</sup> ]
$H$	Total water depth in SST	[m]
$H_w$	Depth of the influent stream opening	[m]
$h$	Characteristic element length scale of the element	[m]
$k$	Turbulent kinetic energy	[m <sup>2</sup> /s <sup>2</sup> ]
$l_m$	Mixing length to calculate the inlet turbulence dissipation rate	[m]
$K, K_i$	Constants in settleability equation by Tacács	[–]
$n$	Constant in settleability equation by Tacács ( $= K$ )	[–]
$N$	Basis function	[–]
$n_i$	Outward unit normal vector	[–]
$p$	General pressure less the hydrostatic pressure	[Pa]

$Pe$	Peclet number	[-]
$Re$	Reynolds number	[-]
$t$	Time	[s]
$U$	Mean horizontal velocity in $r$ (circular tank) and $x$ (rectangular tank) directions	[m/s]
$U_o$	Mean horizontal inlet velocity to the tank	[m/s]
$U_i$	Velocity tensor	[m/s]
$U_i^*$	Intermediate velocity tensor	[m/s]
$V$	Mean vertical velocity in the $y$ direction	[m/s]
$V_s$	Settling velocity of sludge particles	[m]
$W$	Weighting function	[-]
$x$	Horizontal coordinate	[m]
$x_i$	Coordinate tensor	[m]
$y$	Vertical coordinate	[m]

*Superscripts and subscripts*

$o$	Initial conditions
$i, j$	Indices used in tensor notation

## LIST OF FIGURES FOR PART 2

### CHAPTER 2 SECONDARY SETTLING TANKS

<b>Fig 1</b>	Secondary Settling Tank	3
<b>Fig 2</b>	Modelling of fluid-solid flow in SSTs	4

### CHAPTER 3 FUNDAMENTAL EQUATIONS

<b>Fig 3</b>	Modified settling function of Takács	7
<b>Fig 4</b>	Density state equation	8

### CHAPTER 5 EXAMPLE USE OF NUMERICAL MODEL AND EXPERIMENT

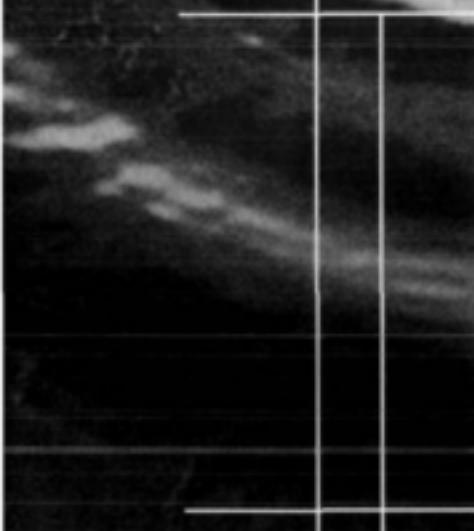
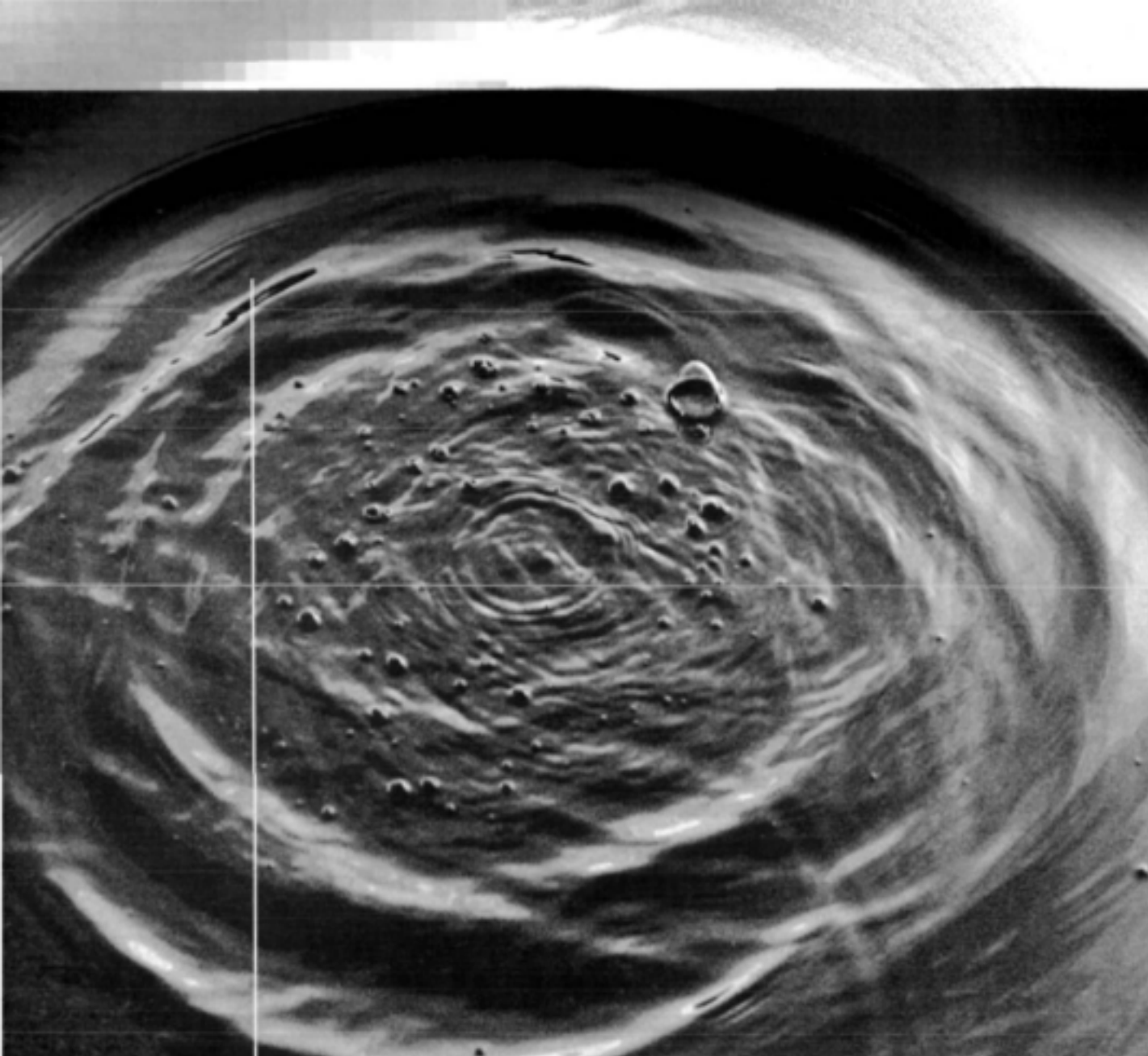
<b>Fig 5</b>	Geometry and boundaries for Darvill Old and New SST, as well as for the Watts SST	
<b>Section 5.2</b>	<b>Simulating of the Darvill Old and New Tank</b>	19
<b>Fig 6</b>	Mesh of Darvill Old Tank (85 x 25 ) and New Tank ( 85 x 58)	24
<b>Fig 7</b>	<u>Darvill Old and New Tank</u> Neural density case: Initial conditions	25
<b>Fig 8</b>	<u>Darvill Old Tank</u> Test 3: After 100 sec to after 10 min Predicted flow pattern and sludge distribution $C$ in g/l	26
<b>Fig 9</b>	<u>Darvill Old Tank</u> Test 3: After 15 min to after 6 hours Predicted flow pattern and sludge distribution $C$ in g/l	27
<b>Fig 10</b>	<u>Darvill Old Tank</u> Test 3: Steady state case Predicted flow pattern and sludge distribution $C$ in g/l	28
<b>Fig 11</b>	<u>Darvill Old Tank</u> Test 3 with a 10 % higher influent flow: Steady state case Predicted flow pattern and sludge distribution $C$ in g/l	28
<b>Fig 12</b>	<u>Darvill New Tank</u> Test 3 with a 10 % higher influent flow: After 100 sec to after 10 min Predicted flow pattern and sludge distribution $C$ in g/l	29
<b>Fig 13</b>	<u>Darvill New Tank</u> Test 3 with a 10 % higher influent flow: After 15 min to after 6 hours Predicted flow pattern and sludge distribution $C$ in g/l	30

<b>Fig 14</b>	<u>Darvill New Tank</u> Test 3 with a 10 % higher influent flow: Steady state case Predicted flow pattern and sludge distribution $C$ in g/l	31
<b>Section 5.3 Simulating of the Watts Tank</b>		
<b>Fig 15</b>	<u>Watts Tank</u> Test1: Predicted flow pattern and sludge distribution $C$ in g/l, using a Schmidt number $\sigma_s$ of 1.0, as well as the predicted turbulent viscosity field $\nu_t$ in m <sup>2</sup> /s	32
<b>Fig 16</b>	<u>Watts Tank</u> Test1: Predicted flow pattern and sludge distribution $C$ in g/l, using the modified Schmidt number $\sigma_{s,}$ , as well as the predicted turbulent viscosity field $\nu_t$ in m <sup>2</sup> /s	34
<b>Fig 17</b>	<u>Watts Tank</u> Test 12: Neutral density case Mesh of 65 x 30 elements and predicted flow pattern	36
<b>Fig 18</b>	<u>Watts Tank</u> Test 12: Neutral density case Predicted turbulent viscosity field $\nu_t$ in m <sup>2</sup> /s	37
<b>Fig 19</b>	<u>Watts Tank</u> Test 12: After 100 sec to after 10 min Predicted flow pattern and sludge distribution $C$ in g/l	38
<b>Fig 20</b>	<u>Watts Tank</u> Test 12: After 15 min to after 6 hours Predicted flow pattern and sludge distribution $C$ in g/l	39
<b>Fig 21</b>	<u>Watts Tank</u> Test 12: Steady state case Predicted flow pattern and sludge distribution $C$ in g/l, as well as the predicted turbulent viscosity field $\nu_t$ in m <sup>2</sup> /s	40
<b>Fig 22</b>	<u>Watts Tank</u> Test 4: Steady state case Predicted flow pattern and sludge distribution $C$ in g/l, as well as the predicted turbulent viscosity field $\nu_t$ in m <sup>2</sup> /s	41

## LIST OF TABLES FOR PART 2

### CHAPTER 5 EXAMPLE USE OF NUMERICAL MODEL AND EXPERIMENT

<b>Table 1</b>	Summary of the loading conditions used for the simulation of the Darvill Old and New Tank, as well as for the Watts Tank	22
<b>Table 2</b>	<u>Darvill Old and New Tank</u> : Loading conditions and model parameter	23
<b>Table 3</b>	<u>Watts Tank</u> : Loading conditions and model parameter	35
<b>Table 4</b>	Summary and comparison of computational and benchmark results	43



Water Research Commission

PO Box 824, Pretoria, 0001, South Africa

Tel: +27 12 330 0340, Fax: +27 12 331 2565

Web: <http://www.wrc.org.za>

1868458601

